2016

The Role of Phosphorylated αB-Crystallin in Age-related Nuclear Cataract

Erin Thornell
University of Wollongong

The Role of Phosphorylated αB-Crystallin in Age-related Nuclear Cataract

A thesis submitted in fulfilment of the requirements for the degree of

Doctor of Philosophy

From

University of Wollongong

School of Biological Sciences

By

Erin Thornell

BSc Adv (hon)

August 2016

Declaration

The work described in this thesis does not contain any material which has been accepted for the award of any other degree or diploma in this or any other University and to the best of my knowledge and belief contains no material previously published by any other person, except where due reference has been acknowledged.

Erin Thornell

August, 2016

Acknowledgements

I would like to start by thanking everyone who has offered guidance and advice over the years, particularly Mike, James, Fran, Amanda, Justin, Lisa and the academic staff at IHMRI and UOW. A small piece of advice can make a huge difference.

I would also like to deeply thank Mark for stepping in when it was most needed, Heath for taking on the primary supervisor role at such a critical point in my PhD and Roger for providing such a high level of expertise in the field.

Finally, I would like to acknowledge and thank the people who donated the tissue I used throughout my studies, and their families.

Publications

Sections of the work described in this thesis have been reported in the following publication:

1. Thornell, E. and Aquilina, A. (2015). *Regulation of αA- and αB-crystallins via phosphorylation in cellular homeostasis.* Cellular and Molecular Life Sciences **72**: 4127-4137.

Abstract

The transparency of the lens is maintained throughout life, at least in part, by the chaperone activity of the small heat shock protein (sHSP) αB-crystallin (αB). However, modified forms of αB, including phosphorylated and deamidated isoforms, accumulate in insoluble protein fractions from the lens with age. This has led to the suggestion that modification of αB is a precursor to age-related nuclear cataract formation. This thesis investigated whether phosphorylated αB could contribute to cataract formation by facilitating the formation of the nucleocortical barrier, a physical barrier to the diffusion of small molecules into the nucleus of the lens that forms at middle age. To determine how phosphorylation may modulate the chaperone activity of αB, single (S19D; S45D; S59D), double (S19D and S45D) and triple (S19D, S45D and S59D) mutants of αB which mimic phosphosphorylation at three key serine residues (Ser19, Ser45 and Ser59) were used in an *in vitro* aggregation assay and their activity compared to wild type (WT) αB. Whilst WTαB failed to inhibit the heat-induced aggregation of creatine phosphokinase (CPK), the triple mutant (i.e. αB S19D, S45D and S59D) inhibited the aggregation of CPK by 83.9±1.3%. Thus, it is concluded that the addition of negative charges to αB, similar to those added by phosphorylation, increases its chaperone activity.

Next, protein was isolated from adult human lenses via sucrose density centrifugation and separated using 2-dimensional sodium dodecylsulphate polyacrylamide gel electrophoresis (2D SDS PAGE) to identify changes in αB phosphorylation and the deamidation of cytoskeletal proteins that occurs with age across different regions of the lens. The amount of multiply phosphorylated αB (i.e. phosphorylated at multiple residues) was increased in high-density protein fractions from the lens (representing membrane-bound protein) compared to low density protein fractions. The amount of multiply phosphorylated αB increased towards the nucleus in the aged lenses. In some high density protein fractions there was also evidence of crosslinked high molecular weight complexes (HMWCs), involving αA-crystallin (αA), αB and cytoskeletal proteins including filensin. This provides evidence for the involvement of α-crystallin, via binding to intermediate filaments, in the formation of a network that supports the fibre cell membrane.

To determine whether the association of αB with fibre cell membranes could also be mediated by direct interactions with membrane pore proteins, a proximity assay was used to

identify interactions between isoforms of αB and the abundant membrane pore proteins aquaporin 0 (AQP0) and connexin 46 (Cx46). Interactions between αB and both AQP0 and Cx46 were restricted to the cortex of the lens in a region coinciding with the putative location of the nucleocortical barrier, although total αB continued to associate with membranes in the nucleus of the lens. This pattern was more prominent for the pSer59 isoform, with minimal interactions between pSer19 αB and membrane pore proteins throughout the lens.

Finally, recombinant human αB was heat-treated under acidic (~pH 3.0), basic (~pH 8.0) and unfolding buffer conditions in order to determine whether it was susceptible to non-enzymatic deamidation, a process known to occur with age in the lens. An additional site of deamidation in αB was identified in the sample that was heat-treated under slightly alkaline (~pH 8.0) buffer conditions (i.e. deamidation occurred at both N146 and N78) compared to the sample heat-treated under acidic buffer conditions (i.e. deamidation occurred only at N146). Although the amount of deamidation at each site was unaffected by protein unfolding, a slight decrease in buffer pH (from ~pH 8.0 to ~pH 7.4) significantly increased the amount of deamidation at N146 and Q151 of αB.

Based on the results of this work, a new model for age-related cataract formation is proposed, whereby phosphorylation of αB induces its association with membrane pore proteins (such as AQP0 and Cx46) and deamidated cytoskeletal components (particularly filensin) that coat the membrane. It is proposed that if these interactions mediate the formation of the nucleocortical barrier at middle age, the inhibition of the transport of glutathione (GSH) and water into the lens nucleus would result in an oxidative environment in the nucleus of the lens. This provides a pathway for protein cross-linking and aggregation of proteins that form the insoluble deposits characteristic of age-related nuclear cataract.

Contents

Table of Figures

Table of Tables

Abbreviations

0P: no phosphomimicking mutation (i.e. WT αB)

1D SDS-PAGE: 1-dimensional sodium dodecyl sulphate polyacrylamide gel electrophoresis

1P: single phosphomimicking mutation (S19D)

2D: 2-dimensional

2P: double phosphomimicking mutation (i.e. S19D; S45D)

3P: triple phosphomomicking mutation (i.e. S19D; S45D; S59D)

αA: αA-crystallin

αB: αB-crystallin

ACD: α-crystallin domain

ANOVA: analysis of variance

ATP: adenosine triphosphate

AQP0: aquaporin 0

BASP1: brain acidic soluble protein 1

BFSP2: beaded filament protein 2 (phakinin)

BSA: bovine serum albumin

cAMP: cyclic adenosine monophosphate

CPK: creatine phosphokinase

Cx46: connexin 46

DAB: diaminobenzidine

DHA: dehydroalanine

DHB: dehydrobutyrine

DTT: dithiothrietol

EDTA: ethylenediaminetetraacetic acid

GFAP: glial fibrillary acid protein

GSH: glutathione

HBSS: Hank’s balanced salt solution

HMW: high molecular weight

HMWCs: high molecular weight complexes

HPLC: high performance liquid chromatography

HRP: horseradish peroxidase

Hsps: heat shock proteins

IEF: isoelectric focusing

iTRAQ: isobaric tag for relative and absolute quantitation

MAP: mitogen-activated protein

MAPKAP: MAP kinase-activate protein

MP20: membrane protein 20

MS: mass spectrometry

MS/MS: tandem MS

nanoLC QTOF: nano liquid chromatography quadrupole time-of-flight

PAR2: protease-activated receptor 2

PBS: phosphate-buffered saline

PFA: paraformaldehyde

pSer19: phosphorylation at Ser19

pSer45: phosphorylation at Ser45

pSer59: phosphorylation at Ser59

PTMs: posttranslational modifications

PVDF: polyvinylidene fluoride

S19D: aspartate substitution at Ser19

S45D: aspartate substitution at Ser45

S59D: aspartate substitution at Ser59

S19D: aspartate substitution at Ser19

S45D: aspartate substitution at Ser45

S59D: aspartate substitution at Ser59

sHSP: small heat shock protein

SOD1: superoxide dismutase 1

TBST: tris-buffered saline – tween 20

TNF-α: tumor necrosis factor α

TNF: tumor necrosis factor

TRAIL: TNF-related apoptosis-inducing ligand

WT: wild type

Chapter 1

Introduction

Sections of the work described in this chapter have been published:

1. Thornell, E. and Aquilina, A. (2015). Regulation of αA- and αB-crystallins via phosphorylation in cellular homeostasis. *Cellular and Molecular Life Sciences***72**: 4127-4137.

Chapter 1

1.1 Introduction

The lens is a transparent structure located in the eye that is responsible for the transmission and focusing of light onto the retina. During life, the lens has negligible protein turnover, and thus lenticular proteins are vulnerable to the accumulation of post-translational modifications and damage that can compromise the transparency of the lens, leading to cataract. The transparency of the lens is therefore maintained, in most cases, throughout life by the chaperone activity of α-crystallins (Sun *et al.*, 1997), which act to ensure lenticular proteins remain in a soluble state. However, α-crystallin is itself vulnerable to post-translational modifications (PTMs), and these are believed to have the ability to alter its chaperone activity. It has been shown that phosphorylated α-crystallin accumulates within lens fibre cells with age (Takemoto and Boyle, 1998), but it is unclear if, and in what way, this may contribute to cataract formation. It has also been proposed that the formation of the nucleocortical barrier, a barrier to diffusion that is known to form in the lens at around middle age, directly contributes to cataract formation (Sweeney and Truscott, 1998; Truscott, 2000; Truscott, 2005) by leading to the formation of an oxidative environment in the centre of the lens. The mechanism behind barrier formation also remains unclear, and any potential link between α-crystallin phosphorylation and barrier formation is yet to be elucidated. This chapter discusses these complimentary theories in the context of the ageing lens.

1.2 The Lens

The lens is located in the eye, anterior to the vitreous humour and posterior to the aqueous humour and the iris. It is held in position by the suspensory ligaments which anchor it to the ciliary body (Ross and Pawlina, 2006) (Figure 1.1). The role of the lens is to bend or refract incoming light that has already passed through the cornea and the pupil at such an angle that the rays focus directly onto the light-sensitive retina, the innermost layer of the wall of the eyeball (Ross and Pawlina, 2006). The lens achieves this through the process of 'accommodation', whereby the curvature of the lens is adjusted by the ciliary muscle to allow light reflected off objects at various distances from the eye to be bent at the correct angle for precise focussing onto the retina (Ross and Pawlina, 2006) (Figure 1.1). Upon striking the

retina, the sensory organ of the eye, light energy is transferred into action potentials, through a process known as 'transduction' (Silverthorn, 2007).

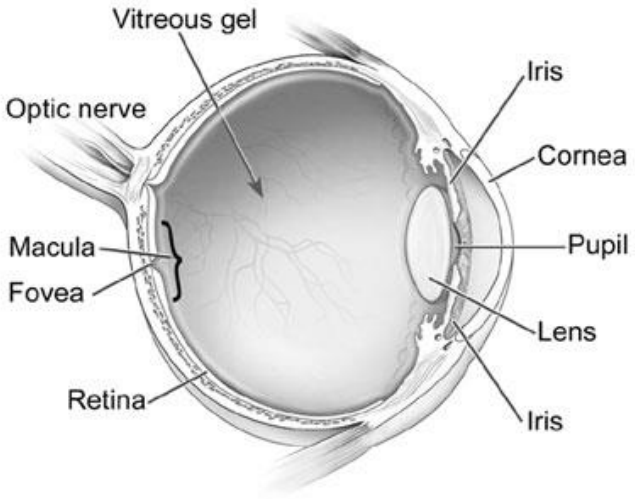

Figure 1.1: Internal and external structures of the eye. The lens is attached to the ciliary body via the suspensory ligaments (not labelled), which act to suspend it in a position anterior to the vitreous humour and posterior to the aqueous humour and iris. Light passes through the cornea and pupil and is transmitted through the lens which, through the process of accommodation, acts to focus the rays directly onto the retina. Image obtained from National Eye Institute (2015a).

Synthesis and growth of the lens commences *in utero* and continues until death (Phelps Brown and Bron, 1996), with the average mature lens reaching 4 mm in width, and 9 mm in diameter (Harper and Shock, 2004). The lens, which is asymmetric and biconvex in shape (Figure 1.2), is entirely covered by a thick but permeable capsule which protects it from bacterial infection whilst allowing the diffusion of materials such as water, ions and proteins via the humours. This capsule, which is composed of connective tissue, notably Type IV collagen, is secreted by the epithelial cells *in utero* (Phelps Brown and Bron, 1996).

Within the capsule, the bulk of the lens consists of a mass of fibre cells covered at the anterior surface by a single layer of epithelial cells which extend as far as the equator (Papaconstantinou, 1967; Grey and Schey, 2009) (Figure 1.2). These epithelial cells migrate

to the equator of the lens as they differentiate into fibre cells, elongate and wrap around the lens, meeting at their tips to form sutures (Papaconstantinou, 1967; Grey and Schey, 2009). Differentiation of epithelial cells into fibre cells involves the degradation of the organelles and nucleus in order to attain the state of transparency required for effective light transmission (Han and Schey, 2006; Grey and Schey, 2009)

This pattern of growth, where the addition of new cells on top of older cells in the centre of the lens, results in the formation of two indiscrete zones (Han and Schey, 2006): the nucleus, defined as the lenticular material that was present at birth; and the cortex, concentric layers of cells that are laid down postnatally (Phelps Brown and Bron, 1996). At around middle-age, a barrier forms between these regions, known as the 'nucleocortical barrier' (Sweeney and Truscott, 1998; Shestopalov and Bassnett, 2000; Cobb and Petrash, 2002b; Truscott, 2005). The precise nature of this barrier is unknown, although it is believed to inhibit the diffusion of water and other molecules between the two regions (Cobb and Petrash, 2002b; Truscott, 2005).

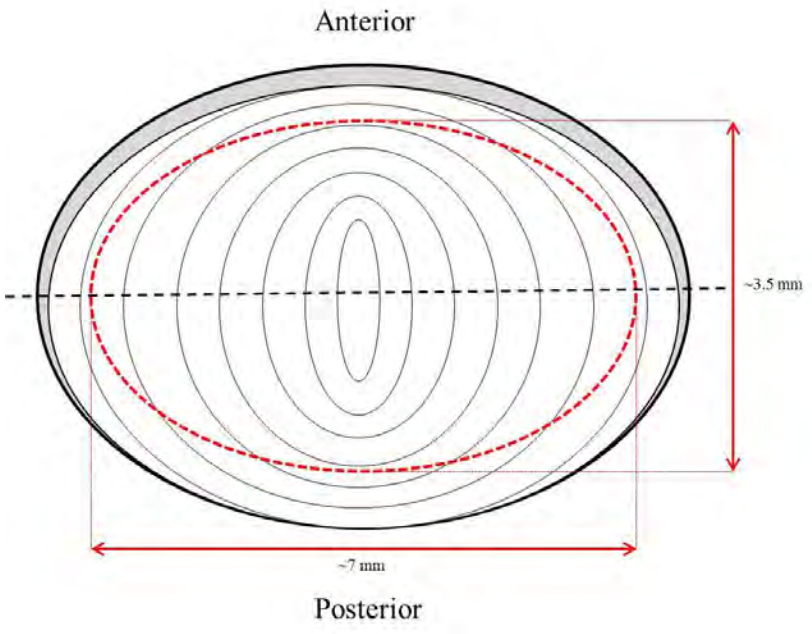

Figure 1.2: Structure of the optical lens along the meridial plane. The lens is composed of concentrically layered fibre cells, covered at the anterior pole by a single layer of epithelial cells, shaded in grey. The outer border of the lens on the equatorial plane is known as the equator, indicated by the black broken line, and is the site of differentiation of the epithelial cells into fibre cells. The purported location of the nucleocortical barrier is indicated by the red broken line. The dimensions of the barrier are as indicated.

The lens proteome

Due to the absence of a nucleus and organelles in lenticular fibre cells, protein synthesis is not possible, thus the lens is particularly prone to degradation with age (Han and Schey, 2006). Most notably, there is a decrease in elasticity that is due, in part, to the loss of α-crystallin (Heys *et al.*, 2007), the formation of protein crosslinks (Phelps Brown and Bron, 1996; Truscott, 2005), and the formation of insoluble high molecular weight (HMW) protein complexes that also cause increased light scattering (Benedek, 1971; Horwitz, 1993; Carver *et al.*, 1996; Phelps Brown and Bron, 1996; Hejtmancik and Kantorow, 2004; Moreau and King, 2012). Other changes in the lens that are associated with age include decreased membrane permeability due to increased chain length and saturation of membrane phospholipids (Merchant *et al.*, 1991), decreased amount and activity of enzymes (Hockwin, 1965; Hockwin *et al.*, 1965; Sethna *et al.*, 1982; Phelps Brown and Bron, 1996; Cobb and Petrash, 2002b), the formation of the nucleocortical barrier (Cobb and Petrash, 2002b; Truscott, 2005) and a range of PTMs that occur to proteins (Lund *et al.*, 1996; Lin *et al.*, 1997; Lampi *et al.*, 1998; Lin *et al.*, 1998; Ma *et al.*, 1998; Hanson *et al.*, 2000; Lapko *et al.*, 2001; MacCoss *et al.*, 2002; Truscott, 2005; Han and Schey, 2006; Wang *et al.*, 2013). These events are highly significant as they contribute to the conditions of presbyopia and cataract (reviewed in Spector, 1995; Phelps Brown and Bron, 1996; Truscott, 2005). Presbyopia, or long-sightedness, occurs around middle-age as a result of the lens failing to accommodate efficiently, whereas cataracts result from the diffusion and obstruction of light transmission by insoluble HMW proteins (Benedek, 1971; Horwitz, 1993; Carver *et al.*, 1996; Phelps Brown and Bron, 1996; Hejtmancik and Kantorow, 2004; Truscott, 2005; Moreau and King, 2012; National Eye Institute, 2015b).

Despite the lack of protein turnover, lenticular cells retain cytoskeletal and membrane protein components. Three cytoskeletal networks exist in the lens i.e. the actin, microtubule and intermediate filament networks (Figure 1.3), each of which retain distinct roles and assemble independently of each other (Quinlan *et al.*, 1999). The actin and microtubule cytoskeletal networks are involved in cellular differentiation and cell transport processes respectively (Quinlan *et al.*, 1999). The lenticular intermediate filament network comprises three filament proteins specific to the lens; vimentin, phakinin and filensin, the latter two of which are lens specific (Quinlan *et al.*, 1999). Phakinin and filensin interact to form a filamentous network (FitzGerald and Graham, 1991; Carter *et al.*, 1995; Quinlan *et al.*, 1999) that is believed to be important in the maintenance of cell morphology and cell membrane architecture (Perng *et*

al., 2007). Both filensin (Sandilands, Prescott, Hutcheson*, et al.*, 1995) and phakinin (Sandilands, Prescott, Carter*, et al.*, 1995) are highly susceptible to cleavage in the lens. It has been shown *in vitro*, that although only a 53 kDa fragment derived from the N-terminal head of filensin is required for filament formation (Masaki and Quinlan, 1997), neither filensin nor phakinin can form a filament without the presence of the other (Carter *et al.*, 1995; Goulielmos *et al.*, 1996). In the lens, phakinin and filensin co-assemble at the fibre cell membrane to form a beaded filament protein (FitzGerald and Graham, 1991; Carter *et al.*, 1995). This structure interacts with αA and αB, which are believed to produce the characteristic beaded appearance of the beaded filament protein (Carter *et al.*, 1995). It has been suggested that the association of the α-crystallins with filensin and phakinin is essential for intermediate filament formation (Ghosh *et al.*, 2005). Additionally, an R120G point mutation of αB has been implicated in the breakdown of the intermediate filament network associated with desmin-related myopathy, being incorporated into the protein aggregates characteristic of the disease (Vicart *et al.*, 1998).

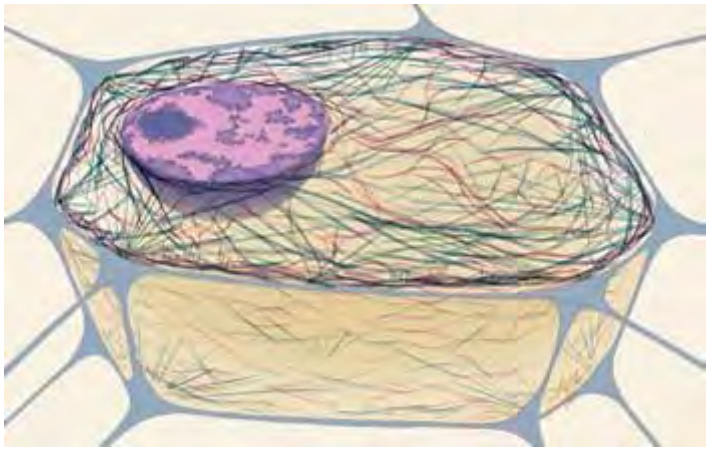

Figure 1.3: Cytoskeletal networks of the cell. Representation of a cell depicting the three cytoskeletal networks; the actin (green), intermediate filament (red) and microtubule (blue) network. Cytoskeletal networks anchor to the cell membrane (grey) and function in cell transport and structural maintenance. The nucleus is indicated by purple sphere. Image obtained from the National Institute of General Medical Sciences (2012).

The most abundant membrane pore proteins in the lens are the aquaporins (Bassnett *et al.*, 2009; Kumari *et al.*, 2011), comprising AQP1, present only in epithelial cells, and AQP0,

present in mature fibre cells (Varadaraj *et al.*, 2007). Both are believed to act as water channels in the lens (Varadaraj *et al.*, 2007; Kumari *et al.*, 2011) with AQP0, constituting over 50% of membrane proteins (Varadaraj *et al.*, 2007), also taking part in cell-to-cell adhesions (Kumari *et al.*, 2011). The second most abundant membrane protein in the lens is membrane protein 20 (MP20), which is thought to be involved in fibre cell junction formation and organisation (Tenbroek *et al.*, 1992). The final family of membrane proteins in the lens are the connexins; Cx43, Cx46 and Cx50. These proteins interact to form hexamer hetero- or homotypic hemichannels (connexons), which align with hemichannels on the surfaces of neighbouring cells to form gap junctions (Molina and Takemoto, 2012). Each of the connexins have distinct distribution patterns within the lens; Cx43 is found exclusively in epithelial cells while both Cx50 and Cx46 exist in mature fibre cells, where Cx50 decreases in abundance towards the nucleus and Cx46 increases in abundance towards the nucleus (Molina and Takemoto, 2012). Like all members of this family, lenticular connexins are involved in ion and small solute transport in the lens (Beyer and Berthoud, 2014). However, Cx46 has also been shown to transport glutathione (GSH) into the nucleus of the lens (Slavi *et al.*, 2014), as well as protect lenticular epithelial cells against hypoxic stress *in vitro* (Banerjee *et al.*, 2010). The remaining 90% of lenticular proteins are comprised of the crystallins (Wistow and Piatigorsky, 1988; Groenen *et al.*, 1994; Han and Schey, 2006).

1.3 Small Heat Shock Proteins and α-Crystallin

1.3.1 Small Heat Shock Proteins (sHsps)

The sHSPs are a ubiquitous family of proteins that typically have a monomeric mass less than 30 kDa (Perng *et al.*, 1999) and reside in the cytosol of cells under physiological conditions (Klemenz *et al.*, 1991b), where they form multisubunit oligomers (Peschek *et al.*, 2009). In most cells, sHsps, (there are 10 isoforms in humans, denoted HSPB1-10), are induced under stress conditions and operate as molecular chaperones by binding exposed hydrophobic regions of partially unfolded proteins, thereby acting to prevent aggregation (de Jong *et al.*, 1998). They differ from other heat shock proteins (Hsps) in that they do not actively aid protein refolding (Bloemendal *et al.*, 2004) and as such their activity is adenosine triphosphate (ATP)-independent (Nicholl and Quinlan, 1994). Members of the sHsp family

are characterised by the presence of a region of conserved amino acid residues known as the 'α-crystallin domain' (ACD), located close to the C-terminus (de Jong *et al.*, 1998). This region is flanked by a hydrophobic N-terminal domain, and a hydrophilic C-terminal tail, both of which are necessary for maintaining chaperone activity (de Jong *et al.*, 1998). The N-terminal domain provides accessible binding sites for exposed hydrophobic regions of partially unfolded proteins, whilst the flexible C-terminal tail interacts with the solvent to maintain solubility (Farnsworth *et al.*, 1998). Both of these domains are variable in sequence and length in the different human sHsps, leading to variation between the activity of different protein species (Peschek *et al.*, 2009), for example in terms of substrate specificity.

1.3.2 α-Crystallin

The crystallins are water-soluble proteins (Sun *et al.*, 1997) present in the cytoplasm of lenticular fibre cells. The crystallin family constitutes 90% (by weight) of the total protein content of the lens (Wistow and Piatigorsky, 1988; Groenen *et al.*, 1994; Han and Schey, 2006), and encompasses three classes of proteins, the α-, β- and γ-crystallins. These proteins are present in the cell at ratios that prevent crystallisation of proteins at high concentrations, and ensure optimal conditions for the reduction of cytoplasmic viscosity, the control of cell volume through the monitoring of osmotic pressure and the regulation of cytoplasmic stability (Tardieu, 1998). In conjunction with this, all three crystallin classes play a structural role in the lens (De Jong *et al.*, 1994; Horwitz *et al.*, 1999; Grey and Schey, 2009), controlling protein-to-protein interactions in order to provide a light-refractive media that optimises light transmission (Carver and Lindner, 1998).

In the human lens, α-crystallin is present at a concentration of 300-450 mg/mL (Fagerholm *et al.*, 1981; Veretout and Tardieu, 1989; Koretz *et al.*, 1998) and consists of two closely related subunits, αA (HSPB4) and αB (HSPB5) (Schoenmakers and Bloemendal, 1968; Van Der Ouderaa *et al.*, 1973; Van Der Ouderaa *et al.*, 1974; Phelps Brown and Bron, 1996; Sun *et al.*, 1997). α-Crystallin is the most abundant of the crystallins, constituting 40% of the total protein content of the lens (Peschek *et al.*, 2009). It was originally thought that the sole function of α-crystallin was to act as a structural protein, increasing the refractive index of the lens above that of the humours (Koretz *et al.*, 1998), a function that it shared with both β- and γ-crystallin (Phelps Brown and Bron, 1996). In this way, it was considered to be a 'required protein', that is, its function was enabled by the protein's general characteristics such as its

solubility and longevity, as opposed to a specific activity (Koretz *et al.*, 1998). However, Ingolia and Craig (1982) observed that a region of α-crystallin showed sequence similarity to the regions of *Drosophila* proteins Hsp23, Hsp22, Hsp26 and Hsp27 (designated the ACD). Further studies found that α-crystallin displayed chaperone activity (Horwitz, 1992), that αB was also induced in NHN 3T3 cells by heat and chemical stress (Klemenz *et al.*, 1991b), and that αB trafficked into the nucleus under stress conditions (Klemenz *et al.*, 1991b). These characteristics, which are shared by all sHsps, confirmed α-crystallin as a member of the sHsp family.

The structure of α-crystallins

The two subunits of α-crystallin, αA and αB, are homologs (Phelps Brown and Bron, 1996; Sun *et al.*, 1997) coded for by different genes on different chromosomes (de Jong *et al.*, 1998). The subunits are both approximately 20 kDa (Sun *et al.*, 1997), share 60% sequence similarity (Peschek *et al.*, 2009) and, in the lens, exist in the cytoplasm at a ratio of three αA subunits to one B subunit (Bloemendal, 1981; De Jong *et al.*, 1994). Each subunit contains a highly conserved ACD composed of seven β-strands that form a β sandwich fold (Laganowsky *et al.*, 2010) (Figure 1.5A), and this domain alone has chaperone activity (Hochberg *et al.*, 2014). The α-crystallin domain is flanked by two globular domains, formed by the N- and C- terminal regions (de Jong *et al.*, 1998), with a highly flexible C-terminal tail at the C-terminus (Carver *et al.*, 1992; Smulders *et al.*, 1998) (Figure 1.4).

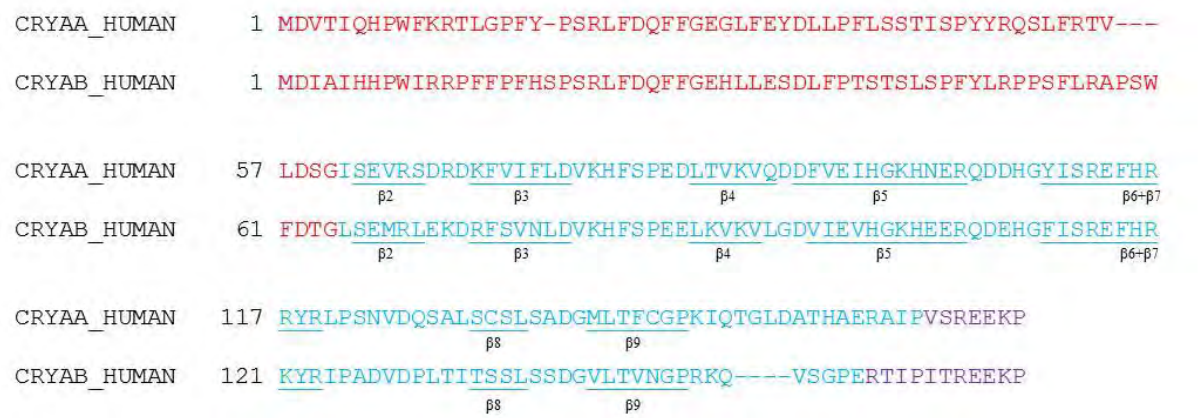

Figure 1.4: Alignment of human αA- and αB-crystallin. Amino acid sequences for human αA (CRYAA_HUMAN, accession number P02489) and αB (CRYAB_HUMAN, accession number P02511) were submitted to the ExPASy SIM alignment tool for alignment. N-terminal domain is indicated with red text, ACD with blue text and the C-terminal domain in purple text. β-Sheet regions of ACD are underlined.

Previous studies have shown that sequences within the α-crystallin domain of αB subunits interact to form dimers that feature an anti-parallel β-sheet at the interface (Bagneris *et al.*, 2009; Laganowsky *et al.*, 2010; Braun *et al.*, 2011; Clark *et al.*, 2011; Jehle *et al.*, 2011) (Figure 1.5A, B). The C-terminal tails of neighbouring dimers then bind to hydrophobic grooves also formed within the α-crystallin domain (Bagneris *et al.*, 2009; Jehle *et al.*, 2010; Laganowsky *et al.*, 2010; Baldwin *et al.*, 2011; Braun *et al.*, 2011; Clark *et al.*, 2011; Jehle *et al.*, 2011), forming a polydisperse population of hetero-oligomers with an average size of 800 kDa (Sun *et al.*, 1997). α-Crystallin oligomers have been reported to exist in two substructural formations: high affinity monomeric and low affinity dimeric substructures (Benesch *et al.*, 2008), the exchange between which is responsible for the moderation of activity.

Due to difficulty in achieving protein crystallisation, the structure of larger oligomers is based largely on conjecture with multiple models being proposed (Tardieu *et al.*, 1986; Augusteyn and Koretz, 1987; Wistow, 1993; Carver *et al.*, 1994; Vanhoudt *et al.*, 2000; Bagneris *et al.*, 2009; Baldwin *et al.*, 2011; Braun *et al.*, 2011; Jehle *et al.*, 2011). More recently, multiple groups have independently proposed a model where hexamers interact to form larger structures that feature a roughly spherical shape with binding sites located either

as pockets on the surface (Jehle *et al.*, 2011), or within the hollow interior accessible through openings in the shell (Haley *et al.*, 1998; Peschek *et al.*, 2009; Braun *et al.*, 2011) (Figure 1.5C). Figure 1.5C depicts the quaternary structure of αB-crystallin based on electron microscopy data obtained by Peschek *et al.*(2009).

It has been reported that αB shows a bias towards a 24meric structure (Braun *et al.*, 2011), which allows the formation of differently sized oligomers via either the association of extra dimers to the external pockets (Jehle *et al.*, 2011) or the addition and subtraction of subunits to the shell itself (Baldwin *et al.*, 2011; Braun *et al.*, 2011). In the latter, the subtraction of subunits would lead to the exposure of hydrophobic regions found on the inner walls (Braun *et al.*, 2011) and extensions (Bagneris *et al.*, 2009), as well as the production of higher-activity smaller oligomers (Peschek *et al.*, 2013) and, eventually, monomers (Aquilina *et al.*, 2004; Benesch *et al.*, 2008). This may allow for the regulation of activity to be mediated by the dissociation of subunits. The importance of the fluidity of the structure has been recently highlighted by Mainz *et al.* (2015) who showed that upon exposure following subunit dissociation, the N-terminal domain is able to undergo conformational changes in order to mimic the properties of different disordered substrate proteins, allowing a wide range of protein interactions essential in order to prevent the amorphous aggregation of substrate proteins. Alternatively, hydrophobic β-sheet structured regions within the static α-crystallin domain are also able to bind substrates with similar properties, enabling a separate pathway for the prevention of amyloid aggregation (Mainz *et al.*, 2015). It has been proposed that the 3:1 ratio of αA to αB subunits in the lens is important in maintaining oligomeric thermal stability (Horwitz *et al.*, 1999), while the dimeric substructure is key in regulating chaperone activity (Aquilina *et al.*, 2004).

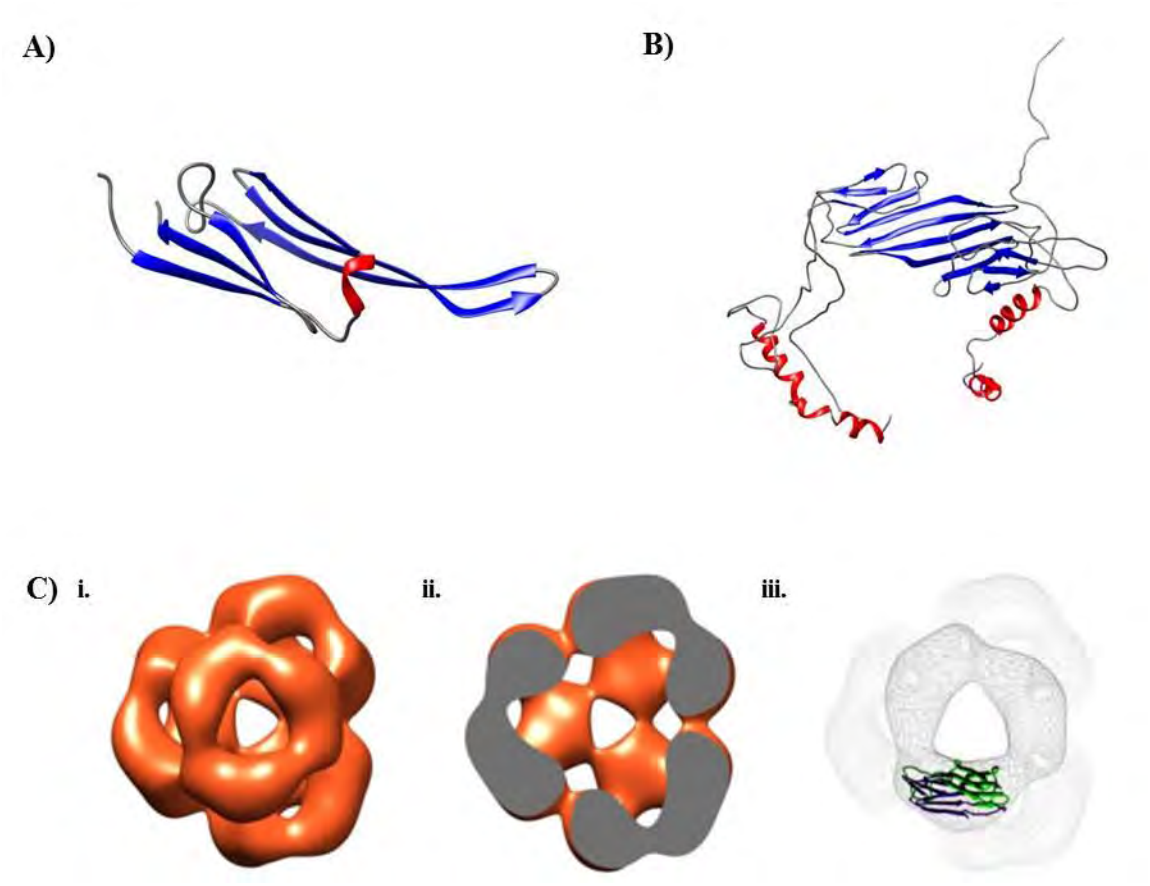

Figure 1.5: Model of recombinant human αB-crystallin structure. Model of the **(A)** ACD (pdb entry 2KLR; Jehle *et al.*(2010)), **(B)** dimer fold (pdb entry 3J07; Jehle *et al.* (2011)) of αB depicted as a ribbon representation (α-helices - red, β-sheets – blue, coils - grey), and the **(C)** 24-mer depicted as **(i)** surface representation, **(ii)** density cross-section and with **(iii)** dimeric α-crystallin domain of Hsp16.5 from *M. jannaschii* overlay (adapted from Peschek *et al.*, 2009).

αA is found almost exclusively in the lens (Peschek *et al.*, 2009) with trace amounts being detected in the thymus, the spleen and the retina (Kantorow and Piatigorsky, 1998). The *HSPB4* gene is located on chromosome 21 (de Jong *et al.*, 1998), the protein has a molecular mass of ~20 kDa and forms polydisperse homo-oligomers ranging in size from 440 to 720 kDa (i.e. containing 22-36 monomers) (Aquilina *et al.*, 2005) . αB is found in relatively high amounts in non-lenticular tissue compared to αA, being detected in the brain, heart, muscle tissue (Peschek *et al.*, 2009), nervous system, retina, iris, thyroid, colon, squamous epithelia, placenta, spermatocytes and tissues subjected to high oxidative stress such as in the kidneys (Kantorow and Piatigorsky, 1998). The *HSPB5* gene is located on chromosome 11 (de Jong

et al., 1998), and multi-angle light scattering data demonstrate that the protein forms homo-oligomers within the range of 400-800 kDa (i.e. containing 20-40 monomers), with an average molecular mass of 540 kDa (Aquilina *et al.*, 2004). The expression of αB in cells has been found to be induced by oncogene expression (Klemenz *et al.*, 1991), osmotic stress (Dasgupta *et al.*, 1992), heat shock (Klemenz *et al.*, 1991b), dexamethasone, cadmium, sodium arsenite (Klemenz *et al.*, 1993) and muscle stretch (Atomi *et al.*, 1990; Kantorow and Piatigorsky, 1998).

1.4 α-Crystallin in Health and Disease

As αB is expressed ubiquitously throughout bodily tissues, the functions it serves are highly diverse. These roles are summarised in Table 1.1.

Table 1.1: Roles of αB-crystallin in non-lenticular tissue.

Function	Mechanism	Reference
Anti-apoptosis	Inhibits caspase-3	Morrison *et al.*, 2003
	Induces GSH expression in response to tumour necrosis factor α (TNFα)	Mehlen *et al.*, 1996
	Protects against damage cause by inflammation following infection	Whiston *et al.*, 2008
	Inhibits caspase-3 activation	Ousman *et al.*, 2007
Protection against oxidative damage	Increases expression of GSH	Mehlen et al., 1996
Maintenance of cytoskeletal integrity	Prevents interactions between intermediate filaments	Perng *et al.*, 1999 Launay *et al.,* 2006
	Binds to intermediate filaments following stress to protect during network remodelling	Djabali *et al.*, 1997
	Prevents aggregation of actin filaments following pH stress	Bennardini *et al*., 1992
Suppression of neurodegeneration	Prevents aggregation of glial fibrillary acidic protein (GFAP)	Hagemann *et al*., 2010
	Prevents aggregation of SOD1 and α-synuclein	Wang *et al*., 2008
Formation of inclusion bodies in protein conformation diseases	Alexander's disease	Head *et al*., 1993 Iwaki *et al.*, 1989
	Alzheimer's disease	Shinohara *et al*., 1993
	Parkinson's disease	Liu *et al.,* 2015
Acts as an oncoprotein	Promotes neoplastic changes and invasiveness of basal-like breast carcinomas	Moyano *et al*., 2006
	Marker for poor prognosis in head and neck cancers	Chin *et al*., 2005
	Overexpressed in laryngeal sarcoma tissues	Yilmaz *et al.*, 2015
	Inhibits TNF-related apoptosis-inducing ligand (TRAIL)-induced apoptosis in various cancer cell lines	Kamradt *et al.*, 2005
Anti-inflammation	Suppresses inflammatory role of nuclear factor kappa-light-chain-enhancer of activated B cells (NF-κB)	Ousman *et al.*, 2007
	Reduce inflammatory cytokine levels following stroke	Arac *et al.,* 2011

Although the deposition or overexpression of αB in diseased tissues is generally interpreted as a sign of pathogenicity, its beneficial role in healthy tissues may suggest that the increased levels of αB are simply a by-product of the stress response in diseased cells, rather than the cause of disease. This is yet to be fully elucidated and as such needs to be taken into consideration when evaluating the pathogenic potential of αB.

Mutations in α-crystallin have also been associated with cataract and various myopathies. These mutations are outlined in Table 1.2.

Table 1.2 Pathologically significant mutations of αA- and αB-crystallin in humans.

Disease	Species	Mutation	Reference
Autosomal dominant congenital cataract	αB	D140N	Liu, Zhang, *et al.*, 2006
		450delA	Berry *et al.*, 2001
		P20S	Liu, Ke, *et al.*, 2006
		R120G	Vicart *et al.*1998
	αA	R116C	Litt *et al.*, 1998 Vanita *et al.*, 2006
		R49C	Mackay *et al.*, 2003
		R116H	Richter *et al.*, 2008
		R54P	Su, Guyo, et al., 2012
Autosomal recessive congenital cataract	αA	W9X	Pras *et al.*, 2000
Desmin-related myopathy	αB	R120G	Vicart *et al.*, 1998
Dilated cardiomyopathy	αB	R157H	Inagaki *et al.*, 2006
		G157S	Pilotto *et al.*, 2006
Myofibrillar myopathy	αB	Q151X	Selcen and Engel, 2003
		464delCT	Selcen and Engel, 2003
Late-onset distal vacuolar myopathy	αB	G154S	Reilich *et al.*, 2010

Central to all of these functions is the ability of αB to act as a molecular chaperone through the binding of destabilised proteins which, in the lens, is also essential for the maintenance of lens transparency.

1.5 Chaperone Activity of α-Crystallin

In conjunction with crystalline-like short-range protein order (Delaye and Tardieu, 1983; Bloemendal *et al.*, 2004), the degeneration of vasculature and innervation *in utero* (Phelps Brown and Bron, 1996) and the degradation of cellular organelles and the nucleus (Han and Schey, 2006), α-crystallin plays a vital role in the maintenance of lens transparency with age through its action as a molecular chaperone (Horwitz, 1992; Sun *et al.*, 1997). Due to the loss of the nucleus and other cellular organelles during the process of fibre cell differentiation, it is often assumed that lenticular fibre cells do not experience protein turnover, meaning that the proteins present in the lens have existed since birth and cannot be replaced (Bloemendal, 1977; Lynnerup *et al.*, 2008; Truscott, 2010). However, more recently it has been suggested that there are low but variable rates of carbon turnover ranging from 1-3% of soluble protein annually throughout the human lifetime (Stewart *et al.*, 2013). Due to this minimal turnover, it is essential that lenticular proteins are long-lived to maintain the integrity of the lens (Bloemendal *et al.*, 2004). Longevity of a protein is determined by its thermodynamic stability, that is, its ability to retain its tertiary or quaternary structure with time, and the presence of an efficient chaperone system in the cell that is able to prevent protein aggregation (Bloemendal *et al.*, 2004). It is with the latter that α-crystallin plays an important role.

The unfolding of cytoplasmic proteins in response to stresses such as heat or ultraviolet radiation (Truscott, 2005) triggers the heat shock response, which acts to inhibit protein synthesis and induce molecular chaperone production (Bloemendal *et al.*, 2004). Molecular chaperones exist as monomers or oligomers both intra- and extracellularly, where they act to preserve the conformation of proteins in solution (Soti and Csermely, 2000). This is achieved by either preventing aggregation, solubilising aggregates that have already formed, assisting in the folding or refolding of misfolded or unfolded proteins, sequestering damaged proteins in insoluble complexes or labelling damaged proteins for degradation (Soti and Csermely, 2000).

Proteins with compromised tertiary structure are partially unfolded and contain hydrophobic regions that remain exposed to the solvent (Carver and Lindner, 1998). These exposed hydrophobic regions can interact with each other eventually causing the protein to precipitate from solution (Carver and Lindner, 1998). In the lens, this leads to the formation of insoluble protein aggregates that cause opacification of the lens, and interfere with light transmission

by scattering the incoming light (Phelps Brown and Bron, 1996). α-Crystallin prevents these aggregates from forming by binding to the exposed hydrophobic regions of proteins that are partially unfolded and on the path to irreversible aggregation (Carver and Lindner, 1998). The complexes formed by α-crystallin and its substrates such β- and γ-crystallins remain soluble until the chaperone is saturated and co-precipitates with the substrate (Lampi *et al.*, 2002; Evans *et al.*, 2008; Acosta-Sampson and King, 2010). It has been reported that mutations to αA (Koteiche and Mchaourab, 2006) and αB (Bova *et al.*, 1999) can induce aggregation by increasing substrate affinity leading to increased binding accelerated co-precipitation. Each α-crystallin assembly can bind multiple substrate molecules, with the exact number being dependent on the substrate and the subunit makeup of α-crystallin (Smulders *et al.*, 1998). It has been proposed that in non-lenticular tissues, the bound substrate may dissociate from the HMWC so it can be presented to the Hsp70 co-chaperone system and be refolded (Horwitz, 1992; Carver and Lindner, 1998).

Intermediately folded states of proteins are inherently unstable (Carver and Lindner, 1998), often differing from those that are on the protein folding pathway, that is, proteins that are in the process of folding into their native state. α-Crystallin is selective, in that it binds exclusively to partially folded or intermediate states of proteins that have left the folding pathway and have entered an off-folding pathway, thereby allowing proteins that are on the folding pathway to achieve their native state (Carver *et al.*, 1993). The chaperone activity of α-crystallin is also non-specific; it binds to hydrophobic regions on diverse proteins, including non-lenticular proteins such as insulin (Smulders *et al.*, 1998), and not to specific amino acid sequences or motifs.

The major substrates of α-crystallin in the lens fibre cell are γ- and β-crystallin (Horwitz, 1992; Horwitz *et al.*, 1999; Hanson *et al.*, 2000; Horwitz, 2000; Acosta-Sampson and King, 2010; Michiel *et al.*, 2010), although interactions with 'house-keeping' enzymes such as enolase (Valasco *et al.*, 1997), cytoskeletal elements (Quinlan, 2002) and membrane associated proteins also occur (Cobb and Petrash, 2002b; Horwitz, 2003). *In vitro,* α-crystallin completely suppresses aggregation of β- and γ-crystallin (Horwitz, 1992; Boyle and Takemoto, 1994; Wang and Spector, 1994; Evans *et al.*, 2008; Acosta-Sampson and King, 2010; Andley *et al.*, 2014) at molar ratios of 12:1 and 10:1 respectively (Horwitz, 1992). Like all sHsps, both the N- and C-terminal regions are vital in maintaining the chaperone activity of the protein with the C-terminal domain maintaining solubility (Carver *et al.*, 1992; Merck

et al., 1993; Carver and Lindner, 1998) and the N-terminal domain promoting oligomerisation (Merck *et al.*, 1992) and providing hydrophobic binding sites (Smulders *et al.*, 1998). Furthermore, it appears that the quaternary structure of the protein (with a hydrophilic exterior and a hydrophobic interior) is vital to its chaperone activity, as it has been observed that the structure is conserved (Farnsworth *et al.*, 1998) and resistant to changes in the amino acid sequence (Smulders *et al.*, 1998). However, further studies have shown that the chaperone activity of α-crystallin can be altered by buffer conditions or the introduction of different surface charges. For example, the addition of calcium or magnesium to buffers, or a decrease in pH has a detrimental effect on activity (Bindels *et al.*, 1985), while the addition of a negative charge to the protein surface, such as through citraconylation, increases activity (Bindels *et al.*, 1985). Significantly, as protein turnover in lenticular fibre cells is negligible, various PTMs have also been found to affect the chaperone activity of α-crystallin, possibly correlating with an observed decrease in α-crystallin chaperone activity with age (Horwitz, 1992; Cherian and Abraham, 1995; Derham and Harding, 1997; Soti and Csermely, 2000).

1.6 Posttranslational Modification of α-Crystallin

Owing to the longevity of lenticular α-crystallins, they are vulnerable to the accumulation of PTMs with age (Masters *et al.*, 1977; Bloemendal *et al.*, 2004; Wilmarth *et al.*, 2006; Sharma and Santhoshkumar, 2009; Truscott and Friedrich, 2016). PTMs have been detected in human lenses using isoelectric focusing and SDS-PAGE (Kramps *et al.*, 1978). Furthermore, it is known that modifications occur from a very young age, with modifications being detectable in foetal lenses (Phelps Brown and Bron, 1996). Perhaps surprisingly, it was noticed in a later study that protein isolated from young lenses (i.e. 17 year old donor) show a similar levels of modification to aged lenses (i.e. 54 to 55 year old donors) , implying the modifications occur relatively early in life (Lampi *et al.*, 1998). Grey and Schey (2009) reported that the amount of intact α-crystallin (i.e. not proteolytically cleaved) decreases with age, with little remaining after the age of 75 (Grey and Schey, 2009). It has also been shown that αB undergoes less

truncation with age compared to αA, suggesting a higher level of stability (Grey and Schey, 2009).

The number of PTMs that can occur to α-crystallin is extensive and include carbamylation , acetylation , disulphide bond formation, oxidation, truncation, deamidation , glycation and phosphorylation (Lund *et al.*, 1996; Lin *et al.*, 1997; Lampi *et al.*, 1998; Lin *et al.*, 1998; Ma *et al.*, 1998; Hanson *et al.*, 2000; Lapko *et al.*, 2001; MacCoss *et al.*, 2002; Han and Schey, 2006; Wang *et al.*, 2013). Phosphorylation of serine residues is the most common modification αB (Kato *et al.*, 1998), and is believed to alter the chaperone activity of the protein (Ito *et al.*, 2001; Koteiche and Mchaourab, 2003; Aquilina *et al.*, 2004; Ecroyd *et al.*, 2007; Benesch *et al.*, 2008). Likewise, deamidation is also common and believed to affect chaperone activity (Gupta and Srivastava, 2004; Fujii *et al.*, 2011). For these reasons, this thesis focuses on the phosphorylation and deamidation of lenticular αB.

1.6.1 Phosphorylation of α-Crystallin

Phosphorylation rates of 33-50% have been reported for human lens αB (Carver and Lindner, 1998; Farnsworth *et al.*, 1998), with phosphorylated products being present from birth (Phelps Brown and Bron, 1996). The phosphorylation process occurs naturally in a state of dynamic equilibrium under physiological conditions in dividing cells (Ito *et al.*, 1997), for example in epithelial cells for αB and in differentiating cells for αA (Phelps Brown and Bron, 1996). Phosphorylation can also be induced stress conditions such as ischemia (Ahmad *et al.*, 2008) and heat stress (Ito *et al.*, 1997).

In vivo, the majority of α-crystallin is phosphorylated via the cyclic adenosine monophosphate (cAMP)-dependent pathway in a reversible serine-specific manner (Kantorow and Piatigorsky, 1998). It has been a long-held belief that the dominant sites of phosphorylation in αB are Ser19, Ser45 and Ser59, and in αA Ser122. Western blots of mitotic U373 human glioma cells revealed that the three phosphorylation sites of αB are regulated separately during mitosis (Kato *et al.*, 1998). The elevated levels of pSer19 (phosphorylated Ser19) and pSer45 (phosphorylated Ser45) and the lower levels of pSer59 (phosphorylated Ser59) detected suggested that each site is phosphorylated by a different kinase (Kato *et al.*, 1998). Purification and activity assays of the different kinases revealed that Ser45 and Ser59 are phosphorylated via p44/42 mitogen-activated protein (MAP) kinase and MAP kinase-activated protein (MAPKAP) kinase-2 respectively (Kato *et al.*, 1998). The

kinase responsible for the phosphorylation of Ser19 has still not identified due to instability of the enzyme, although it was found to be of a similar molecular weight to p44/42 MAP kinase, approximately 60 kDa (Kato *et al.*, 1998). The αA Ser122 residue is also believed to be phosphorylated by MAPKAP kinase-2 as it lies within a recognition site for the enzyme ((Arg/Lys)-X-Pro-Ser) (Kantorow and Piatigorsky, 1998). Despite the dominance of these sites in the literature, a multitude of other sites of phosphorylation for both subunits have been recently reported in the lens (Miesbauer *et al.*, 1994; Kamei *et al.*, 2000; MacCoss *et al.*, 2002; Searle *et al.*, 2005; Wilmarth *et al.*, 2006; Huang *et al.*, 2011; Wang *et al.*, 2013; Wang *et al.*, 2014). These are summarised in Appendix 1, and locations are indicated in Figure 1.7.

Although much less prominent in the literature, non-enzymatic phosphorylation has also been observed in lenticular α-crystallin (Kantorow and Piatigorsky, 1998). Little is known about the mechanism of non-enzymatic phosphorylation in the lens, but it has been shown *in vitro* that both α-crystallin subunits are able to undergo non-enzymatic phosphorylation in the presence of either Mn^+ (Schieven and Martin, 1988) or Mg^+ (Kantorow and Piatigorsky, 1994) and ATP. There is also evidence of a mechanism of non-enzymatic dephosphorylation in the lens that involves the spontaneous β-elimination of phosphate groups from phosphoserine and phosphothreonine residues and the subsequent glutathionylation of the resultant dehydroalanine (DHA) intermediate, resulting in covalent crosslinking (Bessems *et al.*, 1987; Linetsky *et al.*, 2004; Srivastava *et al.*, 2004; Linetsky and LeGrand, 2005; Wang *et al.*, 2014). It is as yet unclear what proportion of the phosphorylation observed in the lens is residual from early enzymatic phosphorylation events, and how much results from subsequent non-enzymatic events. However, it is likely that α-crystallin enzymatically phosphorylated in the metabolically active cells of the outer cortex are gradually dephosphorylated non-enzymatically as they form part of the metabolically inactive nucleus.

Phosphorylation and α-crystallin chaperone activity

The effect that phosphorylation has on the chaperone activity of α-crystallin, if any, has met with contention in the literature. Earlier studies by Ito *et al.* (2001) reported a decrease in chaperone activity when thermal aggregation assays were performed utilising α-crystallin S→D phosphomimics that mimic the negative charge introduced by a phosphate group. They attributed this to an observed decrease in oligomeric size. These findings were supported by Kamei *et al.* (2001) who reported a 30% decrease in the ability of phosphorylated bovine α-crystallin to prevent the heat-induced aggregation of β_L-crystallin. A complimentary study by

Augusteyn *et al.*(2002), however, reported no effect on chaperone activity. More recently, studies utilising mutations that mimic phosphorylation have found that the addition of one or more negative charges onto αB acts to increase target protein affinity (Koteiche and Mchaourab, 2003; Ecroyd *et al.*, 2007), increase oligomeric polydispersity (Ecroyd *et al.*, 2007) and decrease average oligomeric size (Ito *et al.*, 2001; Ecroyd *et al.*, 2007). It has been proposed that such modifications to the N-terminal domain of α-crystallin induces flexibility and structural changes that lead to increased exposure of substrate binding sites (Peschek *et al.*, 2013). Phosphorylation in this region may also interrupt intersubunit interactions, resulting in dissociation of larger oligomers to form smaller oligomers with higher activity (Ecroyd *et al.*, 2007; Peschek *et al.*, 2013).

It has been suggested that this hyperactivity can induce aggregation with the target, rather than prevent it, as the αB reaches saturation and co-deposits with the target proteins (Ecroyd *et al.*, 2007). This is supported by a study by Aquilina *et al.* (2004) that reported both a change in oligomeric substructure, i.e. a preference towards high affinity monomeric substructure and away from low affinity dimeric substructure, coupled with an earlier onset of aggregation with the target protein α-lactalbumin. Taken together, it appears that the hyperactivity observed recently upon phosphorylation of αB may be a result of the increased exposure of substrate binding sites brought about by the dissociation of dimeric subunits. As the precise nature of the relationship between phosphorylation and chaperone activity of αB is uncertain, an aim of the work described in this thesis was to attempt to elucidate whether mimicking phosphorylation of αB, via S→D point mutations, increases or decreases the ability of αB to suppress the heat-induced aggregation of a model substrate.

1.6.2 Deamidation of α-Crystallin

Another major age-related modification of lenticular α-crystallin is deamidation, involving the chemically mediated conversion of asparagine and glutamine residues to aspartate and glutamate residues respectively (Wilmarth *et al.*, 2006). The reaction occurs non-enzymatically, taking one of two pathways depending on the environmental pH. At a neutral or alkaline pH, the reaction follows two steps (Figure 1.6A); the peptide bond nitrogen of the asparagine (or glutamine) residue attacks the carbonyl carbon of the sidechain and forms a succinimide (for asparagine) or glutiminide (for glutamine) ring intermediate, which is then hydrolysed at either the α or β carbon to form aspartate (or glutamate) or iso-aspartate (or iso-

glutamate). Alternatively, at pH<5.0, the amide group on the asparagine (or glutamine) sidechain undergoes direct hydrolysis to produce aspartate (or glutamate) as a sole product (Figure 1.6B).

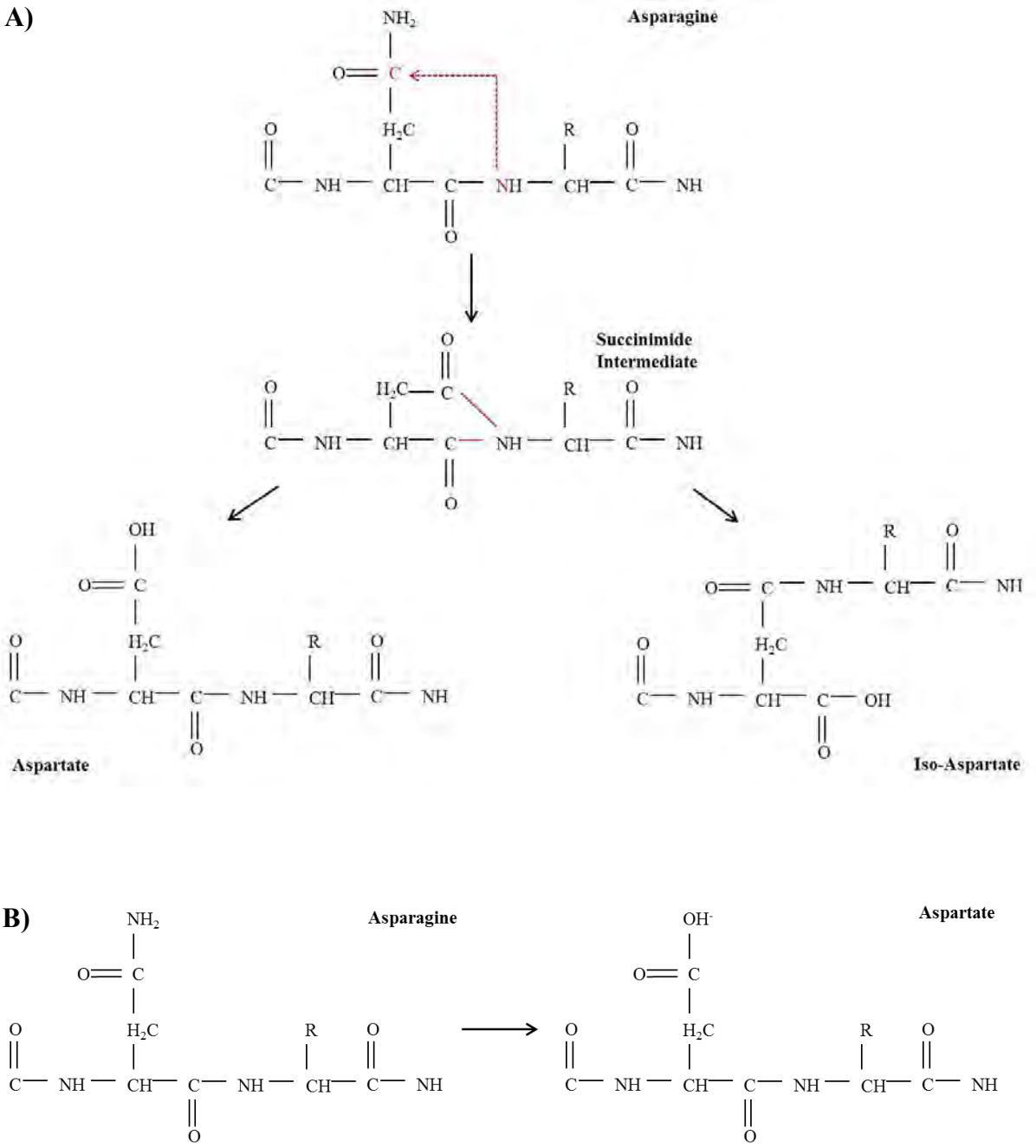

Figure 1.6: Mechanism of deamidation of an asparagine residue. (A) At a neutral or alkaline pH, the peptide bond nitrogen attacks the carbonyl carbon of the asparagine or aspartate sidechain (both shown in red, connected by broken arrow) to form a succinimide ring intermediate, which is then hydrolysed at either the α or β carbonyl group (bonds shown in red), resulting in aspartate or iso-aspartate residues. **(B)** At an acidic pH (i.e. pH<5.0), the amide group of the asparagine sidechain can undergo direct hydrolysis to form an aspartate residue. Note that glutamine forms a 6-member ring (i.e. glutaminide) intermediate via a similar mechanism that undergoes hydrolysis similar to the succinimide intermediate.

Deamidation is restricted to amino acid residues that contain an amide side chain i.e. asparagine and glutamine, and are influenced by the surface exposure of the residue (Lapko *et al.*, 2002) as well as the conformational flexibility of the surrounding residues (Kosky *et al.*, 1999; Hooi *et al.*, 2012; Truscott and Friedrich, 2016). Multiple deamidation sites have been identified in both lenticular αA and αB (Lund *et al.*, 1996; Hanson *et al.*, 2000; Srivastava and Srivastava, 2003; Searle *et al.*, 2005; Wilmarth *et al.*, 2006; Asomugha *et al.*, 2010; Hains and Truscott, 2010), summarised in Appendix 1 with positions indicated in Figure 1.7.

Deamidated α-crystallin is in high abundance in water-insoluble lens fractions, leading to the suggestion that the deamidation of α-crystallin contributes to cataract formation (Srivastava and Srivastava, 2003; Wilmarth *et al.*, 2006). It has also been reported that, in conjunction with other modifications, namely oxidation and C- and N-terminal truncation, deamidation inhibits chaperone activity (Gupta and Srivastava, 2004; Chaves *et al.*, 2008) and induces insolubility of the protein (Lund *et al.*, 1996; Hanson *et al.*, 2000). Structural changes are thought to be responsible for this loss of solubility, for example decreases in β-sheet content (Gupta and Srivastava, 2004), exposure of hydrophobic regions (Hanson *et al.*, 2000; Gupta and Srivastava, 2004) and the formation of intramolecular disulphide bonds in αA (Lund *et al.*, 1996; Hanson *et al.*, 2000). Furthermore, deamidation is known to induce both racemisation (conversion of L- to D-) and isomerisation (conversion of α- to β-) to form L-β-X, D-α-X and D-β-X isotypes that can in turn alter secondary structure (Fujii *et al.*, 2010; Fujii *et al.*, 2016; Truscott and Friedrich, 2016) and cause a loss of function (Fujii *et al.*, 2007; Fujii *et al.*, 2010). High rates of racemisation and isomerisation have been observed at the residues N58, N76, N84 and N151 in lenticular αA, and N62 and N96 in αB (Fujii *et al.*, 2012). Notably, N96 is highly racemised in aged human lenses, where it is thought to interrupt higher order oligomeric assembly (Sakaue *et al.*, 2015; Takata and Fujii, 2015). Locations of all reported deamidation sites are indicated in Figure 1.7.

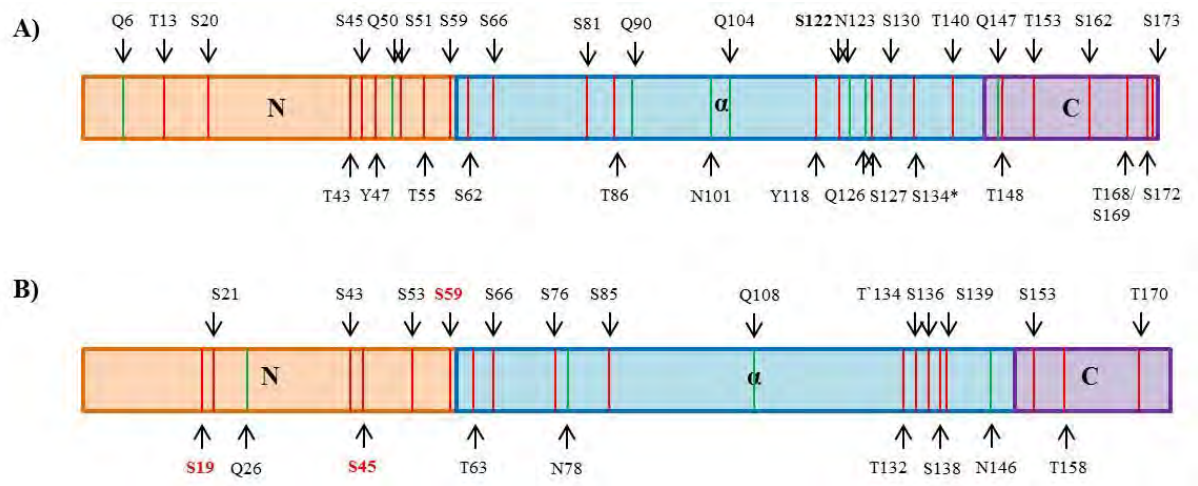

Figure 1.7: Location of reported phosphorylation and deamidation sites of human lenticular αA (A) and αB (B). Depicts full length protein with N-terminal (N-orange), α-crystallin (α-blue) and C-terminal (C-purple) regions indicated. Red bars represent phosphorylation sites and green bars represent deamidation sites; residue identities are labelled with arrows. Phosphorylation sites investigated in this thesis are highlighted in red.

Similar to the α-crystallins, β- and γ-crystallins are heavily deamidated in the insoluble fraction of aged and cataractous human lenses (Lapko et al., 2002; Wilmarth et al., 2006; Hains and Truscott, 2010). Multiple studies have utilized deamidation mimics to investigate the effect deamidation has on the structure and function of these proteins. Deamidation of residues at the dimeric interface has been shown to not affect secondary structure or interfere with dimer formation (Lampi et al., 2006; Takata et al., 2007; Takata et al., 2008). However, the presence of deamidated residues at the oligomeric interface is suggested to alter tertiary structure by interrupting hydrogen bond formation, thereby inhibiting interactions between hetero- and homodimers (Takata et al., 2009). Deamidation has also been shown to destabilise β- and γ-crystallins, inducing aggregation in urea and heat treatment (Kim et al., 2002; Lampi et al., 2002; Flaugh et al., 2006; Lampi et al., 2006; Takata et al., 2007; Takata et al., 2008; Michiel et al., 2010).

1.6.3 Protein crosslinking

Covalent crosslinking has been identified between crystallins, and between crystallins and other proteins (Srivastava *et al.*, 2004; Su, McArthur, Truscott*, et al.*, 2011) in human lenses. Crosslinks formed via DHA intermediates were first identified in human lenses by Linetsky

et al. (2004). Wang *et al.* (2014) later identified such non-disulphide crosslinks between β- and γ-crystallin proteins in lens extracts, and were able to induce formation under physiological conditions *in vitro*. Crosslink formation via this mechanism is believed to occur when phosphoric acid is cleaved from phosphorylated serine or threonine residues by β-elimination, and the resulting DHA or dehydrobutyrine (DHB) intermediates are targeted for nucleophilic attack by GSH (Wang *et al.*, 2014). It has been suggested that this mechanism is a predominant pathway of crosslink formation in lens proteins, thereby contributing to protein aggregation and cataract (Wang *et al.*, 2014).

1.7 Role of Phosphorylated α-Crystallin in Non-lenticular tissues

In non-lenticular tissues, phosphorylated αB-crystallin has been implicated in various cellular responses ranging from cytoprotection in response to stress, the regulation of apoptosis and actin dynamics, and protein quality control. These roles are summarised in Table 1.3.

Table 1.3: Purported roles of phosphorylated αB-crystallin isotypes in non-lenticular tissue.

Role	Mechanism	Residue	Reference
Cytoprotection (inhibition of apoptosis)	Localisation to Z-bands of myocytes following ischemia	Ser59	Hoover *et al.*, 2000 Golenhofen *et al.*, 1999 Golenhofen *et al.*, 1998
		Ser45 and Ser59	Eaton *et al.*, 2001
	Induces Bcl2 expression in myoblasts in presence of TNF-α	Ser59	Adhikari *et al.*, 2011
	Inhibits caspase-3 activation in myocytes following hyperosmotic or hypoxic stress	Ser59	Morrison *et al.*, 2003
	Nuclear speckle formation following heat shock	Ser45 and Ser59	Den Engelsman *et al.*, 2013 Den Engelsman *et al.*, 2005
	Induced by PAR-2 in astrocytes in presence of C2-ceramide and staurosporine	Ser45 and Ser59	Li and Reiser, 2011
	Prevents exosomal secretion of αB in glioma cells	Ser19, Ser45 and Ser59	Kore and Abraham, 2014 Kore and Abraham, 2016
Regulation of apoptosis (promotes apoptosis)	Reduces anti-apoptotic activity of αB in differentiation induced cell death of myoblasts	Ser19, Ser45 and Ser59	Kamradt *et al.*, 2002
	Binds to and inhibits anti-apoptotic activity of Bcl2 in vinblastine treated breast epithelial carcinoma cells	Ser59	Launay *et al.*, 2010
Modulation of actin dynamics	Co-localises with and stabilises cytoskeletal components at focal adhesions in myoblasts treated with vinblastine and cytochalasin D	Ser59	Launay *et al.*, 2006
	Co-localises with proteins of the actin nucleation complex involved with membrane protrusion and cell migration in migratory lenticular epithelial cells	Ser59	Maddala and Rao, 2005
	Negatively modulates actin depolymerisation *in vitro*		Wang and Spector, 1996
Protein quality control	Participates in the ubiquitin-proteasome system to degrade excess protein in disused rat soleus muscle	Ser59	Kato *et al.*, 2002
	Accumulates in and potentially facilitates formation of aggresomes in MG-132 treated glioma cells	Ser59	Ito *et al.*, 2002

1.8 Cataracts

The term cataract refers to any light-scattering opacity in the lens which significantly obstructs vision. It is the leading cause of blindness worldwide, contributing to 48% of all cases (World Health Organisation, 2010). The different classes of cataract can be divided into those that are non-progressive, including congenital nuclear, sutural and coronary cataracts, and those that are progressive, or age-related, with age-related cataract being defined as cataracts that occur past the age of 50 years old, without an obvious cause (Phelps Brown and Bron, 1996). Age-related cataract are thought to result from a combination of genetic, age-related and environmental factors (Hammond *et al.*, 2000). Age-related cataracts encompass three different types: cortical, sub-capsular and nuclear (Phelps Brown and Bron, 1996). Cortical and sub-capsular cataracts are caused by disorder in the cytoplasm or fibre cell membranes (Phelps Brown and Bron, 1996).

Nuclear cataracts differ in that they result from the formation of insoluble protein aggregates that directly obstruct light transmission (Phelps Brown and Bron, 1996). As these aggregates remain insoluble, even in 8 M urea and 6 M guanidine hydrochloride (Truscott and Augusteyn, 1977), it has traditionally been difficult to obtain molecular information regarding the protein composition of the aggregate (Takemoto and Boyle, 1998). Truscott *et al.* (1998), using tryptic digestion and high performance liquid chromatography (HPLC) to purify peptides from the insoluble fraction of human cataractous lens tissue, found αB subunits to be in overabundance when compared with αA and other lenticular proteins, suggesting that αB is more directly involved in age-related cataract formation than αA (Chen *et al.*, 1997; Truscott *et al.*, 1998).

This claim has been supported by work from a number of studies in recent years. The identification of peptides derived from αB as well as αA, βB2-, γs- and βA3-crystallin in high abundance in the insoluble protein fractions from aged human lenses suggests that truncation of these proteins may be involved in protein insolubilisation (Hanson *et al.*, 2000; Santhoshkumar *et al.*, 2008; Su *et al.*, 2010). The addition of peptides αB_{1-18} and $\beta A3/A1_{59-74}$ decreases the chaperone activity of α-crystallin *in vitro*, while $\beta A3/A1_{59-74}$ increases the oligomeric size and induces aggregation of αB homo-oligomers (Santhoshkumar *et al.*, 2008). In separate studies, αA_{66-80} was reported to bind to the C-terminal extension, the chaperone site and the subunit interaction site of αB to form complexes with reduced chaperone activity and solubility compared to αB homo-oligomers (Kannan *et al.*,

2013),while αB_{1-18} was reported to increase the association of α-crystallin to purified membranes *in vitro* (Su, McArthur, Friedrich, et al., 2011). Zhou *et al.* (2015), with the aid of isobaric tag for relative and absolute quantitation (iTRAQ) technology, were able to report that αB, but not αA, was downregulated in the nucleus of cataractous lenses compared to healthy lenses. Datiles III *et al.* (2016), used dynamic light scattering to monitor free lenticular α-crystallin levels in patients over 6-36 months and reported that low base levels of free α-crystallin, as well as faster rates of free α-crystallin loss, positively correlate with increased occurrence and faster progression of nuclear cataract. Finally, Makley *et al.* (2015) were able to reverse R120G associated cataract opacity in mouse lenses *in situ* and in aged-related opacities in human lenses *ex situ* by incubating lenses with 5-cholesten-3b, 25-diol. It is reported that this compound binds to the hydrophobic groove of αB, thereby stabilising the oligomer and preventing aggregation (Makley *et al.*, 2015), suggesting that instability of αB is a contributing factor to cataract formation.

The exact role that phosphorylated αB plays in cataract formation is unclear due to the contention surrounding the effect that phosphorylation has on αB chaperone activity. If activity is decreased upon phosphorylation, aggregates may form as a consequence of the inability of αB to prevent interactions between other proteins (Phelps Brown and Bron, 1996; Ito *et al.*, 2001; Bloemendal *et al.*, 2004; Grey and Schey, 2009). Alternatively, if activity is increased, the affinity of αB to protein substrates may be increased to the point where it binds excessively to substrate and co-deposits prematurely (Aquilina *et al.*, 2004). Additionally, previous studies have found that α-crystallin associates with fibre cell membranes increasingly with both age (Boyle and Takemoto, 1996) and oxidation-induced phosphorylation (Takemoto and Boyle, 1998). The mechanism behind this may be explained by the theory proposed by Aquilina *et al.* (2004). If a change in αB substructure was in fact responsible for the induction of hyperactivity due to the increased exposure of hydrophobic regions, the protein may also have increased affinity with proteins that interact with fibre cell membranes, which in turn could lead to greater localisation of αB with membranes (Aquilina *et al.*, 2004). This phenomenon is of particular interest when considering the formation of the nucleocortical barrier and the role it is believed to play in cataract formation.

1.8.1 Barrier Theory of Cataract Formation

The barrier theory was first proposed by Sweeney and Truscott (Sweeney and Truscott, 1998) following the paradoxical observation that although levels of the reduced form of GSH were observed to decrease in the nucleus of older lenses, concentrations in the cortex often remain within the normal range. In a healthy lens, GSH is synthesised in the cortex and diffuses into the nucleus via gap junctions that are present between fibre cells (Goodenough, 1992). To determine the cause of this phenomenon, Sweeney and Truscott incubated lenses of varying ages in artificial aqueous humor containing labelled [^{35}S] cysteine, which is incorporated into GSH metabolically. Following localisation experiments, the labelled cysteine was found to be homogenously distributed in young lenses. However, only very low amounts of label were detected in the nucleus of older lenses, indicating the presence of a barrier retarding the diffusion of small molecules from the cortex into the nucleus, dubbed the nucleocortical barrier (Sweeney and Truscott, 1998). As a minimum concentration of 2 mM GSH is required to protect proteins from oxidation by reactive small molecules such as ascorbate (Truscott, 2005), it is believed that the decrease in the reduced form of GSH allows the oxidation of proteins leading to the formation of disulphide bonds and thereby aggregate formation (Truscott and Augusteyn, 1977; Truscott, 2005).

Evidence supporting a role for barrier formation in cataractogenesis includes the observation that a sharp decrease in the concentration of reduced GSH always precedes the formation of experimentally induced cataracts (Harding, 1991), the abundance of oxidised proteins in the nucleus of aged lenses (Truscott, 2005) and the coinciding of the putative location of the barrier and the sclerotic zone of cataractous lenses (Sweeney and Truscott, 1998). The process of barrier formation itself is less well understood with multiple theories being proposed, such as the uncoupling of gap junctions as a result of cellular damage or modification of transport proteins (Sweeney and Truscott, 1998). It has also been postulated that changes in lens membrane lipid composition and fibre cell compression may alter lens membrane dynamics (Deeley *et al.*, 2010). These models however have not been extensively studied and little literature regarding them is available.

One well-documented phenomenon that has been proposed as a potential mechanism of barrier formation is the binding of cytosolic proteins to fibre cell membranes with age (Friedrich and Truscott, 2009; Friedrich and Truscott, 2010). Membrane association of fibre cell membranes was first reported by Cenedella and Fleschner (1992), who observed that crystallin and cytoskeletal proteins from bovine lens lysates codeposit with membrane

components as high density bands on sucrose density gradients. Western blotting of these bands indicated that 70% of membrane associated protein consisted of αA and its modified forms, while 20% consisted of β- and γ-crystallins with the remaining components consisting of cytoskeletal proteins (Cenedella and Fleschner, 1992). Later studies involved incubating isolated bovine fibre cell membranes with either purified rat (Chandrasekher and Cenedella, 1997) or recombinant human α-crystallin (Cobb and Petrash, 2002b) to replicate membrane binding *in vitro*. It was reported that α-crystallin was most likely to associate with membranes as part of HMW aggregates (Chandrasekher and Cenedella, 1997; Cobb and Petrash, 2002b) via hydrophobic interactions (Chandrasekher and Cenedella, 1997), and that once bound, chaperone activity was diminished (Cobb and Petrash, 2002b) and the rate of disulphide crosslinking was increased (Chandrasekher and Cenedella, 1997).

Localisation of α-crystallins with plasma membranes in aged and cataractous human lenses was also confirmed using electron microscopy immunolocalisation (Boyle and Takemoto, 1996). Sucrose density centrifugation has been used to isolate high density membrane-bound protein fractions from aged normal (Friedrich and Truscott, 2010) and cataractous (Chandrasekher and Cenedella, 1995) human lenses. It has been shown that the proportion of bound protein to total protein increases with both age (Friedrich and Truscott, 2010) and in cataracts (Chandrasekher and Cenedella, 1995), and is coupled with a decrease in soluble protein (Friedrich and Truscott, 2010). These high-density protein fractions are predominantly composed of modified crystallins (Chandrasekher and Cenedella, 1995; Friedrich and Truscott, 2010), that when separated via 2D SDS-PAGE, focus as a series of negatively charged spots, suggesting the presence of deamidated and/or phosphorylated species (Friedrich and Truscott, 2010).

How these associations with the membrane are mediated i.e. through direct binding to the phospholipid membrane or interactions with cytoskeletal components and integral membrane proteins, is yet to be fully elucidated. It has been proposed, however, that interactions between α-crystallins and membrane pore proteins in the lens maybe be a contributing factor to nucleocortical barrier formation (Cobb and Petrash, 2002b; Friedrich and Truscott, 2009; Friedrich and Truscott, 2010). In short, the accumulation of HMW aggregates at fibre cell membranes are thought to potentially occlude pore proteins, such as AQP0 and Cx46, which are responsible for the transport of water (Gorin *et al.*, 1984) and glutathione (GSH) (Slavi *et al.*, 2014) in the lens respectively. This would account for the fact that both the diffusion of GSH and water is reduced markedly at middle age (Moffat *et al.*, 1999). If obstruction of

Cx46 were to occur, it is believed it may result in an oxidative environment in the nuclear region of the older lens, leaving resident proteins vulnerable to oxidative damage (Truscott, 2005).

Phosphorylation and membrane association of αB-crystallin

This thesis expands upon this model, postulating that phosphorylation-induced hyperactivity of αB is responsible for α-crystallin association with the pore proteins AQP0 and Cx46, resulting in the formation of the nucleocortical barrier. This model is illustrated in Figure 1.8. Although it is postulated that α-crystallin associates with fibre cell membrane components as a HMW complex that includes αA, this thesis focuses mostly on αB. This is based on recent reports that implicate αB, but not αA, in cataract formation (Makley *et al.*, 2015; Datiles III *et al.*, 2016), as well as previous reports showing that αB has comparatively higher chaperone activity (Sun *et al.*, 1997) and lower thermostability (Sun and Liang, 1998; van Boekel *et al.*, 1999; Liang *et al.*, 2000), which may predispose it to stress-induced aggregation.

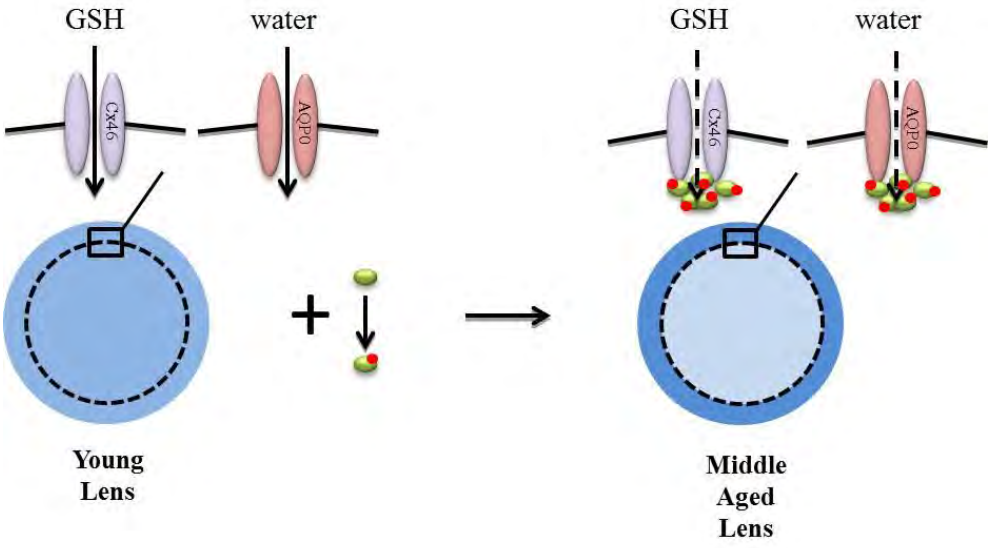

Figure 1.8: Representation of obstructed fibre cell pores. In young lenses, membrane pore proteins (AQP0 represented by pink ovals and Cx46 represented by purple ovals) facilitate the transport of water and GSH into the nucleus of the lens (represented by blue circles where intensity of colour represents concentration of metabolites). As αB becomes phosphorylated with age (green oval, red spot represents phosphate group), hyperactivity causes its association with fibre cell membranes in the barrier region (represented by dotted line), inhibiting diffusion of water/GSH into the nucleus. A similar effect may occur with αA.

Little is known regarding the relationship between protein modification and membrane association of lenticular proteins. It is also important to note that as interactions between α-crystallins and Cx46 or AQP0 have not been detected *in vivo,* obstruction of pore proteins due to membrane association of cytosolic proteins is still largely speculative. However, if barrier formation is indeed instigated by the binding of proteins such as α-crystallins to membrane or cytoskeletal proteins or the fibre cell membranes themselves, characterising the modifications associated with age and protein deposition is likely to give a critical insight into the molecular mechanisms behind barrier formation, and hence cataractogenesis. This thesis attempts to elucidate how protein modification may be involved in barrier formation by identifying what modifications are prevalent in membrane associated fractions, determining how phosphorylation may affect the chaperone activity of αB, and by identifying interactions between unmodified and phosphorylated αB, and the membrane pore proteins Cx46 and AQP0 in human lenses.

1.9 Aims

Post-translational modification and membrane-binding of α-crystallin are two age-related phenomena in lenticular fibre cells that have been implicated in cataractogenesis. However, the relationship between these two events has not been extensively studied. This thesis investigates phosphorylation and deamidation and how they may contribute to protein deposition and membrane-binding in aged human lenses.

The specific aims of this thesis were to:

1. **Determine the effect of phosphorylation on the chaperone activity of αB**
   Present knowledge regarding chaperone activity of phosphorylated αB is conflicting and appears to be dependent on the substrate protein and buffer system. In chapter 3, the chaperone of isoforms of αB containing mutations that mimic phosphorylation were compared to WT αB using a biologically relevant substrate in order to elucidate how the addition of a negative charge (like that added by phosphorylation) modulates the chaperone activity of αB.

2. Characterise the age-related phosphorylation of αB in aged human lenses

Lenticular proteins are susceptible to the accumulation of modifications with age, and it is highly likely such modifications play a role in protein deposition and cataract pathogenesis. In chapter 3, proteomic profiles of human lenses of varying ages were compared, and used to establish patterns of αB phosphorylation across regions of the lens in order to track the relationship between αB phosphorylation and age-related protein insolubilisation and/or membrane association.

3. Elucidate αB localisation at fibre cell membranes

Association of αB with fibre cell membranes has been observed in aged human lenses and may be the origin of nucleocortical barrier formation. In chapter 4, interactions between αB and membrane pore proteins were visualised in order to elucidate how αB localises with fibre cell membranes and to explain how these interactions may obstruct transport GSH *in vivo*.

4. Identify and characterise sites of non-enzymatic αB deamidation *in vitro*

Non-enzymatic deamidation can induce structural changes within proteins that can result in altered activity of the protein. This is relevant for all lens proteins including αB as they exist in an essentially enzymatically inert environment in the lens. In chapter 5, deamidated residues of αB were identified following various storage and treatment conditions in order to determine the susceptibility of specific αB residues to deamidation.

Chapter 2

Methods

Chapter 2

2.1 Materials

2.1.1 Antibodies

Antibodies used and their sources are listed below in Table 2.1.

Table 2.1: Product details for the antibodies used in these experiments. Dilution values are working dilution factors for immunblotting and immunofluorescence experiments.

Antibody	Catalogue number	Source	Supplier	Western Blotting Dilution	Immunofluorescence Dilution
Anti-αB Crystallin (phospho S19)	ab5597	Polyclonal rabbit	Abcam, USA	1:2000	1:200
Anti-αB Crystallin (phospho S45)	ab5598	Polyclonal rabbit	Abcam, USA	1:2000	1:200
Anti-αB Crystallin (phospho S59)	ab5577	Polyclonal rabbit	Abcam, USA	1:2000	1:125
Anti-αB Crystallin	ab13497	Polyclonal rabbit	Abcam, USA	1:1500	1:200
Anti-AQP0 (T-16)	sc-49364	Polyclonal goat	Santa Cruz, USA	N/A	1:150
Anti-connexin 46	sc-20859	Polyclonal goat	Santa Cruz, USA	N/A	1:100
Anti-BFSP2 (phakinin)	ab122476	Polyclonal rabbit	Abcam, USA	N/A	1:120
Anti-rabbit IgG-Peroxidase	A6154	Polyclonal goat	Sigma-Aldrich, USA	1:2500	N'A
Anti-rabbit IgG (H + L), Alexa Fluor® 488	A11034	Polyclonal goat	Invitrogen, USA	N/A	1:200

2.1.2 Reagents and materials

Recombinantly expressed human αB was gifted by Dr Amie Morris (University of Wollongong, Australia) or Dr Megan Kelly (University of Wollongong, Australia). All other reagents were obtained from Sigma-Aldrich (USA) or Amresco (USA) unless otherwise specified. Tris-base was obtained from PanReac AppliChem (Germany). Ethylenediaminetetraacetic acid (EDTA) was obtained from Astral Scientific (Australia). Dithiothreitol (DTT) was obtained from Pro-Lab (Canada). Biolyte® 3/10 Carrier Ampholyte (100x), ReadyStrip™ IPG Strips (17cm, pH 3-10 NL) and the RCDC™ Protein Assay Kit II were obtained from BioRad (USA). Unichrom® methanol and Univar® phosphoric acid and acetic acid were obtained from Ajax Finechem (Australia). SuperSignal™ West Pico Chemiluminescent Substrate and Slide-A-Lyzer ™ MINI Dialysis Devices were obtained from ThermoFisher Scientific (USA). Sequencing Grade Modified Trypsin (porcine) was obtained from Promega (USA). Duolink® products including the reagents Duolink® In Situ PLA® Probe anti-rabbit MINUS, Duolink® In Situ PLA® Probe anti-goat PLUS, Duolink® In Situ Detection Reagents Orange (including ligase and polymerase and dilution buffer solutions) were obtained from Sigma-Aldrich (USA). Wheat germ agglutinin-Alexa 488 was obtained from Invitrogen (USA). A list of buffers used in this work is included in Appendix 2.

2.2 Phosphorylation and membrane-binding events in aged human lenses

2.2.1 Chaperone assays

Recombinant WT αB (referred to as WTαB or 0P) and αB isoforms containing mutations that mimic phosphorylation were expressed and purified by Dr Amie Morris (University of Wollongong, Australia) according to the method previously described by Horwtiz *et al.* (1998). Serine to aspartate (i.e. S→D) point mutations were made at all three dominant phosphorylatable serines (Ito *et al.*, 1997), i.e. S19 (referred to as S19D or 1P), S45 (referred to as S45D), S59 (referred to as S59D), S19 and S45 (referred to as 2P), and S19, S45 and S59 (referred to as 3P). Assays were performed in phosphate buffered saline (PBS; pH 7.4) at 40°C with creatine phosphokinase (CPK) concentrations of 0.125 μM and αB concentrations of 0.5 or 0.25 μM, in 384 well plates (Greiner Bio-One, Austria) with a total volume of 20 μL. Samples were incubated in a POLARstar Omega microplate reader (BMG LABTECH,

Germany) for 10 hours at 43°C with absorbance readings at 360 nm every 60 seconds, with each reading preceded by a 10 second double orbital shake at 100 rpm. To assess the effect of multiple phosphorylation sites, assays were performed for the 0P, 1P, 2P and 3P phosphomutants using CPK concentrations of 0.125 μM and αB concentrations of 0.5 μM or 0.125 μM. To compare the effect of phosphorylation at each residue, single mutants were used and assays were repeated using WTαB, S19D, S45D and S59D phosphomutants. Samples using only CPK at 10 μM or only αBs at 10 μM or 5 μM acted as controls for each set of assays. The ability to prevent aggregation was calculated as the percentage inhibition using the formula: % protection = $((A_{CPK}-A_C)/A_{CPK}) \times 100$ based on the final average absorbance reading where A_C denotes absorbance of sample containing chaperone and A_{CPK} denotes absorbance of CPK control, as previously described (Ecroyd *et al.*, 2007). Assays were performed in triplicate and results are expressed as means ± SD. Results were analysed using analysis of variance (ANOVA) and Tukey's statistical tests where $P<0.05$ was considered statistically significant.

2.2.2 Tissue dissection

Donated human lenses aged 41-77 years of age were sourced from the Lions Eye Bank at the Sydney Eye Hospital and stored at -80°C until use. Tissue was handled according to the tenets of the Declaration of Helsinki. Trephines (6 mm and 4.5 mm) precooled with liquid nitrogen were used to manually dissect lenses into cortical, barrier and nuclear regions according to Figure 2.1.

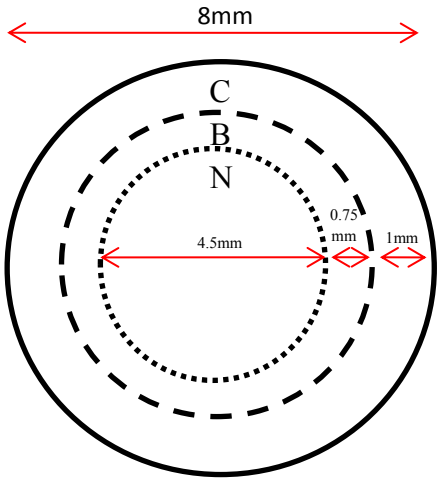

Figure 2.1: Regions of the human lens. Schematic depicts cross section of human lens in the equatorial plane. Cortical (C), barrier (B) and nuclear (N) regions are demarcated by dotted lines and the approximate width of the regions is indicated in mm.

Briefly, decapsulated lenses were placed in precooled polytetrafluoroethylene moulds (DuPont, USA) with a diameter of 8 mm, and a 6 mm trephine was used to excise cortical tissue. From the cylindrical core that remained, approximately 0.5-1 mm of tissue was removed from both ends using a precooled razor blade and was combined with previously excised tissue to provide cortical samples. The remaining tissue was placed again into a precooled 6 mm mould and a 4.5 mm trephine was used to isolate barrier and nuclear tissue samples. Trephines and mould were precooled to -20°C and lenses were kept frozen throughout process with regular submersion in liquid nitrogen.

2.2.3 Density sucrose gradient centrifugation

Sucrose solutions were prepared in sucrose buffer (Appendix 2) and layered into 9 mL centrifuge tubes from bottom to top as follows: 1 mL 80% w/v sucrose, 2 mL 70%, 1.5 mL 60%, 1.5 mL 50%, 1.5 mL 45%, 1.5 mL 25%. Gradient tubes were kept cold on ice while tissue was aspirated in 1 mL of 8% sucrose solution using a 21 g syringe. Homogenised tissue was then layered on top of the gradient, before being overlayed by a further 1 mL of 8% sucrose solution. Tubes were then spun at 100, 000 *g* for 2 hours at 4°C using a swing-

bucket rotor (Ti41; Beckman Coulter, USA) in an Optima-100 XP Ultracentrifuge (Beckman Coulter, USA). Images were taken of the gradient tubes with a digital camera before protein was extracted from bands (SG1-SG6, labelled with decreasing density) using glass pasture pipettes. Sucrose was removed by diluting the sample twofold with sucrose buffer and centrifuging at 4°C at 12281 *g* for 10 minutes in a MIKRO 20 microfuge (Hettich, Germany). Protein was then delipidated by resuspension in 100% v/v ethanol and incubating overnight at -20°C.

2.2.4 Protein quantitation

For 1D SDS-PAGE and western blotting, protein was solubilised in 8 M urea and absorbance at 280 nm was measured using a NanoDrop 2000 system (ThermoFisher Scientific, USA) using 8 M urea as a blank to compensate for absorption caused by urea in the buffer. The A_{280} readings were then used to calculate protein concentration assuming a molar extinction coefficient of 19000 M^{-1} cm^{-1} (Horwitz *et al.*, 1998). Samples were then made up to a final concentration of 1 $mg.mL^{-1}$ using 8 M urea. For 2D electrophoresis, protein was solubilised in SSS buffer and protein concentration was calculated using a RC DC™ Protein Assay Kit II, performed in microfuge tubes according to the manufacturer's instructions. The RC DC™ Protein Assay Kit was selected for quantitation of these samples as it is compatible with buffers that contain high concentrations of reducing agents and detergents such as SSS buffer. Briefly, 125 µL of RC Reagent I was added to 25 µL of sample, vortexed and incubated at room temperature for 1 minute. Following this, 125µL of RC Reagent II was added, and samples were vortexed and centrifuged at 15 000 *g* for 5 minutes using a Centrifuge 5415C (Eppendorf, Germany). The supernatant was removed via aspiration and discarded following centrifugation, before adding 127 µL of Reagent A' (previously prepared by combining DC Reagent S and DC Reagent A at a ratio of 1:5). Samples were then vortexed before being incubated at room temperature for 5 minutes. Samples were again vortexed and 1 mL of DC Reagent B was added, immediately vortexed, and incubated at room temperature for 15 minutes. Following incubation, 120 µL of each sample was transferred into a 98 well microplate (Greiner Bio-One, Austria) and absorbance was read on a Spectramax Plus 384 (Molecular Devices, USA) at a wavelength of 750 nm. Samples were then made up to a final concentration of 1 $mg.mL^{-1}$ using SSS buffer.

2.2.5 1-Dimensional (1D) electrophoresis and western blotting of protein bands

Protein isolated from SG2, SG3 and SG5, and Cortical SG6 bands was quantified and prepared in 8 M urea as described in section 2.2.4. Samples were prepared in 2-times loading buffer (Appendix 2), unfolded by incubation at 37°C for 30 minutes and subjected to SDS PAGE on a 15% v/v gel for one hour at 110V. The gel was stained using Coomassie stain (Appendix 2) for one hour, destained with coomassie destain (Appendix 2) overnight and imaged using a Gel Logic 212 Pro imaging system (Carestream, USA). Relative protein load was compared using ImageJ 1.49v densitometry software (Wayne Rasband, NIH, USA). Duplicate gels (but for the exclusion of the cortical SG6 sample) were prepared and proteins were transferred onto a polyvinylidene fluoride (PVDF) (MerckMillipore, USA) membrane electrophoretically at 30 V overnight at 4°C for western blotting. Briefly, membranes were blocked with 3% w/v bovine serum albumin (BSA) (Sigma, USA) in Tris buffered saline-tween 20 (TBST) (Appendix 2) prior to incubation with individual anti-phosphoserine αB antibodies specific to pSer19, pSer45 and pSer59, or an anti-αB antibody at concentrations outlined in Table 2.1. Blots were washed 3 times for 5 minutes in TBST, prior to labelling with goat anti-rabbit IgG/horse radish peroxidase (HRP). Blots were washed again 3 times for 5 minutes in TBST and developed using SuperSignal^{TM} West Pico Chemiluminescent Substrate and 3,3' –Diaminobenzidine Tetrahydrochloride (DAB) substrate, before being imaged using a Gel Logic 212 Pro imaging system (Carestream, USA). In-gel analysis of scanned images was performed using ImageJ 1.49v densitometry software (Wayne Rasband, NIH, USA). It should be noted that densitometric analysis was limited to the comparison of the relative proportion of each band compared to the total signal for each lane within the same gel as no one sample was run on all gels, therefore preventing comparison between gels. Cross-reactivity of anti-phosphoserine antibodies with αA and unphoshporylated αB was tested by repeating the blots with recombinant αA and αB alongside αB purified from bovine lens lysate.

2.2.6 2-Dimensional (2D) electrophoresis and spot analysis

Protein extracted from SG2, SG3, SG5 and SG6 bands was quantified and prepared in SSS buffer as previously described in section 2.2.4. For each protein extract, 300 µL of sample (i.e. 300 µg protein) was loaded onto a ReadyStrip^{TM} IPG trip (17cm, pH 3-10 NL) via overnight rehydration, and separated by charge using a Protean® IEF system (Biorad, USA) with the following program: 100 V for 1 hour, 300 V for 1 hour, 600 V for 1 hours, 1000 V

for 1 hour, 2000 V for 1 hour, 4000 V for 1 hour, 40000 V for 10 hours, then a 100 V hold. For the second dimension, IEF strips were equilibrated for 20 minutes in equilibration buffer (see Appendix 2) before being layered over 12.5% v/v polyacrylamide gels and subjected to electrophoresis for 5 hours at 45 mA to separate the proteins by mass. Gels were stained with colloidal Coomassie stain (Appendix 2), destained with colloidal destain (Appendix 2) and imaged using a Gel Logic 212 Pro imaging system (Carestream, USA). Scanned images were analysed using ImageJ 1.49v densitometry software (Wayne Rasband, NIH, USA). It should be noted that no protein standards of a known amount were used, therefore densitometric analysis is limited to the comparison of the relative proportion of each spot compared to spot 3 (as it was the most abundant spot on most gels). As such, comparison between gels of the absolute amounts of protein present was not performed. To confirm spot identity, individual protein spots were excised from gels of SG2 protein and were subjected to in-gel tryptic digestion with 1 μg of trypsin at room temperature overnight. Resultant peptides were detected using positive ion nano liquid chromatography quadrupole time-of-flight (NanoLC QTOF) MS (Synapt^{TM} HDMS; Waters, USA) and Masslynx V4.1 software (Waters, USA), and parent proteins were identified by comparison with a peptide match database (UniProt).

2.2.7 Separation of crosslinked complexes

Western blot analysis was used to identify phosphorylated αB species present in the gels present as discrete spots and as components of crosslinked complexes of ~45-90 kDa. Briefly, a region of the gel of the SG3 fraction from the cortex incorporating non-complexed αB spots (~20 kDa) was excised and labelled with anti-phosphoserine αB antibodies specific to the residues pSer19, pSer45 and pSer59 as previously described in section 2.2.5. The blot was then developed using SuperSignal^{TM} West Pico Chemiluminescent Substrate. Blots were scanned and imaged using a Gel Logic 212 Pro imaging system (Carestream, USA). To characterise the protein composition of crosslinked protein complexes, spots (1-10) were excised from the gel, and submitted for MS analysis.

2.2.8 Analysis of crosslinked complexes

The following work was undertaken at the Australian Proteome Analysis Facility (APAF), the infrastructure provided by the Australian Government through the National Collaborative Research Infrastructure Strategy (NCRIS). Briefly, excised spots were subjected to in-gel overnight digestion with 50-150 μg trypsin with resultant peptides being extracted from the

gel with acetonitrile:formic acid. Purported positively and negatively charged peptide bands were excised from the dye front of the barrier and nuclear SG3 gels respectively. Peptides were extracted from the gel spots using sonication and incubation with acetonitrile overnight at 37°C without further digestion. All samples were then concentrated and desalted using a peptide trap (Michrom peptide Captrap, USA). Peptides were separated using an Eksigent Ultra NanoLC system (Eksigent, USA), and analysed using positive ion nanoflow electrospray MS in an information dependent acquisition mode (IDA). The ten largest multiply charged ions (counts>150) observed in the TOF-MS survey scan (*m/z* 350-1500, 0.5 seconds) were further analysed using MS/MS. MS/MS spectra were acquired over 100 milliseconds (*m/z* 100-1500) with rolling collision energy. Peptide identities and modifications were determined by comparison with a human MASCOT database, and deamidated residues were identified based on what potential sites were present on the peptides (i.e. it is important to note that if more than a single potential deamidation site was present on a single peptide, it was not possible to determine which residue was deamidated) Percent deamidation of deamidated filensin sites was calculated by integrating ion chromatograms of precursor peptides, and calculating the relative peak area of the deamidated peptide compared to the total peptide (i.e. deamidated + non-deamidated peptides).

2.3 Characterisation of αB membrane binding in aged human lenses

2.3.1 Tissue sectioning and treatment

Lenses were treated and mounted according to Lim *et al.* (2009). In short, intact lenses were incubated for 24 hours in 0.75% w/v paraformaldehyde (PFA, see Appendix 2) in PBS at 4°C. Lenses were then encased in 6% w/v agarose in PBS prior to being cut in half along the equatorial plane with a razor blade, and incubated again in 0.75% w/v PFA in PBS for a further 24 hours at 4°C. Lens halves were equilibrated for 1 hour in 10% w/v sucrose in PBS, 1 hour in 20% w/v sucrose in PBS and overnight in 30% w/v sucrose in PBS at 4°C. Lens halves were then sectioned at 15 μm at -20°C using a Leica CM1905 cryostat (Leica Microsystems, Germany), and soft mounted onto glass slides. To ensure consistency of

results and in the quality of tissue sections, all lenses used were of a similar age i.e. 62-63 years-old.

2.3.2 Labelling

For direct labelling of αB, sections were washed 3 times with PBS, permeabilised for 30 minutes with 0.25% v/v Triton X-100 in milliQ and blocked with 3% w/v BSA in TBST for a minimum of 1 hour at room temperature. The sections were then labelled with antibodies specific to WTαB, pS19αB, pS45αB or pS59αB using concentrations outlined in Table 2.1. Labelled sections were then washed 3 times for 5 minutes in TBST before being incubated with goat anti-rabbit IgG/Alexa 488 (Table 2.1) in blocking buffer (i.e. 3% w/v BSA in TBST). Sections were washed 3 times for 10 minutes in TBST and mounted with Citifluor™ CFPVOH and AF100 anti-fadent before being imaged on a Leica TCS SPS II confocal microscope (Leica, Germany) and analysed using LAS AF Lite software (Leica, Germany). To label fibre cell membranes, separate lens sections were washed 3 times for 5 minutes with Hank's balanced salt solution (HBSS) buffer (Appendix 2) and incubated with WGA/Alexa 633 diluted (1:200 in HBSS buffer) for 10 minutes at room temperature. Sections were washed 2 times for 5 minutes with HBSS buffer before being mounted, imaged and analysed as previously described.

2.3.3 Duolink® proximity assays

Mounted lens sections were permeabilised and blocked as previously described in section 2.3.2. Sections were then co-labelled with antibodies specific to either WTαB, pS19αB, pS45αB or pS59αB and antibodies specific to either AQP0 or Cx46 in blocking buffer (i.e. 3% w/v BSA in TBST), at concentrations outlined in Table 2.1. Sections were incubated with anti-rabbit and anti-goat PLA® probes for 1 hour at 37°C, and washed twice for 5 minutes with wash buffer A (Appendix 2). Sections were then incubated with ligase according to the manufacturer's instructions for 30 minutes at 37°C and washed twice for 2 minutes in wash buffer A. Sections were then incubated with polymerase according to company instructions for 100 minutes at 37°C in the dark, before being washed twice for 10 minutes in wash buffer B (Appendix 2) and for 1 minute in 0.01x wash buffer B (Appendix 2) in the dark. Sections were allowed to air dry in the dark and mounted with Citifluor™ CFPVOH and AF100 anti-fadent before being imaged on a Leica TCS SPS II confocal microscope (Leica, Germany)

and analysed using LAS AF Lite software (Leica, Germany). Two negative control sections were prepared using no primary antibodies or co-labelling of rabbit polyclonal IgG with goat anti-AQP0 IgG at concentrations outlined in Table 2.1. A positive control section was prepared by co-labelling with polyclonal rabbit anti-BFSP2 antibody and AQP0 at concentrations outlined in Table 1.2, as BFSP2 (also known as phakinin and CP49) is known to associate with AQP0 in human lenses (Rose *et al.*, 2006).

2.4 *In vitro* deamidation of αB

2.4.1 In vitro deamidation of αB under storage conditions

A batch of recombinant human αB expressed and purified by Dr Amie Morris (see section 2.2.1) was stored in 200 mM ammonium acetate (pH 7.0) at -20°C for a minimum of 5 years (referred to as batch 1). To investigate deamidation events under low temperatures and pH following long term storage, the method published by Liao *et al.* (2009) was modified and adapted. Briefly, protein was transferred into 34 mM acetic acid (~pH 3.0) at a concentration of 1 $mg.mL^{-1}$, and incubated at 4°C for a total of 72 hours. Aliquots were taken at 0, 23, 48 and 72 hours, and were snap frozen in liquid nitrogen and stored at -20°C until analysis. To compare deamidation events under varying pH conditions with the addition of heat following long term storage, protein was transferred into either 34 mM acetic acid (~pH 3.0) or 200 mM ammonium acetate (pH 7.0) at a concentration of 1 $mg.mL^{-1}$, and incubated at 50°C for 16 hours. Samples were digested with trypsin at a concentration of 0.5 $\mu g.mL^{-1}$ for either 5 minutes or 2 hours, and resultant peptides were snap frozen in liquid nitrogen and stored at -20°C until analysis. For each experiment, protein samples that had not been subjected to heat treatment were used as controls. Samples were analysed using positive ion NanoLC QTOF MS (Synapt^{TM} HDMS; Waters, USA) using a mass range *m/z* 1800-2000 for the 4°C treated samples to allow detection of intact proteins, and *m/z* 300-1800 for the 50°C treated samples to allow detection of peptides. Data was analysed using Masslynx V4.1 software (Waters, USA). Mass changes were detected in 4°C treated samples by identifying mass shifts in matching peaks between time point samples, and predicted masses were used to identify peptides and potential modifications in the 50°C treated samples.

2.4.2 In vitro deamidation of unfolded αB protein

A second batch of recombinant human αB was donated by Dr Megan Kelly (University of Wollongong, Australia) and stored in 50 mM phosphate buffer (~pH 7.4) at -20°C until use, but for a period of less than 12 months (referred to as batch 2). To determine the rate of deamidation under unfolding conditions following short term storage, protein samples were diluted into either 6 M urea (~pH 8.0) or 1 M ammonium bicarbonate (~pH 8.0) to a final concentration of 2 $mg.mL^{-1}$, and incubated at either 37°C for 4 hours or 50°C for 18 hours respectively. Samples were then transferred back into PBS using Slide-A-Lyzer ^{TM} MINI dialysis cups in order to allow for the slow refolding of the 6 M urea treated sample (Saha and Das, 2007; Benesch *et al.*, 2008). Samples were then snap frozen in liquid nitrogen and stored at -20°C until submission for analysis at APAF. Protein samples in PBS with and without heat treatment at 50°C for 18 hours were prepared and submitted as controls. To compare isoelectric profiles of treated samples, 6 µg aliquots of the urea treated sample and the PBS and PBS heat treated samples were retained prior to submission for MS analysis.

The following work was undertaken at APAF, the infrastructure provided by the Australian Government through the National Collaborative Research Infrastructure Strategy (NCRIS). Prior to MS analysis, 50 µg aliquots of each sample were made up to 0.5 $mg.mL^{-1}$ with ammonium bicarbonate and digested with 2 µg trypsin overnight. Samples were then concentrated and subjected to MS analysis as previously described in section 2.2.7. For further MS/MS analysis, MS/MS spectra were acquired over 200 milliseconds (*m/z* 100-1500) with rolling collision energy for the ten largest multiply charged ions (counts>150) observed in the TOF-MS survey scan (*m/z* 380-1500, 0.25 seconds). Peptide identities and theoretical retention times were determined using a MASCOT database search, and a computer simulation method was used to calculate deamidation percentages of peptides containing asparagine (N) and glutamine (Q) residues. Briefly, this was performed using a peak harvester program to develop a Poisson model for each isotopic distribution (Breen *et al.*, 2000), and then calculating the intensity of the peak corresponding to the deamidated peptide as a proportion of the total intensity of the peaks corresponding to both the deamidated and non-deamidated peptides. Samples were analysed three times, and results were presented as mean ± SD. Results were analysed using ANOVA and Tukey's statistical tests and $P<0.05$ was considered statistically significant.

Chapter 3

Investigation of αB phosphorylation

in the human lens

Chapter 3

3.1 Introduction

Although αB is generally believed to play a protective role in the human lens, it has also been reported to be the dominant protein in insoluble, membrane-bound protein fractions in aged and cataractous human lenses (Cenedella and Fleschner, 1992; Fleschner and Cenedella, 1992; Chandrasekher and Cenedella, 1995; Friedrich and Truscott, 2010). This has led to speculation that membrane association of the protein may be a pivotal step in cataractogenesis (Sweeney and Truscott, 1998; Cobb and Petrash, 2002b; Friedrich and Truscott, 2009). Membrane associated αB has also been shown to have a range of modifications (Friedrich and Truscott, 2010; Wang *et al.*, 2013), including phosphorylation.

To elucidate how phosphorylated αB may participate in pathogenic processes in the lens, it is essential to determine how phosphorylation affects the chaperone activity of the protein. The results from previous studies in this area are conflicting. For example, Ahmad *et al.* (2008) reported that a triple αB phosphomimic (i.e. S19D/S45D/S59D αB) had increased chaperone activity against insulin, citrate synthase and α-synuclein under either reducing conditions or heat stress compared to wild type αB. In contrast, Aquilina *et al.* (2004) reported that a double phosphomimic (i.e. S19D/S45D αB) co-aggregated with α-lactalbumin under reducing conditions, while a single phosphomimic (i.e. S19D αB) retained activity similar to WTαB. Ecroyd *et al.* (2007) later showed that the effect of phosphorylation on αB activity was dependent on the substrate and buffer conditions. For example, αB phosphomimics were more efficient than WTαB at preventing amyloid formation of RCMκ-casein (but not ccβ-Trp), the heat-induced aggregation of catalase, β_L-crystallin and alcohol dehydrogenase, and the DTT-induced aggregation of insulin and α-lactalbumin in phosphate buffer (Ecroyd *et al.*, 2007). However, incubation of αB phosphomimics with α-lactalbumin in ammonium acetate buffer induced aggregation, suggesting that the stability of the chaperone in certain buffers containing ammonium ions may be compromised, leading to hyperactivity and co-precipitation (Ecroyd *et al.*, 2007). A number of phosphorylation-induced structural and kinetic changes in αB oligomers have also been reported, including an increase in subunit exchange (Ahmad *et al.*, 2008), increased polydispersity, loss of dimeric substructure (Aquilina *et al.*, 2004) and an increase in flexibility and solvent accessibility of the N-terminal domain (Peschek *et al.*, 2013).

An indication that protein modification may be involved in pathogenic processes in the lens is the abundance of modifications (including phosphorylation) in protein associated with the

insoluble, membrane associated lens fractions (Wang *et al.*, 2013). Studies have shown an age-related loss of soluble protein in the lens, coupled with an increase of membrane associated protein (Friedrich and Truscott, 2009; Friedrich and Truscott, 2010). This pattern becomes more pronounced towards the nuclear region of lenses (Truscott *et al.*, 2011). It has been shown that these membrane associated fractions are composed predominantly of α-crystallin (Friedrich and Truscott, 2009; Friedrich and Truscott, 2010; Truscott *et al.*, 2011; Wang *et al.*, 2013), with lower levels of β- and γ-crystallins as well as cytoskeletal proteins such as filensin, phakinin and spectrin (Wang *et al.*, 2013). It is believed that α-crystallin becomes tightly bound to membranes though hydrophobic interactions with either phospholipids or integral membrane proteins (Chandrasekher and Cenedella, 1997; Cobb and Petrash, 2000; Truscott *et al.*, 2011). Soluble cytoplasmic HMWCs, consisting of α-crystallin and its substrate proteins, then form low affinity associations with tightly-bound α-crystallin at the membrane (Chandrasekher and Cenedella, 1997; Cobb and Petrash, 2002b; Friedrich and Truscott, 2009). These soluble complexes show higher membrane affinity than native α-crystallin and, once bound, display decreased chaperone activity, although the ability to participate in subunit exchange events is retained (Cobb and Petrash, 2002b). As such, these complexes can recruit more cytoplasmic proteins, incorporating them into the complex (Friedrich and Truscott, 2010).

However, protein modifications present in membrane associated fractions have not been extensively studied. Friedrich and Truscott (2010) identified a pattern of multiple negatively charged spots, corresponding to unmodified and modified αB, on 2D gels of high density membrane associated fractions. However, this study did not differentiate between phosphorylated or deamidated isoforms. More recently, a comprehensive phosphoproteomic study was performed on human fibre cell membrane extracts (Wang *et al.*, 2013). Although this identified seventeen sites of αB and 22 sites of αA phosphorylation, some of which were previously unreported, the study did not differentiate between lens age and region, and did not compare levels with a soluble protein control. A full understanding of the mechanism of membrane association and the role phosphorylation may play in this process is therefore lacking and is the focus of the work presented in this chapter.

Chapter 3

3.2 Experimental Rationale

Creatine phosphokinase is found in the brain, myocardium and skeletal muscle (Baird *et al.*, 2012), and is overexpressed in diseases such as myocardial infarction (Vincent and Rapaport, 1965; Van der Veen and Willebrands, 1966; Goto, 1974) and muscular dystrophies (Van der Veen and Willebrands, 1966; Goto, 1974; Somer *et al.*, 1976). It is commonly used as a substrate for chaperone assays (Dabbs and Wilson, 2014; Wyatt *et al.*, 2015) due to its tendency to reproducibly form amorphous aggregates following thermal stress, and it has previously been shown that non-chaperone proteins have no effect on its aggregation (Dabbs and Wilson, 2014). Both CPK and αB co-exist in skeletal muscle (section 2.2.1). Furthermore, the comparatively low temperature used for these assays (i.e. 40°C) compared to temperatures required to destabilise proteins native to the lens, such as β-crystallins (Ecroyd *et al.*, 2007; Takata *et al.*, 2008), are closer to physiological temperatures experienced by the lens. For these reasons, CPK was selected as a substrate for aggregation assays rather than a native substrate to investigate the activity of αB.

Density sucrose centrifugation has become a well-established method to isolate membrane associated and soluble protein fractions from lens homogenates. This method was previously published by Lampi *et al.* (1992) and Cenedella and Fleschner (1992), and later modified by Friedrich and Truscott (2009; 2010). This current work employed the modified protocol published by Friedrich and Truscott (2009; 2010) to isolate membrane associated protein fractions (section 2.2.3). Prior to this, human donor lenses from different ages were manually dissected into cortical, barrier and nuclear regions to allow for comparison between different lens regions (section 2.2.2). These fractions were then separated by 1D (section 2.2.5) and 2D SDS PAGE (section 2.2.6). As 2D SDS PAGE separates proteins in two dimensions i.e. mass and pI, modified proteins resolve as a series of discrete spots due to the variance in charge bestowed on them by the modification. This method, used previously by Lampi *et al.* (1998) to identify crystallin deamidation and truncation products in human lenses, was therefore employed in order to separate modified forms of αB for more detailed analysis. To identify phosphorylated species of αB, commercially available anti-phosphoserine antibodies specific to pSer19, pSer45 and pSer59 αB were used for western blotting of 1D and 2D gels (section 2.2.5, section 2.2.6). These three residues were selected for study as they are the dominant sites of phosphorylation (Miesbauer *et al.*, 1994; MacCoss *et al.*, 2002), the most extensively studied and corresponding anti-phosphoserine antibodies were readily available. Another

antibody specific to the C-terminal residues of αB was used as a control to detect both phosphorylated and unphosphorylated αB, thereby reflecting the total αB pool. Densitometry software was used on 1D blots to measure relative intensity of spots representing phosphorylated αB in order to compare αB phosphorylation profiles between lens region and density fractions, and with age (section 2.2.5).

Tandem mass spectrometry (MS/MS) is often used to determine peptide identity and to detect modification sites. In-gel tryptic digests of discrete 2D spots were therefore subjected to MS/MS to determine protein identities. This method was also applied to spots within the mass range ~40-95 kDa to identify proteins and modification sites present in crosslinked complexes (section 2.2.7).

3.3 Results

3.3.1 Mimicking phosphorylation activates chaperone activity of αB..

To determine how the addition of a negative charge can affect the chaperone activity of αB, aggregation assays were performed to compare the ability of αB with single (S19D; hereafter 1P), double (S19D/S45D; hereafter 2P) and triple (S19D/S45D/S59D; hereafter 3P) point mutations that mimic phosphorylation to inhibit the heat-induced aggregation of CPK. There was minimal aggregation when WT or 1P αB were incubated alone under these experimental conditions (Figure 3.1C). When present at a molar ratio of $1_{\alpha B}$:1_{CPK}, WTαB (no mutations) increased the amount of aggregation of CPK by 2.8-fold (P=0.001) compared to when CPK incubated alone (Figure 3.1A). In contrast, the amorphous aggregation of CPK was inhibited by 72.3±2.9% (P=0.009) in the presence of 3P αB (Figure 3.1A). The amount of CPK aggregation was also reduced (45.8±7.7%) by 2P αB, although these results did not reach statistical significance (P=0.195) (Figure 3.1A). Incubation with 1P did not significantly affect CPK aggregation (P=0.9) (Figure 3.1A). At a molar ratio of $1_{\alpha B}$:2_{CPK}, each subsequent addition of a mutation that mimics phosphorylation led to a decrease in the amount of CPK aggregation (Figure 3.1B). At this lower concentration of αB, incubation with WT (P=0.9) or 1P αB (P=0.134) did not significantly affect aggregation of CPK. However, 2P αB inhibited aggregation by 41.9±7.5% (P=0.001) and 3P αB inhibited the aggregation of CPK by

83.9±1.3% (P=0.001) (Figure 3.1B). WT, 1P, 2P and 3P αB incubated in the absence of chaperone were used as negative controls (Appendix 3).

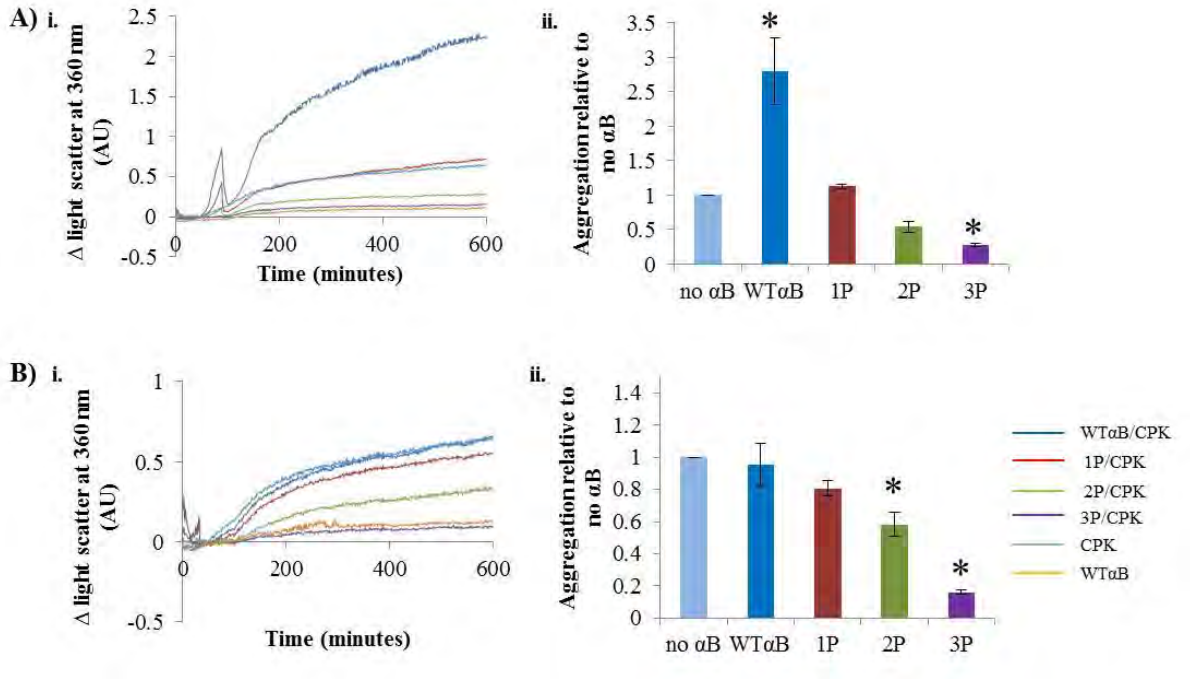

Figure 3.1: Effect of mutations that mimic phosphorylation on the ability of αB to inhibit the heat-induced aggregation of CPK. CPK (0.125 μM) was incubated in PBS (pH 7.4) at 40°C in the presence of WT, 1P, 2P or 3P αB at a concentration of **(A)** 0.5 μM or **(B)** 0.25 μM. (i) The change in light scatter was measured at 360 nm over time. (ii) The amount of aggregation at 600 minutes was calculated as a proportion of the control i.e. no αB. Data are shown as means±1SD (N=3). Differences between group means were tested using a one-way ANOVA and Tukey's post-hoc test (P≤0.01 is indicated by an asterisk). Note – scale of y-axis is different in (A) compared to (B).

To determine if the observed increase in chaperone activity of 2P and 3P αB was due to mutation of a specific residue (e.g. Ser45), the CPK aggregation assays were repeated using phosphomutants with single S→D point mutations at Ser19, Ser45 or Ser59 (i.e. S19D, S45D and S59D αB). Again, there was minimal aggregation observed when CPK was not present in the sample (Figure 3.2C). At a molar ratio of 1_{CPK}:$1_{\alpha B}$, the addition of WTαB significantly increased CPK aggregation by 2-fold (P=0.001) compared to when CPK was incubated alone (Figure 3.2A). At a $1_{\alpha B}$:1_{CPK} ratio, the aggregation of CPK was not significantly affected by incubation with the S19D, S45D or S59D αB phosphomutants (Figure 3.2A). At a molar ratio of $1_{\alpha B}$:4_{CPK}, CPK aggregation was not significantly affected by incubation with any of the αB isoforms (Figure 3.2B). WT, S19D, S45D and S59D incubated in the absence of chaperone were used as negative controls (Appendix 3).

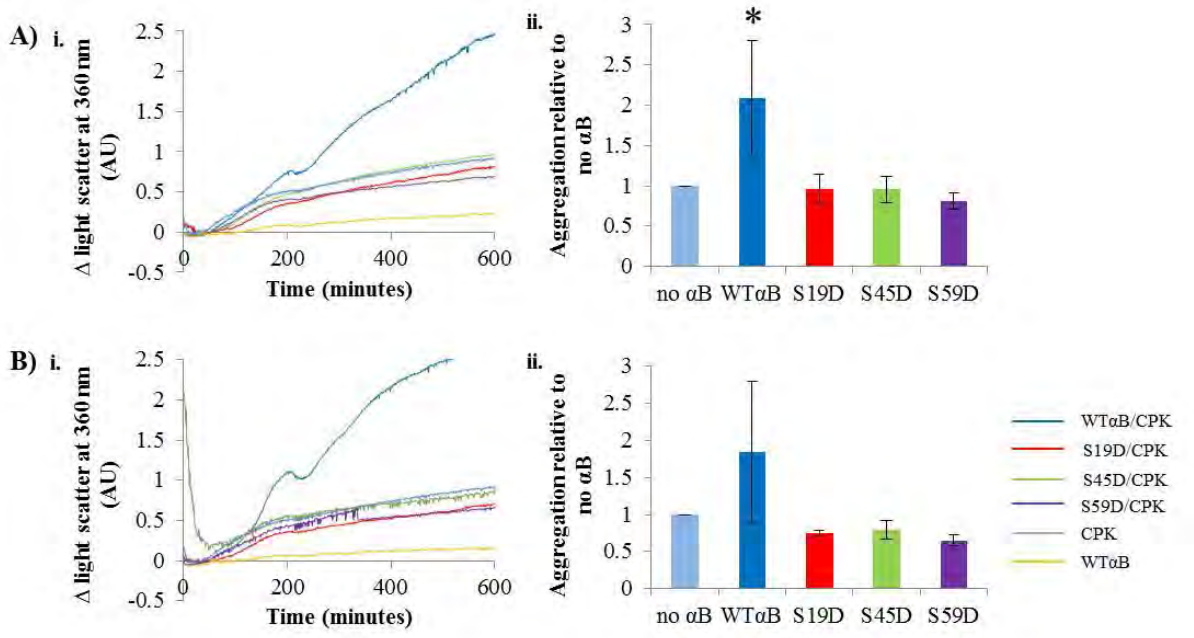

Figure 3.2: Effect of single-site αB phosphomimics on the heat-induced aggregation of CPK. CPK (0.125 µM) was incubated in PBS (pH 7.4) at 40°C in the presence of WT, 1P, 2P or 3P αB at a concentration of **(A)** 0.5 µM or **(B)** 0.125 µM. (i) The change in light scatter was measured at 360 nm over time. (ii) The amount of aggregation measured as light scatter at 600 minutes was calculated as a proportion of the control i.e. no αB. Data are shown as means±1SD (N=3). Differences between group means were tested using a one-way ANOVA and Tukey's post-hoc test (P≤0.01 is indicated by an asterisk).

3.3.2 The amount of multiply phosphorylated αB is increased in the nucleus of aged human lenses and coincides with the formation of high-density protein fractions.

Isolation of high density lens protein fractions

Density sucrose centrifugation was performed separately on two human lenses (aged 41 and 77 years old, representing a younger and an older lens respectively) to investigate how density profiles from different regions of the lens change with age. Prior to centrifugation, each lens was dissected into cortical, barrier and nuclear regions with a trephine (section 2.2.2, Figure 2.1). Protein deposited at density interfaces, was observed as cloudy white bands (sucrose gradient 6-1, SG6-1, in order of increasing density). The amount of protein for each band was measured as a percentage of the total protein in the tube.

The predominant band in the cortical sample from the younger lens was SG3 (Figure 3.3A, B). As the amount of SG3 decreased in the younger lens towards the nucleus, SG5 increased to become the predominant band in the nuclear sample (Figure 3.3A, B). The predominant band in the older lens for all regions (i.e. cortical, barrier and nuclear samples) was SG2 (Figure 3.3A, B).

In the cortical samples, SG6, SG5 and SG3 decreased from 17%, 28% and 38% of the total protein respectively in the younger lens to 14%, 19% and 24% in the older lens (Figure 3.3B, C). The amount of SG4 remained constant (at 10% of the total protein) and SG2 increased from 7% of the total protein in the younger lens to 32% in the older lens (Figure 3.3B, C).

In the barrier region, SG6, SG5, SG4 and SG3 decreased from 17%, 31%, 14% and 38% of the total protein respectively in the younger lens to 14%, 20%, 7% and 16% in the older lens (Figure 3.3B, C). While no SG2 band was evident in the younger lens, SG2 constituted 42% of the total protein in the barrier region from the older lens (Figure 3.3B, C).

In the nuclear samples, SG5, SG4 and SG3 decreased from 44%, 16% and 23% of the total protein respectively in the younger lens to 16%, 8% and 6% in the older lens (Figure 3.3B, C). The amount of SG6 and SG2 increased from 12% and 4% of total protein respectively in the younger lens to 16% and 41% in the older lens (Figure 3.3B, C). Although absent in the nuclear region from the younger lens, and from cortical and barrier samples from both lenses, SG1 constituted 11% of the total protein content in the nuclear sample from the older lens (Figure 3.3B, C).

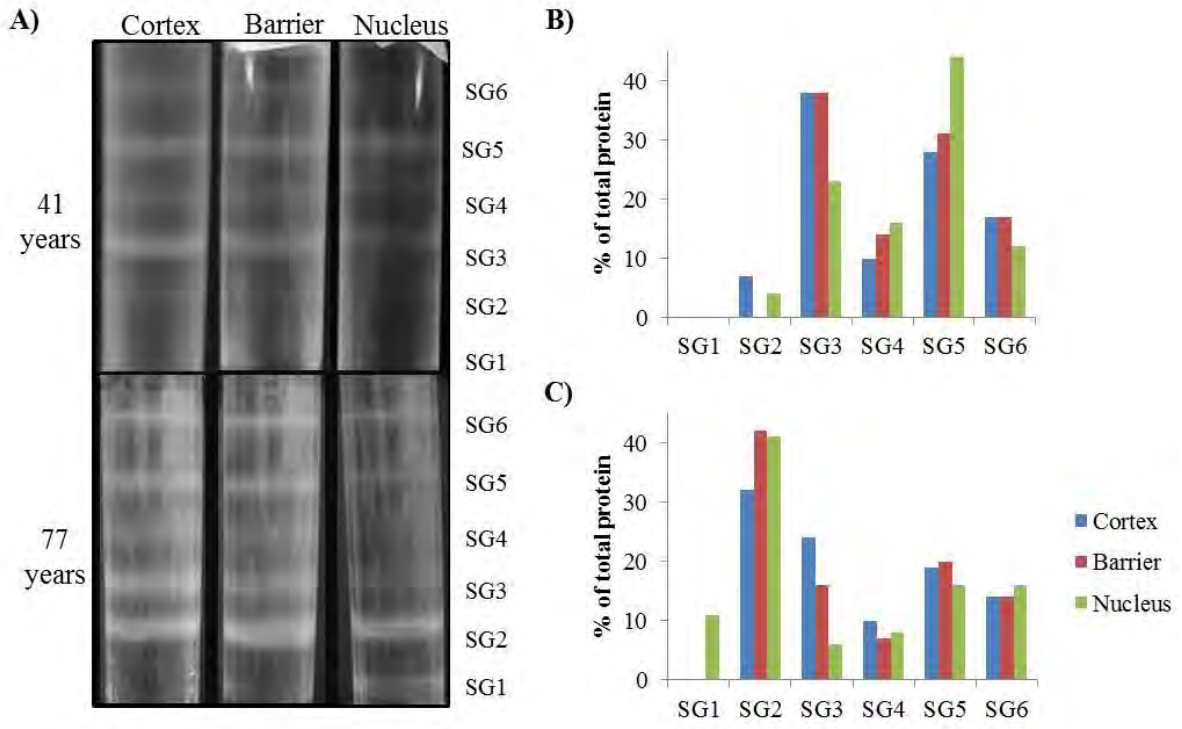

Figure 3.3: Comparison of sucrose density gradient profiles from human lenses as a function of age. **(A)** Human lenses from a 41 year-old and a 77 year-old were manually dissected into cortical, barrier and nuclear regions and density fractions (SG6-SG1) were separated via density sucrose centrifugation. Images were inverted using densitometry software, and the amount of protein for each band was determined by measuring the area under the corresponding peak on the densitometry profile. The relative amount of protein in each band for the **(B)** 41 year-old and the **(C)** 77 year-old lens is expressed as a percentage of the total protein in each tube.

Chapter 3

Comparison of protein composition of sucrose density bands

To compare proteins present in different density fractions, SG2, SG3, SG5 and SG6 were isolated from each region of a 53 year-old human lens and separated using 1D SDS PAGE. Fraction SG4 was not analysed as analysis was limited to high and low density fractions. Additionally, SG4 was a relatively minor component for each lens. As a known amount of standard was not loaded for each gel, densitometry analysis was limited to the comparison of relative proportions compared to the total signal from each lane. A different lens of this age was used in order to obtain sufficient protein yield for each fraction for analysis. Barrier and nuclear SG6 were not analysed due to insufficient protein yields. In the cortical SG6 sample, αB migrated a shorter distance than in the higher density fractions, potentially due to overall lower rates of modification, notably truncation. Levels of protein (observed as discrete bands) increased with decreasing density across all lens regions. Across all regions of the lens and all density fractions, αA and αB were the predominant protein species in these samples (Figure 3.4A, B).

Additional protein bands at 100 kDa, 55 kDa and 40 kDa were also observed in some samples (Figure 3.4A, B). The 100 kDa and 55 kDa bands were exclusively present in high density fractions (i.e. SG2 and SG3) from cortical samples, albeit at low levels (1.1-2.0% and 0.8-1.7% of the total protein respectively) (Figure 3.4A, B). In comparison, the 40 kDa band was observed in samples from all lens regions (Figure 3.4A, B). In cortical samples, levels of the 40 kDa band decreased from 7.6% of the total protein in the SG5 fraction to 3.9% in the SG2 fraction (Figure 3.4A, B). In barrier samples, the 40 kDa band was only observed in the SG3 fraction, accounting for 6.1% of the total protein in the sample (Figure 3.4A, B). Levels of a protein migrating with αA (‘αA’) decreased with increasing density across all lens regions (Figure 3.4A, B). In the cortical samples, ‘αA’ decreased from 16% of the total protein in SG6 to 6.7% in SG2 (Figure 3.4A, B). In barrier and nuclear samples, ‘αA’ decreased from 7.1% to 9.2% of total protein in the SG5 fraction to 6.1% and 5.9% in the SG2 fraction respectively (Figure 3.4A, B). Although the levels of a protein migrating with αB (‘αB’), as a proportion of the total protein, varied across density fractions, a trend towards a decrease in ‘αB’ levels was observed when comparing cortical and nuclear samples across all SG fractions (Figure 3.4A, B). In SG2 fractions, ‘αB’ accounted for 28.5% of the total protein in cortical samples but only 11.5% in nuclear samples (Figure 3.4A, B). Levels of ‘αB’ as a proportion of the total protein in SG3 and SG5 fractions decreased from 24.3% and

31.8% in cortical samples to 19.1% and 24.4% in nuclear samples respectively (Figure 3.4A, B).

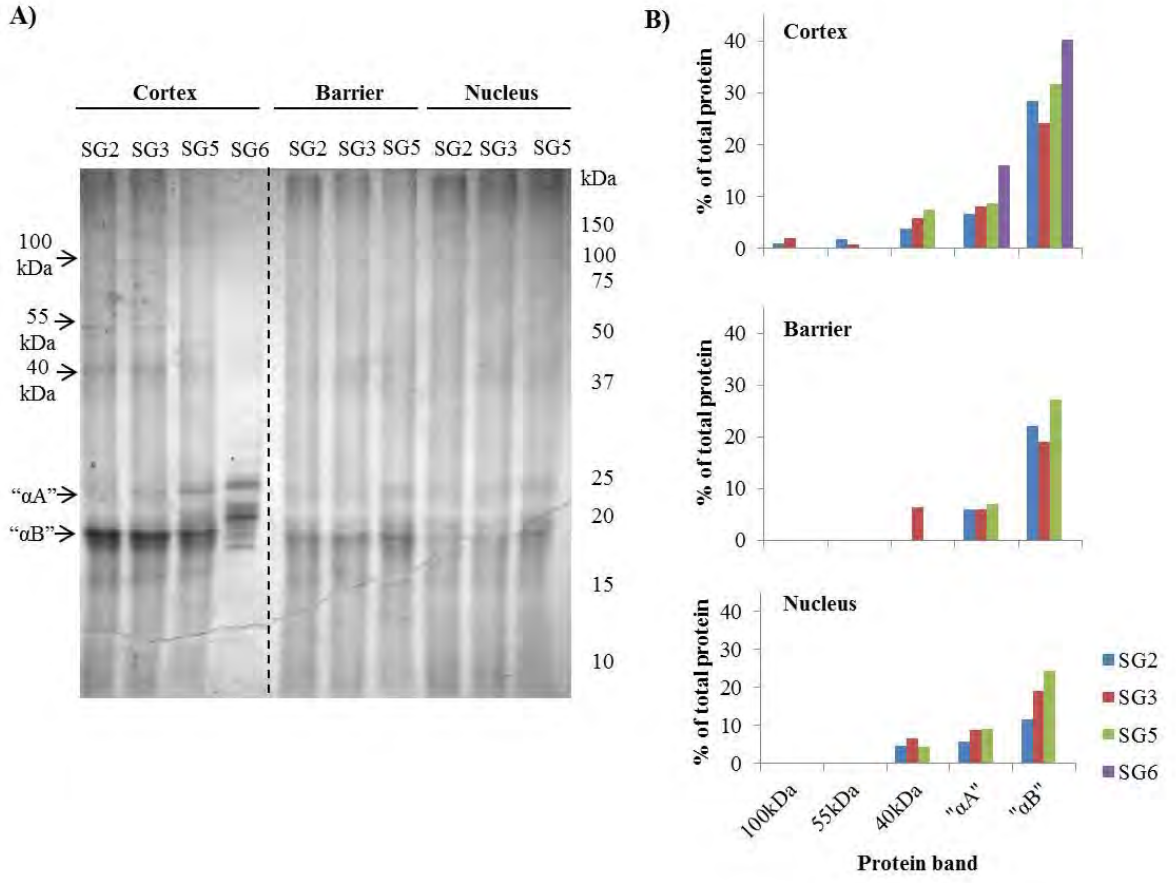

Figure 3.4: Protein components of SG fractions from different regions of a human lens. **(A)** SG2, SG3 and SG5 fractions were isolated from the cortical, barrier and nuclear regions of a 53 year-old female human lens via density sucrose centrifugation and separated using 1D SDS PAGE. The position of dominant protein bands at 100 kDa, 55 kDa, 40 kDa, as well as bands running at the distance of αA and αB are shown on the left. **(B)** The amount of each protein band was measured using densitometry and calculated as a percentage of the total protein in each lane to the closest whole number. Note - an empty lane was digitally excised from the gel and the imaged was merged (indicated by broken line).

Chapter 3

Detection of phosphorylated αB in sucrose density bands

To compare levels of phosphorylated αB across density fractions from each region of this 53 year-old lens, protein from SG2-SG5 from each region was separated on 1D SDS gels, transferred onto PVDF and labelled with antibodies specific to pSer19, pSer45 or pSer59 αB. An identical blot was prepared and labelled with an anti-αB antibody for use as a control to indicate levels of total αB for each sample. Densitometric data for each αB band was standardized against the cortical SG5band for each blot (i.e. density of band was calculated as a proportion of the signal for cortical SG5 band for each blot) as it was found to have the highest level of total protein. Differences in the amount of protein in each sample were accounted for by calculating the relative amount of phosphorylated αB as a proportion of the relative amount of αB in the sample (i.e. density of pαB as a proportion of corresponding band on blot labelled for total αB).

With regards to the pSer19 to total αB ratio between samples, the highest levels of pSer19 αB were found in cortical samples for SG2 (0.9) and SG3 (0.8) (Figure 3.5). In comparison, SG5 had pSer19 αB levels equal to the amount of αB in the sample (Figure 3.5). The relative levels of pSer19 αB were slightly lower in the barrier samples for SG2 (0.6), SG3 (0.8) and SG5 (0.7) (Figure 3.5). The lowest relative levels of pSer19 αB were in nuclear samples for SG2 (0.2), SG3 (0.3) and SG5 (0.6) (Figure 3.5).

With regards to the pSer45 to total αB ratio between samples, the highest levels of pSer45 αB were also in the cortex, with the relative levels the same across all fractions and similar to the amount of αB in the samples (Figure 3.5). The relative levels of pSer45 αB were lower in the barrier samples for SG2 (0.5) and SG3 (0.6). However, relative levels of SG5 were elevated in the barrier sample (1.2) compared to SG2 and SG3 (Figure 3.5). The lowest levels of pSer45 αB were in nuclear samples for SG2 (0.1), SG3 (0.2) and SG5 (0.5) (Figure 3.5).

With regards to the pSer59 to total αB ratio between samples, the highest levels of pSer59 αB were in the barrier for SG2 (0.9), SG3 (0.9) and SG5 (0.8) (Figure 3.5). The relative levels of pSer59 in cortical and nuclear samples were comparable when levels across each of the fractions were averaged (Figure 3.5). In the cortical samples, relative levels of pSer59 were equal to the amount of αB in SG5 (Figure 3.5). However, relative levels of pSer59 were lower for SG2 (0.5) and SG3 (0.8) compared to SG5 (Figure 3.5). In the nuclear samples, the relative levels of pSer59 were equal to the amount of αB in SG2 (Figure 3.5). However,

relative levels of pSer59 were lower in SG3 (0.9) and SG5 (0.4) compared to SG2 (Figure 3.5).

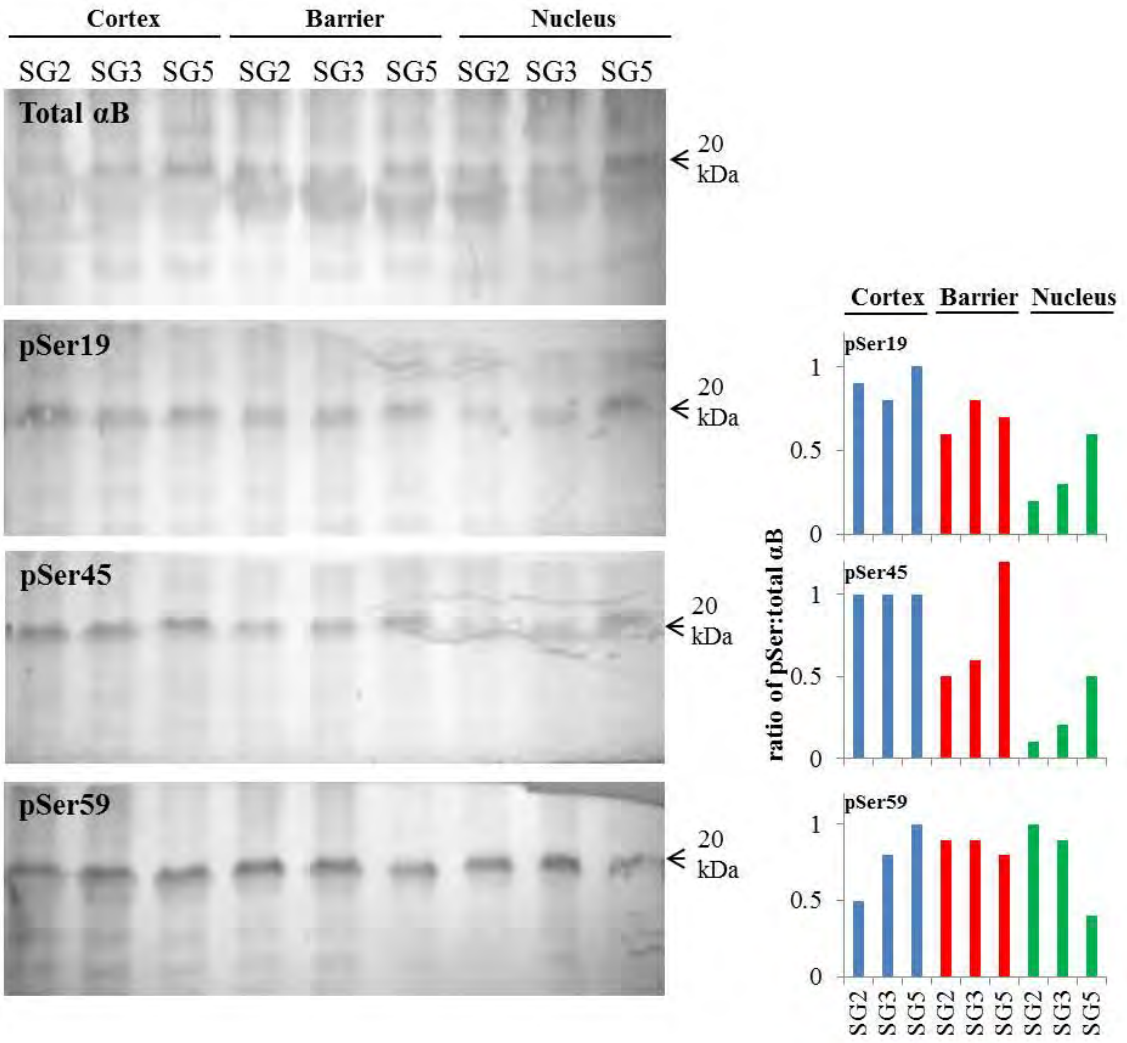

Figure 3.5: Identification of phosphorylated isoforms of αB and their relative amounts in SG fractions from a human lens following 1D SDS-PAGE. SG2, SG3 and SG5 fractions were isolated from the cortical, barrier and nuclear regions of a 53 year-old human lens, separated using 1D SDS PAGE and transferred onto PVDF membranes. Membranes were incubated with anti-αB antibody (total αB) or antiphosphoserine specific antibodies to pSer19, pSer45 or pSer59 αB, and developed with DAB. The intensity of each band was measured using densitometry, standardised to the cortical SG5 band for each membrane, and the relative amount of pαB in each band was calculated as a ratio of the relative amount of αB in that sample.

Chapter 3

2D SDS PAGE separation of modified αB from SG fractions

To compare differences in αB phosphorylation patterns between density fractions and between age groups, SG2, SG3 and SG5 fractions from each region were isolated from a range of human lenses (aged 41-77 years), and separated using 2D SDS PAGE. As corresponding controls for each region, another lens was dissected into cortical, barrier and nuclear regions, and subjected to 2D SDS PAGE without sucrose density centrifugation i.e. separated as a whole homogenate. Spots identified as αB (based on MS analysis and migration patterns) were labelled 1-9 in order of increasing negative charge, and phosphorylated isotypes were identified by immunoblotting with the pSer19, pSer45 and pSer59 αB specific antibodies. The relative intensity for each gel spot was calculated as a ratio of its density compared to that of spot 3 which, based on its pI, corresponds to the unphosphorylated form of αB.

Gel spots 1-3 were not reactive with any of the αB phosphospecific antibodies (Figure 3.6), suggesting these spots correspond to unphosphorylated forms of αB. The differences in migration (i.e. the pI) between these αB isoforms is likely to be due to post-translational modification (e.g. deamidation), other than phosphorylation, that act to change the pI of the protein. The pSer19 antibody reacted with the fewest spots (spots 4-6) (Figure 3.6). The pSer45 antibody reacted with five discrete spots, spots 4-7 and spot 9 (Figure 3.6). The pSer59 antibody reacted with six discrete protein spots, spots 4-9 (Figure 3.6). The existence of protein isoforms that reacted with the phosphospecific antibodies indicates the presence of multiply phosphorylated isoforms of αB in some samples. It should be noted that on the membrane probed with the pSer59 antibody (Figure 3.6), the negative banding of spot 4 is consistent with substrate saturation due to high levels of this isoform in the sample.

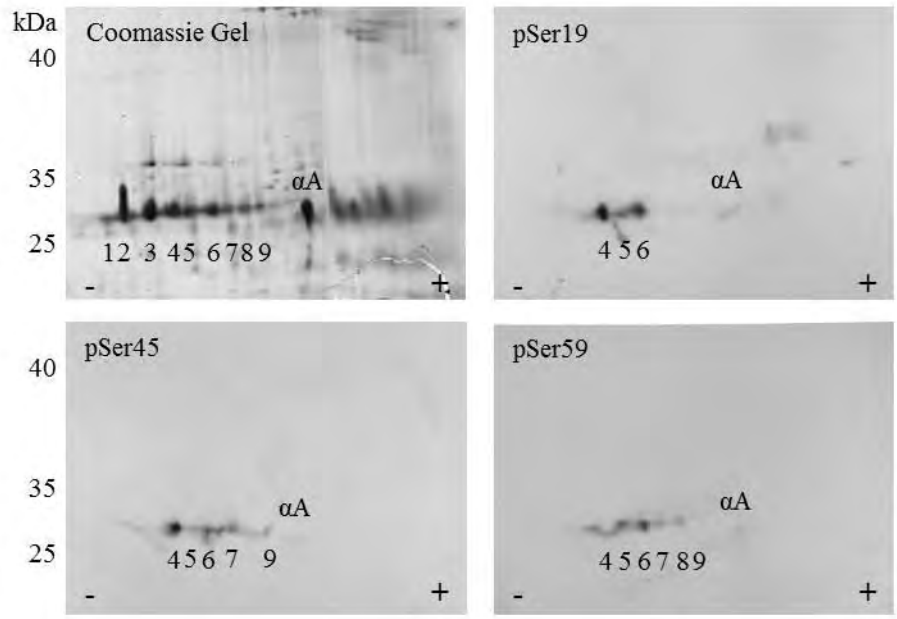

Figure 3.6: Identification of phosphorylated isoforms of αB in SG3 fraction from a 77 year-old human lens following 2D SDS-PAGE. SG3 was isolated from the cortical region of a 77 year-old human lens and separated using 2D SDS PAGE. Sections of the gels were excised and transferred onto PVDF membrane. Membranes were incubated with anti-phosphoserine specific antibodies to pSer19, pSer45 or pSer59 αB, and developed using chemiluminescence on X-ray film. X-ray films were superimposed onto a corresponding Coomassie stained gel section to identify spots (labelled 1-9) corresponding to αB isoforms. The spot previously identified as αA via MS analysis was used as a reference point.

To compare phosphorylation profiles of different density fractions, SG2 and SG3 were isolated from a 77 year-old lens. Due to insufficient protein yields from this lens, SG5 was isolated from a 41 year-old lens. The fractions were then separated using 2D SDS PAGE. Analysis of SG1, SG4, SG6 and cortical SG2 was not performed due to insufficient amounts of proteins in these samples. Homogenised tissue from each region (i.e. cortex, barrier and nucleus) was prepared and analysed for use as corresponding controls.

Control gels

The cortical region gel displayed only two phosphorylated spots, spot 4 and 6, both of which had half the amount of protein (i.e. 0.5-fold) compared to spot 3 from the same gel (Figure 3.7A; Table 3.1). The relative amount of spot 4 remained constant in the barrier control (i.e. 0.5-fold) (Figure 3.7B; Table 3.1). The relative amount of spot 6 decreased slightly in the barrier region compared to the cortical region (i.e. 0.3-fold the amount of protein compared to spot 3 from the barrier region) (Figure 3.7B; Table 3.1). The nuclear region had only one phosphorylated spot, spot 5 (i.e. 0.9-fold the amount of protein as spot 3 from the same gel) (Figure 3.7C; Table 3.1). All control gels, i.e. the cortical, barrier and nuclear whole homogenate gels, also displayed spot 2 (i.e. corresponding to an unphosphorylated isoform of αB) at high levels (Figure 3.7A-C; Table 3.1) (i.e. 1.5-fold for the cortical region, 0.8-fold for the barrier region and 1-fold for the nuclear region.

SG2 gels

Gels of the SG2 fractions demonstrated that there is an increase in phosphorylation levels between the barrier and the nucleus, observed as an increase in the number of multiply phosphorylated spots (i.e. spots 5-9) (Figure 3.7D-E; Table 3.1). The gel of the SG2 fraction from the barrier displayed two phosphorylated spots; spot 5 (i.e. 0.3-fold) and spot 6 (i.e. 0.2-fold the amount of protein compared to spot 3 from the same gel) (Figure 3.7D; Table 3.1). The gel of the SG2 fraction from the nucleus displayed an increase in multiply phosphorylated species compared to both the nuclear control gel (Figure 3.7C) and the SG2 gel from the barrier (Figure 3.7D) as evidenced by an increase in the number of negatively-charged spots (spots 5-9). These had 0.5-fold (spot 5), 0.4-fold (spot 6), 0.4-fold (spot 7), 0.2-fold (spot 8) and 0.1-fold (spot 9) the amount of protein compared to spot 3 from the same gel respectively (Figure 3.7E; Table 3.1). The amounts of spot 2 (i.e. an unphosphorylated isoform of αB observed in the gels), decreased in the SG2 gel from the nucleus compared to the SG2 gel from the barrier (Figure 3.7D-E; Table 3.1) (i.e. 0.8-fold for the barrier and 0.6-

fold the amount of protein compared to from spot 3 from the same gel for the nucleus) (Figure 3.7D-E; Table 3.1). This relative decrease in this unphosphorylated αB could be explained by either the presence of additional modifications that affect pI or an increase in the relative amount of phosphorylated αB in the sample. Spots corresponding to truncated forms of αA were present, predominantly on the nuclear gel. However, the spots were not sufficiently resolved to allow for densitometric analysis.

SG3 gels

All gels of SG3 fractions (i.e. cortical, barrier and nucleus) displayed the maximum number of spots observed amongst the gels (i.e. spots 4-9) (Figure 3.7F-H; Table 3.1) indicating higher levels of αB phosphorylation compared to SG2 and SG5 fractions as well as whole lens homogenates. The relative amounts for spots 4 and 6-8 decreased slightly from the cortex towards the nucleus for the SG3 fraction (i.e. decreased from 0.6-fold, 0.6-fold, 0.3-fold and 0.3-fold in the cortex to 0.5-fold, 0.3-fold, 0.2-fold and 0.2-fold in the nucleus respectively) (Figure 3.7F-H; Table 3.1). The relative amounts of spots 5 and 9 remained consistent in SG3 from the cortex and nucleus (0.3-fold and 0.2-fold the amount of protein compared to spot 3 from the same gel) (Figure 3.7F-H; Table 3.1). Relative amounts of spot 2 decreased in SG3 between the cortex and the nucleus (i.e. 1.3-fold in the cortex to 0.4-fold in the nucleus) (Figure 3.7F-H; Table 3.1). Spot 1 was only present in SG3 from the cortex (Figure 3.7F) and the barrier (Figure 3.7G) (0.3-fold and 0.2-fold the amount of protein compared to spot 3 from each gel). Spots corresponding to truncated forms of αA were present on gels from each region (Figure 3.7F-H, indicated by boxed area). However, the spots were not sufficiently resolved to allow for densitometric analysis.SG5 gels

Gels of SG5 fractions demonstrated a gradual decrease in αB phosphorylation levels towards the nucleus, as evidenced by a decrease in the number and relative amounts of spots (Figure 3.7I-K; Table 3.1). The SG5 gel from the cortex displayed three spots corresponding to phosphorylated αB isoforms i.e. spots 4-6, each having 0.5-fold the amount of protein compared to spot 3 from the same gel (Figure 3.7I; Table 3.1). Relative amounts for spots 4 and 6 were similar to relative amounts of the corresponding spots on the cortical control (Figure 3.7A; Table 3.1). Spot 5 however was not present on the cortical control gel, indicating higher levels of αB phosphorylation in cortical SG5 compared to cortical homogenate (Figure 3.7A, I; Table 3.1). The SG5 gel from the barrier displayed a single spot corresponding to a phosphorylated αB isoform (i.e. spot 4, having 0.6-fold the amount of

protein compared to spot 3 from the same gel) (Figure 3.7J; Table 3.1), indicating levels of αB phosphorylation had decreased compared to the levels in the barrier control (Figure 3.7B). The SG5 gel from the nucleus also only displayed spot 4, the relative amount of which had decreased to 0.3-fold the amount of protein compared to spot 3 from the same gel (Figure 3.7K; Table 3.1). The relative amounts of spot 2 increased in SG5 between the cortex and the nucleus (i.e. from 0.5-fold in the cortex to 0.7-fold in the nucleus) (Figure 3.7I-K; Table 3.1). However, these amounts remained below those observed for spot 2 in the corresponding control gels (Table 3.1).

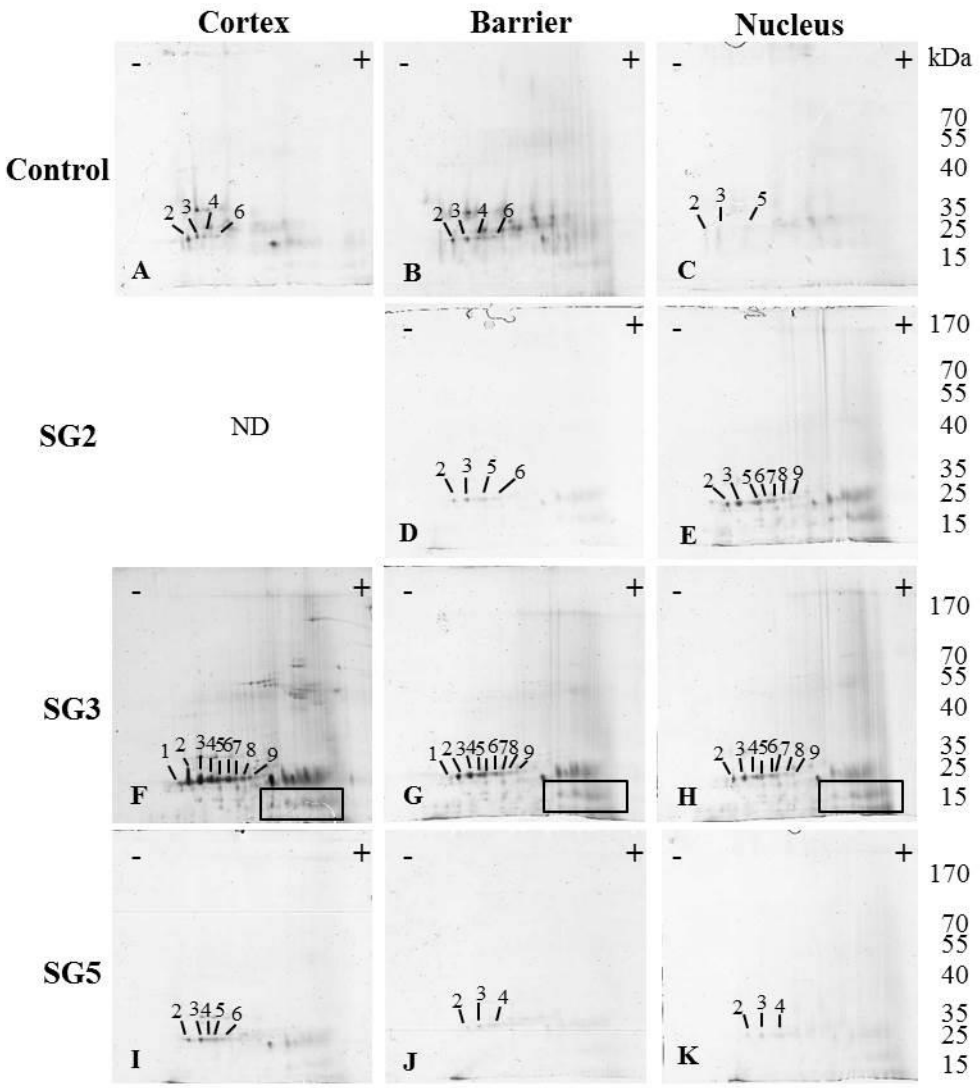

Figure 3.7: Comparison of phosphorylated isoforms of αB in SG fractions from different regions of human lenses. SG2 (D-E) and SG3(F-H) isolated from each region (i.e. cortex, barrier and nucleus) of a 77 year-old human lens, and SG5 (I-K) isolated from each region of a 41 year-old human lens were separated using 2D SDS-PAGE. Tissue homogenate from each region of a 53 year-old lens was separated using 2D SDS-PAGE without prior sucrose density gradient centrifugation for use as a total protein control (A-C). Spot identities for αA and αB were confirmed by MS, and spots corresponding to αB were labelled 1-9. The regions of the gels corresponding to the acidic (+) and basic (-) region of the IEF strip used in the first dimension separation are as indicated. Spots consistent with truncated αA are indicated by boxed region. Samples which could not be analysed due to low yield are indicated by "ND".

Chapter 3

Table 3.1: Relative amounts of αB isoforms in SG fractions from different regions of human lenses. The intensity of αB spots (labelled 1-9; see Figure 3.7) detected in SG2, SG3 (77 year-old lens), SG5 (41 year-old lens) fractions and the control sample (53 year-old lens) from each region of the lens was measured using densitometry and the relative amount calculated as a proportion of spot 3 (corresponding to unmodified αB) from each corresponding gel. Pink shading indicates spots corresponding to unphosphorylated αB isoforms and blue shading indicates spots corresponding to phosphorylated αB isoforms. Samples which could not be analysed due to low yield are indicated by "ND".

	Cortex									**Barrier**									**Nucleus**								
	1	**2**	**3**	**4**	**5**	**6**	**7**	**8**	**9**	**1**	**2**	**3**	**4**	**5**	**6**	**7**	**8**	**9**	**1**	**2**	**3**	**4**	**5**	**6**	**7**	**8**	**9**
Control	0	1.5	1	.5	0	.5	0	0	0	0	.8	1	.5	0	.3	0	0	0	0	1	1	0	.9	0	0	0	0
SG2	ND	ND	ND	ND	ND	ND	ND	ND	ND	0	.8	1	0	.3	.2	0	0	0	0	.6	1	0	.5	.4	.4	.2	.1
SG3	.3	1.3	1	.6	.3	.6	.3	.3	.2	.2	.8	1	.5	.4	.5	.3	.3	.2	0	.4	1	.5	.3	.3	.2	.2	.2
SG5	0	.5	1	.5	.5	.5	0	0	0	0	.5	1	.6	0	0	0	0	0	0	.7	1	.3	0	0	0	0	0

Chapter 3

Comparison of phosphorylated αB in SG2 as a function of age

To compare phosphorylation profiles of membrane associated αB across three lenses of different ages, the same 2D gels of the SG2 fraction from the 77 year-old lens were compared to gels of the SG2 fractions isolated from two younger human lenses (aged 41 and 62 years) that had been separated using 2D SDS PAGE. Analysis of the 41 year-old barrier and 77 year-old cortical region was not performed due to insufficient amount of protein in these samples.

The gels of the cortex and nucleus of the 41 year-old lens both displayed four spots corresponding to phosphorylated αB isoforms; spots 4-8 (Figure 3.8A-B; Table 3.2). The relative amounts of these spots varied between the nucleus and cortex of the 41 year-old lens. Relative amounts of spots 6 and 8 were decreased in the nucleus compared to the cortex (0.4-fold and 0.2-fold in the nucleus compared to 0.7-fold and 0.3-fold in the cortex respectively) (Figure 3.8; Table 3.2). Spot 4 was only present in the cortical sample from the 41 year-old lens, having 0.5-fold the amount of protein compared to spot 3 from the same gel (Figure 3.8A; Table 3.2). The relative amounts of spots 5 and 7 were increased in the nucleus compared to the cortex for the 41 year-old lens (0.7-fold and 0.4-fold in the nucleus compared to 0.5-fold and 0.2-fold in the cortex respectively) (Figure 3.8A-B; Table 3.2). Relative amounts of spot 2 (i.e. corresponding to an unphosphorylated αB isoform) were slightly decreased in the nucleus compared to the cortex for the 41 year-old lens (0.8-fold in the nucleus compared to 0.9-fold in the cortex) (Figure 3.8A-B; Table 3.2).

62 year-old lens

The number and relative amounts of spots corresponding to phosphorylated αB isotypes decreased towards the nucleus in the 62 year-old lens (Figure 3.8C-E; Table 3.2). The cortical gel displayed three spots corresponding to phosphorylated αB isoforms i.e. spots 4-7 (Figure 3.8C). Spots 4-6 had 0.4-fold and spot 7 had 0.3-fold the amount of protein compared to spot 3 from the same gel (Figure 3.8C; Table 3.2). The barrier gel from the 62 year-old lens displayed two spots corresponding to phosphorylated αB isoforms i.e. spots 5 and 6 (Figure 3.8D; Table 3.2). Spot 5 had 0.6-fold and spot 5 had 0.4-fold the amount of protein compared to spot 3 from the same gel (Figure 3.8D; Table 3.2). The nuclear gel from the 62 year-old lens displayed a single spot corresponding to a phosphorylated αB isoform, spot 5 which had 0.2-fold the amount of protein compared to spot 3 from the same gel (Figure 3.8E; Table 3.2).

The relative amount of spot 2 decreased towards the nucleus in the 62 year-old lens (0.5-fold in the nucleus compared to 0.8-fold in the cortex) (Figure 3.8C-E; Table 3.2).

77 year-old lens

The number and relative amounts of spots corresponding to phosphorylated αB isoforms increased towards the nucleus in the 77 year-old lens (Figure 3.8F-G; Table 3.2). The barrier gel from the 77 year-old lens displayed two spots corresponding to phosphorylated αB isoforms, spots 5 and 6 having 0.3-fold and 0.2-fold the amount of protein compared to spot 3 from the same gel respectively (Figure 3.8F; Table 3.2). The nuclear gel from the 77 year-old lens displayed five spots corresponding to phosphorylated αB isoforms, spots 5-9 having 0.5-fold, 0.4-fold, 0.4-fold, 0.2-fold and 0.1-fold the amount of protein compared to spot 3 from the same gel respectively (Figure 3.8G; Table 3.2). The relative amount of spot 2 decreased between the barrier and the nucleus of the 77 year-old lens (0.8-fold in the cortex compared to 0.6-fold in the nucleus) (Figure 3.8F-G; Table 3.2).

Spots corresponding to truncated forms of αA were present on gels for each lens (Figure 3.8). However, the spots were not sufficiently resolved to allow for densitometric analysis.

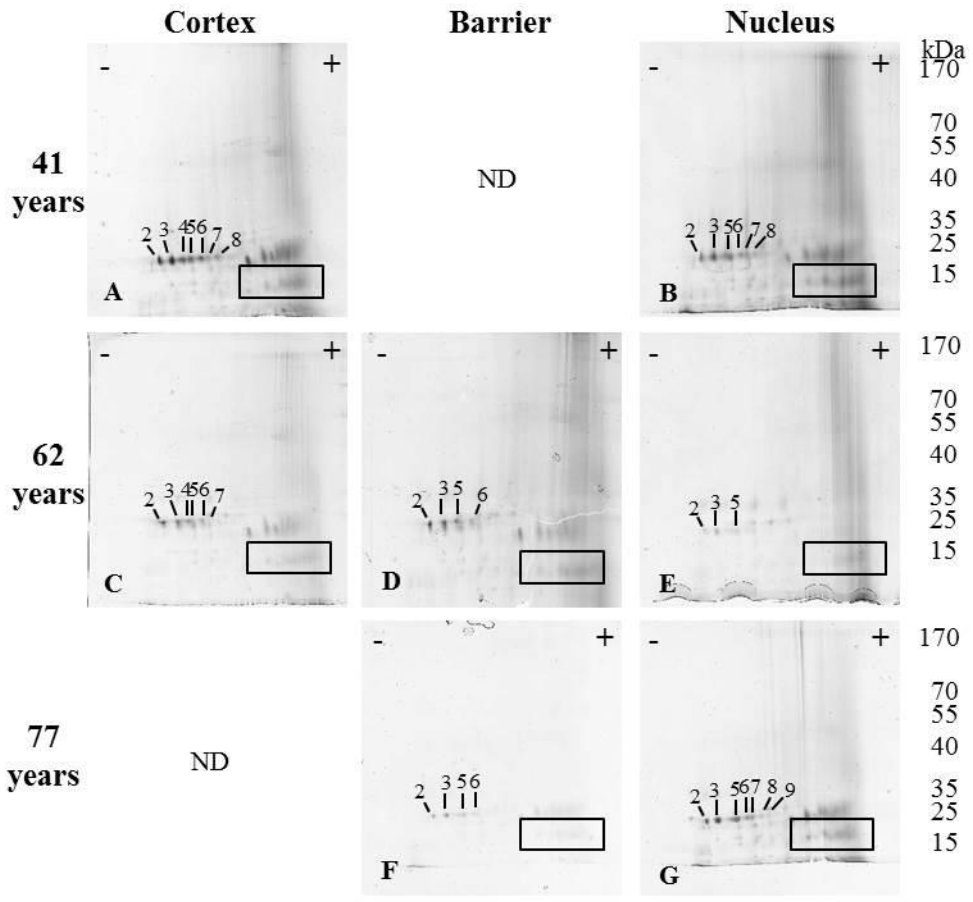

Figure 3.8: Comparison of phosphorylated isoforms of αB in SG2 from different regions of human lenses with age. SG2 from each region of a 41 year-old (A-B), 62 year-old (C-E) and 77 year-old (F-G) human lens was separated using 2D SDS-PAGE. Spots corresponding to αB were identified and labelled 1-9. The regions of the gels corresponding to the acidic (+) and basic (-) region of the IEF strip used in the first dimension separation are as indicated. Spots consistent with truncated αA are indicated by boxed region. Analysis of SG2 from the barrier of the 41 year-old lens and SG2 from the cortex of the 77 year-old lens was not performed due to insufficient protein yields. Samples for which analysis could not be performed due to low yield are indicated by "ND". Note: panels D and E from Figure 3.7 are shown here as panels F and G for comparison against other lenses.

Table 3.2: Relative amounts of αB isoforms from SG2 as a function of age. The intensity of αB spots (labelled 1-9; see Figure 3.8) detected in SG2 from each region of a 41 year-old, 62 year-old and 77 year-old lens was measured using densitometry and the relative amount calculated as a proportion of spot 3 (corresponding to unmodified αB) from each corresponding gel. Pink shading indicates spots corresponding to unphosphorylated αB isoforms and blue shading indicates spots corresponding to phosphorylated αB isoforms. Spots for which not enough protein was isolated for analysis are indicated by "ND".

	Cortex									**Barrier**									**Nucleus**								
	1	**2**	**3**	**4**	**5**	**6**	**7**	**8**	**9**	**1**	**2**	**3**	**4**	**5**	**6**	**7**	**8**	**9**	**1**	**2**	**3**	**4**	**5**	**6**	**7**	**8**	**9**
41	0	.9	1	.5	.5	.7	.2	.3	0	ND	ND	ND	ND	ND	ND	ND	ND	ND	0	.8	1	0	.7	.4	.4	.2	0
62	0	.8	1	.4	.4	.4	.3	0	0	0	.7	1	0	.6	.3	0	0	0	0	.5	1	0	.2	0	0	0	0
77	ND	ND	ND	ND	ND	ND	ND	ND	ND	0	.8	1	0	.3	.2	0	0	0	0	.6	1	0	.5	.4	.4	.2	.1

3.3.3 Modified filensin and crystallins form complexes

Protein from the SG3 fraction from the cortex of the 77 year-old lens was isolated and separated by 2D-SDS-PAGE. A cluster of negatively charged proteins were observed in this fraction, ranging in size from ~40-95 kDa (red boxed zone and expansion, Figure 3.9A). Although most prominent in this gel, similar but fainter spots were also observed in the barrier and nuclear gels from the same lens (Figure 3.7), and on cortical SG2 gels from a 41 and a 62 year-old lens (Figure 3.8). Discrete spots were excised and submitted for MS/MS analysis to determine the composition and modification profile of each. A total of ten spots were analysed and labelled complex 1-10 according to decreasing mass. The proportion of filensin deamidated at each site (as a %) was calculated based on relative peak area for complexes where filensin was the predominant protein (Table 3.3, Figure 3.10). A comprehensive list of identified peptides and modified residues is available in Appendix 3.

With the exception of complex 3, based on the number of tryptic peptides, all spots were predominately (>60%) composed of peptides derived from filensin (~75 kDa), with lower amounts of peptides derived from αA (~20 kDa), αB (~20 kDa), βB1 (~28 kDa), phakinin (~46 kDa), serum albumin (~ 69 kDa), retinol dehydrogenase (~55 kDa) and actin, cytoplasmic 1 (~42 kDa) (Figure 3.9B). Complex 1 resolved as a discrete spot of ~95 kDa with a pI of ~4.5 (Figure 3.9A), and was found to be composed of peptides derived from filensin (83%), phakinin (7%) and αA (4%) (Figure 3.9B). From complex 1, four sites of filensin deamidation (N383, N478, N145 and N304) and two of oxidation (M649 and M207) were identified (Figure 3.9A). The proportion of filensin peptides deamidated at N478, N145 and N304 was calculated from the peak areas from the ion chromatograms (Figure 3.10) and found to be 25.2%, 7% and 42.2% respectively (Table 3.3). For N383, only the deamidated peptide was detected in complex 1 (Table 3.3).

Complex 2 resolved as a discrete spot of ~60 kDa with a pI of ~5 (Figure 3.9A), and was shown to be composed of peptides derived from filensin (74%), phakinin (5%), αA (3%), βB1 (6%), retinal dehydrogenase (4%) and αB (5%) (Figure 3.9B). From complex 2, a single site of filensin oxidation (M207), and five of deamidation (N155, N145, N304, N383, N268) were identified, as well as a single αB oxidation (M68) site (Figure 3.9A). The proportion of filensin peptides deamidated at residues N155 and N304 was 3.8% and 34.7% respectively (Table 3.3). The peptide containing both N145 and N155 had a percent deamidation of 12.4% (Table 3.3). For N383, only the deamidated peptide was detected in complex 2 (Table 3.3).

Complex 3 resolved as a discrete spot of ~55 kDa with a pI of ~4 (Figure 3.9A), and had a unique protein profile predominantly composed of peptides derived from brain acidic soluble protein 1 (BASP1, 54%), with lower amounts of filensin (22%), phakinin (9%), αA (4%), serum albumin (6%) and αB (4%) (Figure 3.9B). From complex 3, a single site of filensin oxidation (M649) was identified, as well as single site of BASP 1 deamidation (N218) (Figure 3.9A).

Complexes 4-9 resolved as a cluster of spots with similar mass (~45 kDa) and pIs ranging from 5.8 -6 (Figure 3.9A). Complex 4 had a pI of ~6.2 (Figure 3.3.9A) and was composed of peptides derived from filensin (86%), αA (2%), βB1 (6%) and αB (2%) (Figure 3.9B). From complex 4, a single αB deamidation site (N146) was identified, as well as four deamidation (N268, N304, N145 and N155) and a single oxidation (M207) site from filensin (Figure 3.9A). The proportion of filensin peptides deamidated at N155 and N304 was 3.5% and 29.2% respectively (Table 3.3). The peptide containing both N145 and N155 was deamidated 2.5% (Table 3.3).

Complex 5 had a pI of ~6 (Figure 3.9A) and was shown to be composed of peptides derived from filensin (85%), αA (3%), βB1 (5%) and αB (3%) (Figure 3.9B). From complex 5, three sites of filensin deamidation (N304, N145 and N155) and a single site of oxidation (M207) was identified (Figure 3.9A). The proportion of filensin peptides deamidated at N155 and N304 was 3.8% and 56% respectively (Table 3.3). The peptide containing both N145 and N155 was deamidated 2.8% (Table 3.3).

Complex 6 had a pI of 5.9 (Figure 3.9A) and was shown to be composed of peptides derived from filensin (80%), αA (4%), serum albumin (4%), βB1 (5%) and αB (4%) (Figure 3.9B). From complex 6, a single site of αB deamidation (N146) was identified, as well as four sites of deamidation (N318, N304, N145 and N155) and a single site of oxidation (M207) from filensin (Figure 3.9A). The proportion of filensin peptides deamidated at N155 and N304 was 3.5% and 59.4% respectively (Table 3.3). The peptide containing both N145 and N155 was deamidated 2.7% (Table 3.3). For N318, only the deamidated peptide was detected (Table 3.3).

Complex 7 had a pI of ~5.8 (Figure 3.9A) and was shown to be composed of peptides derived from filensin (78%), αA (3%), serum albumin (5%), βB1 (5%) and αB (5%) (Figure 3.9B). From complex 7, a single site of αB deamidation (N146) was identified, as well as three sites of deamidation (N304, N145 and N155) and as a single site of oxidation (M207)

from filensin (Figure 3.9A). The proportion of filensin peptides deamidated at N155 and N304 was 3.5% and 56.7% respectively (Table 3.3). The peptide containing both N145 and N155 was deamidated 2.9% (Table 3.3).

Complexes 8-9 were shown to have a slightly lower mass than complexes 4-7 (~42 kDa), while having pIs similar to complex 6 and complex 7 respectively (~5.8 – 5.9) (Figure 3.9A). Complex 8 was shown to be composed of peptides derived from filensin (83%), αA (4%), βB2 (5%) and αB (5%) (Figure 3.9B). From complex 8, a single site of αB deamidation (M146) was identified, as well as four sites of deamidation (N155, N145, N304 and N318) and a single site of oxidation (M207) from filensin (Figure 3.9A). The proportion of filensin peptides deamidated at N155 and N304 was 3.7% and 42.3% respectively (Table 3.3). The peptide containing both N145 and N155 was deamidated 3.4% (Table 3.3). For N318, only the deamidated peptide was detected (Table 3.3).

Complex 9 was shown to be composed of peptides derived from filensin (71%), phakinin (2%), αA (5%), βB1 (9%) and αB (8%) (Figure 3.9B). From complex 9, five sites of filensin deamidation (N145, N155, N478, N304 and N268) were identified, as well as two sites of deamidation (N78 and N146) and single site of oxidation (M68) from αB (Figure 3.9A). The proportion of filensin peptides deamidated at N155 and N304 was 5.3% and 44.2% respectively (Table 3.3). The peptide containing both N145 and N155 was deamidated 3.3% (Table 3.3). For N478, only the deamidated peptide was detected (Table 3.3).

Complex 10 resolved as a discrete spot of ~40 kDa with a pI of ~4 (Figure 3.9A), and was shown to be composed of peptides derived from filensin (60%), phakinin (14%), αA (6%) and actin, cytoplasmic 1 (10%) (Figure 3.9B). From complex 10, two sites of filensin deamidation (N478 and N304) and two sites of phosphorylation (S488 and T450) were identified (Figure 3.9A). The proportion of filensin peptides deamidated at N155, N304 and N478 was calculated at 2%, 66.8% and 71.2% respectively (Table 3.3).

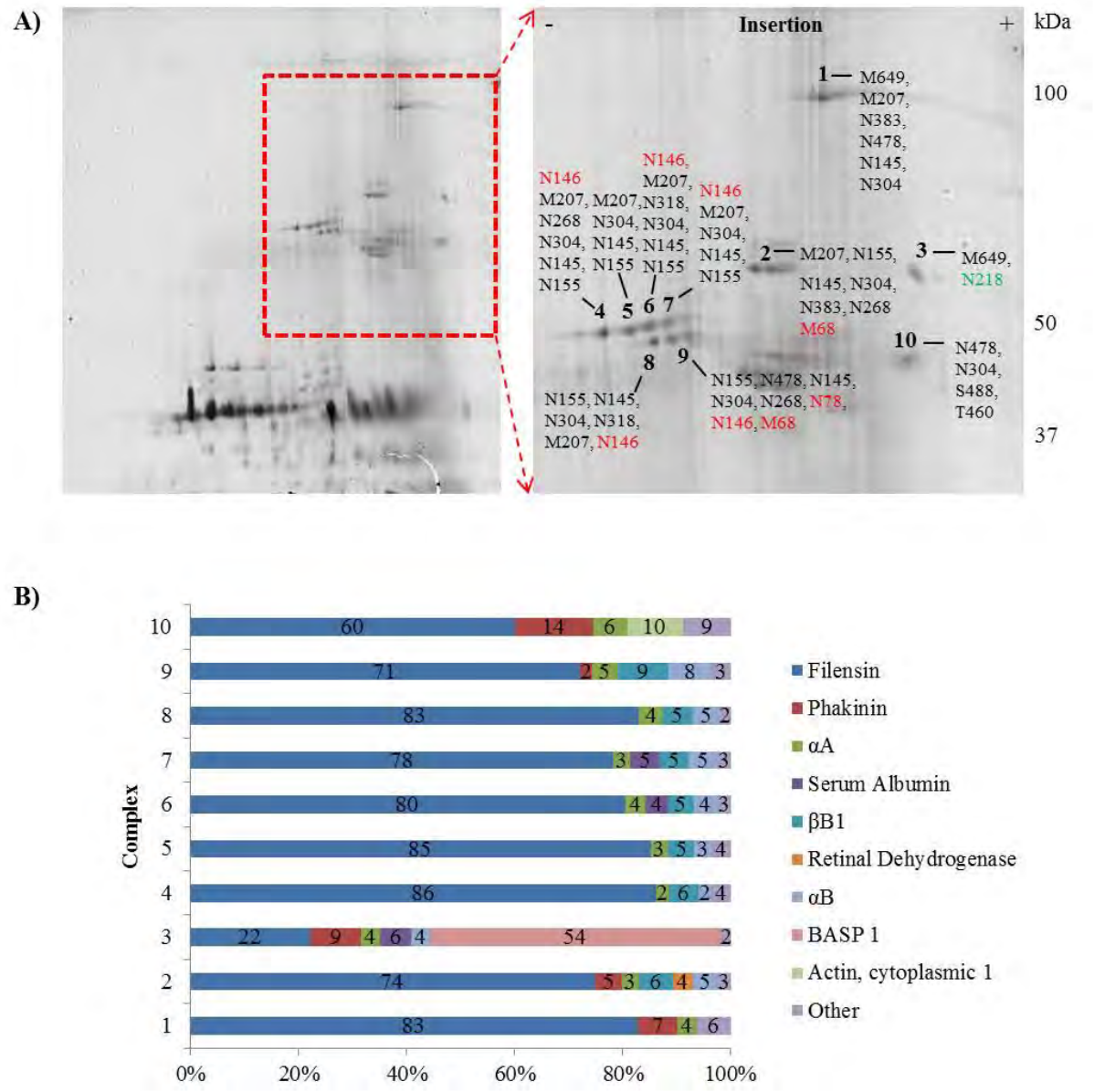

Figure 3.9: Identification of proteins and modified residues from protein complexes in the SG3 fraction from the cortex of the 77 year-old human lens. Discrete spots (labelled 1-10; inset) were excised from the gel of the SG3 fraction from the cortex of the 77 year-old lens (Figure 3.3.7), digested with trypsin and characterised using MS/MS. **(B)** Proteins that constituted ≥2% of the total peptide hits were identified for each spot by comparison with a peptide database. **(A)** Modified residues within each spot were identified for filensin (in black), αB (in red) and brain acid soluble protein 1 (BASP 1) (in green).

Table 3.3: Deamidation of filensin in crosslinked complexes (see Figure 3.9). The proportion of filensin deamidated in each 2D gel spot following tryptic digestion and analysis of peptides. Values are expressed as the amount of deamidated peptide as a proportion of the total amount of that peptide (i.e. deamidated + and non-deamidated peptide), calculated using the relative peak areas from the ion chromatograms of the mass spectra. Residues located in regions of the protein not included within the sequence coverage (i.e. cleaved regions) are indicated by a dash. Peptides that were not detected are indicated with (ND). Residues located within the same tryptic peptide are indicated with an asterisk.

Complex	N145*	N155	N145/N155*	N304	N318	N383	N478
1	7%	0%		42.2%	n.d.	100%	25.2%
2		3.8%	12.4%	34.7%	0%	100%	-
4		3.5%	2.5%	29.2%	0%	-	-
5		3.8%	2.8%	56%	0%	-	-
6		3.5%	2.7%	59.4%	100%	-	-
7		3.5%	2.9%	56.7%	ND	-	-
8		3.7%	3.4%	42.3%	100%	-	-
9		5.3%	3.3%	44.2%	ND	ND	100%
10		2%	0%	66.8%	ND	ND	71.2%

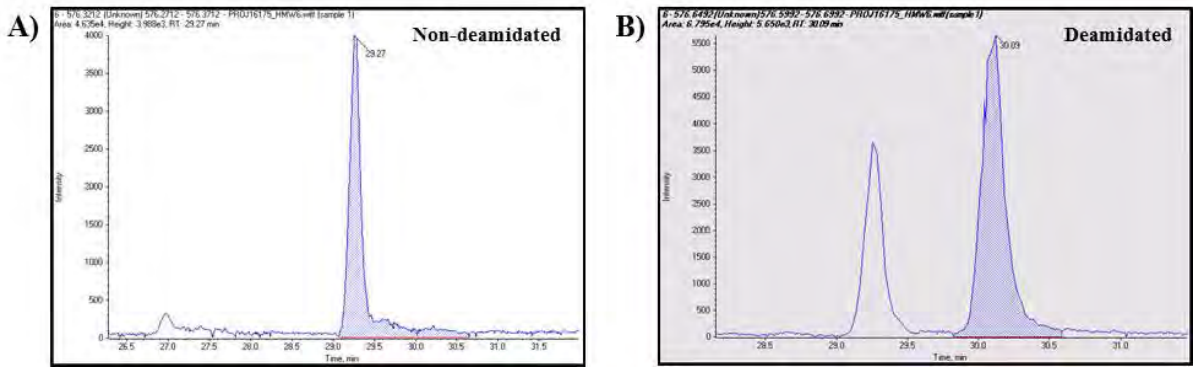

Figure 3.10: Ion chromatogram of filensin tryptic peptide 294-308 of mass 1726.9 Da. Ion chromatograms were integrated for each precursor peptide containing a deamidation site to calculate peak area for the **(A)** non-deamidated and **(B)** deamidated peptide. Relative peak area for each deamidated peptide was calculated as a proportion of total amount of peptide (i.e.deamidated + non-deamidated peptide) to calculate the percent deamidation at each site.

Chapter 3

3.4 Discussion

3.4.1 Substitution of Asp at Ser19, Ser45 and S59 of αB increases chaperone activity in a cumulative manner.

The results of this work demonstrate that at a $1_{\alpha B}$:1_{CPK} molar ratio, WT αB significantly increased aggregation of CPK (Figure 3.1A; Figure 3.2A), however this isoform suppressed aggregation when CPK was present in excess (i.e. $1_{\alpha B}$:2_{CPK} or $1_{\alpha B}$:4_{CPK}). Furthermore, the activity of αB and its ability to suppress aggregation was increased by the mutations that mimic phosphorylation (Figure 3.1). Although a trend of increased activity with an increasing number of mutations that mimic phsophorylation was observed, the only statistically significant results obtained were for the double and triple αB phosphomutants (i.e. 2P and 3P) (Figure 3.1). While the presence of 2P at a $1_{\alpha B}$:1_{CPK} molar ratio was able to inhibit aggregation of CPK by 41.9%, the addition of an extra negative charge (i.e. 3P) led to an 83.9% inhibition of CPK aggregation (Figure 3.1B). Additionally, 3P was the only phosphomutant to significantly suppress aggregation of CPK at a $1_{\alpha B}$:1_{CPK} molar ratio (Figure 3.1A). It has been postulated that multiple aspartate substitutions may induce hyperactivity of αB and that this leads to co-aggregation of the substrate and the chaperone protein under certain conditions (Aquilina *et al.*, 2004). However, Ecroyd *et al.* (2007) demonstrated that the use of buffer systems containing ammonium ions (e.g. ammonium acetate) has the ability to destabilize 3P αB, leading to co-precipitation with the substrate (although this effect is ameliorated by increases in pH). Furthermore, the addition of mutations that mimic phosphorylation and destabilization of substrate proteins have both been shown to increase αB substrate affinity (Koteiche and Mchaourab, 2003). Studies of an Δ41-58 αB mutant (a mutant form of αB where residues 41-58 have been deleted) have shown that its ability to prevent the heat-induced aggregation of fully unfolded citrate synthase is reduced compared to WTαB, however, its activity is comparable to WTαB in regards to inhibiting the aggregation of partially unfolded β_L-crystallin and alcohol dehydrogenase (Ghosh *et al.*, 2006). This may explain why some studies, such as that by Aquilina *et al.* (2004), have reported co-precipitation of αB phosphomimics with substrate proteins, i.e. destabilization of the chaperone and/or substrate increased the affinity of the interaction to the point that both proteins co-precipitate from solution.

The results of this study are consistent with previous reports that αB phosphomimics are more efficient than WTαB at protecting against stress-induced protein aggregation (Ghosh *et*

al., 2006; Ecroyd *et al.*, 2007; Ahmad *et al.*, 2008). As αB remains stable in the buffer system used for this study (i.e. PBS, pH 7.4) (Ecroyd *et al.*, 2007), it appears that the presence of mutations that mimic phosphorylation increase the chaperone activity of αB without inducing hyperactivity (Figure 3.1). These results do confirm however that αB can induce the aggregation of substrate proteins when the chaperone activity is reduced, suggesting that phosphorylation-induced increases in αB activity may be pivotal for maintaining cellular homeostasis in the lens.

To confirm that an increase in chaperone activity was the cumulative effect of multiple mutations that mimic phosphorylation and not the result of a particular single mutation, the chaperone activity of αB with single serine-to-aspartate mutations at Ser19, Ser45 and Ser59 were compared (Figure 3.2). No αB isoform with a single mutation to mimic phosphorylation was able to significantly reduce the aggregation of CPK compared to WTαB (Figure 3.2). This is consistent with the previous finding that αB isoforms with a single mutation to mimic phosphorylation have similar activity to WTαB (Aquilina *et al.*, 2004). Moreover, these results demonstrate that the significant increase in chaperone activity observed for 2P and 3P (Figure 3.1) is due to the cumulative effect of multiple serine-to-aspartate substitutions, suggesting that multiple phosphorylation events may be required *in situ* to enhance the chaperone activity of αB.

3.4.2 Loss of soluble αA and αB may involve phosphorylation

It is important to note that it has previously been shown that lens proteins are already heavily modified by early adulthood (Lampi *et al.*, 1998), therefore feotal lenses would have provided a more suitable control for this study. Unfortunately, feotal lenses were unavailable for use, therefore lenses that covered the age when barrier and cataract formation occur (41–77 years) were used.

Previous studies have reported that α-crystallin binds to fibre cell membranes with age, forming high density fractions that can be isolated using density sucrose centrifugation (Friedrich and Truscott, 2009; Friedrich and Truscott, 2010). The density profiles of this work support these findings, i.e. there is a loss of low density soluble protein coupled with an increase in high density membrane associated protein with age (Figure 3.3). This was further validated by 1D SDS PAGE, where the relative amount of bands corresponding to monomeric αA and αB (i.e. corresponding to a band of 20 kDa, labeled ‘αA’ and ‘αB’ as the

bands were not definitively identified by MS analysis) decreased in the high density samples (i.e. SG2 and SG3) from the cortex concomitant with the appearance of bands of ~40 kDa, ~55 kDa and ~100 kDa compared to the lowest density sample (i.e. SG6) (Figure 3.4). Spots with similar masses were resolved following 2D SDS PAGE of the cortical SG3 fraction, and were found to contain, among other proteins, αA and αB (Figure 3.9). This suggests that the loss of αA and αB in the cortex is a consequence of their incorporation into soluble higher molecular weight complexes. Furthermore, the relative amount of αA and αB (i.e. amount of monomeric αA and αB compared to the total protein) was decreased in nuclear SG fractions compared to cortical SG fractions (Figure 3.4). As this loss was concomitant with an increase in protein smearing that was immunoreactive to αB (Figure 3.5), this suggests that loss of αA and αB in the nucleus may be due to insolubilisation events. This is consistent with αA and αB forming soluble complexes with substrate proteins in the cortex, which later become insoluble in the nucleus. Similar to previous reports (Friedrich and Truscott, 2009; Friedrich and Truscott, 2010), αA and αB were shown to be the predominant protein species in the high density fractions i.e. SG2 and SG3 (Figure 3.4). The loss of αA or αB, whether via incorporation into complexes (i.e. in the cortex) or insolubilisation (i.e. in the nucleus) (Figure 3.4), could then potentially render the resident proteins susceptible to insolubilisation. This is supported by a recent report that showed a negative correlation between free α-crystallin levels (i.e. α-crystallin not involved in HMWCs) and the prevalence and progression of nuclear cataract (Datiles III *et al.*, 2016), suggesting that free α-crystallin loss is a phenomenon that precedes cataract in aged but otherwise healthy lenses.

When pSer19, pSer45 and pSer59 αB levels were compared across density fractions and lens regions (Figure 3.5), it was shown that pSer19 and pSer45 were elevated in low density fractions (i.e. SG5) compared to high density fractions. As this soluble state may allow higher levels of activity and substrate accessibility, it is proposed that this reflects a physiological role for these isoforms *in vivo*. A similar preference (i.e. increased levels in SG5) was shown for pSer59 αB in cortical tissue. However, pSer59 αB was elevated in high density fractions (i.e. SG2) compared to low density fractions in nuclear tissue, suggesting that phosphorylation at this site may be associated with membrane association in the nucleus. As single serine-to-aspartate substitutions were found to be insufficient to significantly affect the chaperone activity of αB (Figure 3.2), it remains unclear how the charge provided by a single phosphorylated residue could so significantly affect the behaviour of αB *in vivo*. It is

therefore likely that pSer59 works in conjunction with other phosphorylatable residues to induce hyperactivity that could lead to αB membrane association.

This is supported by data from the 2D western blots (Figure 3.6) that indicated that, although αB was more likely to be phosphorylated at Ser19 when overall phosphorylation levels were low (i.e. 1-3 phosphorylated residues), pSer59 (and to a lesser extent pSer45) were present in multiply phosphorylated species (i.e. 4-6 phosphorylated residues). This suggests that the increased ability of pSer59 to alter the membrane association of αB is a product of its tendency to be present in more multiply phosphorylated species. The reason why pSer59 and pSer45 are more often associated with highly phosphorylated species of αB while pSer19 is associated with lower overall phosphorylation levels is unclear. It is possible that phosphorylation at Ser59 or Ser45 induces structural changes that make neighbouring sites more susceptible to phosphorylation. For example, Ser59 has been shown to directly contact the β3 region of the α-crystallin domain (Jehle *et al.*, 2010) and mutations within the neighbouring region of Ser59 (Trp60-Ser66) were shown to alter oligomeric size and subunit exchange rates between αA and αB (Sreelakshmi and Sharma, 2005). Likewise, Ser45 is located within a substrate recognition and subunit interaction site (i.e. Ser41-Pro58) (Ghosh *et al.*, 2005; Ghosh *et al.*, 2006). It is therefore plausible that phosphorylation at Ser59 or Ser45 may induce subunit dissociation, resulting in exposure of otherwise occluded residues, increasing the likelihood of further phosphorylation events. As the number of phosphorylation events increases, increased exposure of binding sites caused by alterations in subunit exchange dynamics, may in turn increase chaperone activity of the protein (Ahmad *et al.*, 2008). As Ser19 lies within a substrate recognition site (Trp9-Pro20), but not a subunit interaction site (Ghosh *et al.*, 2005), it would be expected that this process would not apply to phosphorylation at this residue. Furthermore, the comparatively low number of spots corresponding to phosphorylated αB that reacted with anti-pSer19 antibody suggests that phosphorylation at Ser19 occurs early and inhibits phosphorylation of other residues, preventing the formation of multiply phosphorylated isoforms.

It was observed that the amount of multiply phosphorylated αB increased in higher density fractions such that the predominant isoforms in SG2 had 2-4 phosphate groups (i.e. spots 2-4) while only the monophosphorylated isoform (i.e. spot 4) was present in SG5 from the barrier and nucleus (Figure 3.7; Table 3.1). This further implicates multiply phosphorylated αB isoforms with the formation of high density and membrane-bound fractions. Additionally, while the amount of multiply phosphorylated isoforms was decreased in the nucleus

compared to the cortex for SG3 and SG5, multiply phosphorylated isoforms were increased in the nucleus for SG2 (Figure 3.7; Table 3.1). A similar pattern was observed for pSer59, which was elevated in the nuclear and barrier samples compared to the cortical sample for SG2 while pSer19 and pSer45 were decreased (Figure 3.5). These results again suggest a link between phosphorylation at Ser59, αB hyperphosphorylation, and in turn membrane binding. Furthermore, the fact that the increased amount of multiply phosphorylated isoforms was only observed in the nucleus of the 77 year-old lens (Figure 3.5) suggests that the switch to pathogenicity is gradual and occurs at later stages of life.

3.4.3 Deamidation and oxidation of filensin may contribute to HMWC formation

Clusters of spots between ~40-95 kDa were observed within the acidic region of SG3 and cortical SG2 2D gels (Figure 3.7; Figure 3.8). As their masses were similar to the ~40-100 kDa bands observed following 1D separation (Figure 3.4), it was inferred they represent these species. The dominant protein species for each complex (with the exception of complex 3) was filensin. Intact filensin has a mass of ~75 kDa and is known to undergo extensive truncation in the lens (Sandilands, Prescott, Hutcheson*, et al.*, 1995; Su, McArthur, Truscott*, et al.*, 2011), producing largely N-terminal fragments. As the mass of each of the complexes (with the exception of complex 1) was below 75 kDa, filensin must be present as truncated forms. No spot consistent with intact non-crosslinked filensin was present (Figure 3.9). Sequence coverage of filensin from each spot suggests that filensin undergoes truncation at both N- and C-termini, with filensin from complex 1 remaining the most intact (24-652) (Figure 3.11A). Notably, complex 1 exceeds the mass expected mass for intact filensin. Sequence coverage for complexes 3 and 10 suggests that filensin from these complexes underwent further N-terminal truncation (78-652 and 78-630 respectively), while complexes 2 and 4-9 underwent further C-terminal truncation (24-411 for complex 2, 24-362 for complexes 4-8 and 24-483 for complex 9). Others have reported cleavage of filensin in HMWCs (Srivastava *et al.*, 2004; Su, McArthur, Truscott*, et al.*, 2011). The cleavage of filensin reported here is not as extensive as that previously reported from similar HMWCs by Srivastava *et al.* (2004). For this study, peptides were detected that covered the residues 24-652 (Figure 3.11A). Srivastava *et al.* (2004) detected peptides from residues 79-239 of filensin, suggesting more extensive truncation than that observed for this study, particularly at the C-terminus.

Compared to the number of peptides detected derived from filensin, fewer peptides derived from αA were detected in each complex, and fewer peptides derived from αB (complexes 2-9) and phakinin (complexes 1-3 and 9-10) were detected in some complexes (Figure 3. 9). These proteins are well documented to interact with filensin in lens fibre cells (Carter *et al.*, 1995; Djabali *et al.*, 1997), where they assemble to form beaded-chain filaments at fibre cell membranes (Goulielmos *et al.*, 1996). Additionally, filensin is also known to act as a substrate for αB following stress (Muchowski *et al.*, 1999). The co-migration of αA and αB with filensin despite having a much smaller mass (~20 kDa) than what was observed (i.e. 40 kDa), suggests that these proteins exist together as soluble, covalently crosslinked complexes in the lens. Notably, the peptides matching to αA and αB were derived solely from the N- and α-crystallin domains of the proteins, covering the residues 12-99 for αA (Figure 3.11A) and 12-146 for αB (Figure 3.11B). This suggests that αA and αB involved in these complexes may also be N- and C-terminally truncated. This is consistent with the presence of spots corresponding to truncated αA on 2D gels from the SG2 and SG3 fractions (Figure 3.7, Figure 3.8). Sequence coverage of αA and αB also indicates that the proteins are further truncated in some complexes. Sequence coverage of αA from complexes 1, 3 and 7 indicated further C-terminal truncation (13-78, 13-65 and 13-88 respectively). Sequence coverage of αB indicated further C-terminal truncation (12-103) from complex 5 as well as N- and C-terminal truncation (75-103) from complex 3. This suggests that interaction sites and crosslinking regions for intermediate filaments lie within residues 13-65 for αA and 75-103 for αB.

A)

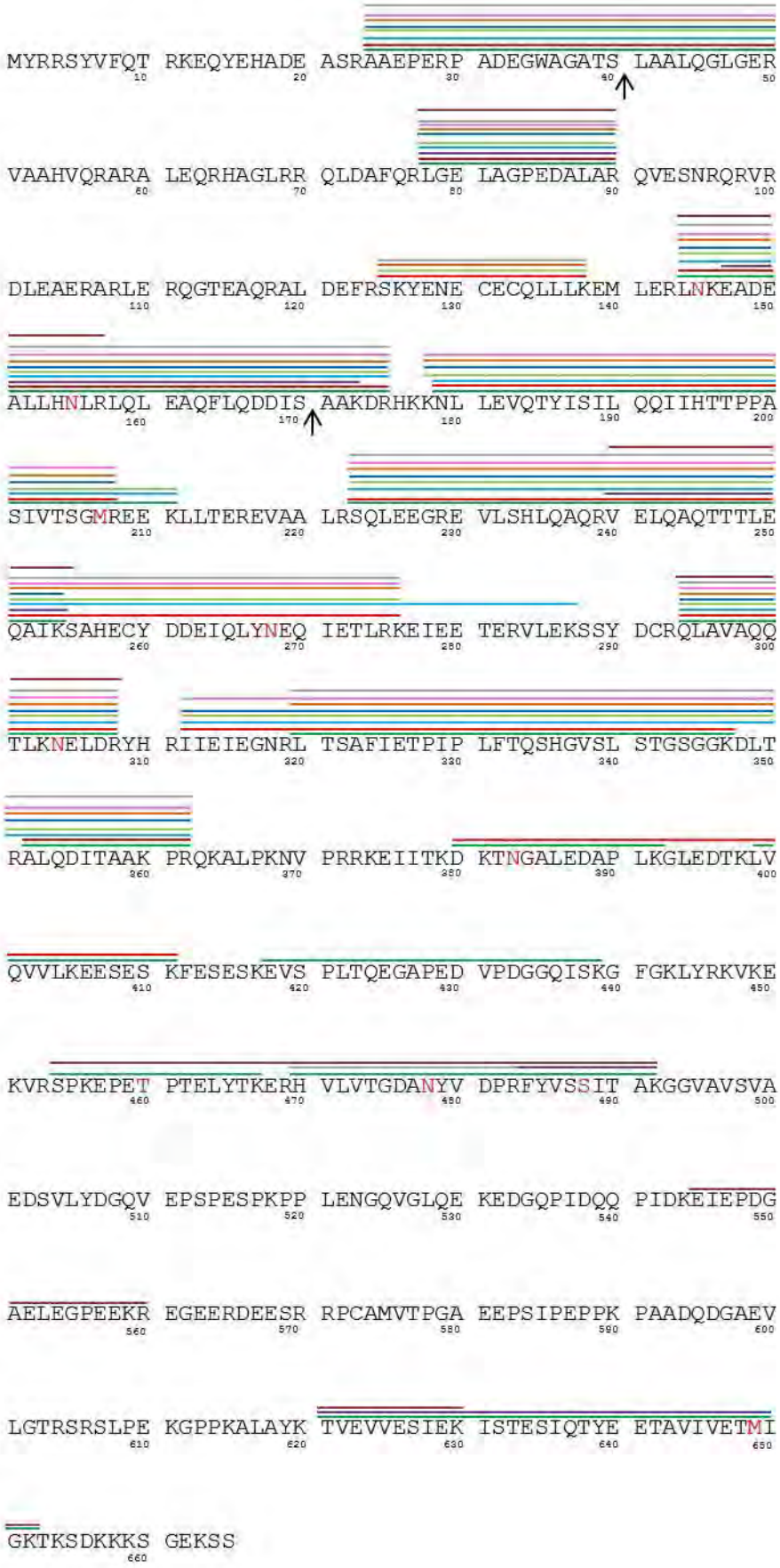
MYRRSYVFQT RKEQYEHADE ASRAAEPERP ADEGWAGATS LAALQGLGER
VAAHVQRARA LEQRHAGLRR QLDAFQRLGE LAGPEDALAR QVESNRQRVR
DLEAERARLE RQGTEAQRAL DEFRSKYENE CECQLLLKEM LERLNKEADE
ALLHNLRLQL EAQFLQDDIS AAKDRHKKNL LEVQTYISIL QQIIHTTPPA
SIVTSGMREE KLLTEREVAA LRSQLEEGRE VLSHLQAQRV ELQAQTTTLE
QAIKSAHECY DDEIQLYNEQ IETLRKEIEE TERVLEKSSY DCRQLAVAQQ
TLKNELDRYH RIIEIEGNRL TSAFIETPIP LFTQSHGVSL STGSGGKDLT
RALQDITAAK PRQKALPKNV PRRKEIITKD KTNGALEDAP LKGLEDTKLV
QVVLKEESES KFESESKEVS PLTQEGAPED VPDGGQISKG FGKLYRKVKE
KVRSPKEPET PTELYTKERH VLVTGDANYV DPRFYVSSIT AKGGVAVSVA
EDSVLYDGQV EPSPESPKPP LENGQVGLQE KEDGQPIDQQ PIDKEIEPDG
AELEGPEEKR EGEERDEESR RPCAMVTPGA EEPSIPEPPK PAADQDGAEV
LGTRSRSLPE KGPPKALAYK TVEVVESIEK ISTESIQTYE ETAVIVETMI
GKTKSDKKKS GEKSS

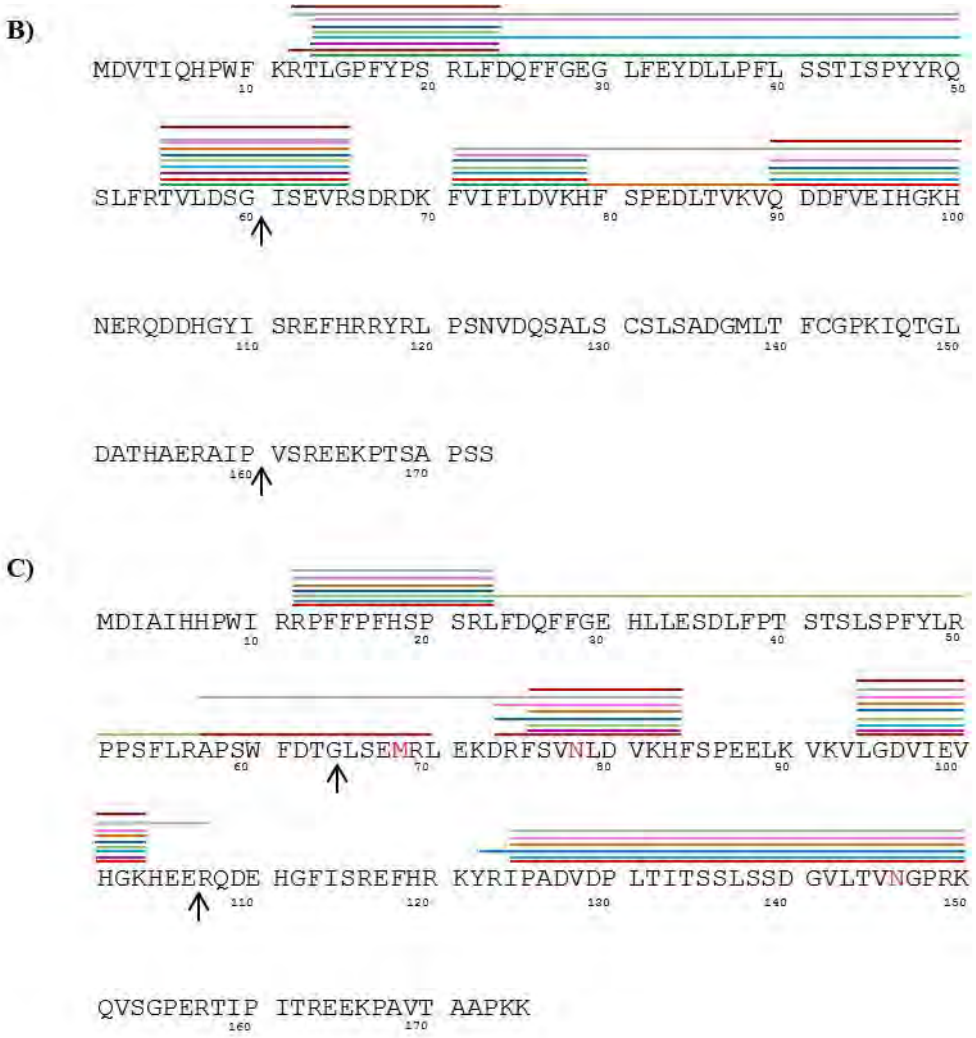

Figure 3.11: Sequence coverage of filensin. Sequence coverage of **(A)** filensin, **(B)** αA and **(C)** αB precursor peptides following tryptic digestion. Regions detected are indicated by the presence of coloured lines corresponding to each 2D spots from which the peptides were obtained: spot 1 (dark green), spot 2 (red), spot 3 (purple), spot 4 (light blue), spot 5 (light green), spot 6 (dark blue), spot 7 (orange), spot 8 (pink), spot 9 (grey) and spot 10 (brown). Modified residues are highlighted in red. Boundaries of the head (1-40), rod (41-320) and tail (321-665) domains of filensin, and the N- (1-60 and 1-64 respectively), ACD (61-160 and 65-156 respectively) and C-terminal (161-173 and 157-175 respectively) domains of αA and αB are marked with arrows.

Low levels of actin (complex 10), serum albumin (complex 3 and complexes 6-7), retinal dehydrogenase (complex 2) and βB1-crystallin (complex 2 and complexes 4-9) were also observed in some complexes (Figure 3.9B). To our knowledge, these proteins have not been previously reported to associate with filensin. Complex 3 is unusual in that BASP 1, not filensin, was the major component (Figure 3.9). BASP 1 is a membrane protein that has been detected in the brain (Mosevitsky, 2005), axonal termini, testis, kidney, spleen, thymus (Mosevitsky *et al.*, 1997) and, more recently, in the lens (Bagchi *et al.*, 2008; Truscott *et al.*, 2011). In the lens, BASP 1 is most abundant in the cortex, where it has been suggested to be involved in membrane deformation and the formation ball and socket joints (Wenke *et al.*, 2016). Although it has a reported mass of ~23 kDa (Mosevitsky *et al.*, 1997), in this study it migrated to a distance corresponding to a protein of α55 kDa (Figure 3.9). Although this may indicate crosslinking of the protein, BASP 1 has been reported to show retarded migration patterns on SDS PAGE gels caused by interactions with non-ionic detergents (Mosevitsky *et al.*, 1997). The abnormal migration pattern of BASP 1 in this study is therefore unlikely to be caused exclusively by protein crosslinking. The presence of these complexes in a high density fraction (i.e. SG3), and the high levels of membrane associated proteins (i.e. filensin, phakinin, actin and BASP1), suggests that the spots may be derived from soluble HMWCs that had localised at fibre cell membranes (Chandrasekher and Cenedella, 1997; Cobb and Petrash, 2002b; Friedrich and Truscott, 2009).

High molecular weight complexes have been reported in lens extracts previously, occurring from a young age (Srivastava *et al.*, 2004; Su, McArthur, Truscott*, et al.*, 2011) and increasing in abundance and complexity with age (Srivastava *et al.*, 2004). Su *et al.*(2011) reported complexes composed exclusively of crosslinked crystallin proteins in the water-soluble fraction of human lenses. Previously, Srivastava *et al.* (2004) reported complexes in the urea-soluble fractions of human lenses formed by crystallin proteins, predominantly αA, along with lower levels of intermediate filament proteins. As intermediate filaments were only detected in complexes from lenses over 25 years of age, it was suggested that the incorporation of intermediate filaments into such complexes is age-related (Srivastava *et al.*, 2004). In contrast, this study reports filensin as the predominant protein component of crosslinked complexes, with lower levels of αA (Figure 3.9). However, as Srivastava *et al.* (2004) were unable to resolve discrete HMW spots in lenses older than 41 years-old, it is possible that the increased incorporation of filensin reported here is a continuation of this age-related process. Srivastava *et al.* (2004) also identified modifications to αA, including C-

terminal truncation, oxidation, conversion of serine to DHA and formylation, suggesting that modified αA (particularly oxidised and DHA-containing αA) contributes to the formation of HMWCs by mediating crosslink formation (Srivastava *et al.*, 2004). In the current study, no modifications to αA were identified (Appendix 3). However, filensin was observed to be heavily deamidated (Figure 3.9), suggesting that modified filensin (particularly deamidated filensin) may be more highly involved in complex formation. It is important to note that a limitation of 2D SDS PAGE analysis is bias regarding which proteins are able to penetrate the different dimensions of the gel. Although the effect of this is perhaps ameliorated by the fact the complexes appear crosslinked, it is possible that proteins exist as part of these complexes *in situ* that were not able to be detected.

There have been few reports of how filensin is modified in human lenses. Wilmarth *et al.* (2006) reported extensive deamidation (i.e. 23 sites), as well as a single phosphorylation site (S5), two sites of pyroglutamic acid formation (Q71 and Q294) and five sites of carbamylation (V51, L144, E230, Q294 and S607). Su *et al.* (2011) observed truncation of filensin, reporting products of 60 kDa, 53 kDa, 43 kDa and 24 kDa, predominantly in urea soluble fractions. In the current study, seven previously identified sites of deamidation were observed (N145, N155, N304, N318, N383, N478) as well as a previously unreported site, N268 (Figure 3.9A). The most abundant site of deamidation was N304, with between 29.2-66.8% of this residue deamidated in the complexes studied in this work (Table 3.3). Whilst the high degree of deamidation at this site suggests that deamidation at this residue is involved in complex formation, the degree of deamidation did not directly correlate with the size of the complex, i.e. the amount of deamidation did not increase correspondingly with the mass of the complex (Figure 3.9, Table 3.3). Residue N304 lies within the rod domain of the protein (Hess *et al.*, 1998), a region of intermediate filament proteins are highly conserved and predominantly composed of α-helices (Hess *et al.*, 1998). As deamidation typically requires a high level of conformational flexibility to occur (Paranandi *et al.*, 1994; Kosky *et al.*, 1999; Hooi *et al.*, 2012; Truscott and Friedrich, 2016), the high degree of deamidation in this region may suggest that filensin is, at least partially, unfolded in the lens. Other filensin residues with a high degree of deamidation were N383 (100%) and N478 (25.2-100%) (Table 3.3), both of which are positioned within the tail domain of the protein. Although having a high proportion of these residues deamidated when present in complexes, including those with a higher molecular mass (i.e. complexes 1 and 2), N383 and N478 were often not detected in the complexes. This is most likely due to C-terminal truncation of filensin.

Deamidation at N318 was only detected in filensin from complexes 6 and 8, although in these complexes it was always deamidated (100%) (Table 3.3). Spots 6 and 8 co-migrated in the first dimension on the 2D gel, but were separated in the second dimension, demonstrating that they differ in mass (Figure 3.9A). This suggests they correspond to truncated forms of the same isotype. However, as the sequence coverage was identical for both following tryptic digestion, it cannot be determined where the truncation site is located. Additionally, as the mass of these complexes does not vary substantially from the other complexes identified in which N318 was not deamidated (i.e. complexes 4-5, 7 and 9), it is unclear how this residue is involved in complex formation. With regards to residues N145 and N155, these were often located on the same peptide, which made it difficult to determine the exact site of deamidation. However, as the proportion of deamidation was consistently low for this peptide in each complex (Figure 3.3), it is unlikely that deamidation at these two residues plays an important role in complex formation.

Notably, in a previous study, 14 of the deamidation sites identified were found to be at glutamine residues (Wilmarth *et al.*, 2006). This is unusual as asparagine residues are known to be deamidated much more readily than glutamine residues due to energetic stability of the succinimide intermediate compared to the glutaminide intermediate (Wright, 1991; Robinson, 2002; Robinson and Robinson, 2004a; Hains and Truscott, 2010). This may suggest that filensin has a tertiary structure that favours glutamine deamidation. However, in contrast, in this work there was a strong preference towards deamidation of asparagine residues (Figure 3.9A). This is in accordance with previous research that indicated that asparagine residues of αB undergo deamidation at 3-fold the rate of glutamine residues in aged human lenses (Hains and Truscott, 2010). However, the possibility that deamidated asparagine residues were more readily detected than glutamine by the selected treatment and analysis procedure cannot be excluded. A slight preference was shown for deamidation of residues within the rod domain of the protein, with 5 of the 8 potential deamidation sites being found to be deamidated in this work compared to 2 of the 4 potential deamidation sites in the tail domain being observed. Interestingly, no deamidation was detected in the head domain of filensin, although this is likely to be due to the absence of asparagine residues in this region, in addition to N-terminal truncation (Figure 3.11A).

The rod domain of filensin, together with phakinin form the beaded-chain filament, localising at fibre cell membranes in the outer cortex before becoming distributed in the cytoplasm in the inner cortex, while the tail domain remains localised at the membrane (Sandilands,

Prescott, Carter*, et al.*, 1995; Oka *et al.*, 2008). As deamidation is able to induce structural changes including partial protein unfolding (Kim *et al.*, 2002; Flaugh *et al.*, 2006; Hains and Truscott, 2010; Lampi *et al.*, 2014; Soulby *et al.*, 2015; Takata and Fujii, 2015), it is possible that the high degree of deamidation in these complexes, together with any previous unfolding that contributes to deamidation in this domain, enables filensin to recruit proteins, including αB, from the cytoplasm, forming HMWCs that localize at fibre cell membranes. Alternatively, high levels of deamidation of cytoplasmic filensin may induce further membrane association of the protein, which may account for the presence of the complexes in the barrier and nuclear regions of the 77 year-old lens (Figure 3.7).

Although filensin from each complex had between 2-5 deamidated sites, no obvious pattern was observed between migration rate and extent of either deamidation or phosphorylation. Nor was there any observed pattern that was dependent on the protein composition, other than a decrease in pI induced by the presence of phakinin (Figure 3.9A). Two sites of phosphorylation of filensin previously reported by Wang *et al.* (2013) were also observed in this study (i.e. S488 and T460). This work also identified two oxidation sites (M649 and M207) in complexes 1-7 (Figure 3.9A). To our knowledge, this is the first report of oxidation of filensin in lens tissue. Two oxidised residues in filensin were identified in complex 1, which had a molecular mass of ~95 kDa, whereas only single oxidized residues were identified in complexes 2-7 which had masses of ~45 kDa (Figure 3.9A). This 2-fold increase in mass observed for complex 1 is probably explained by less truncation of the C-terminal residues (as evidenced by increased sequence coverage). However, as the spots were digested with trypsin, and there was no consistent pattern between sequence coverage and complex size for the other complexes, and it is not possible to establish this definitively. Moreover, as the increase in sequence coverage was not sufficient to account for a 2-fold increase in mass, it is possible that increased oxidation contributes to a greater degree of crosslinking and hence higher molecular weight complexes. However, it should be noted that oxidation of methionine can take place artifactually.

A single oxidation site was observed for αB (M68) but did this not appear to correlate with migration patterns of the proteins i.e. did not correlate with increased mass or pI of the complexes (Figure 3.9A). Oxidation of lenticular proteins has repeatedly been found to be increased in cataractous lenses and in insoluble lens fractions (Garner and Spector, 1980; Lund *et al.*, 1996; Boscia *et al.*, 2000; Hanson *et al.*, 2000). As oxidation can induce protein crosslinking, the increase in mass observed for complex 1 (Figure 3.9A) could be due to

increased levels of protein crosslinks between filensin and other proteins in the complex, or an increased rate of protein recruitment from the cytoplasm. Despite the common assertion that oxidation and oxidative damage is the direct factor leading to cataract formation (Truscott, 2005), relatively little is known about the factors that contribute to the oxidative environment of the lens. To more fully comprehend the exact mechanism behind cataract formation, this needs to be further investigated.

3.5 Conclusion

It is apparent that phosphorylation may be necessary to maintain chaperone activity of αB. However, increased levels of multiply phosphorylation αB in high density lens fractions and in the nuclear region of aged lenses offers an insight into a potentially pathogenic role for the phosphorylated protein. Although αB participates in complexes that localise at fibre cell membranes, how this may be regulated by phosphorylation and how this may be involved in cataract formation remains to be elucidated. However, as deamidation of several sites of filensin was a consistent feature of the HMWCs analysed in this chapter, this suggests that deamidation and potential partial unfolding of intermediate filaments, particularly filensin, is an important factor in recruiting αB and phosphorylated αB to fibre cell membranes. This would then result in an overall loss of non-complexed αB, reducing the ability of αB to maintain the solubility of protein complexes in the lens, ultimately contributing to cataract formation. In this chapter, we propose that the barrier region of the lens acts a transition zone between the cortex and the barrier, characterised by an increase in αB phosphorylation, complex formation and membrane binding, the onset of which is potentially an important step in cataract formation.

Chapter 4

Investigation of αB association with fibre cell membranes

Chapter 4

4.1 Introduction

It is generally accepted that the accumulation of oxidative damage of lenticular proteins is the direct cause of nuclear cataract formation, resulting in protein crosslinking and aggregation (Truscott, 2005). Early stage cataractous lenses have been shown to have higher levels of oxidative stress compared to healthy lenses (Li *et al.*, 2009). Higher rates of oxidation were also observed in membrane fractions from cataractous (Garner and Spector, 1980) and diabetic lenses (Boscia *et al.*, 2000) compared to healthy lenses, and higher rates of αA oxidation and protein crosslinking has been observed in insoluble protein fractions compared to soluble fractions (Lund *et al.*, 1996).

The burden of oxidative damage in the lens is generally minimised by high concentrations of reduced GSH. However, the GSH concentration decreases in the nucleus of lenses prior to cataract formation (Reddy and Giblin, 1984; Giblin, 2000; Truscott, 2005). Some contention surrounds the mechanism of GSH loss. It has been proposed that the breakdown of the redox cycle responsible for keeping GSH in its reduced form (Giblin, 2000), or the loss of activity of enzymes involved in GSH production i.e. glutathione synthetase and γ-glutamylcysteine synthetase (Rathbun *et al.*, 1993), may be involved. As GSH is synthesised in the cortex and is dependent on pore proteins for transport into the nucleus, an alternative hypothesis stipulates that the presence of an impediment to GSH transport may be responsible (Sweeney and Truscott, 1998).

This phenomenon was first observed by Sweeney and Truscott (1998), following the incubation of human lenses in [^{35}S] cysteine to mimic GSH transport. Although [^{35}S] cysteine diffused uniformly throughout the nucleus of the young lenses, diffusion was restricted to the cortex of aged lenses (Sweeney and Truscott, 1998). Notably, this point of obstruction was consistent between lenses, and coincided with the sclerotic zones as well as the point where GSH levels decrease dramatically in cataractous lenses (Sweeney and Truscott, 1998). This suggests that a physical barrier at the interface of the cortical and nuclear regions, known as the nucleocortical barrier, is responsible for the loss of GSH in the nuclear region of aged lenses (Sweeney and Truscott, 1998). This was later supported by Moffat and Pope (2002), who reported a similar deficit in the transport of water into the nucleus of aged lenses. It is not currently clear how or why this barrier forms, although explanations such as changes in sphingolipid distribution have been proposed (Deeley *et al.*, 2010). Alternatively, is has been proposed that the age-related membrane-binding of proteins, largely α-crystallins, may be

responsible for this impediment, obstructing pore proteins to prevent the transport of GSH as well as water (Cobb and Petrash, 2002b; Friedrich and Truscott, 2009; Friedrich and Truscott, 2010). However, the mode of α-crystallin association with fibre cell membranes has not been elucidated; it is unclear as to whether membrane association is mediated by αB interaction with membrane phospholipids, or with membrane pore proteins (e.g. Cx46 and AQP0).

Although αA and αB have been shown to protect AQP0 against thermal stress *in vitro* (Swamy-Mruthinti *et al.*, 2013) and to interact with AQP0 following co-transfection into HeLa cells (Liu and Liang, 2008), direct interactions between αB and AQP0 *in situ* are yet to be reported. To our knowledge, αB has not been previously reported to interact with Cx46 in human lenses. However, if interactions between αB and AQP0 and/or Cx46 *in situ* can be confirmed, this would provide evidence that αB contributes to barrier formation by mechanically blocking the transport of GSH from middle age onwards. This chapter describes work aimed at mapping the membrane association of αB isoforms across aged human lens sections, and to determine what, if any, effect phosphorylation has on its membrane association. Additionally, interactions between αB isoforms and AQP0 and Cx46 were mapped across aged human lens sections in order to determine how αB membrane association may contribute to barrier formation.

4.2 Experimental Rationale

Determination of the distribution and membrane association of αB in the lens has often involved techniques that necessitate tissue homogenisation such as electrophoresis and MS, inevitably leading to loss of spatial integrity of the tissue. To overcome this, immunoconfocal microscopy was utilised to detect αB isoforms, and to visualise (with fine detail) its subcellular distribution across intact human lens sections (sections 2.3.1 and 2.3.2). The putative location of the nucleocortical barrier i.e. the point at which membrane association would be expected to peak if involved in barrier formation, was determined based on the previous study by Sweeney and Trucsott (1998) that reported that diffusion becomes obstructed 0.5-1 mm in from the periphery of the lens.

Chapter 4

Potential interactions between two or more proteins have traditionally been identified through methods such as co-immunoprecipitation or co-localisation experiments. These technologies however have limitations. For example, co-immunoprecipitation involves tissue homogenisation that results in a loss of spatial detail and can introduce artefactual protein interactions. Additionally, conventional microscopy techniques used for co-localisation experiments can only localise proteins to an accuracy of 200 nm. Information relating to direct protein interactions is therefore limited. By utilising a commercially available proximity ligation assay kit (Duolink®, Sigma, USA), this study was able to detect likely direct interactions between αB isoforms (i.e. total, pSer19 and pSer59), and AQP0 or Cx46 (section 2.3.1 and 2.3.3). Proximity ligation assays involve labelling two proteins of interest with antibodies with attached short oligonucleotides. These oligonucleotides anneal when in close proximity (i.e. ≤40 nm), and with the addition of polymerase, ligase and fluorescently-labelled nucleotides, produce a fluorescent product able to be detected using confocal microscopy (Figure 4.1)

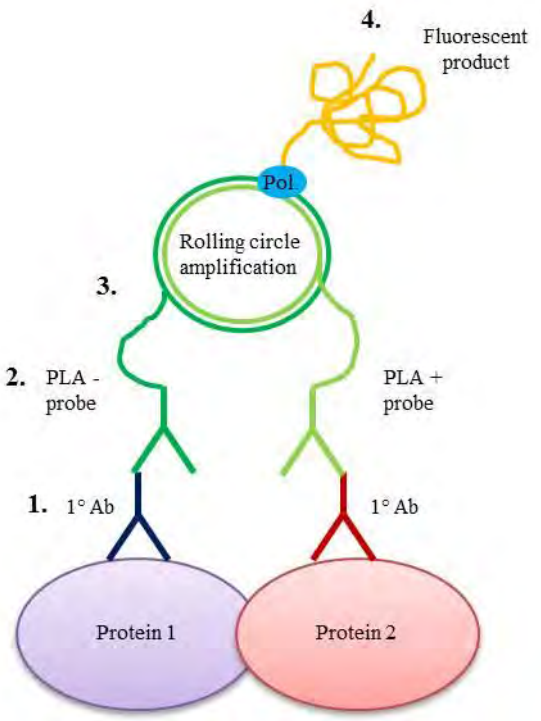

Figure 4.1: Summary of proximity ligation assay protocol. 1. Two proteins of interest are labelled with primary antibodies derived from two different species. 2. PLA + and PLA – probes with attached oligonucleotides bind the primary antibodies. 3. The addition of ligase anneals oligonucleotides forming a circle. 3. The addition of polymerase causes rolling circle amplification of annealed oligonucleotides. 4. Amplification results in fluorescent produced able to be detected via fluorescent microscopy.

As the reaction only proceeds when the proteins of interest are within 40 nm of each other, a signal is only produced when the proteins are in close enough proximity for direct interaction and therefore interaction is highly likely. Furthermore, as the fluorescent product is produced through an amplification reaction, the assay is highly sensitive (i.e. able to detect relatively low levels of interaction *in situ*), with each signal representing a single interaction. This method was selected as it maintains spatial integrity of the tissue while indicating possible interactions based on proximity of the proteins of interest with higher resolution than other co-localisation techniques. As pSer19 and pSer59 of αB were previously found to be associated with low and high levels of total phosphorylation respectively (section 3.3.2), they were selected for use in this study in order to compare the effect of phosphorylation on membrane association. AQP0 and Cx46 were selected due to their reported roles in water (Gorin *et al.*, 1984) and GSH transport (Slavi *et al.*, 2014) respectively.

4.3 Results

4.3.1 Phosphorylated αB becomes predominantly membrane associated by 500 µm in from the outside of the lens.

Human lens tissue sections were labelled for pSer19, pSer45 and pSer59 αB and imaged using confocal microscopy in order to map phosphorylated αB (pαB) membrane association throughout the lens. Each αB phosphoisoform was found to associate with fibre cell membranes, with the extent of association increasing towards the nucleus of the lens (Figure 4.2Ai-iii, v-x, B). Zones of membrane interaction were identified based on degree of membrane association of αB. In the outer ~150 µm of the sections (zone 1), each of the αB phosphoisoforms were distributed in the cytoplasm (Figure 4.2B). In the region ~150-500 µm in from the periphery of the lens (zone 2), each αB phosphoisoform was partially membrane associated (Figure 4.2B). In the region starting from ~500 µm from the periphery and continuing towards the centre (i.e. ~5 mm from the periphery, zone 3), each αB phosphoisoform was completely membrane associated with minimal amounts being distributed in the cytoplasm (Figure 4.2B). Non-specific binding of secondary antibodies was tested for by labelling a tissue section with rabbit IgG. Minimal background staining was detected (Figure 4.1 iv).

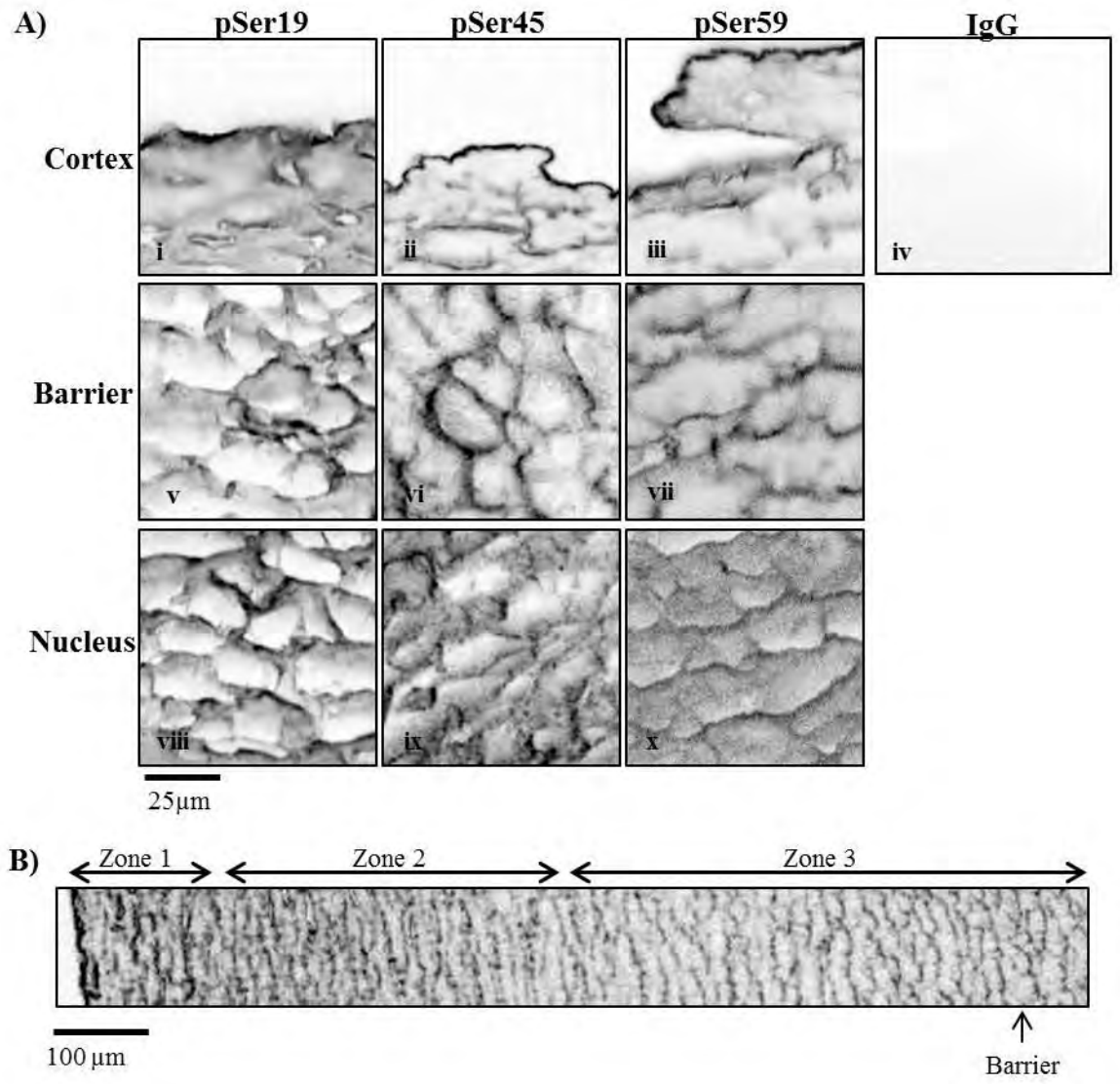

Figure 4.2: Localisation of pαB at fibre cell membranes in human lenses. Sections were obtained from a 63 year-old human lens using a cryostat and labelled with rabbit anti-pSer19, pSer45 or pSer59 αB antibodies. A separate section was labelled with rabbit IgG for use as a negative isotype control. Alexa-488 conjugated goat anti-rabbit antibody was used to visualize sections by confocal microscopy. **(A)** Images were obtained from the periphery (cortex), 1 mm inside the periphery (barrier) and the centre (nucleus) of each section. **(B)** Tiled images were obtained of the outer 1.1 mm of each section (pSer59 shown). Zones of cytosolic pαB distribution (zone 1), partial membrane association (zone 2), complete membrane association (zone 3), and putative location of the nucleocortical barrier were identified and marked.

4.3.2 αB and phosphorylated αB associate directly with membrane pore proteins AQP0 and Cx46.

It was previously shown that pαB becomes predominantly associated with cell membranes as the cells are located closer to the lens nucleus (section 4.3.1). This association could involve interactions with phospholipids or membrane pore proteins. To investigate this aspect further, proximity ligation assays were performed on human lens sections from a 62 year-old lens using a Duolink® labelling kit to visualise and map interactions between αB, pSer19 and pSer59 αB, and AQP0 across the lens. Direct interactions between each αB isoform and AQP0 were detected. The majority of interactions occurred in the outer 500 μm of the lens with the incidence of interaction decreasing towards the nucleus (Figure 4.3Ai-iii, C). Interactions between AQP0 and total αB (i.e. αB) were abundant in the outer cortex (Figure 4.3A, C). At a discrete point, ~500 μm from the lens periphery, the number of interactions decreased dramatically compared to the outer cortex (Figure 4.3C). Interactions between AQP0 and total αB continued to gradually decrease from this point towards the nucleus, where interactions were sparse (Figure 4.3Ai-iii, C).

Interactions between AQP0 and pSer19 αB were minimal throughout the lens section (Figure 4.3iv-vi, C), with a slightly higher number of interactions occurring in the outer cortex (i.e. the outer 500 μm) (Figure 4.3Aiv).

Interactions between AQP0 and pSer59 αB were abundant in the outer cortex (Figure 4.3Avii, C). At a discrete point, ~500 μm from the lens periphery, the number of interactions decreased dramatically compared to the outer cortex, similar to that observed for total αB (Figure 4.3C). From this point, interactions between AQP0 and pSer59 αB were sparse and changed little in abundance towards the nucleus (Figure 4.3C).

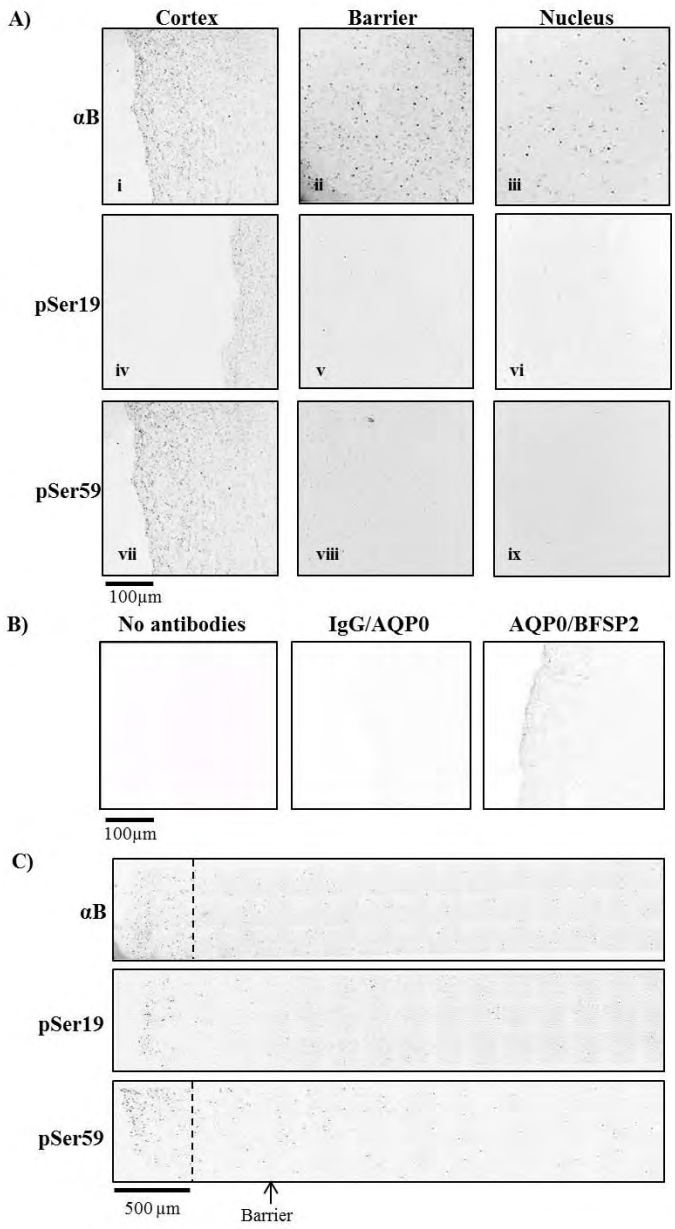

Figure 4.3: Direct association of αB with AQP0. Sections were obtained from a 62 year-old human lens using a cryostat and co-labelled with rabbit anti-αB, pSer19 or pSer59 αB and goat anti-AQP0 antibody. Separate sections were incubated with TBST (no antibodies) or goat anti-AQP0 and rabbit IgG for use as negative controls, or goat anti-AQP0 and rabbit anti-BFSP2 for use as a positive control. A Duolink® assay kit was used to detect interactions, and sections were visualised by confocal microscopy. **(A)** Images were obtained from the periphery (cortex), 1 mm inside the periphery (barrier) and the centre (nucleus) of each section. **(B)** Control images were obtained from the periphery (cortex). **(C)** Tiled images were obtained of the outer 4 mm of each section. The putative location of the nucleocortical barrier is indicated, and a dashed line is used to indicate where signal decreases.

Chapter 4

Proximity assays were performed on human lens sections from a 62 year-old lens using a Duolink® labelling kit to visualise and map interactions between αB, pSer19 and pSer59 αB, and Cx46 across the lens. Direct interactions between each of the αB isoforms and Cx46 were detected. The majority of interactions occurred in the outer 250 µm of the lens with the incidence of interaction decreasing towards the nucleus (Figure 4.4B). Interactions between Cx46 and total αB (i.e. αB) or pSer19 αB were minimal throughout the lens section, with a slightly higher number of interactions occurring in the outer cortex (i.e. the outer 250 µm) (Figure 4.4A, B). By contrast, interactions between Cx46 and pSer59 αB were abundant in the outer cortex (Figure 4.4A, B). At a discrete point, ~250 µm from the lens periphery, the number of interactions between Cx46 and pSer59 decreased dramatically compared to the outer cortex (Figure 4.4B). From this point, interactions between Cx46 and pSer59 αB decreased gradually in abundance towards the nucleus (Figure 4.4B).

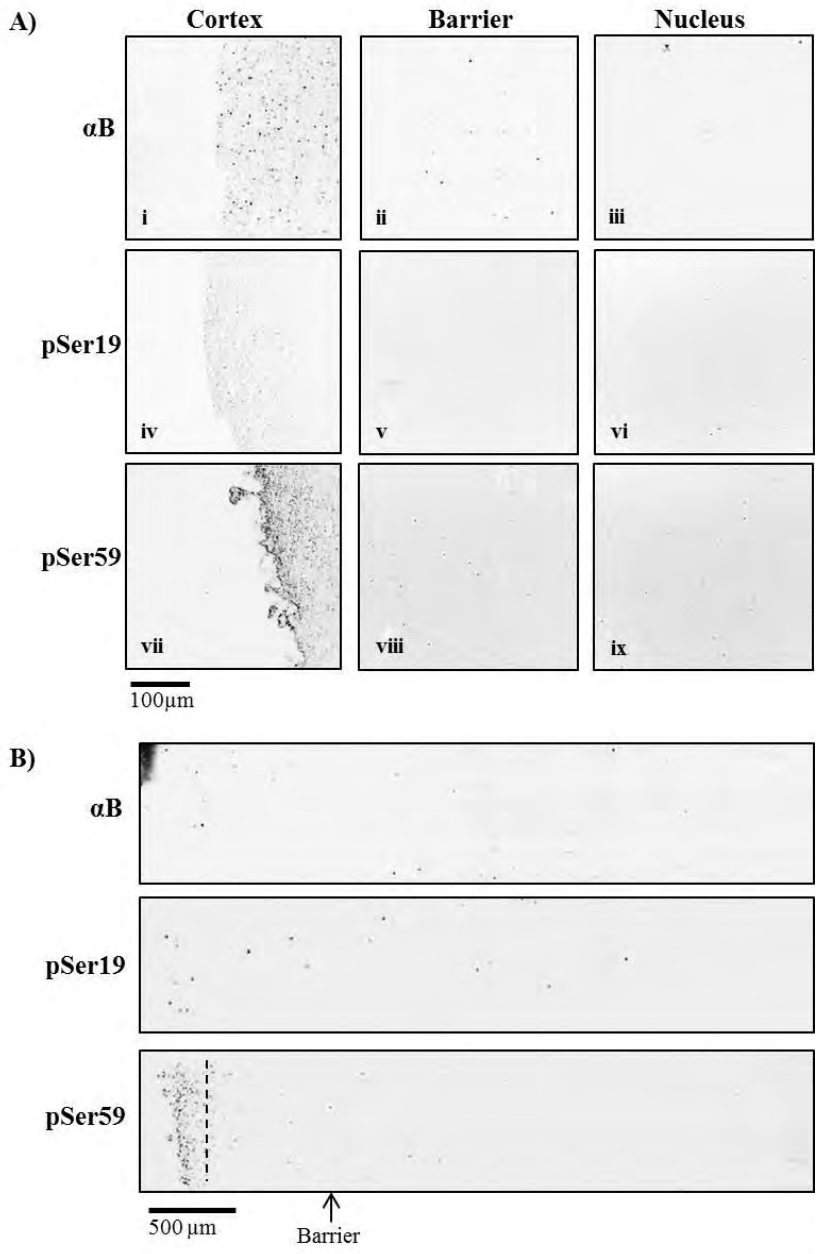

Figure 4.4: Direct association of αB with Cx46. Sections were obtained from a 62 year-old human lens using a cryostat and co-labelled with rabbit anti-αB, pSer19 or pSer59αB and goat anti-Cx46 antibody. Separate sections were incubated with TBST (no antibodies) or goat anti-AQP0 and rabbit IgG for use as negative controls, or goat anti-AQP0 and rabbit anti-BFSP2 for use as a positive control. A Duolink® assay kit was used to detect interactions, and sections were visualised by confocal microscopy. **(A)** Images were obtained from the periphery (cortex), from 1 mm inside the periphery (barrier) and the centre (nucleus) of each section. **(B)** Tiled images were obtained of the outer 4 mm of each section. The putative location of the nucleocortical barrier is indicated with an arrow, and a dashed line is used to indicate where signal decreases. See Figure 5.3 for control images.

Chapter 4

4.4 Discussion

4.4.1 αB and phosphorylated αB membrane-binding coincides with location of barrier

To determine whether the association of phosphorylated or non-phosphorylated isoforms of αB with fibre cell membranes may be involved in the formation of the nucleocortical barrier, aged human lens sections were labelled for the pSer19, pSer45 and pSer59 αB isoforms, and cellular distribution was visualised across lens sections. Each of the phosphorylated αB isoforms tested were found to associate with fibre cell membranes (Figure 4.2A), and all followed a similar pattern of distribution. The association patterns occurred in three zones (zones 1-3) throughout the coronal cross section of the lens, with the extent of membrane association increasing towards the nucleus (Figure 4.2). Complete membrane association of αB occurred from a point ~500 μm interior to the periphery of the lens and continued towards the centre (i.e. zone 3) (Figure 4.2B). Notably, Sweeney and Truscott (1998) observed that the diffusion of [^{35}S] in aged human lenses was abruptly disrupted at a point ~500 μm in from the periphery of the lens. This point, which indicated the presence of a physical barrier to diffusion (Sweeney and Truscott, 1998), approximately coincides with the location of zone 3 in this study (Figure 4.2B), suggesting that large-scale membrane association of phosphorylated αB may be implicated in barrier formation. This is consistent with previous results from 2D gels that indicated that α-crystallin was the predominant protein to associate with fibre cell membranes, the majority of which was phosphorylated (Friedrich and Truscott, 2010).

As only lenses of a narrow age range were analysed, it cannot be confirmed whether the location of these zones change with age. However, as it is likely that the distribution pattern is the result of an age-related process that begins at the newly deposited cells at the lens periphery, it is likely that the zones remain at a consistent distance from the periphery, similar to the barrier region described by Sweeney and Truscott (1998).

4.4.2 αB and phosphorylated αB associates directly with membrane pore proteins AQP0 and Cx46

To determine whether interactions with membrane proteins may be responsible for αB membrane association, proximity ligase assays were performed on aged human lens sections to visualize interactions between αB isoforms (total, pSer19 and pSer59 αB), and AQP0 and Cx46 across the lens cross section. Each of the αB isoforms tested gave results consistent

with interaction with AQP0 (Figure 4.3) and Cx46 (Figure 4.4) at fibre cell membranes. These interactions occurred preferentially in the cortex; interactions involving AQP0 were largely restricted to the outer 500 μm of the cortex (Figure 4.3C) and interactions with Cx46 predominantly occurred in the outer 250 μm of the cortex (Figure 4.4B). This distinct pattern was more pronounced for interactions involving pSer59 αB than for pSer19 αB, for which interactions were minimal throughout the lens section. As it was previously shown that pSer59 is more common in multiply phosphorylated αB species compared to pSer19 (section 3.3.2), this may suggest that the presence of multiple phosphorylated residues in αB may increase its interaction with AQP0 and Cx46. This may be due to structural changes induced by phosphorylation, that act to increase substrate affinity (Aquilina *et al.*, 2004). Alternatively, as it was previously suggested that pSer19 may inhibit phosphorylation at other residues in αB (section 3.4.2), it is also conceivable that pSer19 decreases αB membrane binding capacity. Further membrane binding assays are required in the future to further elucidate the mechanism by which αB associates with membrane proteins.

The lens regions where interactions were most abundant (i.e. outer 500 μm for AQP0 and outer 250 μm for Cx46), coincide with zones 2 and 3 (Figure 4.2B). These are the same regions in which the association of phosphorylated αB isoforms with membranes increases. Together, this suggests that the αB membrane association observed in this region is mediated by interactions with AQP0 and Cx46, or that αB co-localises with Cx46 and AQP0 due to association with the fibre cell membrane such that it is in very close proximity to the membrane proteins. As this region also coincides with the putative location of the nucleocortical barrier (Sweeney and Truscott, 1998), it is likely that interactions between αB isoforms and AQP0 and Cx46, whether direct or via fibre cell membranes, contribute to the inhibition of diffusion in the barrier region of aged lenses.

As AQP0 and Cx46 are responsible for the transport of water (Gorin *et al.*, 1984) and GSH (Slavi *et al.*, 2014) into the nucleus of the lens respectively, any event that decreases the transport activity of these proteins would be detrimental to the lens. In fact, mutations of both AQP0 (Francis *et al.*, 2000; Ganesan *et al.*, 2012; Hu *et al.*, 2012; Kumari *et al.*, 2013) and Cx46 (Burdon *et al.*, 2004; Wang and Zhu, 2012), which affect channel formation, have been implicated in autosomal congenital cataract. With regards to mutations that lead to a loss of Cx46 function, it has previously been proposed that the decrease in GSH transport into the nucleus is responsible for nuclear cataract formation (Cobb and Petrash, 2002b; Friedrich and Truscott, 2009; Friedrich and Truscott, 2010) as it leads to a highly oxidative environment

conducive to protein cross-linking and proteolysis (Reddy and Giblin, 1984; Giblin, 2000; Truscott, 2005). In support of this, Cx46 knockout mice develop nuclear cataract characterised by proteolysis of crystallin proteins (Gong *et al.*, 1997). Additionally, in this study, crosslinked complexes were previously identified in high density lens fractions (section 3.3.3). It is therefore likely that the obstruction of AQP0 and Cx46 channels by αB in the cortex of the lens is a contributing factor in barrier formation, which leads to subsequent damage and eventual cataract formation.

The association of αB with fibre cell membranes was found throughout the nucleus of the lens (Figure 4.2), despite interactions between αB and AQP0 and Cx46 being localised in the cortex (Figure 4.3, Figure 4.4). This suggests that αB membrane association in the nucleus may be mediated via interactions with membrane lipids, cytoskeletal proteins or additional membrane proteins other than AQP0 and Cx46. It is, however, difficult to exclude the presence of interactions with AQP0 and Cx46 in the nucleus as a possibility. It is possible that the accumulation of HMWCs at fibre cell membranes prevents the proteins of interest from being accessed by antibodies and therefore being detected. However, as these lens sections were washed with PBS prior to labelling, this is less likely to be a significant factor.

Alternatively, truncation of AQP0 and Cx46, which increases in the nucleus of the lens (Ball *et al.*, 2004; Grey *et al.*, 2009; Wang and Schey, 2009), could conceivably affect either αB interaction or antibody detection of AQP0 and Cx46. Truncation sites of AQP0 have been identified at Asn246 (Ball *et al.*, 2004; Grey *et al.*, 2009), Pro249, Asn259, Thr260, Gln261 and Ala262 (Ball *et al.*, 2004), resulting in the loss of the C-terminal residues. As the antibody used for this study was specific to a sequence within the region Gly100 to Asp150 of AQP0 (Santa Cruz Biotechnology, Inc., personal correspondence), it is therefore more likely that the decrease in interactions in the nucleus is due to αB dissociation from AQP0, as opposed to a loss of antibody recognition sequences within AQP0. This may suggest that the αB binding site for AQP0 lies within the C-terminus. Although it is not possible to exclude C-terminal truncation of AQP0 itself as a factor in decreased function (Gonen *et al.*, 2004; Korlimbinis *et al.*, 2009), another study suggests that AQP0 function is not strongly affected by C-terminal truncation *in vivo* (Ball *et al.*, 2003). This is likely due to the regulation of AQP0 water permeability, whereby increased Ca^{+} and decreased pH increases the permeability of AQP0 to compensate for the loss of non-truncated protein (Varadaraj *et al.*, 2005). Truncation sites for human Cx46 have been less extensively studied, although a multitude of cleavage sites have been identified for bovine Cx46. These sites include Asn124,

Leu255 (Shearer *et al.*, 2008; Wang and Schey, 2009), Gly121, His122, Asp124, Gly251, Asn259, Ile267, Phe269, Tyr273, Ala274, Ser278, Ser284, Ala285, Glu344, Gly347, Gln352 and Gly2 (Wang and Schey, 2009)). These residues lie within the C-terminus, cytoplasmic loop and N-terminal regions of the protein, and within close proximity of the recognition site for the antibody used in this study, i.e. residues 375-425 of human Cx46 (Santa Cruz Biotechnology, Inc., personal correspondence). This makes it impossible to determine whether the decrease in interaction between αB isoforms and Cx46 in the nucleus compared to the cortex is due to truncation of the αB binding site or the antibody recognition site. The narrower region of interaction for Cx46 with αB compared to AQP0 (i.e. 250 μm versus 500 μm) in the lens is consistent with a higher rate of truncation of Cx46, at an earlier age. As Cx46 truncation occurs so extensively in all regions of the protein (Shearer *et al.*, 2008; Wang and Schey, 2009), the effect of truncation itself on Cx46 function in the lens is worthy of further investigation.

Ultimately, as interactions between αB and Cx46 or AQP0 were not observed in the nucleus of the lens, it remains unclear how αB associates with the membrane in this region and how this may affect transport in the lens. However, as transport in the lens occurs from the cortex into the nucleus, interactions that occur in the cortex, such as those identified in this thesis, are more likely to be the primary cause to any obstruction to diffusion.

4.5 Conclusions

Isoforms, including phosphorylated isoforms, of αB interact with fibre cell membranes, in part, through interactions with the membrane pore proteins AQP0 and Cx46. This provides a mechanism for αB membrane association to be directly involved in the inhibition of small metabolite transport, notably that of GSH. This impediment to GSH transport into the lens nucleus and the loss of re-reduction of oxidized GSH in the cortex, is likely to result in the oxidation of nuclear proteins leading to the formation of protein crosslinking and ultimately cataract formation. Additionally, it appears that phosphorylation increases membrane binding capacity of αB, potentially resulting in increased interactions between αB and AQP0 and Cx46 in the cortex of the aged lens. Thus, this work provides some insight into the interactions between αB and fibre cell membranes, particularly in the lens cortex. However, it

is also important to note that some limitations to this research exist. As only a single lens was investigated, further studies utilizing multiple lenses across a broader age range will need to be undertaken in order to confirm and extend these findings. As the control antibody was the same used for the AQP0 experiment for which very little non-specific binding was observed, an IgG/Cx46 negative control was not performed, but should be incorporated into future experiments to exclude the possibility of non-specific interactions . In addition, although the results suggest it is highly likely that αB directly interacts with Cx46 and AQP0 *in vivo* in the cortical and barrier region, these findings would be strengthened if direct interaction could be confirmed through other methods such as immunoprecipitation assays, in order to exclude the possibility of co-localisation of αB with Cx46 and AQP0 due to interactions with other membrane components.

Chapter 5

Investigation of non-enzymatic deamidation of αB

Chapter 5

5.1 Introduction

Deamidation involves the conversion of asparagine and glutamine residues to aspartate and glutamate residues respectively (Figure 1.5). In the lens, deamidation is believed to occur primarily via non-enzymatic reactions (Hains and Truscott, 2010). The susceptibility of residues to deamidation is affected primarily by the surrounding residues (Robinson *et al.*, 1970; Robinson *et al.*, 1974; Robinson and Robinson, 1991; Wright, 1991; Robinson and Robinson, 2001) which have both a steric and catalytic effect (Robinson and Robinson, 2004b), the secondary structure with deamidation being facilitated by more flexible α-helical structures as opposed to β-sheets (Paranandi *et al.*, 1994; Kosky *et al.*, 1999; Hooi *et al.*, 2012; Truscott and Friedrich, 2016), and tertiary (Kossiakoff, 1988) and quaternary structure, with surface exposed residues being more susceptible (Lapko *et al.*, 2002). Deamidation of αB at N146 reduces chaperone activity, decreases hydrophobic exposure and increases oligomeric size compared to WTαB (Gupta and Srivastava, 2004; Asomugha *et al.*, 2011). Deamidation at either N146 or N78 has also been reported to increase association of αB with βA3-crystallin *in vitro* (Tiwary *et al.*, 2015). Deamidation is known to destabilise β- and γ-crystallins triggering aggregation (Kim *et al.*, 2002; Lampi *et al.*, 2002; Flaugh *et al.*, 2006; Lampi *et al.*, 2006; Takata *et al.*, 2007; Takata *et al.*, 2008; Michiel *et al.*, 2010) as well as interrupting H-bond formation at oligomeric interfaces causing predominantly tertiary structural changes (Lampi *et al.*, 2006; Takata *et al.*, 2007; Takata *et al.*, 2008; Takata *et al.*, 2009) and interfering with hetero-oligomeric interactions with other β-crystallins (Takata *et al.*, 2009). As such, it is speculated to be involved in cataract formation, also being elevated in insoluble human lens fractions compared to soluble fractions (Hanson *et al.*, 2000; Srivastava and Srivastava, 2003). Isomerisation of αB at Asp96 resulting from deamidation, is believed to partially unfold the protein, making it more susceptible to cleavage (Takata and Fujii, 2015).

Outside of the lens, deamidation can be induced by acidic or basic conditions. The mechanisms behind these reactions differ; acidic environments (pH<5.0) allow direct hydrolysis of the amide group of asparagine and glutamine residues (Catak *et al.*, 2009) (Figure 1.5B). Under neutral to basic environments, cyclic intermediates are produced that are then hydrolysed to form aspartate and glutamate (Geiger and Clarke, 1987; Capasso *et al.*, 1991; Wright, 1991; Catak *et al.*, 2009) (Figure 1.5A). Deamidation at asparagine residues forms a succinimide (i.e. 5-member ring) intermediate (Geiger and Clarke, 1987) while

glutamine forms a glutaminide (6-member ring) intermediate (Capasso *et al.*, 1991; Wright, 1991). As the reaction is non-enzymatic, spontaneous deamidation of proteins can occur. For example, insulin has been reported to undergo non-enzymatic deamidation during storage at -15°C (Berson and Yalow, 1966). However, the susceptibility of αB to non-enzymatic deamidation under storage conditions has not been previously studied. As deamidation can alter the structure and function of proteins (Gupta and Srivastava, 2004; Asomugha *et al.*, 2011; Tiwary *et al.*, 2015), the presence of deamidated residues can be problematic for experimental interpretation (such as for functional studies of proteins). The susceptibility of proteins to deamidation and the impact it can have on function therefore needs to be considered when interpreting data. This chapter examines deamidation of αB when stored at -20°C and 4°C, as well as following heat-treatment under different buffer conditions, in order to determine the susceptibility of αB to non-enzymatic deamidation *in vitro*.

5.2 Experimental Rationale

To determine which αB residues are susceptible to non-enzymatic deamidation under different buffer conditions, a protocol was developed to induce deamidation using heat treatment under different pH and unfolding buffer conditions. A protocol developed by Liao *et al.* (2009) used low concentrations of acetic acid (0.03-0.14M) coupled with high temperatures (121ºC), to induce deamidation in wheat gluten while avoiding other modifications (i.e. hydrolysis and isomerisation) that can be introduced with other acids (e.g. hydrochloric acid and phosphoric acid). An inherent obstacle in this procedure is the instability of Hsps at such high temperatures. In an attempt to overcome this, the protocol was modified to incorporate lower temperatures and increased incubation times. To determine the effect of pH on deamidation, ammonium acetate (~pH 7.0), ammonium bicarbonate (~pH 8.0) and acetic acid (~pH 3.0) were used as buffer systems in order to compare which residues were susceptible to deamidation via the succinimide intermediate (basic conditions) versus direct hydrolysis pathway (acidic conditions) (section 2.4.1). Proteins were also heat-treated with urea in order determine the effect of protein unfolding on αB deamidation. For this experiment, lower temperatures and shorter incubation times were

used to prevent protein aggregation (section 2.4.2). Experimental conditions are described in Table 5.1.

Table 5.1: Experimental conditions for each of the αB samples analysed in this section of work.

Section	Batch	Storage	Buffer	Incubation	Digestion	Analysis
5.3.1	1	5 years at -20°C	34 mM acetic acid	0-72 hours at 4°C		MS
5.3.2	1	5 years at -20°C	34 mM acetic acid or 200 mM ammonium acetate	16 hours at 50 °C ± 5 minutes at 100°C	5 minutes or 2 hours	MS
5.3.3	1	1 year at -20°C	6 M urea or	4 hours at 37 °C	overnight	MS/MS (APAF)
5.3.3	2	1 year at -20°C	1 M ammonium bicarbonate	18 hours at 50°C	overnight	MS/MS (APAF)

5.3 Results

5.3.1 Modifications following incubation in acetic acid at 4°C

Recombinant human αB (i.e. batch 1) that had been stored at -20°C in 200 mM ammonium acetate (for a minimum of 5 years) was incubated in 34 mM acetic acid (~pH 3.0) at 4°C for 0-72 hours before being analysed by MS to determine if modifications occurred to the protein under these conditions. The dominant peak for each sample, peak A, had a mass of 20159.5 Da, consistent with unmodified αB (Figure 5.1, Table 5.2). The mass of peak A remained consistent following incubation at 4°C (Figure 5.1, Table 5.2). In the sample that was not incubated (i.e. control), another peak, peak B (20174.4 Da) showed a 15 Da increase in mass compared to peak A, consistent with the addition of a methyl group (Figure 5.1, Table 5.2). The mass of peak B increased by a further 3 Da after a 24 hour incubation at 4°C, and by another 2 Da after a 72 hour incubation at 4°C (Table 5.2). This 5 Da increase of peak B over 72 hours of incubation is consistent with deamidation at 5 sites.

In the control sample (i.e. not incubated), a peak at 20200.8 Da (peak C) showed a mass increase of 41.3 Da compared to peak A, consistent with acetylation of αB (Figure 5.1, Table 5.2). The mass of peak C increased by 1 Da after a 72 hour incubation at 4°C (Table 5.2),

consistent with deamidation at a single site. The control sample also contained a peak corresponding to a mass of 20257.4 Da (peak D) (Figure 5.1, Table 5.2). The increase in mass of peak D over peak A, 39.9 is consistent with pyro-carbamidomethylation of the protein (Figure 5.1, Table 5.2). The mass of peak D remained constant following incubation at 4°C, but was increased in relative amount compared to peak A following a 24 hour incubation before decreasing again following a 48 hour incubation, suggesting decomposition of the compound upon further incubation. It is important to note that as the samples were not subjected to tryptic digestion, the location and nature of modifications could not be confirmed.

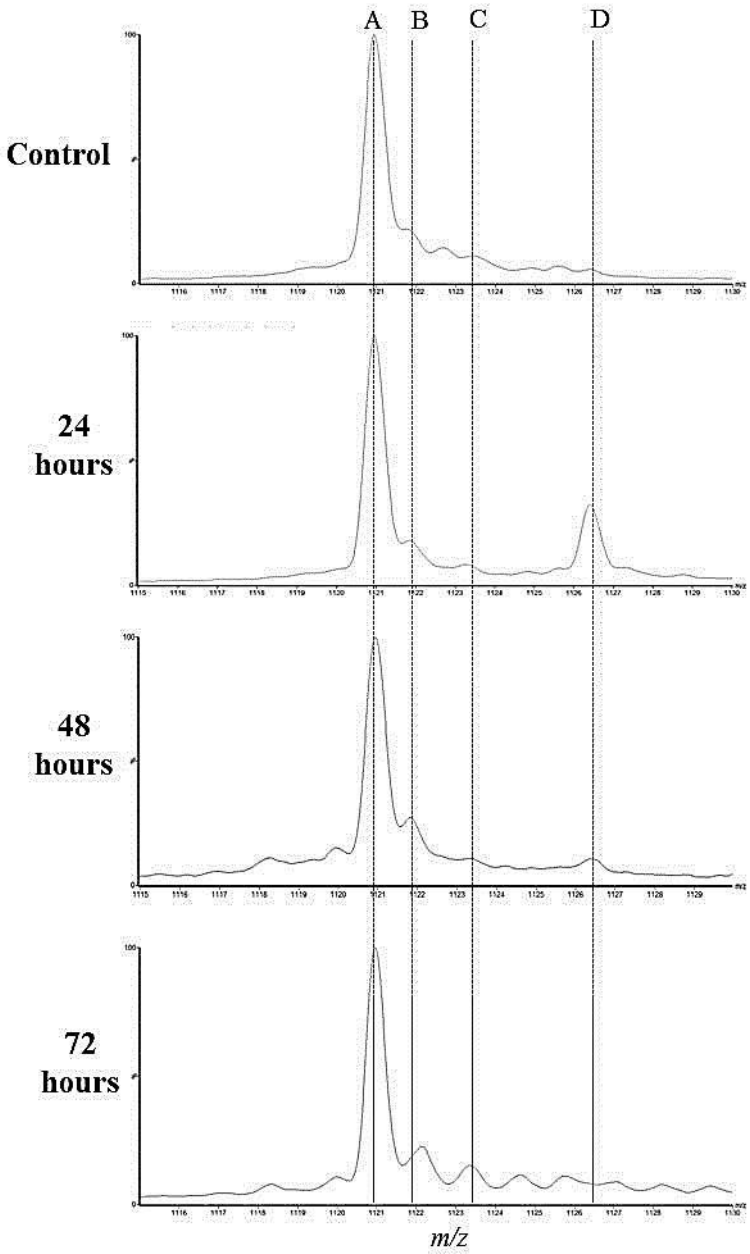

Figure 5.1: Mass spectra of αB following incubation at 4°C for 0-72 hours. Recombinant human αB was incubated at 4°C for 0-72 hours in 34 mM acetic acid (~pH 3.0) at a concentration of 1 mg.mL^{-1}. The protein was then analysed using MS. The position of 4 prominent peaks in the mass spectrum are labelled A-D and indicated on each spectra with a dashed line.

Table 5.2: Masses of αB isoforms calculated from the peaks identified by MS following incubation at 4°C for 0-72 hours. Recombinant human αB was incubated at 4°C for 24-72 hours in 34 mM acetic acid (~pH 3.0) at a concentration of 1 $mg.mL^{-1}$. The protein was analysed using MS and masses of peaks were calculated using Masslynx software. Peak D was not present (NP) in the sample incubated for 72 hours.

Length of incubation	A	B	C	D
0 hours	20159.5	20174.4	20200.8	20257.4
24 hours	20159.5	20177.7	20201	20257.7
48 hours	20159.1	20177.9	20201.2	20257.6
72 hours	20159.4	20179.6	20201.5	NP

5.3.2 Deamidation under acidic or basic conditions

To determine which asparagine or glutamine residues in αB residues were susceptible to heat-induced deamidation under acidic or basic conditions, recombinant human αB (batch 1) was incubated at 50°C for 2 hours in either 34 mM acetic acid (i.e. acidic sample; ~pH 3.0) or 200 mM ammonium acetate (i.e. basic sample; ~pH 7.0). The protein was then digested with trypsin for 5 minutes and analysed by MS. Complete tryptic digestion of αB yielded 21 peptides, five of which contain an asparagine or glutamine residue. For the control sample, 11 αB tryptic peptides were identified (Table 5.3, Figure 5.2). A single deamidation site was identified at N146 on peptide 124-149 (Table 5.3, Figure 5.2). Following incubation under acidic conditions, 7 αB tryptic peptides were identified, 6 of which were the same peptides as identified in the control sample (Table 5.3, Figure 5.2). No extra deamidation sites were identified following incubation under acidic conditions (Table 5.3, Figure 5.2). Following incubation under basic conditions, 8 αB tryptic peptides were identified, 7 of which were the same peptide as identified in the control sample (Table 5.3, Figure 5.2). The same deamidation site (N146) was identified on peptide 124-149 as observed in the control sample, however, no additional deamidation sites were identified when the protein was incubated under basic conditions (Table 5.2, Figure 5.2).

Table 5.3: αB tryptic peptides identified following incubation at 50°C for 2 hours + 100°C for 5 minutes. Recombinant human αB was incubated at 50°C for 2 hours followed by 5 minutes at 100°C in either 34 mM acetic acid (acidic; ~pH 3.0) or 200 mM ammonium acetate (basic; ~pH 7.0) at a concentration of 1 $mg.mL^{-1}$. Protein was digested with trypsin for 5 minutes and analysed using MS, and peptide masses were calculated using Masslynx software. Predicted masses were used to identify peptides and modification sites. Protein that was not incubated was analysed as a control. Modified residues are highlighted in red.

m/z	Expected Mass	Residues	Modification	Sequence	Observed Mass
Control					
588.2	588.3	117-120		EFHR	588.2
656.9	1313.7	124-149	N146	IPADVDPLTITSSLSSDGVL TVNGPR	1313.6
700.4	700.4	158-163		TIPITR	700.4
772.3	772.4	151-157		QVSGPER	772.3
900.5	900.5	150-157		KQVSGPER	900.5
1088.5	1088.5	108-116		QDEHGFISR	1088.5
1140.6	1140.6	164-174		EEKPAVTAAPK	1140.6
1268.7	1268.7	164-175		EEKPAVTAAPKK	1268.7
1374.6	1374.7	12-22		RPFFPFHSPSR	1374.6
1388.7	1388.7	1-11		MDIAIHHPWIR	1388.7
1496.6	1496.7	57-69		APSWFDTGLSEMR	1496.6
Acidic					
700.4	700.4	158-163		TIPITR	700.4
772.4	772.4	151-157		QVSGPER	772.4
900.4	900.5	150-157		KQVSGPER	900.4
986.5	986.5	83-90		HFSPEELK	986.5
1088.5	1088.5	108-116		QDEHGFISR	1088.5
1140.6	1140.6	164-174		EEKPAVTAAPK	1140.6
1268.7	1268.7	164-175		EEKPAVTAAPKK	1268.7
Basic					
588.3	588.3	117-120		EFHR	588.3
700.4	700.4	158-163		TIPITR	700.4
772.4	772.4	151-157		QVSGPER	772.4
900.5	900.5	150-157		KQVSGPER	900.5
1140.6	1140.6	164-174		EEKPAVTAAPK	1140.6
1165.6	1165.7	93-103		VLGDVIEVHGK	1165.6
1268.7	1268.7	164-175		EEKPAVTAAPKK	1268.7
656.9	1313.7	124-149	N146	IPADVDPLTITSSLSSDGVL TVNGPR	1313.6

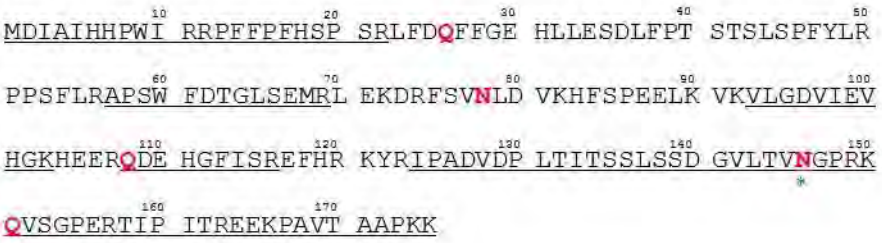

Figure 5.2: Sequence coverage of αB following heat treatment and 5 minute tryptic digestion. Regions of αB identified by tryptic digestion and subsequent MS analysis are underlined. Potential deamidation sites are highlighted in red. The deamidated residue (i.e. N146) is indicated by a green asterisk.

To determine whether additional deamidated residues could be detected by increasing the incubation and digestion time, recombinant human αB was incubated for 16 hours at 50°C, digested with trypsin for 2 hours and analysed by MS. For the control sample, 6 αB tryptic peptides were identified (Table 5.4). No deamidation sites were identified (Table 5.4, Figure 5.3D). Following incubation under acidic conditions, 3 αB tryptic peptides were identified, 2 of which were the same peptide identified in the control sample (Table 5.4). A single deamidation site was identified at N146 on peptide 124-149 (Figure 5.3B, D, Table 5.4). Following incubation under basic conditions, 6 αB tryptic peptides were identified, 3 of which were the same peptide identified in the control sample (Table 5.4). The same deamidation site (N146) was identified on peptide 124-149 as observed following incubation under acidic conditions (Figure 5.3C, D, Table 5.4). However, an additional deamidation at N78 was identified on peptide 75-82 following incubation under basic conditions (Figure 5.3C, D, Table 5.4). Deamidation at this site was not observed following the shorter incubation time (Figure 5.2, Table 5.3).

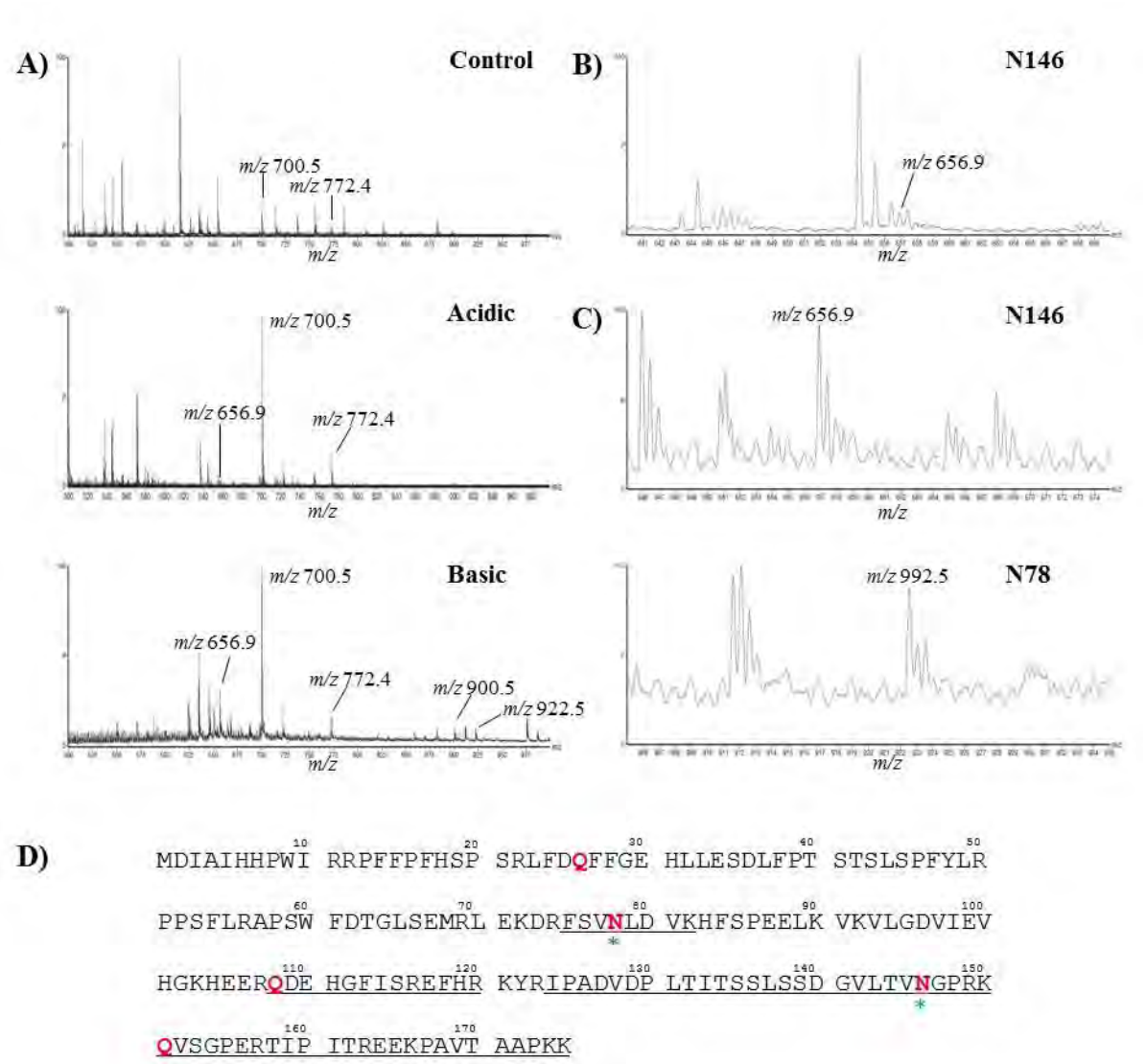

Figure 5.3: Mass spectra of αB tryptic digests following incubation at 50°C for 16 hours. Recombinant human αB was incubated at 50°C for 16 hours in either 34 mM acetic acid (acidic; ~pH 3.0) or 200 mM ammonium acetate (basic; ~pH 7.0) at a concentration of 1 mg.mL^{-1}. **(A)** Protein was digested with trypsin for 2 hours and analysed using MS. Predicted masses were used to identify peptides (some of which are labelled in the spectra above, refer to 5.3) and modification sites detected following treatment with **(B)** acidic or **(C)** basic conditions. Peaks corresponding to a deamidated peptides are labelled with their *m/z* value (B, C). Protein that was not incubated was analysed as a control. **(D)** Regions of αB identified following heat treatment and 2 hour tryptic digestion and subsequent MS analysis were mapped onto the protein sequence. Potential deamidation sites are highlighted in red. Deamidated residues are indicated by a green asterisk.

Table 5.4: αB tryptic peptides identified following incubation at 50°C for 16 hours. Recombinant human αB was incubated at 50°C for 16 hours in either 34 mM acetic acid (~pH 3.0) or 200 mM ammonium acetate (~pH 7.0) at a concentration of 1 $mg.mL^{-1}$. Protein was digested with trypsin for 2 hours and analysed using MS, and peptide masses were calculated using Masslynx software. Predicted masses were used to identify peptides and modification sites. Protein that was not incubated was analysed as a control. Modified residues are highlighted in red.

m/z	Expected Mass	Residues	Modification	Sequence	Observed mass
Control					
588.3	588.3	117-120		EFHR	588.3
700.5	700.4	158-163		TIPITR	700.5
772.4	772.4	151-157		QVSGPER	772.4
900.5	900.5	150-157		KQVSGPER	900.5
1088.5	1088.5	108-116		QDEHGFISR	1088.5
1140.6	1140.6	164-174		EEKPAVTAAPK	1140.6
ACIDIC					
656.9	1313.7	124-149	N146	IPADVDPLTITSSLSSDGVL TVNGPR	1313.8
700.5	700.4	158-163		TIPITR	700.5
772.4	772.4	151-157		QVSGPER	772.4
BASIC					
656.9	1313.7	124-149	N146	IPADVDPLTITSSLSSDGVL TVNGPR	1313.8
700.5	700.4	158-163		TIPITR	700.5
772.4	772.4	151-157		QVSGPER	772.4
900.6	900.5	150-157		KQVSGPER	900.6
1268.8	1268.7	164-175		EEKPAVTAAPKK	1268.8
922.5	922.5	75-82	N78	FSVNLDVK	922.5

5.3.3 Deamidation under folding and unfolding conditions

To determine which αB residues were susceptible to deamidation under folding and unfolding conditions, recombinant human αB (i.e. batch 2) that had been stored at -20°C for <1 year was incubated in 1 M ammonium bicarbonate (~pH 8.0) for 18 hours at 50°C or in 6 M urea (~pH 8.0) for 4 hours at 37°C, digested with trypsin overnight and analysed using MS. The sample treated with 6 M urea was incubated at a lower temperature for a shorter time period to prevent insolubilisation of the unfolded protein. Protein in PBS (~pH 7.4) with and without heating for 18 hours at 50°C were used as controls. From each of the samples, 8 deamidated αB tryptic peptides (denoted peptide 1-8) were identified (site of modification given in parentheses); peptide 1 - 75-82 (N78); peptide 2 - 75-90 (N78); peptide 3 - 124-149 (N146); peptide 4 - 150-157 (Q151); peptide 5 - 23-46 (Q26); peptide 6 - 108-116 (Q108); peptide 7 - 151-157 (Q151); peptide 8 - 122-149 (N146) (Figure 5.3). There was no significant difference in amount of deamidation between each treatment for peptides 1-6 (Figure 5.4, Table 5.5).

One-way ANOVA analysis indicated that there was a significant effect of treatment on the amount of deamidation of peptide 7 that contains Q151 [$F(3, 8) = 11.8$, $p = 0.003$]. The amount of deamidation of peptide 7 was significantly increased in the heat-treated PBS sample (i.e. PBS + heat, 26.8±4.6%) compared to the other samples ($P \leq 0.05$, Figure 5.4, Table 5.5). All other samples had similar levels of deamidation for Q151 (Figure 5.4, Table 5.5).

One-way ANOVA analysis indicated that there was a significant effect of treatment on the amount of deamidation of peptide 8 that contains N146 [$F(3, 44) = 8.99$, $p = 0.0001$]. The amount of deamidation of peptide 8 was significantly increased in the PBS-treated sample (64.5±6.2%) compared to the samples in ABC that were heat-treated (i.e. ABC ± heat, 49.7±6%) or urea-treated (i.e. urea + heat, 55.6±6.8, $P \leq 0.05$; Figure 5.4, Table 5.5). The amount of deamidation of peptide 8 was also significantly increased in the heat-treated PBS sample (i.e. PBS + heat, 59±9.2%) compared to the sample in ABC that was heat-treated (i.e. ABC + heat, $P \leq 0.05$), but not the heat-treated urea sample (Figure 5.4, Table 5.5). There was no significant difference in the amount of deamidation of peptide 8 between the PBS and heat-treated PBS samples, or the heat-treated ABC (i.e. ABC + heat) and urea (i.e. urea + heat) samples (Figure 5.4, Table 5.5).

Table 5.5: Percentage of αB deamidation following heat treatment in urea or ammonium bicarbonate buffer. Recombinant human αB was incubated at 37°C for 4 hours in 6 M urea (~pH 8.0) or at 50°C for 18 hours in 1 M ammonium bicarbonate (ABC; ~pH 8.0), at a concentration of 2 $mg.mL^{-1}$. Protein was digested with trypsin and analysed using MS/MS. Peptides and modified residues were identified using a MASCOT database search, and percentage deamidation for each peptide (1-8) was calculated using a computer simulation method. Differences between treatments were tested using a one-way ANOVA ($P \leq 0.05$ shaded grey) and post-hoc Tukey's tests ($P \leq 0.05$ marked with asterisk). Values are presented as means±1SD. Samples were anlaysed in triplicate, n = number of observations of that peptide.

Peptide	Residues	Deamidation site	ABC + heat	PBS	PBS + heat	Urea + heat
1 (n=3)	75-82	N78	19.4±5.8	16.2±5.4	21±5.1	24.4±5.1
2 (n=12)	75-90	N78	55.7±19.1	59.8±19.5	54.5±21.4	59.8±22.2
3 (n=12)	124-149	N146	44.9±9.7	58.2±8.9	52.4±9.8	50±13.6
4 (n=3)	150-157	Q151	14.7±10	15.2±8.4	15.5±1.4	5±2
5 (n=9)	23-46	Q26	50.7±7.3	52.9±9.1	51.2±13.3	55.9±4.1
6 (n=6)	108-116	Q108	23.9±6.6	25.1+12.2	18.5±3.3	17.4±7.8
7 (n=3)	151-157	Q151	11.4±2.7	17.3±2.4	26.8±4.6*	18.2±2.6
8 (n=12)	122-149	N146	49.7±6	64.5±6.2*	59±9.2*	55.6±6.8

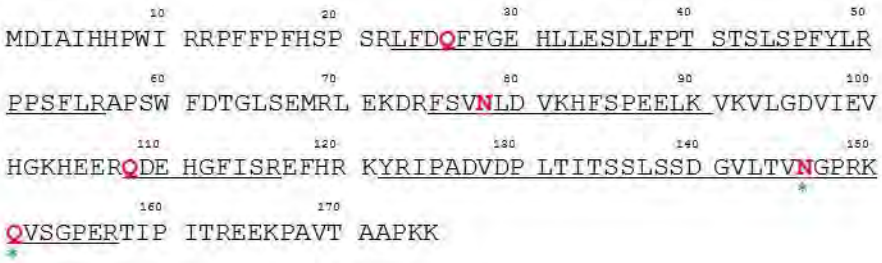

Figure 5.4: Sequence coverage of αB following heat treatment in folding or unfolding conditions and overnight tryptic digestion. Regions of αB identified by tryptic digestion and subsequent MS/MS analysis are underlined. Deamidated residues are highlighted in red. Deamidated residues that show statistical significance between treatments ($P \leq 0.05$) as calculated by one-way ANOVA are indicated by a green asterisk.

5.4 Discussion

Recombinant proteins are a convenient way to study protein structure and function *in vitro*. However, recombinant proteins are prone to the accumulation of non-enzymatic modifications, even under frozen storage conditions (Berson and Yalow, 1966). Modified forms of αB (including methylated, deamidated and pyro-carbamidomethylation) were present in protein that had been stored at -20°C in 200 mM ammonium acetate (~pH 7.0) for 5 years (Figure 5.1, Table 5.2). Unfortunately, the protein used as a control for these experiments (i.e. not heat treated) had been stored under frozen conditions for a minimum of one year. As such, it is impossible to determine whether the modifications present were introduced during protein expression or during storage. The use of a recently expressed protein batch as a control would help elucidate this in future experiments. It was possible however, to determine whether further incubation in non-frozen conditions could contribute to the introduction of further modifications.

When αB was incubated at 4°C, the majority of the additional modifications (the dominant being deamidation) were introduced within the first 24 hours (Figure 5.1, Table 5.2). This suggests that deamidation of αB occurs readily and spontaneously under common experimental and storage conditions, as previously observed by Hao *et al.* (2011).

An additional site of deamidation (i.e. N78) was identified when αB was heat-treated in a basic buffer (200 mM ammonium acetate, ~pH 8.0) compared to an acidic buffer (34 mM acetic acid, ~pH 3.0) (Table 5.3, Table 5.4). These treatments induce deamidation via two different pathways i.e. via a succinimide ring intermediate (basic conditions), and via direct hydrolysis (acidic conditions) (Geiger and Clarke, 1987; Catak *et al.*, 2009). The sample heat-treated in ammonium acetate (~pH 8.0) showed the highest number of deamidated residues (N78 and N146) (Figure 5.3, Table 5.4), with the peak corresponding to deamidation at N146 (*m/z* 656.9) being more prominent in this sample compared to the sample heat-treated in acetic acid (~pH 3.0) (Figure 5.3 compare panels B, C). This is consistent with αB being preferentially deamidated via the succinimide intermediate pathway rather than direct hydrolysis *in vitro*. This is most likely due to higher thermodynamic favourability of the succinimide forming pathway (Catak *et al.*, 2009). Takemoto *et al.* (2001) reported that γ-crystallin in human cataractous lenses undergoes deamidation via this same pathway, as indicated by the formation of iso-aspartate, demonstrating that this pathway to deamidation occurs *in vivo*.

It is important to note that deamidation at N78 was only detected when the samples were subjected to the longer digestion time (i.e. 2 hours versus 5 minutes). Although overall peptide coverage was higher for the samples subjected to the 5 minute digestion, the peptide containing N78 was not detected (Figure 5.3). Therefore, repeat experiments incorporating overnight digestion of samples may lead to the identification of deamidation at more residues. Furthermore, a limitation for identifying PTMs of whole proteins is the accuracy and sensitivity of the mass spectrometer used. Although the samples were run on the same day and using the same setting to help ensure accuracy, only a single replicate was performed. This is particularly pertinent regarding the identification of deamidation, as the modification only introduces a mass change of 1 Da, a change too small for many mass spectrometres to detect. The mass of peak B increased by 3 Da in the first 24 hours of incubation and by a further 2 Da by 72 hours (Table 5.2). Although this is consistent with deamidation at five sites, a possibility given that deamidation occurs relatively rapidly in acidic buffers, the finding is tentative and would need to be confirmed with higher resolution mass spectrometry.

Hydrolysis of the succinimide intermediate has been reported to be the rate-limiting step in deamidation via this mechanism (Catak *et al.*, 2009). A significant decrease in the amount of αB deamidation at N146 and Q151 was observed in samples heat-treated in urea and ABC

(~pH 8.0) compared to samples in PBS (pH 7.4) (Figure 5.4, Table 5.5). This suggests that hydrolysis of the succinimide intermediate occurs faster at slightly acidic pH, and that even slight increases in pH may therefore act to reduce heat-induced deamidation. The lens has a pH gradient that decreases from ~pH 7.2 in the cortex (Bassnett *et al.*, 1987; Eckert, 2002) to ~pH 6.7 in the nucleus (Bassnett *et al.*, 1987). If this slight decrease in intracellular pH is sufficient to affect αB deamidation, this may provide another explanation (in addition to protein longevity) for the high levels of deamidation in the nucleus of aged lenses (Siebinga *et al.*, 1992; Hains and Truscott, 2007). As deamidation, particularly at N146, reduces the chaperone activity of αB (Gupta and Srivastava, 2004; Asomugha *et al.*, 2011), the higher incidence of αB deamidation, associated with the decrease in pH in the nucleus, may facilitate the formation of nuclear cataract in the lens.

Isomerisation resulting from deamidation following the succinimide intermediate pathway is reported to increase the susceptibility of proteins to tryptic cleavage by inducing partial unfolding (Takata and Fujii, 2015). However, following longer heat-treatment and digestion times, the number of αB tryptic peptides identified decreased as the number of deamidated residues increased (Table 5.3, Table 5.4). Additionally, when N78 was identified on two separate peptides (i.e. peptide1 and peptide 2; Table 5.5), the presence of an additional 8 residues on peptide 2 led to an increase in the average amount of deamidation detected on that peptide by 37% (Figure 5.4, Table 5.5). This was not observed for other residues. If deamidation at N78 occurred during heat-treatment, this finding suggests that deamidation at N78 protects surrounding residues from cleavage. Several studies have reported that peptides derived from crystallin proteins form HMWCs during the onset of age-related cataract formation (Ramalho *et al.*, 1996; Santhoshkumar *et al.*, 2008; Su *et al.*, 2015). These peptides are believed to form via autolytic cleavage at serine residues in the lens nucleus with age (Su *et al.*, 2012). Notably, there is a serine residue one residue away from N78 (Figure 5.3), and thus this region may be susceptible to autolytic cleavage in the lens. However, if deamidation of N78 inhibits cleavage of αB *in vivo*, this may act as a protective mechanism to prevent protein cleavage that could lead to cataract. The possibility that N78 deamidation may not be involved in cataract formation is supported by previous findings that deamidation at N78 does not affect the chaperone activity or oligomeric size of αB (Gupta and Srivastava, 2004).

Hains and Truscott (2010) previously reported that αB was deamidated at asparagine residues at a ~3-fold higher rate than glutamine residues in the human lens. This can likely be attributed to the lower thermodynamic stability of succinimide intermediates formed by

asparagine residues (Wright, 1991; Robinson and Robinson, 2004a; Li *et al.*, 2010). With the exception of N78 in peptide 1 and Q26 in peptide 5, the current results support this finding of a higher rate of deamidation at asparagine residues compared to glutamines (Figure 5.4, Table 5.5). Deamidation of N78 (peptide 2) and N146 (peptide 3 and peptide 8) was, on average, 3.3-fold higher than the amount of deamidation measured at Q151 (peptide 4 and peptide 7) and Q108 (peptide 6). However, the average amount of deamidation for asparagine and glutamine residues reported here (46.5% and 26.2%, respectively) were higher than the amount reported by Hains and Truscott (2010) *in vivo* (22.6% and 6.6%, respectively). This difference can be attributed to different experimental conditions (i.e. *in vivo* versus *in vitro* conditions) as well high levels of deamidated Q26 (peptide 5) in this work. When Q26 is excluded from the analysis, asparagine and glutamine were deamidated to the same extent as reported by Hains and Truscott (i.e. 3:1) (2010), thus suggesting a similar preference for asparagine residue deamidation *in vitro*. As Q26 is located within an α-helical region it may be expected to be deamidated to a lesser extent than Q151 which lies within an unstructured coil region (Figure 5.5A). Additionally, as all three glutamine residues (i.e. Q26, Q108 and Q151) are surface exposed (Figure 5.5B), the mechanism of the higher amount of deamidation at Q26 (peptide 5) compared to Q151 (peptide 4 and peptide 7) and Q108 (peptide 6) (Figure 5.4, Table 5.5) is currently unclear.

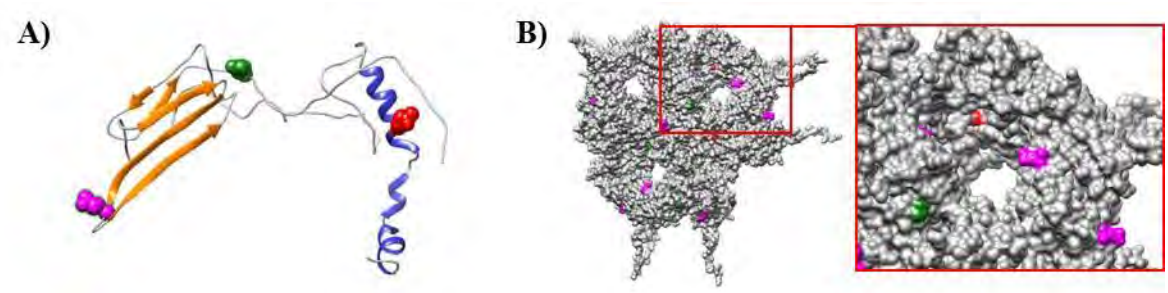

Figure 5.5: Model of αB indicating location of Q26, Q108 and Q151. Model of the **(A)** monomer depicted as a ribbon representation (β-sheets – orange, α-helices – blue, coil – grey) and the **(B)** 24mer depicted as a surface representation of human αB (pdb entry 3J07; Jehle *et al.* (2011)). The deamidated residues Q26 (red), Q108 (magenta) and Q151 (green) are solvent exposed. The red box indicates the area presented as inset.

The only residues for which the amount of deamidation was significantly affected by treatment were N146 (peptide 8) and Q151 (peptide 7), whereby changes in buffer pH, but not protein unfolding, increased the amount of deamidation of these sites (Figure 5.4, Table 5.5). These residues lie within five residues of each other (Figure 5.4); N146 lies within the β9-strand of the ACD and Q151 lies within the hinge loop region (Laganowsky *et al.*, 2010). As deamidation of these sites was not affected by unfolding (Table 5.5), this suggests that surface exposure was not a limiting factor. This was confirmed by mapping the location of N146 and Q151 in a structural model of oligomeric αB (Figure 5.4). Both residues are highly solvent exposed in the αB oligomer (Figure 5.5A), making them susceptible to non-enzymatic deamidation. Deamidation is also facilitated by the conformational flexibility of the surrounding region (Truscott and Friedrich, 2016), as well as the presence of neighbouring glycine and basic residues (Hains and Truscott, 2010). As such, the flexibility of the surrounding hinge loop region may facilitate deamidation of N146 and Q151. Deamidation of N146 and Q151 may also be further facilitated by the presence of neighbouring glycine (G147) and arginine residues (R149) respectively, accounting for the high amount of deamidation at these residues in this study. As the amount of deamidation of N146 and Q151 was affected by pH, this suggests that the surrounding region may also undergo conformational changes at lower pHs that make these residues more susceptible to deamidation, such as a further increase in conformational flexibility. Moreover, since the amount of deamidation was significantly increased in the heat-treated PBS sample compared to the untreated PBS sample for N146 but not Q151 (Figure 5.4, Table 5.5), this suggests that Q151 is more susceptible to deamidation under conditions that promote changes in conformation than N146.

In addition to being highly solvent exposed, N146 is positioned in close proximity to the subunit interaction site of αB (Figure 5.6). As deamidation induces a structural change in the protein, it is likely that deamidation of N146 may interfere with subunit interactions, causing the dissociation of dimers from the αB oligomer. It has previously been shown that αB deamidation mutants (N146D and N78D αB) have increased binding affinity for βA3-crystallin compared to WTαB (Tiwary *et al.*, 2015). It is therefore plausible that dimer dissociation induced by deamidation at N146 may result in the exposure of substrate binding sites, thereby increasing the substrate affinity of αB. This can be tested experimentally by measuring structural changes in N146D and N78D mutants using techniques such as circular dichroism. Changes in hydrophobic exposure can be examined using intrinsic tryptophan

fluorescence, and resulting changes in oligomeric size can then be observed using methods such as size exclusion chromatography or native mass spectrometry. If this results in irreversible substrate binding, this may account for the high levels of deamidation observed in insoluble protein fractions from human lenses (Hanson *et al.*, 2000; Srivastava and Srivastava, 2003).

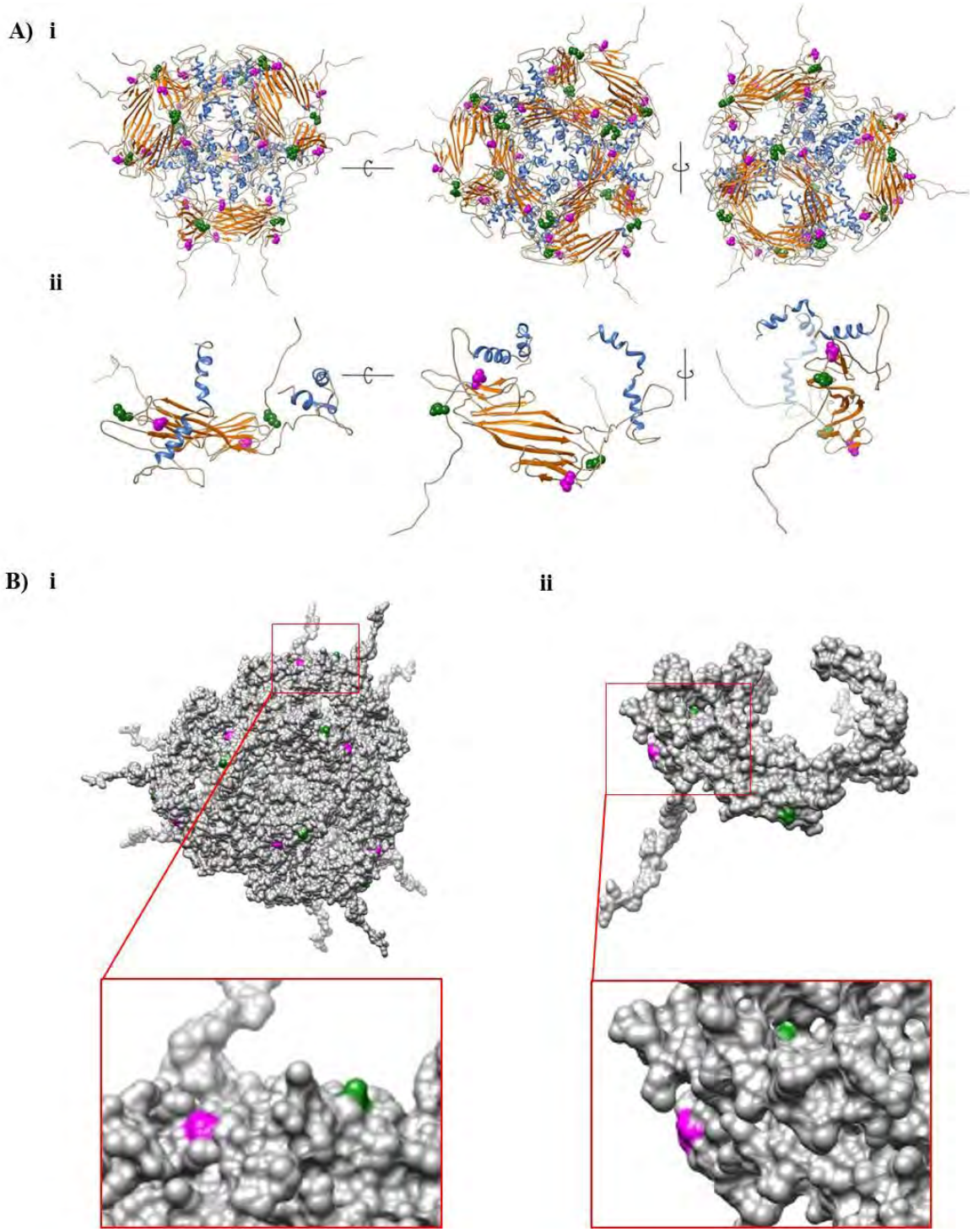

Figure 5.6: A model of the structure of oligomeric αB highlighting the position of deamidation sites N146 and Q151 identified in this work. Model of the 24-mer (i) and dimer forms (ii) of αB (pdb entry 3J07; Jehle *et al.* (2011)) depicted as a **(A)** ribbon representation and as a **(B)** surface representation highlighting the secondary structure elements (β-sheets – orange, α-helices – blue). The deamidated residues N146 (green) and Q151 (magenta) are highly solvent exposed at the surface of the oligomer, and are located in close proximity to sites of subunit interaction. Red boxes indicate area presented as inset.

Chapter 5

5.5 Conclusion

Non-enzymatic deamidation of αB has been implicated in protein insolubilisation in the lens and cataract formation. To study this, *in vitro* studies often use recombinant protein as an experimental model. However, non-enzymatic deamidation of αB resulting from expression, storage or treatment conditions can affect the structure and therefore function of the protein. The results in this chapter indicate that deamidation of αB at Q151 and N146 can be induced by common buffer and treatment conditions i.e. neutral pH and high temperatures. It is therefore important to consider the presence of deamidated residues in recombinant proteins, and how this may affect protein function and chaperone assays. Such modifications need to be taken into account to interpret experimental results appropriately. As similar conditions to those that were shown to induce deamidation *in vitro* exist in the nucleus of the aging lens, these results also provide an insight into the susceptibility and potential consequences of non-enzymatic deamidation *in vivo*.

Chapter 6

Conclusions and future directions

Chapter 6

6.1 Conclusions

Despite its pivotal role in maintaining the health and transparency of the lens, αB has also been implicated in various pathological states (Shinohara *et al.*, 1993; Chin *et al.*, 2005; Kamradt *et al.*, 2005; Moyano *et al.*, 2006; Liu *et al.*, 2015; Yilmaz *et al.*, 2015). This thesis investigated the possible role that phosphorylated αB plays in age-related cataract formation by addressing four separate aims. The first aim was to determine how the addition of a negative charge, similar to that added by phosphorylation, modulates the chaperone activity of αB. To achieve this, the ability of αB isoforms with mutations that mimic phosphorylation to inhibit the heat-induced aggregation of CPK was assessed using aggregation assays. The second aim was to compare αB phosphorylation profiles across different regions, sucrose density gradient fractions and ages of human lenses in order to determine whether αB phosphorylation could be involved in protein insolubilisation. This was achieved by isolating fractions from lenses using sucrose density gradient centrifugation, and assessing the phosphorylated status of αB in the fractions by 2D SDS-PAGE. The constituents of HMWCs were determined, and modification sites identified, by MS/MS analysis of 2D spots with masses of 40-100 kDa. The third aim was to identify interactions between αB and abundant membrane proteins (AQP0 and Cx46) at fibre cell membranes to determine how association of αB with membranes may contribute to barrier formation. This was achieved by co-labelling lens sections for αB and membrane proteins using a Duolink® proximity assay kit, and visualising interactions across the section using confocal microscopy. The final aim was to determine which αB residues are susceptible to non-enzymatic deamidation. To do this, recombinant human αB was heat-treated under acidic (~pH 3.0), alkaline (~pH 8.0) and unfolding buffer conditions, and deamidation sites were identified using MS. Taken together, the results of the current thesis suggest that αB participates in multiple pathways that ultimately can facilitate cataract formation in the lens.

6.2 A potential role of phosphorylation and deamidation

Previous studies have provided conflicting results into how the addition of a negative charge, designed to mimic phosphorylation, affects the chaperone activity of αB (Ito *et al.*, 2001;

Kamei *et al.*, 2001; Augusteyn *et al.*, 2002; Aquilina *et al.*, 2004; Ecroyd *et al.*, 2007). The results of this study indicate that WTαB, at concentrations equal to the substrate, induces protein aggregation following heat treatment (section 3.3.1). Although it is likely that this occurs via co-deposition of αB with the substrate protein (Aquilina *et al.*, 2004; Ecroyd *et al.*, 2007), this was not confirmed in the present study. The ability of αB to inhibit the aggregation of substrate (i.e. CPK) was, however, significantly increased with the addition of multiple negative charges, such that the introduction of 3 negative charges (via aspartate substitution at Ser19, Ser45 and Ser59) inhibited CPK aggregation by 83.9±1.3% (section 3.3.1). These results are consistent with previous findings that mutations that mimic phosphorylation of αB act to increase its capacity to inhibit stress-induced protein aggregation compared to the WT chaperone (Ghosh *et al.*, 2006; Ecroyd *et al.*, 2007; Ahmad *et al.*, 2008). It has been proposed that this increase in chaperone activity is a result of the dissociation of αB oligomers into higher activity monomers (Ecroyd *et al.*, 2007; Peschek *et al.*, 2013) which have higher substrate affinity (Koteiche and Mchaourab, 2003; Ecroyd *et al.*, 2007). If a similar mechanism occurs in the lens acts to maintain sufficient αB activity to maintain protein solubility. It is possible, however, that if substrate affinity is increased to the point of irreversible substrate binding, co-deposition of αB with the substrate protein may occur (Aquilina *et al.*, 2004; Ecroyd *et al.*, 2007).

Although mutations of cytoskeletal proteins in the lens have been implicated in cataract formation (Conley *et al.*, 2000; Jakobs *et al.*, 2000; Alizadeh *et al.*, 2002; Alizadeh *et al.*, 2003; Ramachandran *et al.*, 2007; Muller *et al.*, 2009), modification of these proteins have been largely overlooked. This study reported evidence of the formation of crosslinked protein complexes involving αA, αB and filensin, suggesting that the association of αB with fibre cell membranes may be mediated by interactions with cytoskeletal components. Such complexes have been reported previously, but have not been well characterised in lenses over the age of 45 (Srivastava *et al.*, 2004). The predominance of αA, particularly C-terminally truncated αA, in these complexes led to the suggestion that they were first formed via crosslinking between crystallin proteins (Srivastava *et al.*, 2004). Furthermore, it was suggested that these crosslinks were mediated by αA oxidation and serine to DHA conversion, with the age-related addition of intermediate filaments, including filensin, in older lenses (Srivastava *et al.*, 2004). This study characterised HMWCs isolated from a 77 year-old lens; filensin was found to be the predominant protein in these complexes, followed by αA (Figure 3.9). Without further comparisons with lenses from different age ranges, it remains to be established

whether the predominance of filensin in the complexes isolated from this older lens is a result of the age-related incorporation of intermediate filaments into crosslinked crystallin complexes, or the result of age-related binding of crystallins to the intermediate network.

While filensin, αA and αB in the HMWCs were all N- and C-terminally truncated, αA was more extensively truncated than previously reported (Srivastava *et al.*, 2004), suggesting that proteolytic cleavage, particularly of αA, may contribute to complex formation. Additionally, a high degree of deamidation of filensin was also detected, particularly at N303 (29.2-66.8% for each complex), which resides in the rod domain of the protein (Table 3.3). High levels of deamidation were also detected at N383 and N478 in the tail domain (Table 3.3). However, as peptides containing N383 and N478 were not detected for most complexes (likely due to C-terminal truncation), this suggests that N303 plays a larger role in complex formation. It remains to be determined how deamidation at N383 contributes to complex formation. However, as deamidation-induced isomerisation can cause partial unfolding of proteins (Takata and Fujii, 2015), it is conceivable that structural changes in filensin caused by deamidation at N303, in conjunction with increased substrate affinity of phosphorylated αB, may trigger αB to associate with the intermediate network at fibre cell membranes.

Together these results suggest that, whether through direct interaction or by accumulation of proteins at fibre cell membranes, the association of αB at fibre cell membranes may obstruct membrane pores, contributing to the formation of the nucleocortical barrier at middle age.

Based on the results of the work presented here, a new model of how αB contributes to age-related nuclear cataract formation in proposed (Figure 6.1).

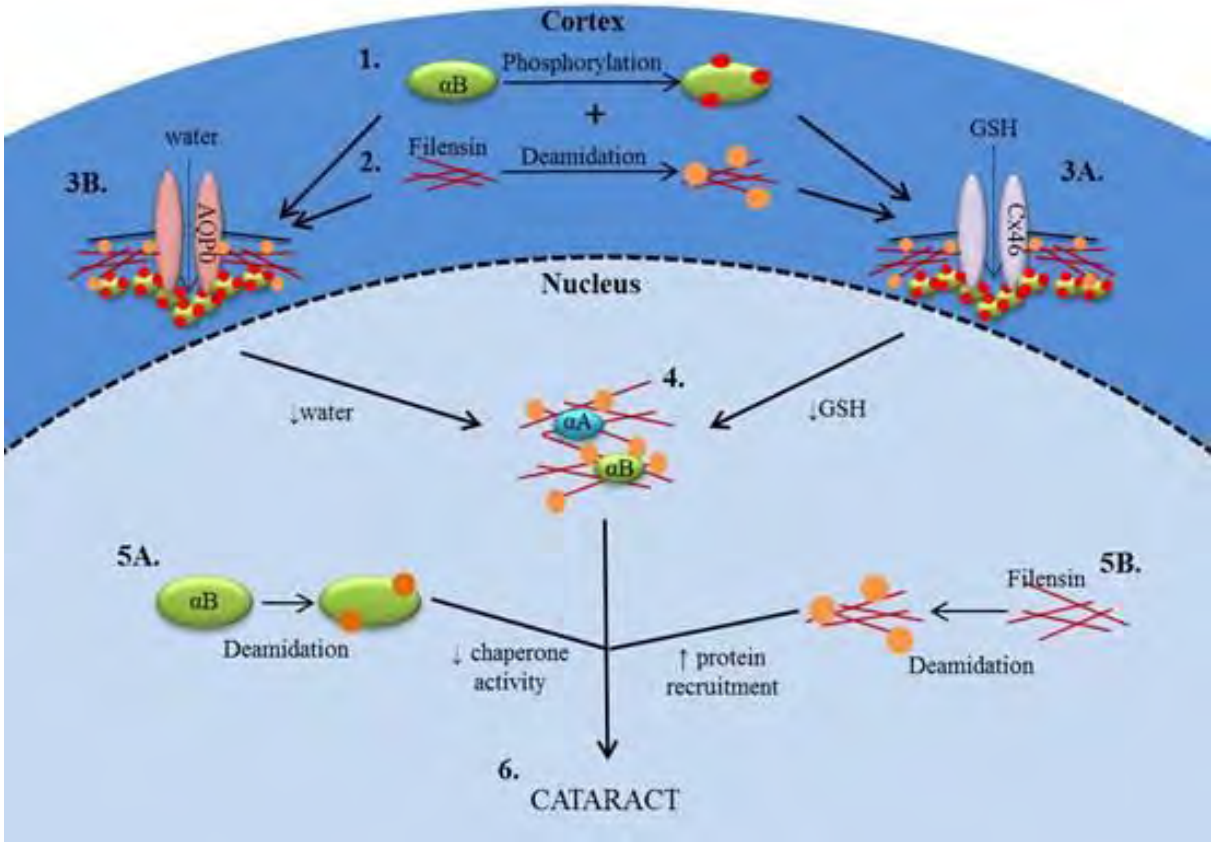

Figure 6.1: Possible roles of αB in age-related nuclear cataractogenesis. In aged lenses, (1) phosphorylation (red circles) of multiple serine residues in cortical αB (green oval) results in an increase in the chaperone activity of αB. (2) Deamidation (orange circles) of cytoskeletal proteins, including filensin (red lines), induces protein unfolding, increasing substrate affinity of cytoskeletal proteins and, together with the increase in the chaperone activity of αB, induces association of αB at fibre cell membranes. Association of αB with fibre cell membranes occludes (3A) Cx46 pores (purple ovals) inhibiting GSH transport, and (3B) AQP0 pores (pink ovals) inhibiting water transport from the cortex (dark blue) into the nucleus (light blue), leading to the formation of the nucleocortical barrier (dashed line) at middle age. (4) An increased level of oxidation in the nucleus, as a result of decreased GSH transport from the cortex, results in the formation of crosslinked HMW protein complexes involving filensin, αA (blue oval) and αB. (5A) Age-related, non-enzymatic deamidation of αB (e.g. at N146 and Q151) decreases the chaperone activity of the remaining non-complexed αBand (5B) deamidation of nuclear proteins, such as filensin, increases the recruitment of proteins into HMWCs. (6) Reduced activity of non-complexed αB, and the loss of soluble, chaperone-active αB into HMWCs in the nucleus results in these protein complexes becoming insoluble. Together with protein oxidation, this leads to nuclear cataract formation.

6.2.1 Barrier to GSH transport

To investigate how the association of αB at fibre cell membranes may be involved in barrier formation, 2D profiles of membrane proteins fractions were compared (section 3.3.2), and the distribution of interactions between αB and abundant membrane pore proteins (i.e. Cx46 and AQP0) was mapped across human lens sections (section 4.3.2).

Two dimensional electrophoretic profiles of high density protein fractions of aged human lenses showed increased amounts of highly phosphorylated αB isotypes compared to low density fractions (section 3.3.2). As these high density fractions have previously been shown to represent membrane associated protein (Friedrich and Truscott, 2009; Friedrich and Truscott, 2010), this suggests that increased αB phosphorylation leads to increased membrane association.

The association of αB with Cx46 and AQP0 was restricted to the cortical region of the lens (outer 500 μm for AQP0 and outer 250 μm for Cx46) (section 4.3, section 4.4.2) (section 3.4.2). This region coincides with the onset of the association of αB with fibre cell membranes (i.e. zone 3) (section 4.3.1) and the putative location of the nucleocortical barrier (section 4.4.2). It has been previously postulated that the presence of this barrier may cause the decrease in nuclear GSH that is believed to be a precursor to cataract formation (Cobb and Petrash, 2002b; Friedrich and Truscott, 2009; Friedrich and Truscott, 2010). The association of αB with membrane proteins, particularly Cx46, reported in this study supports this hypothesis. If, as a result of this association between αB and Cx46, these gap junctions become obstructed, GSH transport into the nucleus may be hindered leading to a decrease in nuclear GSH concentrations and the accumulation of oxidative protein damage (Figure 6.1). This would potentially result in the formation of HMWCs, such as those observed during this study (section 3.4.3). Furthermore, the presence of an additional oxidation site at M649 on filensin corresponded with a ~2-fold increase in the size of the complexes reported in this study (section 3.4.3). It has been proposed that the insolubility of such complexes is the dominant pathway leading to insoluble protein associated with cataract formation (Smulders *et al.*, 1998). Additionally, the increased susceptibility of proteins to non-enzymatic deamidation in the nucleus could also contribute to the recruitment of proteins into HMWCs, while reducing the chaperone activity of αB (Gupta and Srivastava, 2004; Asomugha *et al.*, 2011). The loss of soluble and chaperone-active αB, due to its incorporation into crosslinked complexes, could then be a mitigating factor in cataract formation (Figure 6.1).

Chapter 6

6.3 Future directions

This study utilised αB phosphomimics to determine how phosphorylation may affect the chaperone activity of αB (section 3.3.1). Phosphomimics are often used as they impart a negative charge to proteins similar to phosphorylation, while allowing the targeting of specific residues to give a homogeneous product. However, as phosphomimics are non-physiological and impart a single charge compared to the double negative charge introduced by phosphorylation, their relevance as models of the effect of phosphorylation is limited. Although some residue specificity is lost, protein kinases are commercially available, and can be used to induce phosphorylation of recombinant protein *in vitro*. For example, commercially available MAPKAP2, the kinase responsible for phosphorylation of Ser59 (Kato *et al.*, 1998), could be used to phosphorylate Ser59 of αB *in vitro*. This would provide a more physiologically relevant model of phosphorylated αB, and may provide further insight into how the chaperone activity of αB is regulated by phosphorylation.

Although interactions between αB and membrane proteins (i.e. Cx46 and AQP0) were observed in this work (section 4.3.2), it is possible that membrane association could also be mediated by association of αB with cytoskeletal components or membrane phospholipids. Previous reports regarding this have been conflicting. For example, Mulders *et al.* (1985) reported that α-crystallin associated only with fibre cell membrane extracts that retained some native proteins, while association with artificial phospholipid vesicles only occurred when the vesicles had been reconstituted with MP26 (Mulders *et al.*, 1985). However, Cobb and Petrash (2002a) later reported that α-crystallin was able to bind artificial phospholipid bilayers in the absence of all proteins. Performing further substrate binding and membrane affinity assays may elucidate the precise nature by which αB associates with membranes cells from the lens. Furthermore, the use of αB phosphomimics for such assays would provide further insight into how phosphorylation affects this process.

Deamidation of αB at both N146 and Q151 was increased by heat-treatment under neutral conditions (Table 5.5, section 5.4). While deamidation at N146 is well characterised and known to reduce chaperone activity of αB (Gupta and Srivastava, 2004; Asomugha *et al.*, 2011), deamidation at Q151 has not been investigated due to its relatively low abundance *in vivo*. Mutants that mimic deamidation at asparagine residues of αB (i.e. N→D substitutions) have been extensively used to study the functional impact of deamidation of proteins (Gupta and Srivastava, 2004; Asomugha *et al.*, 2011; Tiwary *et al.*, 2015). Additionally, Q85E and

Chapter 6

Q180E mutants have been used previously for structural studies of βA3-crystallin (Takata *et al.*, 2008). However, to our knowledge, studies utilising Q→E mutants to mimic deamidation at glutamine residues of αB have not been previously attempted. Performing aggregation assays utilising αB Q→E deamidation mimics may help elucidate whether deamidation at Q151 has a similar detrimental effect on αB function.

6.4 Conclusion

The results of this work provide evidence of a role for αB in multiple pathways that culminate in the formation of age-related nuclear cataract. The model described in this thesis proposes that phosphorylation of αB increases its molecular chaperone activity, thereby inducing association with highly deamidated intermediate filament proteins (i.e. filensin) at fibre cell membranes. This results in the occlusion of membrane pore proteins, including Cx46 and AQP0, leading to the formation of a physical barrier to diffusion into the nucleus i.e. the nucleocortical barrier. The presence of this barrier inhibits the transport of GSH into the nucleus of the lens, leading to low levels of nuclear GSH and the accumulation of oxidative damage, resulting in the formation of crosslinked HMW complexes involving αB. The accumulation of non-enzymatic deamidation of αB, together with the loss of soluble, chaperone-active αB, is then suggested to lead to the insolubilisation of HMW complexes, resulting in cataract formation.

Chapter 7

References

Chapter 7

Acosta-Sampson, L. and J. A. King (2010). Partially unfolded aggregation intermediates of human γD-, γC- and γS-crystallin are recognised and bound by human αB-crystallin chaperone. *The Journal of Molecular Biology* **401**: 134-152.

Adhikari, A. S., B. N. Singh, K. S. Rao and M. Rao (2011). αB-Crystallin, a small heat shock protein, modulates NF-κB activity in a phosphorylation-dependent manner and protects muscle myoblasts from TNF-α induced toxicity. *Biochimica et Biophysica Acta* **1813**: 1532-1542.

Ahmad, F., B. Raman, T. Ramakrishna and M. Rao (2008). Effect of phosphorylation of αB-crystallin: differences in stability, subunit exchange and chaperone activity of homo and mixed oligomers of αB-crystallin and its phosphorylation-mimicking mutant. *Journal of Molecular Biology* **375**: 1040-1051.

Alizadeh, A., J. I. Clark, T. Seeberger, J. F. Hess, T. Blankenship and P. G. FitzGerald (2003). Targeted deletion of the lens fibre cell-specific intermediate filament protein filensin. *Investigative Ophthalmology and Visual Science* **44**: 5252-5258.

Alizadeh, A., J. I. Clark, T. Seeberger, J. F. Hess, T. Blankenship, A. Spicer and P. G. FitzGerald (2002). Targeted genomic deletion of the lens-specific intermediate filament protein CP49. *Investigative Ophthalmology and Visual Science* **43**: 3722-3727.

Andley, U. P., J. P. Malone and R. R. Townsend (2014). In vivo substrates of the lens molecular chaperones αA-crystallin and αB-crystallin. *PLoS ONE* **9**: e95507.

Aquilina, J. A., J. L. P. Benesch, L. L. Ding, O. Yaron, J. Horwitz and C. V. Robinson (2004). Phosphorylation of αB-crystallin alters chaperone function through loss of dimeric substructure. *Journal of Biological Chemistry* **279**: 28675-28680.

Aquilina, J. A., J. L. P. Benesch, L. L. Ding, O. Yaron, J. Horwitz and C. V. Robinson (2005). Subunit exchange of polydisperse proteins: mass spectrometry reveals consequences of α-crystallin truncation. *Journal of Biological Chemistry* **280**: 14485-14491.

Arac, A., S. E. Brownell, J. B. Rothbard, C. Chen, R. M. Ko, M. P. Pereira, G. W. Albers, L. Steinman and G. K. Steinberg (2011). Systemic augmentation of αB-crystallin provides therapeutic benefit twelve hours post-stroke onset via immune modulation. *Proceedings of the National Academy of Science* **108**: 13287-13292.

Arrigo, A.-P., S. Simon, B. Gibert, C. Kretz-Remy, M. Nivon, A. Czekalla, D. Guillet, M. Moulin, C. Diaz-Latoud and P. Vicart (2007). Hsp27 (HspB1) and αB-crystallin (HspB5) as therapautic targets. *FEBS Letters* **581**: 3665-3874.

Chapter 7

Asomugha, C. O., R. Gupta and O. P. Srivastava (2010). Identification of crystallin modifications in the human lens cortex and nucleus using laser capture microdissection and CyDye labelling. *Molecular Vision* **16**: 476-494.

Asomugha, C. O., R. Gupta and O. P. Srivastava (2011). Structural and functional roles of deamidation of N146 and/or truncation of NH_2- or COOH-termini in human αB-crystallin. *Molecular Vision* **17**: 2407-2420.

Atomi, Y., S. Yamada and Y. M. Hong (1990). Dynamic expression of αB-crystallin in skeletal muscle. *Proceedings of the Japan Academy. Ser B.* **66**: 203-208.

Augusteyn, R. C. and J. F. Koretz (1987). A possible structure for α-crystallin. *FEBS Letters* **222**: 1-5.

Augusteyn, R. C., L. Murnane, A. Nicola and A. Stevens (2002). Chaperone activity in the lens. *Clinical and Experimental Optometry* **85**: 83-90.

Bagchi, M., S. Kousis and H. Maisel (2008). BASP1 in the lens. *Journal of Cellular Biochemistry* **105**: 699-207.

Bagneris, C., O. A. Bateman, C. E. Naylor, N. Cronin, W. C. Boelens, N. H. Keep and C. Slingsby (2009). Crystal structures of α-crystallin domain dimers of αB-crystallin and Hsp20. *Journal of Molecular Biology* **392**: 1242-1252.

Baird, M. F., S. M. Graham, J. S. Baker and J. F. Bickerstaff (2012). Creatine-kinase- and exercise-related muscle damage implications for muscle performance and recovery. *Journal of Nutrition and Metabolism* **2012**: 1-13.

Baldwin, A. J., H. Lioe, G. R. Hilton, L. A. Baker, J. L. Rubinstein, L. E. Kay and J. L. P. Benesch (2011). The polydispersity of αB-crystallin is rationalised by an interconverting polyhedral architecture. *Structure* **19**: 1855-1863.

Ball, L. E., D. L. Garland, R. K. Crouch and K. L. Schey (2004). Posttranslational modifications of aquaporin 0 (AQP0) in the normal human lens: spatial and temporal occurrence. *Biochemistry* **43**: 9856-9865.

Ball, L. E., M. Little, M. W. Nowak, R. K. Crouch and K. L. Schey (2003). Water permeability of C-terminally truncated aquaporin 0 (AQP0 1-243) observed in the aging human lens. *Investigative Opthalmology and Visual Science* **44**: 4820-4828.

Chapter 7

Banerjee, D., G. Gakhar, D. Madgwick, A. Hurt, D. J. Takemoto and T. A. Nguyen (2010). A novel role of gap junction connexin46 protein to protect breast tumors from hypoxia. *International Journal of Cancer* **127**: 839-848.

Bassnett, S., P. C. Croghan and G. Duncan (1987). Diffusion of lactate and its role in determining intracellular pH in the lens of the eye. *Experimental Eye Research* **44**: 143-147.

Bassnett, S., P. A. Wilmarth and L. L. David (2009). The membrane proteome of the mouse lens fibre cell. *Molecular Vision* **15**: 2448-2463.

Benedek, G. B. (1971). Theory of transparency of the eye. *Applied Optics* **10**: 459-473.

Benesch, J. L. P., M. Ayoub, C. V. Robinson and J. A. Aquilina (2008). Small heat shock protein activity is regulated by variable oligomeric substructure. *J Biol Chem* **283**: 28513-28517.

Bennardini, F., A. Wrzosek and M. Chiesi (1992). αB-Crystallin in cardiac tissue. Association with actin and desmin filaments. *Circulation Research* **71**: 288-294.

Berry, V., P. Francis, M. A. Reddy, D. Collyer, E. Vithana, I. Mackay, G. Dawson, A. H. Carey, A. Moore, S. S. Bhattacharya and R. A. Quinlan (2001). αB-Crystallin gene (*CRYAB)* mutation causes dominant congenital posterior polar cataract in human. *American Journal of Human Genetics* **69**: 1141-1145.

Berson, S. A. and R. S. Yalow (1966). Deamidation of insulin during storage in frozen state. *Diabetes* **15**: 875-879.

Bessems, G. J., H. J. Rennen and H. J. Hoenders (1987). Lanthionine, a protein cross-link in cataractous human lenses. *Experimental Eye Research* **44**: 691-695.

Beyer, E. C. and V. M. Berthoud (2014). Connexin hemichannels in the lens. *Fronteirs in Physiology* **5**: 20.

Bindels, J. G., L. W. Misdom and H. J. Hoenders (1985). The reaction of citraconic anhydride with bovine α-crystallin lysine residues: surface probing and dissociation-reassociation studies. *Biochimica et Biophysica Acta* **828**: 255-260.

Bloemendal, H. (1977). The vertebrate eye lens. *Science* **197**: 127-138.

Bloemendal, H. (1981). Molecular and Cellular Biology of the Eye Lens. New York, Wiley-Blackwell.

Chapter 7

Bloemendal, H., W. W. de Jong, R. Jaenicke, N. H. Lubsen, C. Slingsby and A. Tardieu (2004). Ageing and vision: structure, stability and function of lens crystallins. *Progress in Biophysics and Molecular Biology* **86**: 407-485.

Boscia, F., I. Grattagliano, G. Vendemiale, T. Micelli-Ferrari and E. Altomare (2000). Protein oxidation and lens opacity in humans. *Investigative Opthalmology and Visual Science* **41**: 2461-2465.

Bova, M. P., O. Yaron, Q. Huang, L. Ding, D. A. Haley, P. L. Stewart and J. Horwitz (1999). Mutation R120G in αB-crystallin, which is linked to desmin-related myopathy, results in an irregular structure and defective chaperone-like function. *Proceedings of the National Academy of Sciences* **96**: 6137-6142.

Boyle, D. and L. Takemoto (1994). Characterisation of the α-γ and α-β complex: evidence for an *in vivo* functional role of α-crystallin as a molecular chaperone. *Experimental Eye Research* **58**: 9-16.

Boyle, D. and L. Takemoto (1996). EM immunolocalisation of α-crystallins: association with the plasma membrane from normal and cataractous human lenses. *Current Eye Research* **15**: 577-582.

Braun, N., M. Zacharias, J. Peschek, A. Kastenmuller, J. Zou, M. Hanzlik, M. Haslbek, J. Rappsilber, J. Buchner and S. Weinkauf (2011). Multiple molecular architectures of the eye lens chaperone αB-crystallin elucidated by a triple hybrid approach. *Proceedings of the National Academy of Science* **108**: 20491-20496.

Breen, E. J., F. G. Hopwood, K. L. Williams and M. R. Wilkins (2000). Automatic Poisson peak harvesting for high throughput protein identification. *Electrophoresis* **21**: 2243-2251.

Burdon, K. P., M. G. Wirth, D. A. Mackey, -. E. Russell, I. M., J. E. Craig, J. E. Elder, J. L. Dickinson and M. M. Sale (2004). A novel mutation in the Connexin 46 gene causes autosomal dominant congenital cataract with incomplete penetrance. *Journal of Medical Genetics* **41**: 106.

Capasso, S., L. Mazzarella, F. Sica and A. Zagari (1991). First evidence of spontaneous deamidation of glutamine residue via cyclic imide to α- and γ-glutamic residue under physiological conditions. *Journal of the Chemical Society, Chemical Communications*: 1667-1668.

Carter, J. M., A. M. Hutcheson and R. A. Quinlan (1995). *In vitro* studies on the assembly properties of the lens proteins CP49, CP115: coassembly with α-crystallin but not with vimentin. *Exp Eye Res* **60**: 181-192.

Chapter 7

Carver, J. A., J. A. Aquilina and R. J. W. Truscott (1993). An investiagtion into the stability of α-crystallin by NMR spectroscopy: evidence for a two domain structure. *Biochimica et Biophysica Acta* **1164**: 22-28.

Carver, J. A., J. A. Aquilina and R. J. W. Truscott (1994). A possible chaperone-like quaternary structure for α-crystallin. *Experimental Eye Research* **59**: 231-234.

Carver, J. A., J. A. Aquilina, R. J. W. Truscott and G. B. Ralston (1992). Identification by ^{1}H NMR spectroscopy of flexible C-terminal extensions in bovine lens α-crystallin. *Federation of European Biochemical Societies* **311**: 143-149.

Carver, J. A. and R. A. Lindner (1998). NMR spectroscopy of α-crystallin. Insights into the structure, interactions and chaperone action of small heat-shock proteins. *International Journal of Biological Macromolecules* **22**: 197-209.

Carver, J. A., K. A. Nicholls, J. A. Aquilina and R. J. W. Truscott (1996). Age-related changes in bovine α-crystallin and high-molecular-weight protein. *Experimental Eye Research* **63**: 639-647.

Catak, S., G. Monard, V. Aviyente and M. F. Ruiz-Lopez (2009). Deamidation of asparagine residues: direct hyrdolysis versus succinimide-mediated deamidation mechanisms. *Journal of Physical Chemistry* **113**: 1111-1120.

Cenedella, R. J. and C. R. Fleschner (1992). Selective association of crystallins with lens 'native' membrane during dynamic cataractogenesis. *Curr Eye Res* **11**: 801-815.

Chandrasekher, G. and R. J. Cenedella (1995). Protein associated with human lens "native" membrane during aging and cataract formation. *Experimental Eye Research* **60**: 707-717.

Chandrasekher, G. and R. J. Cenedella (1997). Properties of α-crystallin bound to lens membrane: probing organisation at the membrane surface. *Experimental Eye Research* **64**: 423-430.

Chaves, J. M., K. Srivastava, R. Gupta and O. P. Srivastava (2008). Structural and functional roles of deamidation and/or truncation of N- or C-termini in human αA-crystallin. *Biochemistry* **47**: 10069-10083.

Chen, Y. C., G. E. Reid, R. J. Simpson and R. J. W. Truscott (1997). Molecular evidence for the involvement of α-crystallin in the colouration/crosslinking of crystallins in age-related nuclear cataract. *Experimental Eye Research* **65**: 835-840.

Chapter 7

Cherian, M. and E. C. Abraham (1995). Decreased molecular chaperone property of α-crystallins due to posttranslational modifications. *Biochemical and Biophysical Research Communications* **208**: 675-679.

Chin, D., D. M. Boyle, R. M. Williams, K. Ferguson, N. Pandeya, J. Pedley, C. M. Campbell, D. R. Theile, P. G. Parsons and W. B. Coman (2005). αB-Crystallin, a new independent marker for poor prognosis in head and neck cancer. *The Laryngoscope* **115**: 1239-1242.

Clark, A. R., C. E. Naylor, C. Bagneris, N. H. Keep and C. Slingsby (2011). Crystal structure of R120G disease mutant of human αB-crystallin domain dimer shows closure of a groove. *Journal of Molecular Biology* **408**: 118-134.

Cobb, B., A. and J. M. Petrash (2000). Characterisation of α-crystallin-plasma membrane binding. *Journal of Biological Chemistry* **275**: 6664-6672.

Cobb, B., A. and J. M. Petrash (2002a). Factors influencing α-crystallin association with phospholipid vesicles. *Molecular Vision* **8**: 85-93.

Cobb, B. A. and J. M. Petrash (2002b). α-Crystallin chaperone-like activity and membrane binding in age-related cataracts *Biochemistry* **41**: 483-490.

Conley, Y. P., D. Erturk, A. Keverline, T. S. Mah, A. Keravala, L. R. Barnes, A. Bruchis, J. F. Hess, P. G. FitzGerald, D. E. Weeks, R. E. Ferrell and M. B. Gorin (2000). A juvenile-onset, progressive cataract locus on chromosome 3q21-q22 is associated with a missense mutation in the beaded filament structural protein-2. *American Journal of Human Genetics* **66**: 1426-1431.

Dabbs, R. A. and M. R. Wilson (2014). Expression and purification of chaperone-active recombinant clusterin. *PLoS ONE* **9**: e86989.

Dasgupta, S., T. C. Hohman and D. Carper (1992). Hypertonic stress induces αB-crystallin expression. *Experimental Eye Research* **54**: 461-470.

Datiles III, M. B., R. R. Ansari, J. Yoshida, H. Brown, A. I. Zambrano, J. Tian, S. Vitale, J. S. Zigler, F. L. Ferris III, S. K. West and W. J. Stark (2016). Longitudinal study of age-related cataract using dynamic light scattering. *Ophthalmology* **123**: 248-254.

de Jong, W. W., G.-J. Caspers and J. A. M. Leunissen (1998). Genealogy of the α-crystallin-small heat-shock protein superfamily. *International Journal of Biological Macromolecules* **22**: 151-162.

Chapter 7

De Jong, W. W., N. H. Lubsen and H. J. Kraft (1994). Molecular evolution of the eye lens. *Progress in Retinal Eye Research* **13**: 391-422.

Deeley, J. M., J. A. Hankin, M. G. Friedrich, R. C. Murphy, R. J. W. Truscott, T. W. Mitchell and S. J. Blanksby (2010). Sphingolipid distribution changes with age in the human lens. *Journal of Lipid Research* **51**: 2753-2760.

Delaye, M. and A. Tardieu (1983). Short range order of crystallin proteins accounts for lens transparency. *Nature* **302**: 415-417.

den Engelsman, J., D. Gerrits, W. W. de Jong, J. Robbins, K. Kato and W. C. Boelens (2005). Nuclear import of αB-crystallin is phosphorylation-dependent and hampered by hyperphosphorylation of the myopathy-related mutant R120G. *Journal of Biological Chemistry* **280**: 37139-37148.

den Engelsman, J., C. van de Schootbrugge, J. Yong, G. J. M. Pruijn and W. C. Boelens (2013). Pseudophosphorylated αB-crystallin is a nuclear chaperone imported into the nucleus with help of the SMN complex. *PLoS ONE* **8**: 73489-73498.

Derham, B. K. and J. J. Harding (1997). Effect of aging on the chaperone-like function of human α-crystallin assessed by three methods. *Biochemical Journal* **328**: 763-768.

Djabali, K., B. de Nechaud, F. Landon and M.-M. Portier (1997). αB-Crystallin interacts with intermediate filaments in response to stress. *Journal of Cell Science* **110**: 2759-2769.

Eaton, P., W. Fuller, J. R. Bell and M. J. Shattock (2001). αB-crystallin translocation and phopshorylation: signal transduction pathways and preconditioning in the isolated rat heart *Journal of Molecular and Cellular Cardiology* **33**: 1659-1671.

Eckert, R. (2002). pH gating of lens fibre connexins. *Pflugers Archiv* **443**: 843-851.

Ecroyd, H., S. Meehan, J. Horwitz, J. A. Aquilina, J. L. P. Benesch, C. V. Robinson, C. E. Macphee and J. A. Carver (2007). Mimicking phosphorylation of αB-crystallin affects its chaperone activity. *Biochemical Journal* **401**: 129-141.

Evans, P., C. Slingsby and B. A. Wallace (2008). Association of partially unfolded lens βB2-crystallins with the α-crystallin chaperone. *The Biochemical Journal* **409**: 691-699.

Fagerholm, P. P., B. T. Philipson and B. Lindstrom (1981). Normal human lens-the distribution of proteins. *Experimental Eye Research* **33**: 615-620.

Chapter 7

Farnsworth, P. N., H. Frauwith, B. Groth-Vasselli and K. Singh (1998). Refinement of 3D structure of bovine lens αA-crystallin. *International Journal of Biological Macromolecules* **22**: 175-185.

FitzGerald, P. G. and D. Graham (1991). Ultrastructural localisation of αA-crystallin to the bovine lens fibre cell cytoskeleton. *Current Eye Research* **10**: 417-436.

Flaugh, S. L., I. A. Mills and J. A. King (2006). Glutamine deamidation detsabilises human γD-crystallin and lowers the kinetic barrier to unfolding. *The Journal of Biological Chemistry* **281**: 30782-30793.

Fleschner, C. R. and R. J. Cenedella (1992). Examination of a lens "native" plasma emmbrane fraction and its associated crystallins. *Current Eye Research* **11**: 739-752.

Francis, P., J.-J. Chung, M. Yasui, V. Berry, A. Moore, M. K. Wyatt, G. Wistow, S. S. Bhattacharya and P. Agre (2000). Function impairment of lens aquaporin in two families with dominantly inherited cataracts. *Human Molecular Genetics* **9**: 2329-2334.

Friedrich, M. G. and R. J. W. Truscott (2009). Membrane association of proteins in the aging human lens: profound changes take place in the fifth decade of life. *Investigative Ophthalmology and Visual Science* **50**: 4768-4793.

Friedrich, M. G. and R. J. W. Truscott (2010). Large-scale binding of α-crystallin to cell membranes of aged normal lenses: a phenomenon that can be induced by mild thermal stress. *Investigative Ophthalmolology and Visual Science* **51**: 5145-5152.

Fujii, N., N. Fujii, M. Kida and T. Kinouchi (2010). Influence of Lβ-, Dα- and Dβ-Asp isomers of the Asp-76 residue on the properties of αA-crystallin 70-88 peptide. *Amino Acids* **39**: 1393-1399.

Fujii, N., T. Kawaguchi, H. Sasaki and N. Fujii (2011). Simultaneous stereoinversion and isomerisation at the Asp-4 residue in βB2-crystallin from the aged human eye lenses. *Biochemistry* **50**: 8628-8635.

Fujii, N., H. Sakaue, H. Sasaki and N. Fujii (2012). A rapid, comprehensive liquid chromatography-mass spectrometry (LC-MS)-based survey of the Asp isomers in crystallins from human cataract lenses. *Journal of Biological Chemistry* **287**: 39992-40002.

Fujii, N., Y. Shimmyo, M. Sakai, Y. Sadakane, T. Nakamura, Y. Morimoto, T. Kinouchi, Y. Goto and K. Lampi (2007). Age-related changes of α-crystallin aggregate in human lens. *Amino Acids* **32**: 87-94.

Chapter 7

Fujii, N., T. Takata, N. Fujii and K. Aki (2016). Isomerisation of aspartyl residues in crystallins and influence upon cataract. *Biochimica et Biophysica Acta* **1860**: 183-191.

Ganesan, S. K., J. W. Kyle, P. J. Minogue and S. Sathiyavedu (2012). An MIP/AQP0 mutation with impaired trafficking and function underlies an autosomal dominant congenital lamellar cataract. *Experimental Eye Research* **110**: 136-141.

Garner, M. H. and A. Spector (1980). Selective oxidation of cysteine and methionine in normal and senile cataractous lenses. *Proceedings of the National Academy of Sciences* **77**: 1274-1277.

Geiger, T. and S. Clarke (1987). Deamidation, isomerisation and racemisation at asparaginyl and aspartyl residues in peptides. Succinimide-linked reactions that contribute to protein degradation. *Journal of Biological Chemistry* **262**: 785-794.

Ghosh, J. G., M. R. Estrada and J. I. Clark (2005). Interactive domains for chaperone activity in the small heat shock protein, human αB-crystallin. *Biochemistry* **44**: 14854-14869.

Ghosh, J. G., A. K. Shenoy and J. I. Clark (2006). N- and C-terminal motifs in human αB-crystallin play an important role in the recognition, selection, solubilisation of substrates. *Biochemistry* **45**: 13847-13854.

Giblin, F. J. (2000). Gluathione: a vital lens antioxidant. *Journal of Ocular Pharmacology and Therapeutics* **16**: 121-135.

Golenhofen, N., P. Htun, W. Ness, R. Koob, W. Schaper and D. Drenckhahn (1999). Binding of the stress protein αB-crystallin to cardiac myofibrils correlates with the degree of myocardial damage during ischemia/reperfusion *in vivo*. *Journal of Molecular and Cellular Cardiology* **31**: 569-580.

Golenhofen, N., W. Ness, R. Koob, P. Htun, W. Schaper and D. Drenckhahn (1998). Ischemia-induced phosphorylation and translocation of stress protein αB-crystallin to Z lines of myocardium. *American Journal of Physiology* **274**: 1457-1464.

Gonen, T., Y. Cheng, J. Kistler and T. Walz (2004). Aquaporin-0 membrane junctions form upon proteolytic cleavage. *Journal of Molecular Biology* **342**: 1337-1345.

Gong, X., E. Li, G. Klier, Q. Huang, Y. Wu, H. Lei, N. M. Kumar, J. Horwitz and N. B. Gilula (1997). Disruption of alpha3 connexin gene ledas to proteolysis and cataractogenesis in mice. *Cell* **12**: 833-843.

Goodenough, D. A. (1992). The crystalline lens: a system networked by gap junctional intercellular communication. *Seminars in Cell Biology* **3**: 49-58.

Gorin, M. B., S. Yancey, S. B. Cline, J.-P. Revel and J. Horwitz (1984). The major intrinsic protein (MIP) of the bovine lens fibre membrane: characterisation and structure based on cDNA cloning. *Cell* **30**: 49-59.

Goto, I. (1974). Creatine phosphokinase isoenzymes in neuromuscular disorders. *Journal of the American Medical Association* **31**: 116-119.

Goulielmos, G. G., F. Gounari, S. Remington, S. Muller, M. Haner, U. Aebi and S. D. Georgatos (1996). Filensin and phakinin form a novel type of beaded intermediate filaments and coassemble *de novo* in cultered cells. *The Journal of Cell Biology* **132**: 643-655.

Grey, A. C., P. Chaurand, R. M. Caprioli and K. L. Schey (2009). MALDI imaging mass spectrometry of integral membrane proteins from ocular lens and retinal tissue. *Journal of Proteome Research* **8**: 3278-3283.

Grey, A. C. and K. L. Schey (2009). Age-related changes in the spatial distribution of human lens α-crystallin products by MALDI imaging mass spectrometry. *Investigative Ophthalmology and Visual Science* **50**: 4319-4329.

Groenen, P. J., K. B. Merck, W. W. De Jong and H. Bloemendal (1994). Structure and modifications of the junior chaperone α-crystallin: from lens transparency to molecular pathology. *225*(1-19).

Gupta, R. and O. P. Srivastava (2004). Effect of deamidation of Asparagine 146 on functional and structural properties of human lens αB-crystallin. *Investigative Ophthalmology and Visual Science* **45**: 206-214.

Hagemann, T. L., W. C. Boelens, E. F. Wawrousek and A. Messing (2009). Suppression of GFAP toxicity by αB-crystallin in mouse models of Alexander disease. *Hum Mol Genet* **18**: 1190-1199.

Hains, P. G. and R. J. W. Truscott (2007). Post-translational modifications in the nuclear region of young, aged, and cataract human lenses. *Journal of Proteome Research* **6**: 3935-3943.

Hains, P. G. and R. J. W. Truscott (2010). Age-dependent deamidation of lifelong proteins in the human lens. *Investigative Ophthalmology and Visual Science* **51**: 3107-3114.

Haley, D. A., J. Horwitz and P. L. Stewart (1998). The small heat-shock protein, αB-crystallin, has a variable quaternary structure. *Journal of Molecular Biology* **277**: 27-35.

Hammond, C. J., H. Snieder, T. D. Spector and C. E. Gilbert (2000). Genetic and environmental factors in age-related nuclear cataracts in monozygotic and dizygotic twins. *The New England Journal of Medicine* **342**: 1786-1790.

Han, J. and K. L. Schey (2006). MALDI tissue imaging of ocular lens α-crystallin. *Investigative Ophthalmology and Visual Science* **47**: 2990-2996.

Hanson, S. R., A. Hasan, D. L. Smith and J. B. Smith (2000). The major *in vivo* modifications of the human water-soluble lens crystallins are disulphide bonds, deamidation, methionine oxidation and backbone cleavage. *Experimental Eye Research* **71**: 195-207.

Hao, P., Y. Ren, A. J. Alpert and S. K. Sze (2011). Detection, evaluation and minimisation of nonenzymatic deamidation in proteomic sample preparation. *Molecular and Cellular Proteomics* **10**: O111.009381.

Harding, J. J. (1991). Cataract biochemistry, epidemiology and pharmacology. London, Chapman and Hall.

Harper, R. A. and J. P. Shock (2004). Lens. Vaughan and Ashbury's General Ophthalmology. P. Riordan-Eva and J. P. Whitcher. USA, Lange Medical Books/McGraw-Hill**:** 173-181.

Head, M., E. Corbin and J. Goldman (1993). Overexpression and abnormal modification of the stress proteins αB-crystallin and Hsp27 in Alexanders disease. *American Journal of Pathology* **143**: 1743-1753.

Hejtmancik, J. F. and M. Kantorow (2004). Molecular genetics of age-related cataract. *Experimental Eye Research* **79**: 3-9.

Hess, J. F., J. T. Casselman, A. P. Kong and P. G. FitzGerald (1998). Primary sequence, secondary structure, gene structure, and assembly properties suggests that lens-specific cytoskeletal protein filensin represents a novel class of intermediate filament protein. *Experimental Eye Research* **66**: 625-644.

Heys, K. R., M. G. Friedrich and R. J. W. Truscott (2007). Presbyopia and heat: changes associated with aging of the human lens suggest a functional role for the small heat shock protein, α-crystallin, in maintaining lens flexibility. *Aging Cell* **6**: 807-815.

Hochberg, G. K. A., H. Ecroyd, C. Liu, D. Cox, D. Cascio, M. R. Sawaya, M. P. Collier, J. Stroud, J. A. Carver, A. J. Baldwin, C. V. Robinson, D. S. Eisenberg, J. L. P. Benesch and A.

Laganowsky (2014). The structured core domain of αB-crystallin can preven amyloid fibrillation and associated toxicity. *Proceedings of the National Academy of Sciences* **111**: 1562-1570.

Hockwin, O. (1965). Enzyme activities in relationship to age and phosphorylated intermediates in energy metabolism. *Investigative Ophthalmology* **4**: 496-501.

Hockwin, O., E. Noll and W. Licht (1965). Influence of age on enzyme activities of lenses. *Ophthalmologica* **150**: 187-195.

Hooi, M. Y. S., M. J. Raftery and R. J. W. Truscott (2012). Age-dependent deamidation of glutamine residues in human γS-crystallin: deamidation and unstructured regions. *Protein Science* **21**: 1074-1079.

Hoover, H. E., D. J. Thuerauf, J. J. Martindale and C. C. Glembotski (2000). αB-Crystallin gene induction and phosphorylation by MKK6-activated p38. *Journal of Biological Chemistry* **275**: 23825-23833.

Horwitz, J. (1992). α-Crystallin can function as a molecular chaperone. *Proceedings of the National Academy of Science USA* **89**: 10449-10453.

Horwitz, J. (1993). The function of α-crystallin. *Investigative Ophthalmology and Visual Science* **34**: 10-22.

Horwitz, J. (2000). The function of α-crystallin in vision. *Seminars in Cell and Developmental Biology* **11**: 53-60.

Horwitz, J. (2003). α-Crystallin. *Experimental Eye Research* **76**: 145-153.

Horwitz, J., M. P. Bova, L. Ding, D. A. Haley and P. L. Stewart (1999). Lens α-crystallin: function and structure. *Eye* **13**: 403-408.

Horwitz, J., Q.-L. Huang, L. L. Ding and M. P. Bova (1998). Lens α-crystallin: chaperone-like properties. *Methods in Enzymology* **290**: 365-383.

Hu, S., B. Wang, Y. Qi and H. Lin (2012). The Arg233Lys AQP0 mutation disturbs aquaporin0-calmodulin interaction causing polymorphic congenital cataract. *PLoS ONE* **7**: 37637.

Huang, C.-H., Y.-T. Wang, C.-F. Tsai, Y.-J. Chen, J.-S. Lee and S.-H. Chiou (2011). Phosphoproteomics characterisation of novel phosphorylated sites of lens proteins fom normal and cataractous human eye lenses. *Molecular Vision* **17**: 186-198.

Inagaki, N., T. Hayashi, T. Arimura, Y. Koga, M. Takahashi, H. Shibata, K. Teraoka, T. Chikamori, A. Yamashina and A. Kimura (2006). αB-Crystallin mutation in dilated cardiomyopathy. *Biochemical and Biophysical Research Communications* **342**: 379-386.

Ingolia, T. D. and E. A. Craig (1982). Four small *Drosophila* heat shock proteins are related to each other and to mammalian α-crystallin. *Proceedings of the National Academy of Science USA* **79**: 2360-2364.

Ito, H., A. Kamei, I. Iwamoto, Y. Inaguma, R. Garcia-Mata, E. Sztul and K. Kato (2002). Inhibition of proteasomes induces accumulation, phosphorylation, and recruitment of Hsp27and αB-crystallin to aggresomes. *Journal of Biochemistry* **131**: 593-603.

Ito, H., K. Kamei, I. Iwamoto, Y. Inaguma, D. Nohara and K. Kato (2001). Phosphorylation-induced change of the oligomerization state of αB-crystallin. *Journal of Biological Chemistry* **276**: 5346-5352.

Ito, H., K. Okamoto, H. Nakayama, T. Isobe and K. Kato (1997). Phosphorylation of αB-crystallin in response to various types of stress. *Journal of Biological Chemistry* **272**: 29934-29941.

Iwaki, T., A. Kume-Iwaki, R. K. H. Liem and J. E. Goldman (1989). αB-Crystallin is expressed in non-lenticular tissues and accumulates in Alexander's disease brain. *Cell*

57: 71-78.

Jakobs, P. M., J. F. Hess, P. G. FitzGerald, P. Kramer, R. G. Weleber and M. Litt (2000). Autosomal-dominant congenital cataract associated with a deletion mutation in the human beaded filament protein gene BFSP2. *American Journal of Human Genetics* **66**: 1432-1436.

Jehle, S., P. Rajagopal, B. Bardiaux, S. Markovic, R. Kuhne, J. R. Stout, V. A. Higman, R. E. Klevit, B.-J. van Rossum and H. Oschkinat (2010). Solid-state NMR and SAXS studies provide a structural basis for the activation of αB-crystallin oligomers. *Nature* **17**: 1037-1043.

Jehle, S., B. S. Vollmar, B. Bardiaux, K. K. Dove, P. Rajagopal, T. Gonen, H. Oschkinat and R. E. Klevit (2011). N-terminal domain of αB-crystallin provides a conformational switchfor multimerization and structural heterogeneity. *Proceedings of the National Academy of Science* **108**: 6409-6414.

Kamei, A., T. Hamaguchi, N. Matsuura, H. Iwase and K. Masuda (2000). Post-translational modification of αB-crystallin of normal human lenses. *Biological and Pharmaceutical Bulletin* **23**: 226-230.

Kamei, A., T. Hamaguchi, N. Matsuura and K. Masuda (2001). Does post-translational modification influence chaperone-like activity of α-crystallin? 1. study on phosphorylation. *Biological and Pharmaceutical Bulletin* **24**: 96-99.

Kamradt, M. C., F. Chen, S. Sam and V. L. Cryns (2002). The small heat shock protein αB-crystallin negatively regulates apoptosis during myogenic differentiation by inhibiting caspase-3 activation. *Journal of Biological Chemistry* **277**: 38731-38736.

Kamradt, M. C., M. Lu, M. E. Werner, T. Kwan, F. Chen, A. Strohecker, S. Oshita, J. C. Wilkinson, C. Yu, P. G. Oliver, C. S. Duckett, D. J. Buchsbaum, A. F. LoBuglio, V. C. Jordan and V. L. Cryns (2005). The small heat shock protein αB-crystallin is a novel inhibitor of TRAIL-induced apoptosis that suppresses the activation of caspase 3. *Journal of Biological Chemistry* **280**: 11059-11066.

Kannan, R., P. Santhoshkumar, B. P. Mooney and K. K. Sharma (2013). αA66-80 peptide interacts with soluble α-crystallin and induces its aggregation and precipitation: a contribution to age-related catarcat formarion. *Biochemistry* **52**: 10.1021/bi301662w.

Kantorow, M. and J. Piatigorsky (1994). α-Crystallin/small heat shock protein has autokinase activity. *Biochemistry* **91**: 3112-3116.

Kantorow, M. and J. Piatigorsky (1998). Phosphorylations of αA- and αB-crystallin. *International Journal of Biological Macromolecules* **22**: 307-314.

Kato, K., H. Ito, A. Kamei, I. Iwamoto and Y. Inaguma (2002). Innervation-dependent phosphorylation and accumulation of αB-crystallin and Hsp27 as insoluble complexes in disused muscle. *Federation of American Societies for Experimental Biology* **16**: 1432-1434.

Kato, K., H. Ito, K. Kamei, Y. Inaguma, I. Iwamoto and S. Saga (1998). Phosphorylation of αB-crystallin in mitotic cells and identification of enzymatic activites responsible for phosphorylation. *Journal of Biological Chemistry* **273**: 28346-28354.

Kim, Y. H., D. M. Kapfer, J. Boekhorst, N. H. Lubsen, H. P. Bachinger, T. R. Shearer, L. L. David, J. B. Feix and K. Lampi (2002). Deamidation, but not truncation, decreases the urea stability of a lens structural protein, βB1-crystallin. *Biochemistry* **41**: 14076-14084.

Klemenz, R., A. C. Andres, E. Frohli, R. Schafer and A. Aoyama (1993). Expression of the murine small heat shock proteins Hsp25 and αB-crystallin in the absence of stress. *Journal of Cell Biology* **120**: 639-645.

Klemenz, R., E. Frohli, A. Aoyama, S. Hoffmann, R. J. Simpson, R. L. Moritz and R. Schafer (1991). αB-crystallin accumulation is a specific response to Ha-ras and v-mos oncogene expression in mouse NIH 3T3 fibroblasts. *Molecular and Cellular Biology* **11**: 803-812.

Klemenz, R., E. Frohli, R. Steiger, H., R. Schafer and A. Aoyama (1991b). αB-Crystallin is a small heat shock protein. *Proceedings of the National Academy of Science USA* **88**: 3652-3656.

Kore, R. A. and E. C. Abraham (2014). Inflammatory cytokines, interleukin-1 β and tumor necrosis factor-α, upregulated in glioblastoma multiforme, raise the levels of CRYAB inexosomes secreted by U393 glioma cells. *Biochemical and Biophysical Research Communications* **453**: 326-331.

Koretz, J. F., E. W. Doss and J. N. LaButti (1998). Environmental factors influencing the chaperone-like activity of α-crystallin. *International Journal of Biological Macromolecules* **22**: 283-294.

Korlimbinis, A., Y. Berry, D. Thibault, K. L. Schey and R. J. W. Truscott (2009). Protein aging: truncation of aquaporin 0 in human lens regions is a continuous age-related process. *Experimental Eye Research* **88**: 966-973.

Kosky, A. A., A. O. Razzaq, M. J. Treuheit and D. N. Brems (1999). The effects of α-helix on the stability of Asn residues: deamidation rates in peptides of varying helicity. *Protein Science* **8**: 2519-2523.

Kossiakoff, A. (1988). Tertiary structure is a major determinant to protein deamidation. *Science* **240**: 191-194.

Koteiche, H. A. and H. S. Mchaourab (2003). Mechanism of chaperone function in small heat-shock proteins: phosphorylation-induced activation of two-mode binding in αB-crystallin. *Journal of Biological Chemistry* **278**: 10361-10367.

Koteiche, H. A. and H. S. Mchaourab (2006). Mechanism of a hereditary cataract phenotype: mutations in αA-crystallin activate subtrate binding. *The Journal of Biological Chemistry* **281**: 14273-14279.

Kramps, J. A., W. W. De Jong, J. Wollensak and H. J. Hoenders (1978). The polypeptide chains of α-crystallin from old human eye lenses. *Biochimica et Biophysica Acta* **533**: 487-495.

Kumari, S. S., S. Eswaramoorthy, R. Mathias and K. Varadaraj (2011). Unique and analogous of aquaporin 0 for fibre cell architecture and ocular lens transparency. *Biochimica et Biophysica Acta* **1812**: 1089-1097.

Chapter 7

Kumari, S. S., J. Gandhi, M. H. Mustehsan, S. Eren and K. Varadaraj (2013). Functional characterisation of an AQP0 missense mutation, R33C, that causes dominant congenital lens cataract reveals impared cell-cell adhesion. *Experimental Eye Research* **116**: 371-385.

Laganowsky, A., J. L. P. Benesch, M. Landau, L. Ding, M. R. Sawaya, D. Cascio, Q. Huang, C. V. Robinson, J. Horwitz and D. Eisenberg (2010). Crystal structures of truncated αA- and αB-crystallins reveal structural mechanisms of polydispersity important for eye lens function. *Protein Science* **19**: 1031-1043.

Lampi, K., K. K. Amyx, P. Ahmann and E. A. Steel (2006). Deamidation in human lens βB2-crystallin destabilises the dimer. *Biochemistry* **45**: 3146-3153.

Lampi, K., L. L. David and T. R. Shearer (1992). Association of calpain with insoluble pellet of rat lens. *Experimental Eye Research* **55**: 369-375.

Lampi, K., Y. H. Kim, H. P. Bachinger, B. A. Boswell, R. A. Lindner, J. A. Carver, T. R. Shearer, L. L. David and D. M. Kapfer (2002). Decreased heat stability and increased chaperone requirement of modified human βB1-crystallins. *Molecular Vision* **8**: 359-366.

Lampi, K., P. A. Wilmarth, M. R. Murray and L. L. David (2014). Lens β-crytsallins: the role of deamidation and related modifications in aging and cataract. *Progress in Biophysics and Molecular Biology* **115**: 21-31.

Lampi, K. J., Z. Ma, S. R. Hanson, H. Azuma, M. Shih, T. R. Shearer, L. L. David, D. L. Smith and J. B. Smith (1998). Age-related changes in human lens crystallins identified by two-dimensional electrophoresis and mass spectrometry. . *Experimental Eye Research* **67**: 31-43.

Lapko, V. N., A. G. Purkiss, D. L. Smith and J. B. Smith (2002). Deamidation in human gamma S-crystallin from cataractous lenses is influenced by surface exposure. *Biochemistry* **41**: 8638-8648.

Lapko, V. N., D. L. Smith and J. B. Smith (2001). *In vivo* carbamylation and acetylation of water-soluble human lens αB-crystallin lysine 92. *Protein Science* **10**: 1130-1136.

Launay, N., B. Goudeau, K. Kato, P. Vicart and A. Lilienbaum (2006). Cell signaling pathways to αB-crystallin following stresses of the cytoskeleton. *Experimental Cell Research* **312**: 3570-3584.

Launay, N., A. Tarze, P. Vicart and A. Lilienbaum (2010). Serine 59 phosphorylation of αB-crystallin down-regulates its anti-apoptotic function by binding and sequestering Bcl-2 in breast cancer cells. *Journal of Biological Chemistry* **285**: 37324-37332.

Li, L., J. S. Duker, Y. Yoshida, E. Niki, H. Rasmussen, R. M. Russell and J. K.-. Yeum (2009). Oxidative stress and antioxidant status in older adults with early cataract. *Eye* **23**: 1464-1468.

Li, R. and G. Reiser (2011). Phosphorylation of Ser45 and Ser59 of αB-crystallin and p38/extracellular regulated kinase activity determine αB-crystallin-mediated protection of rat brain astrocytes from C2-ceramide- and staurosporine-induced cell death. *Journal of Neurochemistry* **118**: 354-364.

Li, X., C. Lin and P. B. O'Connor (2010). Glutamine deamidation: differentiation of glutamic acid and gamma-glutamic acid in peptides by electron capture dissociation. *Analytical Chemistry* **82**: 3606-3615.

Liang, J.-N., T.-X. Sun and N. J. Akhtar (2000). Heat-induced conformational change of human lens recombinant αA- and αB-crystallins. *Molecular Vision* **6**: 10-14.

Liao, L., M. Zhao, J. Ren, H. Zhao, C. Cui and X. Hu (2009). Effect of acetic acid deamidation-induced modification on functional and nutritional properties and conformation of wheat gluten. *Society of Chemical Industry* **90**: 409-417.

Lim, J. C., K. L. Walker, T. Sherwin, K. L. Schey and P. J. Donaldson (2009). Confocal microscopy reveals zones of membrane remodelling in the outer cortex of the human lens. *Investigative Opthalmology and Visual Science* **50**: 4304-4310.

Lin, P., J. B. Smith and D. L. Smith (1997). *In vivo* modification of the C-terminal lysine of human lens αB-crystallin. *Experimental Eye Research* **65**: 673-680.

Lin, P. P., R. C. Barry, D. L. Smith and J. B. Smith (1998). *In vivo* acetylation identified at lysine 70 of human lens αA-crystallin. *Protein Science* **7**: 1451-1457.

Linetsky, M., J. M. W. Hill, R. LeGrand and F. Hu (2004). Dehydroalanine crosslinks in human lenses. *Experimental Eye Research* **79**: 499-512.

Linetsky, M. and R. LeGrand (2005). Glutathionylation of lens proteins through the formation of a thioether bond. *Molecular and Cellular Biochemistry* **272**: 133-144.

Litt, M., P. Kramer, D. M. LaMorticella, W. Murphey, E. W. Lovrien and R. G. Weleber (1998). Autosomal dominant congenital cataract associated with a missense mutation in the human α-crystallin gene *CRYAA*. *Human Molecular Genetics* **7**: 471-474.

Liu, B. F. and J. J. Liang (2008). Confocal fluorescence microscopy study of interaction between len MIP26/AQP0 and crystallins in living cells. *Journal of Cellular Biochemistry* **104**: 51-58.

Liu, M., T. Ke, Z. Wang, Q. Yang, W. Chang, F. Jiang, Z. Tang, H. Li, X. Ren, X. Wang, T. Wang, Q. Li, J. Yang, J. Liu and Q. K. Wang (2006). Identification of *CRYAB* mutation associated with autosomal dominant posterior polar cataract in a Chinese family. *Investigative Ophthalmology and Visual Science* **47**: 3461-3466.

Liu, Y., X. Zhang, L. Luo, M. Wu, R. Zeng, G. Cheng, B. Hu, B. Liu, J. J. Liang and F. Shang (2006). A novel αB-crystallin mutation associated with autosomal dominant congenital lamellar cataract. *Investigative Ophthalmology and Visual Science* **47**: 1069-1075.

Liu, Y., Q. Zhou, M. Tang, N. Fu, W. Shao, S. Zhang, Y. Yin, R. Zeng, X. Wang, G. Hu and J. Zhou (2015). Upregulation of αB-crystallin expression in the substantia nigra of patients with Parkinson's disease. *Neurobiology of Aging* **36**: 1686-1691.

Lund, A. L., J. B. Smith and D. L. Smith (1996). Modifications of the water-insoluble human lens α-crystallins. *Experimental Eye Research* **63**: 661-672.

Lynnerup, N., H. Kjeldsen, S. Heegaard, C. Jacobsen and J. Heinemeier (2008). Radiocarbon dating of the human eye lens crystallins reveal proteins without carbon turnover throughout life. *PLoS ONE* **3**(e1529).

Ma, Z., S. R. Hanson, K. J. Lampi, L. L. David, D. L. Smith and J. B. Smith (1998). Age-related changes in human lens crystallins identified by HLPC and mass spectrometry. *Experimental Eye Research* **67**: 21-30.

MacCoss, M. J., W. H. McDonald, A. Saraf, R. Sadygov, J. M. Clark, J. J. Tasto , K. L. Gould, D. Wolters, M. Washburn, A. Weiss, J. L. Clark and J. R. Yates (2002). Shotgun identification of protein modifications from protein complexes and lens tissue. *Proceedings of the National Academy of Science* **99**: 7900-7905.

Mackay, D. S., U. P. Andley and A. Shiels (2003). Cell death triggered by a novel mutation in the αA-crystallin gene underlies autosomal dominant cataract linked to chromosome 21q. *European Journal of Human Genetics* **11**: 784-793.

Mainz, A., J. Peschek, M. Stavropoulou, K. C. Back, B. Bardiaux, S. Asami, E. Prade, C. Peters, S. Weinkauf, J. Buchner and B. Reif (2015). The chaperone αB-crystallin uses different interfaces to capture an amorphous and an amyloid client. *Nature Structural and Molecular Biology* **22**: 898-908.

Chapter 7

Makley, L. N., K. A. McMenimen, B. T. DeVree, J. W. Goldman, B. N. McGlasson, P. Rajagopal, B. M. Dunyak, T. J. McQuade, A. T. Thompson, R. Sunahara, R. E. Klevit, U. P. Andley and J. E. Gestwicki (2015). Pharmacological chaperone for α-crystallin partially restores transparency in cataract models. *Science* **350**: 674-677.

Masaki, S. and R. A. Quinlan (1997). Gene structure and sequence comparisons of the eye lens specific protein, filensin, from rat and mouse: implications for protein classification and assembly. *Gene* **201**: 11-20.

Masters, P. M., J. L. Bada and J. S. Zigler (1977). Aspartic acid racemisation in the human lens during ageing and in cataract formation. *Nature* **268**: 71-73.

Mehlen, P., C. Kretz-Remy, X. Preville and A.-P. Arrigo (1996). Human hsp27, *Drosophila* hsp27 and human αB-crystallin expression-mediated increase in glutathione is essential for the protective activity of these proteins against TNFα-induced cell death. *The EMBO Journal* **15**: 2695-2706.

Merchant, T. E., J. H. Lass, P. Meneses, J. V. Greiner and T. Glonek (1991). Human crystalline lens phospholipid analysis with age. *Investigative Ophthalmology and Visual Science* **32**: 549-555.

Merck, K. B., W. A. de Haard-Hoekman, B. B. Oude Essink, H. Bloemendal and W. W. De Jong (1992). Expression and aggregation of recombinant αA-crystallin and its two domains. *Biochimica et Biophysica Acta* **1130**: 267-276.

Merck, K. B., J. Horwitz, M. Kersten, P. Overkamp, M. Gaestel, H. Bloemendal and W. W. De Jong (1993). Comparison of the homologous carboxyl-terminal domain and tail of α-crystallin and small heat shock protein. *Molecular Biology Reports* **18**: 209-215.

Michiel, M., E. Duprat, F. Skouri-Panet, S. Finet, A. Tardieu and K. Lampi (2010). Aggregation of deamidated human βB2-crystallin and incomplete rescue by α-crystallin chaperone. *Experimental Eye Research* **90**: 688-698.

Miesbauer, L. R., X. Zhou, Z. Yang, Z. Yang, Y. Sun, D. L. Smith and J. B. Smith (1994). Post-translational modifications of water-soluble human lens crystallins from young adults. *Journal of Biological Chemistry* **269**: 12494-12502.

Moffat, B. A., K. A. Landman, R. J. W. Truscott, M. H. Sweeney and J. M. Pope (1999). Age-related changes in the kinetics of water transport in normal human lenses. *Experimental Eye Research* **69**: 663-669.

Moffat, B. A. and J. M. Pope (2002). Anisotropic water transport in the human eye lens studied by diffusion tensor NMR micro-imaging. *Experimental Eye Research* **74**: 677-687.

Molina, S. A. and D. J. Takemoto (2012). The role of connexin 46 promoter in lens and other hypoxic tissues. *Communicative and Integrative Biology* **5**: 114-117.

Moreau, K. L. and J. A. King (2012). Protein misfolding and aggregation in cataract disease and prospects for prevention. *Trends in Molecular Medicine* **18**: 273-282.

Morrison, L. E., H. E. Hoover, D. J. Thuerauf and C. C. Glembotski (2003). Mimicking phosphorylation of αB-crystallin on Serine-59 is necessary and sufficient to provide maximal protection of cardial myocytes from apoptosis. *Circ Res* **92**: 203-211.

Mosevitsky, M. I. (2005). Nerve ending "signal" proteins GAP-43, MARCKS and BASP1. *International Review of Cytology* **245**: 245-325.

Mosevitsky, M. I., J. P. Capony, G. Y. Skladchikova, V. A. Novitskaya, A. Y. Plekhanov and V. V. Zakharov (1997). The BASP1 family of myristoylated proteins abundant in axonal termini. Primary structure analysis and physico-chemical properties. *Biochimie* **79**: 373-384.

Moyano, J. V., J. R. Evans, F. Chen, M. Lu, M. E. Werner, F. Yehiely, L. K. Diaz, D. Turbin, G. Karaca, E. Wiley, T. O. Nielsen, C. M. Perou and V. L. Cryns (2006). αB-Crystallin is a novel oncoprotein that predicts poor clinical outcome in breast cancer. *Journal of Clinical Investigation* **116**: 261-270.

Muchowski, P. J., M. M. Valdez and J. I. Clark (1999). αB-Crystallin selectively targets intermediate filament proteins during thermal stress. *Investigative Opthalmology and Visual Science* **40**: 951-958.

Mulders, J. W. M., J. Stokkermans, J. A. M. Leunissen, E. L. Benedetti, H. Bloemendal and W. W. de Jong (1985). Interaction of α-crystallin with plasma membranes. Affinity for MP26. *European Journal of Biochemistry* **152**: 721-728.

Muller, M., S. Bhattacharya, T. Moore, Q. Prescott, T. Wedig, H. Herrmann and T. M. Magin (2009). Dominant cataract formation in association with a vimentin assembly disrupting mutation. *Human Molecular Genetics* **18**: 1052-1057.

National Eye Institute, N. I. o. H. (2015a). "Drawing of the Eye." Retrieved 12.02.16, from nei.nih.gov/health/eyediagram.

National Eye Institute, N. I. o. H. (2015b). "Facts about cataract.". Retrieved 21.02.2016, from nei.nih.gov/health/cataract/cataract_facts.

Nicholl, I. D. and R. A. Quinlan (1994). Chaperone activity of α-crystallins modulates intermediate filament assembly. *The EMBO Journal* **13**: 945-953.

NIGMS (2012). "Inside the Cell." Retrieved 10th August, 2016, from publications.nigms.nih.gov/insidethecell/chapter1.

Oka, M., H. Kudo, N. Sugama, Y. Asami and M. Takehana (2008). The function of filensin and phakinin in lens transparency. *Molecular Vision* **14**: 815-822.

Ousman, S. S., B. H. Tomooka, J. M. van Noort, E. F. Wawrousek, K. C. O'Connor, D. A. Hafler, R. A. Sobel, W. H. Robinson and L. Steinman (2007). Protective and therapeutic role for αB-crystallin in autoimmune demyelination. *Nature* **448**: 474-481.

Papaconstantinou, J. (1967). Molecular aspects of lens cell differentiation. *Science* **21**: 338-346.

Paranandi, M. V., A. W. Guzzetta, W. S. Hancock and D. W. Aswad (1994). Deamidation and isoaspartate formation during *in vitro* aging of recombinant tissue plasminogen activator. *The Journal of Biological Chemistry* **269**: 243-253.

Perng, M.-D., Q. Zhang and R. A. Quinlan (2007). Insights into the beaded filament of the eye lens. *Experimental Cell Research* **313**: 2180-2188.

Perng, M. D., L. Cairns, P. van den IJssel, A. Prescott, A. M. Hutcheson and R. A. Quinlan (1999). Intermediate filament interactions can be altered by HSP27 and αB-crystallin. *Journal of Cell Science* **112**: 2099-2112.

Peschek, J., N. Braun, T. M. Franzmann, Y. Georgalis, M. Halsbeck, S. Weinkaut and J. Buchner (2009). The eye lens chaperone α-crystallin forms defined globular bodies. *Proceedings of the National Academy of Sciences* **106**: 13272-13277.

Peschek, J., N. Braun, J. Rohrburg, K. C. Back, T. Kriehuber, A. Kastenmuller, S. Weinkauf and J. Buchner (2013). Regulated structural transitions unleash the chaperone activity of αB-crystallin. *Proceedings of the National Academy of Science* **110**: 3780-3789.

Phelps Brown, N. and A. J. Bron (1996). Lens Disorders: A clinical manual of cataract diagnosis. Oxford, Butterworth-Heinamann.

Pilotto, A., N. Marziliano, M. Pasotti, M. Grasso, A. M. Costante and E. Arbustini (2006). αB-Crystallin mutation in dilated cardiomyopathies: low prevalence in a consecutive series of 200 unrelated probands. . *Biochem Biophys Res Commun* **346**: 1115-1117.

Chapter 7

Pras, E., M. Frydman, E. Levy-Nissenbaum, T. Bakhan, R. J., E. I. Assia and B. Goldman (2000). A nonsense mutation (W9X) in *CRYAA* causes autosomal recessive cataract in an inbred Persian Jewish family. *Investigative Ophthalmology and Visual Science* **41**: 3511-3515.

Quinlan, R. (2002). Cytoskeletal competence requires protein chaperones. Small Stress Proteins. A. P. Arrigo and W. E. G. Muller. Berlin, Springer**:** 219-228.

Quinlan, R. A., A. Sandilands, J. E. Procter, A. R. Prescott, A. M. Hutcheson, R. Dahm, C. Gribbon, P. Wallace and J. M. Carter (1999). They eye lens cytoskeleton. *Eye* **13**: 409-416.

Ramachandran, R. D., V. Perumalsamy and J. F. Hejtmancik (2007). Autosomal recessive juvenile onset cataract associated with mutation in BFSP1. *Human Genetics* **121**: 475-482.

Ramalho, J., C. Marques, P. Pereira and M. C. Mota (1996). Crystallin composition of human cataractous lens may be modulated by protein glycation. *Graefe's Archive for Clinical and Experimental Ophthalmology* **234**: S232-238.

Rathbun, W. B., A. J. Schmidt and A. M. Holleschau (1993). Activity loss of glutathione synthesis enzymes associated with human subcapsular cataract. *Investigative Opthalmology and Visual Science* **34**: 2049-2054.

Reddy, V. N. and F. J. Giblin (1984). Metabolsim and function of glutathione in the lens. *Ciba Foundation Symposium* **106**: 65-87.

Reilich, P., B. Schoser, N. Schramm, S. Krause, J. Schessl, W. Kress, J. Muller-Hocker, M. C. Walter and H. Lochmuller (2010). The p.G154S mutation of the αB-crystallin gene (*CRYAB*) causes late-onset distal myopathy. *Neuromuscular Disorders* **20**: 255-259.

Richter, L., P. Flodman, F. B. von-Bischhoffshausen, D. Burch, S. Brown, L. Nguyen, J. Turner, M. A. Spence and J. B. Bateman (2008). Clinical variability of autosomal dominant cataract, microcornea and corneal opacity and novel mutation in the αA-crystallin gene (*CRYAA*). *American Journal of Medical Genetics* **146**: 833-842.

Robinson, A. B., J. H. McKerrow and P. Cary (1970). Controlled deamidation of peptides and proteins: an experimental hazard and a possible biological timer. *Proceedings of the National Academy of Sciences* **66**: 753-757.

Robinson, A. B., J. H. McKerrow and M. Legaz (1974). Sequence dependent deamidation rates for model peptides of cytochrome C. *International Journal of Peptide and Protein Research* **6**: 31-35.

Chapter 7

Robinson, A. B. and L. R. Robinson (1991). Distribution of glutamine and asparagine residues and their near neighbours in peptides and proteins. *Proceedings of the National Academy of Sciences* **88**: 8880-8884.

Robinson, N. E. (2002). Protein deamidation. *Proceedings of the National Academy of Sciences* **99**: 5283-5288.

Robinson, N. E. and A. B. Robinson (2001). Prediction of protein deamidation rates from primary and three-dimensional structure. *Proceedings of the National Academy of Sciences* **98**.

Robinson, N. E. and A. B. Robinson (2004a). Molecular clocks: deamidation of asparaginyl and glutaminyl residues in peptides and proteins. Cave Junction, OR, Althouse Press.

Robinson, N. E. and A. B. Robinson (2004b). Prediction of primary structure deamidation rates of asparaginyl and glutaminyl peptides through steric and catalytic effects. *The Journal of Peptide research* **63**: 437-448.

Rose, K. M. L., R. G. Gourdie, A. R. Prescott, R. A. Quinlan, R. K. Crouch and K. L. Schey (2006). The C terminus of lens aquaporin 0 interacts with the cytoskeletal proteins filensin and CP49. . *Investigative Ophthalmology and Visual Science* **47**: 1562-1570.

Ross, M. H. and W. Pawlina (2006). Histology: A text and atlas. USA, Lippincott Williams and Wilkins.

Saha, S. and K. P. Das (2007). Unfolding and refolding of bovine α-crystallin in urea and its chaperone activity. *The Protein Journal* **26**: 315-326.

Sakaue, H., T. Takata, N. Fujii, H. Sasaki and N. Fujii (2015). αB- and βA3-crystallins containing D-aspartic acids exist in a monomeric state. *Biochimica et Biophysica Acta* **1854**: 1-9.

Sandilands, A., A. R. Prescott, J. M. Carter, A. M. Hutcheson, R. A. Quinlan, J. Richards and P. G. FitzGerald (1995). Vimentin and CP49/filensin form distinct networks in the lens which are independently modulated during lens fibre cell differentiation. *Journal of Cell Science* **108**: 1397-1406.

Sandilands, A., A. R. Prescott, A. M. Hutcheson, R. A. Quinlan, J. T. Casselman and P. G. FitzGerald (1995). Filensin in proteolytically processed during lens fibre cell differentiation by multiple pathways. *European Journal of Cell Biology* **67**: 238-253.

Santhoshkumar, P., P. Udupa, R. Murugesan and K. K. Sharma (2008). Significance of interactions of low molecular weight crystallin fragments in lens aging and cataract formation. *Journal of Biological Chemistry* **283**: 8477-8485.

Schieven, G. and G. S. Martin (1988). Nonenzymatic phosphorylation of tyrosine and serine by ATP is catalyzed by manganese but not magnesium. *Journal of Biological Chemistry* **263**: 15590-15593.

Schoenmakers, J. G. G. and H. Bloemendal (1968). Subunits of α-crystallin from adult and embryonic cattle lens. *Nature* **220**: 790-791.

Searle, B. C., S. Dasari, P. A. Wilmarth, M. Turner, A. P. Reddy, L. L. David and S. R. Nagalla (2005). Identification of protein modifications using MS/MS de novo sequencing and the open SeaAlignment algorithm. *Journal of Proteome Research* **4**: 546-554.

Selcen, D. and A. G. Engel (2003). Myofibrillar myopathy caused by novel dominant negative αB-crystallin mutations. *Annals of Neurology* **54**: 804-810.

Sethna, S. S., A. M. Holleschau and W. B. Rathbun (1982). Activity of glutathione synthesis enzymes in human lens related to age. *Current Eye Research*: 735-742.

Sharma, K. K. and P. Santhoshkumar (2009). Lens aging: effects of crystallins. . *Biochimica et Biophysica Acta* **1790**: 1095-1108.

Shearer, D., W. Ens, K. Standing and G. Valdimarsson (2008). Posttranslational modifications in lens fibre connexins identified by off-line-HPLC WALD-quadrupole time-of-flight mass spectrometry. *Investigative Opthalmology and Visual Science* **49**: 1553-1562.

Shestopalov, V. I. and S. Bassnett (2000). Expression of autofluorescent proteins reveals a novel protein permeable pathway between cells in the lens core. *Journal of Cell Science* **113**: 1913-1921.

Shinohara, H., Y. Inaguma, S. Goto, T. Inagaki and K. Kato (1993). αB-Crystallin and Hsp28 are enhance in the cerebral cortex of patients with Alzheimer's disease. *Journal of the Neurological Sciences* **119**: 203-208.

Siebinga, I., G. F. J. M. Vrensen, K. Otto, G. J. Puppels, d. F. F. M. Mul and J. Greve (1992). Ageing and changes in protein conformation in the human lens: a Raman microspectroscopic study. *Experimental Eye Research* **54**: 759 - 767.

Silverthorn, D. U. (2007). Human Physiology: An integrated approach. San Francisco, Pearson International Edition.

Chapter 7

Slavi, N., C. Rubinos, L. Li, C. Sellitto, T. W. White, R. Mathias and M. Srinivas (2014). Connexin 46 (Cx46) gap junctions provide a pathway for the delivery of glutathione to the lens nucleus. *The Journal of Biological Chemistry* **289**: 32694-32702.

Smulders, R. H. P. H., M. A. M. Van Boekel and W. W. De Jong (1998). Mutations and modifications support a 'pitted-flexiball' model for α-crystallin. *International Journal of Biological Macromolecules* **22**: 187-196.

Somer, H., V. Dubowitz and M. Donner (1976). Creatine kinase isoenzymes in neuromuscular diseases. *Journal of the Neurological Sciences* **29**: 129-136.

Soti, C. and P. Csermely (2000). Molecular chaperones and the aging process. *Biogerontology* **1**: 225-233.

Soulby, A. J., J. W. Heal, M. P. Barrow, R. A. Roemer and P. B. O'Connor (2015). Does deamidation cause protein unfolding? A top-down tandem mass spectrometry study. *Protein Science* **24**: 850-860.

Spector, A. (1995). Oxidative stress-induced cataract: mechanism of action. *FASEB Journal* **9**: 1173-1182.

Sreelakshmi, Y. and K. K. Sharma (2005). Recognition sequence 2 (residues 60-71) plays a role in oligomerisation and exchange dynamics of αB-crystallin. *Biochemistry* **44**: 12245-12252.

Srivastava, O. P., M. C. Kirk and K. Srivastava (2004). Characterization of covalent multimers of crystallins in aging human lenses. *Journal of Biological Chemistry* **279**: 10901-10909.

Srivastava, O. P. and K. Srivastava (2003). Existence of deamidated αB-crystallin fragments in normal and cataractous human lenses. *Molecular Vision* **9**: 110-118.

Stewart, D. N., J. Lango, K. P. Nambiar, M. J. S. Falso, P. G. FitzGerald, D. M. Rocke, B. D. Hammock and B. A. Buchholz (2013). Carbon turnover in the water-soluble protein of the adult human lens. *Molecular Vision* **19**: 463-475.

Su, D., Y. Guo, Q. Li, L. Guan, S. Zhu and X. Ma (2012). A novel mutation in *CRYAA* is associated with autosomal dominant suture cataracts in a Chinese family. *Molecular Vision* **18**: 3057-3063.

Su, S.-P., J. D. McArthur, R. J. W. Truscott and J. A. Aquilina (2011). Truncation, cross-linking and interactions of crystallins and intermediate filament proteins in the aging human lens. . *Biochimica et Biophysica Acta* **1814**: 647-656.

Su , S. P., B. Lyons, M. G. Friedrich, J. D. McArthur, X. Song, D. Xavier, R. J. W. Truscott and J. A. Aquilina (2012). Molecular signatures of long-lived proteins: autolytic cleavage adjacent to serine residues. *Aging Cell* **11**: 1125-1127.

Su, S. P., J. D. MacArthur and J. A. Aquilina (2010). Localisation of low molecular weight crystallin peptides in the aging human lens using a MALDI mass spectrometry imaging approach. *Experimental Eye Research* **91**: 97-103.

Su, S. P., J. D. McArthur, M. G. Friedrich, R. J. W. Truscott and J. A. Aquilina (2011). Understanding the α-crystallin cell membrane conjunction. *Molecular Vision* **17**: 2798-2807.

Su, S. P., X. Song, D. Xavier and J. A. Aquilina (2015). Age-related cleavages of crystallins in human lens cortical fibre cells generate a plethora of endogenous peptides and high molecular weight complexes. *Proteins* **83**: 1878-1886.

Sun, T.-X. and J.-N. Liang (1998). Intermolecular exchange and stabilisation of recombinant human αA- and αB-crystallin. *The Journal of Biological Chemistry* **273**: 286-290.

Sun, T. X., B. K. Das and J. J. N. Liang (1997). Conformational and functional differences between recombinant human lens αA- and αB-crystallin. *Journal of Biological Chemistry* **272**: 6220-6225.

Swamy-Mruthinti, S., V. Srinivas, J. E. Hansen and C. M. Rao (2013). Thermal stress induced aggregation of aquaporin 0 (AQP0) and protection by α-crystallin via its chaperone function. *PLoS ONE* **8**: 80404.

Sweeney, M. H. J. and R. J. W. Truscott (1998). An impediment to glutathione diffusion in older human lenses: a possible precondition for nuclear cataract. *Experimental Eye Research* **67**: 587-595.

Takata, T. and N. Fujii (2015). Effect of Asp 96 isomerisation on the properties of a lens αB-crystallin-derived short peptide. *Journal of Pharmaceutical and Biomedical Analysis* **116**: 139-144.

Takata, T., J. T. Oxford, B. Demeler and K. J. Lampi (2008). Deamidation destabilises and triggers aggregation of a lens protein, βA3-crystallin. . *Protein Science* **17**: 1565-1575.

Takata, T., J. T. Oxford and K. Lampi (2007). Deamidation alters the structure and decreases the stability of human lens βA3-crystallin. *Biochemistry* **46**: 8861-8871.

Takata, T., L. G. Woodbury and K. Lampi (2009). Deamidation alters interactions of β-crystallins in hetero-oligomers. *Molecular Vision* **15**: 241-249.

Takemoto, L. and D. Boyle (1998). The possible role of α-crystallins in human senile cataractogenesis. *International Journal of Biological Macromolecules* **22**: 331-337.

Takemoto, L., N. Fujii and D. Boyle (2001). Mechanisms of asparagine deamidation during human senile cataractogenesis. *Experimental Eye Research* **72**: 559-563.

Tardieu, A. (1998). α-crystallin quaternary structure and interactive properties control eye lens transparency. *International Journal of Biological Macromolecules* **22**: 211-217.

Tardieu, A., D. Laporte, P. Licinio, B. Krop and M. Delaye (1986). Calf lens α-crystallin quaternary structure: a three-layer tetrahedral model. *Journal of Molecular Biology* **192**: 711-724.

Tenbroek, E., M. Arneson, L. Jarvis and C. Louis (1992). The distribution of the fibre cell intrinsic membrane proteins MP20 and connexin46 in the bovine lens. *Journal of Cell Science* **103**: 245-257.

Tiwary, E., S. Hegde, S. Purushotham, C. Deivanayagam and O. P. Srivastava (2015). Interaction of βA3-crystallin with deamidated mutants of αA- and αB-crystallins. *PLoS ONE* **10**: e0144621.

Truscott, R. J. W. (2000). Age-related nuclear cataract: a lens transport problem. *Ophthalmic Research* **32**: 185-194.

Truscott, R. J. W. (2005). Age-related nuclear cataract- oxidation is the key. *Experimental Eye Research* **80**: 709-725.

Truscott, R. J. W. (2010). Are ancient proteins responsible for the age-related decline in health and fitness? *Rejuvination Research* **13**: 83-89.

Truscott, R. J. W. and R. C. Augusteyn (1977). The state of sulfhydral groups in normal and cataractous lenses. *Experimental Eye Research* **25**: 139-148.

Truscott, R. J. W., Y. C. Chen and D. C. Shaw (1998). Evidence for the participation of αB-crystallin in human age-related nuclear cataract. *International Journal of Biological Macromolecules* **22**: 321-330.

Truscott, R. J. W., S. Comte-Walters, Z. Ablonczy, J. H. Schwake, Y. Berry, A. Korlimbinis, M. G. Friedrich and K. L. Schey (2011). Tight binding of proteins to membranes from older human cells. *AGE* **33**: 543-554.

Truscott, R. J. W. and M. G. Friedrich (2016). The etiology of human age-related cataract. Proteins don't last forever. *Biochimica et Biophysica Acta-General Subjects* **1860**: 192-198.

Valasco, P. T., T. J. Lukas, S. N. P. Murthy, Y. Duglas-Tabor, D. L. Garland and L. Lorand (1997). Heirarhcy of lens proteins requiring protection against heat induced precipitation by the α-crystallin chaperone. *Experimental Eye Research* **65**: 497-505.

van Boekel, M. A. M., F. de Lange, W. J. de Grip and W. W. de Jong (1999). Eye lens αA- and αB-crystallin: complex stability versus chaperone-like activity. *Biochimica et Biophysica Acta* **1434**: 114-123.

Van Der Ouderaa, F. J., W. W. De Jong and H. Bloemendal (1973). The amino acid sequence of the αA_2 chain of bovine α-crystallin. . *European Journal of Biochemisty* **39**: 207-222.

Van Der Ouderaa, F. J., W. W. De Jong, A. Hilderink and H. Bloemendal (1974). The amino acid sequence of the αB_2 chain of bovine α-crystallin. *European Journal of Biochemistry* **49**: 157-168.

Van der Veen, K. J. and A. F. Willebrands (1966). Isoenzymes of creatine phosphokinase in tissue extracts and in normal and pathological sera. *Clinica Chimica Acta* **13**: 312-316.

Vanhoudt, J., S. Abgar, T. Aerts and J. Clauwaert (2000). A small-angle X-ray solution scattering study of bovine α-crystallin. *European Journal of Biochemistry* **267**: 3848-3858.

Vanita, V., J. R. Singh, J. F. Hejtmancik, P. Nurnberg, H. C. Hennies, D. Singh and K. Sperling (2006). A novel fan-shaped cataract-microcornea syndrome caused by a mutation of *CRYAA* in an Indian family. *Molecular Vision* **12**: 518-522.

Varadaraj, K., S. Kumari, A. Shiels and R. Mathias (2005). Regulation of aquaporin water permeability in the lens. *Investigative Ophthalmology and Visual Science* **46**: 1393-1402.

Varadaraj, K., S. S. Kumari and R. T. Mathias (2007). Functional expression of aquaporins in embryonic, postnatal, and adult mouse lenses. *Developmental Dynamics* **236**: 1319-1928.

Veretout, F. and A. Tardieu (1989). The protein concentration gradient within eye lens might originate from constant osmotic pressure coupled to differential interactive properties of crystallins. *European Biophysics Journal* **17**: 61-68.

Vicart, P., A. Caron, P. Guicheney, Z. Li, M.-C. Prevost, A. Faure, D. Chateau, F. Chapon, F. Tome, J.-M. Dupret, D. Paulin and M. Fardeau (1998). A missense mutation in the αB-crystallin chaperone gene causes a desmin-related myopathy. *Nature Genetics* **20**: 92-95.

Vincent, W. R. and E. Rapaport (1965). Serum creatine phosphokinase in the diagnosis of acute myocardial infarction. *The American Journal of Cardiology* **15**: 17-26.

Wang, J., E. Martin , V. Gonzales, D. R. Borchelt and M. K. Lee (2008). Differential regulation of sHsps in transgenic mouse models of nuerodegenerative diseases. *Neurobiol Aging* **29**: 586-597.

Wang, K. and A. Spector (1996). α-Crystallin stabilizes actin filaments and prevents cytochalasin-induced depolymerization in a phosphorylation-dependent manner. *European Journal of Biochemistry* **242**: 56-66.

Wang, K. J. and A. Spector (1994). The chaperone activity of bovine α-crystallin. *The Journal of Biological Chemistry* **269**: 13601-13608.

Wang, K. J. and S. Q. Zhu (2012). A novel p.F206I mutation in Cx46 associated with autosomal dominant congenital cataract. *Molecular Vision* **18**: 968-973.

Wang, Z., J. Han, L. L. David and K. L. Schey (2013). Proteomics and phosphoproteomics analysis of human lens fibre cell membranes. *Investigative Ophthalmology and Visual Science* **54**: 1135-1143.

Wang, Z., B. Lyons, R. J. W. Truscott and K. L. Schey (2014). Human protein aging: modification and crosslinking through dehydroalanine and dehydrobutyrine intermediates. *Aging Cell* **13**: 226-234.

Wang, Z. and K. L. Schey (2009). Phosphorylation and truncation sites of bovine lens connexin 46 and connexin 50. *Experimental Eye Research* **89**: 898-904.

Wenke, J. L., W. H. McDonald and K. L. Schey (2016). Spatially directed proteomics of the human lens outer cortex reveals an intermediate filament switch associated with the remodeling zone. *Investigative Ophthalmology and Visual Science* **57**: 4108-4114.

Whiston, E. A., N. Sugi, M. C. Kamradt, M. Krevosky, C. Sack, S. R. Heimer, M. Engelbert, E. F. Wawrousek, M. S. Gilmore, B. R. Ksander and M. S. Gregory (2008). αB-Crystallin protects retinal tissue during Staphylococcus aureus-induced endophthlamitis. *Infection and Immunity* **76**: 1781-1790.

Wilmarth, P. A., S. Tanner, S. Dasari, S. R. Nagalla, M. A. Riviere, V. Bafna, P. A. Pevzner and L. L. David (2006). Age-related changes in humans crystallins determined from comparative analysis of post-translational modifications in young and aged lenses: does deamidation contribute to crystallin insolubility. *Journal of Proteome Research* **5**: 2554-2566.

Wistow, G. (1993). Possible tetramer-based quaternary structures for α-crystallins and small heat shock proteins. *Experimental Eye Research* **56**: 729-732.

Wistow, G. and J. Piatigorsky (1988). Lens crystallins: the evolution and expression of proteins for a highly specialised tissue. *Annual Review of Biochemistry* **57**: 479-504.

World Health Organisation (2010). "Priority eye diseases.". Retrieved May 7th, 2010, from www.who.int.

Wright, H. T. (1991). Nonenzymatic deamidation of asparaginyl and glutaminyl residues in proteins. *Critical Reviews in Biochemistry and Molecular Biology* **26**: 1-52.

Wyatt, A. R., J. R. Kumita, N. E. Farrawell, C. M. Dobson and M. R. Wilson (2015). α2-Macroglobulin is acutely sensitive to freezing and lyophilisation: implications for structural and functional studies. *PLoS ONE* **10**: e0130036.

Yilmaz, M., O. F. Karatas, B. Yuceturk, H. Dag, M. Yener and M. Ozen (2015). αB-Crystallin expression in human laryngeal squamous cell carcinoma tissues. *Head and Neck* **37**: 1344-1348.

Zhou, H. Y., H. Yan, L. L. Wang, W. J. Yan, Y. B. Shui and D. C. Beebe (2015). Quantitative proteomics analysis by iTRAQ in human nuclear cataracts of different ages and normal lens nuclei. *Proteomics Clinical Applications* **9**: 776-786.

APPENDIX

APPENDIX

Appendix 1

Phosphorylation sites identified in human lens αA-crystallin.

Site	Reference
S20	Wang *et al.*, 2013; Wang *et al.*, 2014
S45	Wang *et al.*, 2013; MacCoss *et al.*, 2002
S51	Wang *et al.*, 2013
S59	Wang *et al.*, 2013; Wang *et al.*, 2014
S62	Wang *et al.*, 2013; Wang *et al.*, 2014
S66	Huang *et al.*, 2011; Wang *et al.*, 2013
S81	Huang *et al.*, 2011 ; Wang *et al.*, 2013
S122	Wilmarth *et al.*, 2013; Wang *et al.*, 2013; Searle *et al.*, 2004; MacCoss *et al.*, 2002; Miesbauer *et al.*, 1994
S127	Wang *et al.*, 2013
S130	Wang *et al.*, 2013
S134*	Previously unreported
S162	Wang *et al.*, 2013; Wang *et al.*, 2014
S172	Wang *et al.*, 2013
S173	Wang *et al.*, 2013
T13	MacCoss *et al.*, 2002; Wang *et al.*, 2013; Wang *et al.*, 2014
T43	Wang *et al.*, 2013
T55	Wang *et al.*, 2013
T86	Wang *et al.*, 2013
T140	MacCoss *et al.*, 2002
T148	Huang *et al.*, 2011; Wang *et al.*, 2013; Wang *et al.*, 201
T168/S169	Wang *et al.*, 2013
T153	Huang *et al.*, 2011; Wang *et al.*, 2013
Y47	Wang *et al.*, 2013
Y118	Wang *et al.*, 2013

APPENDIX

Phosphorylation sites identified in human lens αB-crystallin.

S19	Wang *et al.*, 2013; Wilmarth *et al.*, 2006; Huang *et al.*, 2011; MacCoss *et al.*, 2002; Miesbauer *et al.*, 1994
S21	Huang *et al.*, 2011; Wang *et al.*, 2013; MacCoss *et al.*, 2002
S43	Wang *et al.*, 2013; MacCoss *et al.*, 2002
S45	MacCoss *et al.*, 2002; Miesbauer *et al.*, 1994; Wang *et al.*, 2013
S53	Wang *et al.*, 2013; Wang *et al.*, 2014; MacCoss *et al.*, 2002
S59	Wilmarth *et al.*, 2006; Huang *et al.*, 2011; Wang *et al.*, 2013; Wang *et al.*, 2014; Searle *et al.*, 2004; MacCoss *et al.*, 2002; Kamei *et al.*, 2000; Miesbauer *et al.*, 1994
S66	Wang *et al.*, 2013
S76	Wilmarth *et al.*, 2006; Huang *et al.*, 2011; Wang *et al.*, 2013; MacCoss *et al.*, 2002
S85	Wang *et al.*, 2013
S136	Wang *et al.*, 2013
S138	Wang *et al.*, 2013; Wang *et al.*, 2014
S139	Huang *et al.*, 2011; Wang *et al.*, 2013; Wang *et al.*, 2014
S153	Wang *et al.*, 2013
T63	Wang *et al.*, 2013
T170	Wang *et al.*, 2014
T132	Wang *et al.*, 2013
T134	Wang *et al.*, 2013
T158	Wang *et al.*, 2013

APPENDIX

Deamidation sites identified in human lens αA and αB-crystallin.

Subunit	Site	Reference
αA	Q6	Lund *et al.*, 1996; Hanson *et al.*, 2000; Searle *et al.*, 2005; Wilmarth *et al.*, 2006
	Q50	Lund *et al.*, 1996; Wilmarth *et al.*, 2006
	Q90	Lund *et al.*, 1996; Hanson *et al.*, 2000; Searle *et al.*, 2005; Hains and Truscott, 2010
	Q104	Hanson *et al.*, 2000; Hains and Truscott, 2010
	Q126	Wilmarth *et al.*, 2006 ; Hains and Truscott, 2010
	Q147	Lund *et al.*, 1996; Hanson *et al.*, 2000; Searle *et al.*, 2005; Hains and Truscott, 2010
	N101	Lund *et al.*, 1996; Wilmarth *et al.*, 2006
	N123	Searle *et al.*, 2005; Wilmarth *et al.*, 2006; Hains and Truscott, 2010
αB	Q26	Wilmarth *et al.*, 2006; Hains and Truscott, 2010
	Q108	Lund *et al.*, 1996; Hanson *et al.*, 2000; Srivastava and Srivastava, 2003; Hains and Truscott, 2010
	N78	Hanson *et al.*, 2000; Hains and Truscott, 2010
	N146	Searle *et al.*, 2005; Wilmarth *et al.*, 2006; Asomugha *et al.*, 2010; Hains and Truscott, 2010

APPENDIX

Appendix 2

Buffers:

PBS: 137 mM NaCl, 2.7 mM KCl, 12.5 mM Na_2HPO_4, 1 mM KH_2PO_4, pH 7.4

Sucrose buffer: 10 mM Tris-base, 2 mM EDTA, 2 mM BME, adjusted to pH 8.0 with 10 M HCl

SSS buffer: 8 M Urea, 100 mM DTT, 4% w/v CHAPS, 0.8% v/v 100x BioLyte® 3/10 Carrier Ampholyte, 100 mM Tris-base

2 times loading buffer: 125 mM Tris-HCl, 0.03% w/v bromophenol blue, 33% glycerol, 3.3% w/v SDS. Prior to use, 1 M DTT in 10 mM sodium acetate (pH 5.2) was added at the ratio 1:4, for a final DTT concentration of 200 mM.

Coomassie stain: 40% v/v methanol, 10% v/v acetic acid, 0.2% w/v coomassie blue R in milli-Q water

Coomassie destain: 40% v/v methanol, 10% v/v acetic acid in milli-Q water

HBSS buffer: 137 mM NaCl, 5.4 mM KCl, 250 mM Na_2HPO_4, 0.01% w/v glucose, 440 µM KH_2PO_4, 1.3 mM $CaCl_2$, 1 mM $MgSO_4$, 4.2 mM $NaHCO_3$, pH 7.3

TBST: 20 mM Tris-base, 150 mM NaCl, 0.17% Tween-20, adjusted to pH 7.5 with 10 M HCl

TBS: 20 mM Tris-base, 150 mM NaCl, adjusted to pH 7.5 with 10 M HCl

DAB working solution: one DAB tablet was solubilised in TBS, with 12 µL of 30% hydrogen peroxide added prior to use.

Equilibration buffer: 6 M Urea, 0.1% w/v SDS, 300 mM Tris-HCl, 20% v/v Glycerol, 0.1% w/v DTT, 2.5% v/v acrylamide, pH 8.8

Colloidal coomassie stain: 1.3 M ammonium sulphate, 3% v/v phosphoric acid, 0.1% w/v coomassie G, 34% v/v methanol in milli-Q water. N.B. Coomassie G was solubilised in ammonium sulphate solution before adding phosphoric acid and methanol to reach final concentrations.

Colloidal destain: 1% v/v acetic acid in milli-Q water

PFA: PFA was added to PBS to a final concentration of 0.75% w/v. A few drops of 10 M NaOH were added and the solution was heated at 80°C until fully solubilised, before the pH was adjusted to 7.4.

Wash buffer A: 0.01 M Tris-base, 0.15 M NaCl, 0.05% v/v Tween-20, adjusted to pH 7.4 with 10 M HCl

APPENDIX

Wash buffer B: 0.2 M Tris-base, 0.1M NaCl, adjusted to pH 7.5 with 10 M HCl

0.01x wash buffer B: 100x dilution of wash buffer B

APPENDIX

Appendix 3

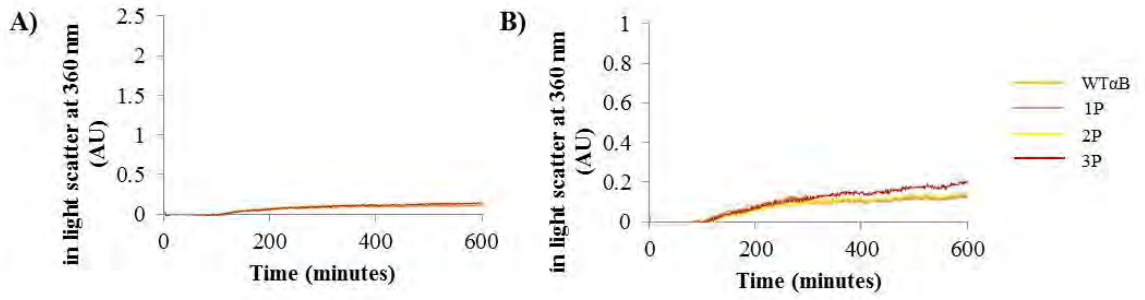

Heat induced aggregation of WTαB and αB containing single, double or triple mutations that mimic phosphorylation. WT, 1P, 2P or 3P αB was incubated in PBS (pH 7.4) at 40°C at a concentration of either **(A)** 0.5 µM or **(B)** 0.25 µM, and the change in light scatter at 360 nm was measured over time.

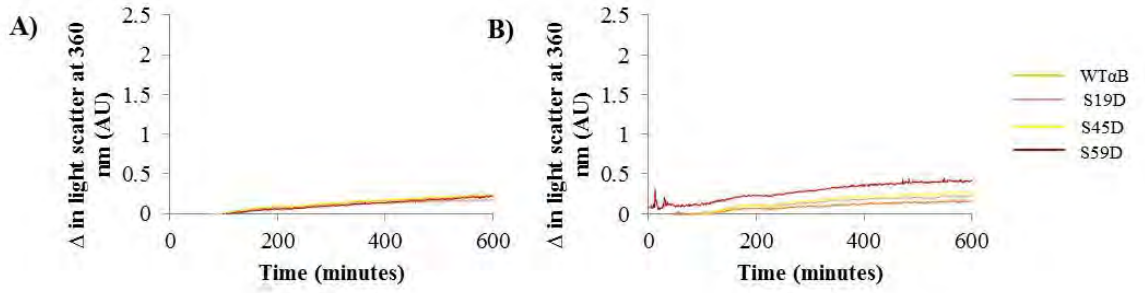

Heat induced aggregation of WTαB and αB containing mutations that mimic phosphorylation at Ser19, Ser45 or Ser59. WT, S19D, S45D or S59D αB was incubated in PBS (pH 7.4) at 40°C at a concentration of either **(A)** 0.5 µM or **(B)** 0.125 µM, and the change in light scatter at 360 nm was measured over time.

APPENDIX

Results of ANOVA of CPK aggregation assays. Test performed on experimental end-point values from data presented in Figures 3.3.1 and 3.3.2 for relative amount of CPK aggregation following incubation with αB (at molar ratios of 1cpk:$1_{\alpha B}$, 1cpk:$2_{\alpha B}$ or 1cpk:$1_{\alpha B}$) with multiple or single aspartate substitutions. N=3

	P	F	Fcrit
Multiple 1cpk:$1_{\alpha B}$ (data in Figure 3.3.1A)	6.26^{-11}	52.8	2.5
Multiple 1cpk:$2_{\alpha B}$ (data in Figure 3.3.1B)	1.36^{-11}	63.1	2.5
Single 1cpk:$1_{\alpha B}$ (data in Figure 3.3.2A)	3.67^{-7}	18.3	2.5
Single 1cpk:$4_{\alpha B}$ (data in Figure 3.3.2B)	1.54^{-4}	7.8	2.5

Tukey's test of aggregation assay performed on data presented in Figure 3.1A: Test performed on experimental end-point values for relative amount of CPK aggregation following incubation with αB (at molar ratios of 1cpk:$1_{\alpha B}$) with single (1P), double (2P) or triple (3P) aspartate substitutions. Statistical significance at P<0.05 shaded in dark green, P<0.01 shaded in light green. N=3.

	CPK	WT/CPK	1P/CPK	2P/CPK	3P/CPK	WT	1P	2P	3P
CPK		0.001	0.9	0.195	0.009	0.003	0.003	0.005	0.007
WT/CPK	0.001		0.001	0.001	0.001	0.001	0.001	0.001	0.001
1P/CPK	0.9	0.001		0.049	0.002	0.001	0.001	0.001	0.001
2P/CPK	0.195	0.001	0.049		0.769	0.497	0.515	0.631	0.693
3P/CPK	0.009	0.001	0.002	0.769		0.9	0.9	0.9	0.9
WT	0.003	0.001	0.001	0.497	0.9		0.9	0.9	0.9
1P	0.003	0.001	0.001	0.515	0.9	0.9		0.9	0.9
2P	0.005	0.001	0.001	0.631	0.9	0.9	0.9		0.9
3P	0.007	0.001	0.001	0.693	0.9	0.9	0.9	0.9	

Tukey's test of aggregation assay performed on data presented in Figure 3.1B: Test performed on experimental end-point values for relative amount of CPK aggregation

APPENDIX

following incubation with αB (at molar ratios of 1cpk:$2_{\alpha B}$) with single (1P), double (2P) or triple (3P) aspartate substitutions. Statistical significance at P<0.05 shaded in dark green, P<0.01 shaded in light green. N=3.

	CPK	WT/CPK	1P/CPK	2P/CPK	3P/CPK	WT	1P	2P	3P
CPK		0.9	0.134	0.001	0.001	0.001	0.001	0.001	0.001
WT/CPK	0.9		0.392	0.001	0.001	0.001	0.001	0.001	0.001
1P/CPK	0.134	0.392		0.049	0.001	0.001	0.001	0.001	0.001
2P/CPK	0.001	0.001	0.049		0.001	0.001	0.001	0.001	0.008
3P/CPK	0.001	0.001	0.001	0.001		0.9	0.9	0.9	0.513
WT	0.001	0.001	0.001	0.001	0.9		0.9	0.9	0.43
1P	0.001	0.001	0.001	0.001	0.9	0.9		0.9	0.579
2P	0.001	0.001	0.001	0.001	0.9	0.9	0.9		0.62
3P	0.001	0.001	0.001	0.008	0.513	0.43	0.579	0.62	

Tukey's test of aggregation assay performed on data presented in Figure 3.2A: Test performed on experimental end-point values for relative amount of CPK aggregation following incubation with αB (at molar ratios of 1cpk:$1_{\alpha B}$) with single aspartate substitutions at Ser19 (S19D), Ser45 (S45D) or Ser59 (S59D). Statistical significance at P<0.05 shaded in dark green, P<0.01 shaded in light green. N=3.

	CPK	WTαB/CPK	S19D/CPK	S45D/CPK	S59D/CPK	WTαB	S19D	S45D	S59D
CPK		0.001	0.9	0.9	0.9	0.031	0.025	0.022	0.02
WTαB/CPK	0.001		0.001	0.001	0.001	0.001	0.001	0.001	0.001
S19D/CPK	0.9	0.001		0.9	0.9	0.044	0.035	0.031	0.028
S45D/CPK	0.9	0.001	0.9		0.9	0.049	0.04	0.035	0.031
S59D/CPK	0.9	0.001	0.9	0.9		0.177	0.148	0.131	0.12
WTαB	0.031	0.001	0.044	0.049	0.177		0.9	0.9	0.9
S19D	0.025	0.001	0.035	0.04	0.148	0.9		0.9	0.9
S45D	0.022	0.001	0.031	0.035	0.131	0.9	0.9		0.9
S59D	0.02	0.001	0.028	0.031	0.12	0.9	0.9	0.9	

APPENDIX

Tukey's test of aggregation assay performed on data presented in Figure 3.2B: Test performed on experimental end-point values for relative amount of CPK aggregation following incubation with αB (at molar ratios of 1cpk:$4_{\alpha B}$) with single aspartate substitutions at Ser19 (S19D), Ser45 (S45D) or Ser59 (S59D). Statistical significance at P<0.05 shaded in dark green, P<0.01 shaded in light green. N=3.

	CPK	WTαB/CPK	S19D/CPK	S45D/CPK	S59D/CPK	WTαB	S19D	S45D	S59D
CPK		0.1	0.9	0.9	0.9	0.116	0.166	0.138	0.307
WTαB/CPK	0.1		0.017	0.024	0.008	0.001	0.001	0.001	0.001
S19D/CPK	0.9	0.017		0.9	0.9	0.476	0.585	0.529	0.79
S45D/CPK	0.9	0.024	0.9		0.9	0.39	0.5	0.443	0.705
S59D/CPK	0.9	0.008	0.9	0.9		0.684	0.792	0.736	0.9
WTαB	0.116	0.001	0.476	0.39	0.684		0.9	0.9	0.9
S19D	0.166	0.001	0.585	0.5	0.792	0.9		0.9	0.9
S45D	0.138	0.001	0.529	0.443	0.736	0.9	0.9		0.9
S59D	0.307	0.001	0.79	0.705	0.9	0.9	0.9	0.9	

APPENDIX

Peptides detected from HMW1-10: peptides were detected using MS/MS (APAF) and identified by comparison with a peptide database. Modified residues in peptide sequences are highlighted red.

Protein	Mass	Peptide Mass (Da)	Residues	Sequence	Modification	Mod. Site
Complex 1						
Filensin	74499	797.54	399-405	K.LVQVVLK.E		
		1014.54	484-492	R.FYVSSITAK.G		
		1098.64	294-303	R.QLAVAQQTLK.N		
		1131.6	621-630	K.TVEVVESIEK.I		
		1182.67	352-362	R.ALQDITAAKPR.Q		
		1279.66	147-157	K.EADEALLHNLR.L		
		1306.63	457-467	K.EPETPTELYTK.E		
		1310.68	78-90	R.LGELAGPEDALAR.Q		
		1371.69	380-392	K.DKTDGALEDAPLK.G	Deamidation	N383
		1486.83	399-411	K.LVQVVLKEESESK.F		
		1554.78	470-483	R.HVLVTGDANYVDPR.F		
		1555.76	470-483	R.HVLVTGDADYVDPR.F	Deamidation	N478
		1618.81	454-467	R.SPKEPETPTELYTK.E		
		1634.87	144-157	R.LNKEADEALLHNLR.L		
		1635.86	144-157	R.LDKEADEALLHNLR.L	Deamidation	N145
		1671.9	240-254	R.VELQAQTTTLEQAIK.S		
		1725.94	294-308	R.QLAVAQQTLKNELDR.Y		
		1726.92	294-308	R.QLAVAQQTLKDELDR.Y	Deamidation	N304
		1788.93	158-173	R.LQLEAQFLQDDISAAK.D		
		1979	223-239	R.SQLEEGREVLSHLQAQR.V		
		2060	158-175	R.LQLEAQFLQDDISAAKDR.H		
		2252.1	418-439	K.EVSPLTQEGAPEDVPDGGQISK.G		
		2457.22	631-652	K.ISTESIQTYEETAVIVETMIGK.T	Oxidation	M649
		2722.33	24-50	R.AAEPERPADEGWAGATSLAALQGLGER.V		
		2831.47	320-347	R.LTSAFIETPIPLFTQSHGVSLSTGSGGK.D		
		3338.79	179-208	K.NLLEVQTYISILQQIIHTTPPASIVTSGMR.E	Oxidation	M207
		3724.97	179-211	K.NLLEVQTYISILQQIIHTTPPASIVTSGMREEK.L	Oxidation	M207
Phakinin	45851	1265.62	201-211	K.AAEEEINSLYK.V		
		1359.79	77-89	R.ALGISSVFLQGLR.S		
		1878.98	122-137	K.VHALEQVSQELETQLR.M		
		2081	174-191	R.LMLQTETIQAGADDFKER.Y	Oxidation	M175
		2179.1	221-239	K.MDLESQIESLKEELGSLSR.N	Oxidation	M221
αA-Crystrallin	19897	979.57	71-78	K.FVIFLDVK.H		
		1036.53	13-21	R.TLGPFYPSR.L		
		1174.62	55-65	R.TVLDSGISEVR.S		
		3363.64	22-49	R.LFDQFFGEGLFEYDLLPFLSSTISPYYR.Q		
γS-Crystallin	20993	1728.89	159-174	R.KPIDWGAASPAVQSFR.R		
		1896.98	132-146	K.VLEGVWIFYELPNYR.G		
Serum Albumin	69321	1622.78	233-245	K.DVFLGMFLYEYAR.R		
		1638.77	233-245	K.DVFLGMFLYEYAR.R	Oxidation	M238
Vimentin	53619	1168.71	130-139	K.ILLAELEQLK.G		
		1532.84	223-235	R.KVESLQEEIAFLK.K		
		1538.9	130-143	K.ILLAELEQLKGQGK.S		
Complex 2						
Filensin	74499	942.51	312-319	R.IIEIEGNR.L		
		1098.64	294-303	R.QLAVAQQTLK.N		
		1182.67	352-362	R.ALQDITAAKPR.Q		
		1279.65	147-157	K.EADEALLHNLR.L		
		1280.64	147-157	K.EADEALLHDLR.L	Deamidation	N155
		1310.68	78-90	R.LGELAGPEDALAR.Q		
		1371.69	380-392	K.DKTDGALEDAPLK.G	Deamidation	N383
		1486.82	399-411	K.LVQVVLKEESESK.F		
		1634.87	144-157	R.LNKEADEALLHNLR.L		
		1635.86	144-157	R.LNKEADEALLHDLR.L	Deamidation	N155
		1635.86	144-157	R.LDKEADEALLHNLR.L	Deamidation	N145
		1671.9	240-254	R.VELQAQTTTLEQAIK.S		
		1725.94	294-308	R.QLAVAQQTLKNELDR.Y		

APPENDIX

		1726.92	294-308	R.QLAVAQQTLKDELDR.Y	Deamidation	N304
		1771.88	382-398	K.TDGALEDAPLKGLEDTK.L	Deamidation	N383
		1788.93	158-173	R.LQLEAQFLQDDISAAK.D		
		1840.87	125-138	R.SKYENECECQLLLK.E	2 Propionamide	C131, C133
		1979.02	223-239	R.SQLEEGREVLSHLQAQR.V		
		2060.05	158-175	R.LQLEAQFLQDDISAAKDR.H		
		2639.18	255-275	K.SAHECYDDEIQLYNEQIETLR.K	Propionamide	C259
		2722.33	24-50	R.AAEPERPADEGWAGATSLAALQGLGER.V		
		2767.28	255-276	K.SAHECYDDEIQLYNEQIETLRK.E	Propionamide	C259
		2768.26	255-276	K.SAHECYDDEIQLYDEQIETLRK.E	Propionamide, Deamidation	C259, N268
		2831.47	320-347	R.LTSAFIETPIPLFTQSHGVSLSTGSGGK.D		
		3338.79	179-208	K.NLLEVQTYISILQQIIHTTPPASIVTSGMR.E	Oxidation	M207
Phakinin	45851	1265.61	201-211	K.AAEEEINSLYK.V		
		1353.72	90-103	R.SSGLATVPAPGLER.D		
		1359.79	77-89	R.ALGISSVFLQGLR.S		
		1801.92	6-22	R.VVVDLPTSASSSMPLQR.R	Oxidation	M18
		1878.98	122-137	K.VHALEQVSQELETQLR.M		
		2081.01	174-191	R.LMLQTETIQAGADDFKER.Y	Oxidation	M175
		2442.18	319-339	R.VELHNTSCQVQSLQAETESLR.A	Propionamide	C326
βB1-Crystallin	28006	1124.59	151-160	K.ISLFEGANFK.G		
		1449.76	61-72	R.LVVFELENFQGR.R		
		1456.7	203-214	R.GYQYLLEPGDFR.H		
		1718.82	188-202	K.VSSGTWVGYQYPGYR.G		
		2007.04	93-110	R.SIIVSAGPWVAFEQSNFR.G		
Retinal Dehydrogenase 1	54827	1188.6	69-78	R.QAFQIGSPWR.T		
		1396.66	101-113	R.LLLATMESMDGGK.L	2 Oxidation, Deamidation	M106, M109, N110
		1543.77	144-156	R.TIPIDGNFFTYTR.H		
		1589.77	421-435	R.ANDTFYGLSAGVFTK.D	Deamidation	N423
		1644.8	309-321	R.IFVEESIYDEFVR.R		
		1745.94	396-410	R.IAKEEIFGPVQQIMK.F	Oxidation	M409
αB-Crystallin	20146	1164.65	93-103	K.VLGDVIEVHGK.H		
		1191.62	73-82	K.DRFSVNLDVK.H		
		1373.67	12-22	R.RPFFPFHSPSR.L		
		1511.67	57-69	R.APSWFDTGLSEMR.L	Oxidation	M68
		2623.37	124-149	R.IPADVDPLTITSSLSSDGVLTVNGPR.K		
αA-Crystallin	19897	979.57	71-78	K.FVIFLDVK.H		
		1036.53	13-21	R.TLGPFYPSR.L		
		1174.62	55-65	R.TVLDSGISEVR.S		
		1192.63	12-21	K.RTLGPFYPSR.L		
		1285.63	89-99	K.VQDDFVEIHGK.H		
βB2-Crystallin	23365	1407.74	109-120	K.IILYENPNFTGK.K		
		1725.8	173-188	K.DSSDFGAPHPQVQSVR.R		
		2189.01	169-188	K.GDYKDSSDFGAPHPQVQSVR.R		
γS-Crystallin	20993	1516.73	8-19	K.ITFYEDKNFQGR.R		
		1728.89	159-174	R.KPIDWGAASPAVQSFR.R		
		1896.98	132-146	K.VLEGVWIFYELPNYR.G		
Serum Albumin	69321	1638.93	438-452	K.KVPQVSTPTLVEVSR.N		
Glutathione Synthetase	52352	940.57	26-34	R.ALAEGVLLR.T		
βA3-Crystallin	25134	1454.7	33-44	K.ITIYDQENFQGK.R		
Tubulin α-1A	50104	1084.61	78-86	K.EIIDLVLDR.I		
γD-Crystallin	20725	1270.6	143-152	R.QYLLMPGDYR.R	Oxidation	M147
γC-Crystallin	20865	1364.72	143-152	R.QYLLRPQEYR.R		
Tubulin β-4A	49554	1038.59	310-318	R.YLTVAAVFR.G		
Complex 3						
Brain Acid Soluble Protein 1	22680	1774.85	103-121	K.APEQEQAAPGPAAGGEAPK.A		
		2297.13	98-121	K.AEPPKAPEQEQAAPGPAAGGEAPK.A		
		2635.23	122-149	K.AAEAAAAPAESAAPAAGEEPSKEEGEPK.K		
		2763.36	199-226	K.AQGPAASAEEPKPVEAPAADSDQTVTVK.E	Deamidation	N218
Filensin	74499	1014.54	484-492	R.FYVSSITAK.G		
		1131.6	621-630	K.TVEVVESIEK.I		
		1279.65	147-157	K.EADEALLHNLR.L		

APPENDIX

		1310.68	78-90	R.LGELAGPEDALAR.Q		
		1671.9	240-254	R.VELQAQTTTLEQAIK.S		
		1788.93	158-173	R.LQLEAQFLQDDISAAK.D		
		2457.22	631-652	K.ISTESIQTYEETAVIVETMIGK.T	Oxidation	M649
Phakinin	45851	1265.61	201-211	K.AAEEEINSLYK.V		
		1359.79	77-89	R.ALGISSVFLQGLR.S		
		2081.01	174-191	R.LMLQTETIQAGADDFKER.Y	Oxidation	M175
		2179.07	221-239	K.MDLESQIESLKEELGSLSR.N	Oxidation	M221
Serum Albumin	69321	1622.78	233-245	K.DVFLGMFLYEYAR.R		
		1638.77	233-245	K.DVFLGMFLYEYAR.R	Oxidation	M238
αA-Crystallin	19897	1036.53	13-21	R.TLGPFYPSR.L		
		1174.62	55-65	R.TVLDSGISEVR.S		
βB1-Crystallin	28006	1449.76	61-72	R.LVVFELENFQGR.R		
αB-Crystallin	20146	920.5	75-82	R.FSVNLDVK.H		
		1164.65	93-103	K.VLGDVIEVHGK.H		
Complex 4						
Filensin	74499	942.51	312-319	R.IIEIEGNR.L		
		1098.64	294-303	R.QLAVAQQTLK.N		
		1182.67	352-362	R.ALQDITAAKPR.Q		
		1279.65	147-157	K.EADEALLHNLR.L		
		1280.64	147-157	K.EADEALLHDLR.L	Deamidation	N155
		1310.68	78-90	R.LGELAGPEDALAR.Q		
		1373.7	277-287	K.EIEETERVLEK.S		
		1634.87	144-157	R.LNKEADEALLHNLR.L		
		1635.86	144-157	R.LNKEADEALLHDLR.L	Deamidation	N155
		1635.86	144-157	R.LDKEADEALLHNLR.L	Deamidation	N145
		1671.9	240-254	R.VELQAQTTTLEQAIK.S		
		1725.94	294-308	R.QLAVAQQTLKNELDR.Y		
		1726.92	294-308	R.QLAVAQQTLKDELDR.Y	Deamidation	N304
		1788.93	158-173	R.LQLEAQFLQDDISAAK.D		
		1979.03	223-239	R.SQLEEGREVLSHLQAQR.V		
		2060.05	158-175	R.LQLEAQFLQDDISAAKDR.H		
		2639.18	255-275	K.SAHECYDDEIQLYNEQIETLR.K	Propionamide	C259
		2722.33	24-50	R.AAEPERPADEGWAGATSLAALQGLGER.V		
		2767.28	255-276	K.SAHECYDDEIQLYNEQIETLRK.E	Propionamide	C259
		2768.26	255-276	K.SAHECYDDEIQLYDEQIETLRK.E	Propionamide, Deamidation	C259 N268
		2831.47	320-347	R.LTSAFIETPIPLFTQSHGVSLSTGSGGK.D		
		3051.55	147-173	K.EADEALLHDLRLQLEAQFLQDDISAAK.D	Deamidation	N155
		3316.73	320-351	R.LTSAFIETPIPLFTQSHGVSLSTGSGGKDLTR.A		
		3338.79	179-208	K.NLLEVQTYISILQQIIHTTPPASIVTSGMR.E	Oxidation	M207
		3466.89	178-208	K.KNLLEVQTYISILQQIIHTTPPASIVTSGMR.E	Oxidation	M207
		3724.97	179-211	K.NLLEVQTYISILQQIIHTTPPASIVTSGMREEK.L	Oxidation	M207
		3755.97	312-347	R.IIEIEGNRLTSAFIETPIPLFTQSHGVSLSTGSGGK.D		
βB1-Crystallin	28006	1124.59	151-160	K.ISLFEGANFK.G		
		1449.77	61-72	R.LVVFELENFQGR.R		
		1456.7	203-214	R.GYQYLLEPGDFR.H		
		2007.02	93-110	R.SIIVSAGPWVAFEQSNFR.G		
		2439.13	161-182	K.GNTIEIQGDDAPSLWVYGFSDR.V		
αB-Crystallin	20146	1164.65	93-103	K.VLGDVIEVHGK.H		
		1373.7	12-22	R.RPFFPFHSPSR.L		
		2623.37	124-149	R.IPADVDPLTITSSLSSDGVLTVNGPR.K		
		2624.35	124-149	R.IPADVDPLTITSSLSSDGVLTVDGPR.K	Deamidation	N146
αA-Crystallin		979.57	71-78	K.FVIFLDVK.H		
		1036.53	13-21	R.TLGPFYPSR.L		
		1174.62	55-65	R.TVLDSGISEVR.S		
		1285.63	88-98	K.VQDDFVEIHGK.H		
		3363.64	22-49	R.LFDQFFGEGLFEYDLLPFLSSTISPYYR.Q		
βB2-Crystallin	23365	1407.74	109-120	K.IILYENPNFTGK.K		
		1759.83	146-160	R.VQSGTWVGYQYPGYR.G		
		2189.01	169-188	K.GDYKDSSDFGAPHPQVQSVR.R		
γS-Crystallin	20993	1516.73	8-19	K.ITFYEDKNFQGR.R		
		1896.98	132-146	K.VLEGVWIFYELPNYR.G		
Phakinin	45851	1359.79	77-89	R.ALGISSVFLQGLR.S		
Niban-like Protein 2	77364	2663.21	641-663	K.SSANWILAASLLSCSCFRSGFHR.D	Phosphorylation, Propionamide	S655, C656

APPENDIX

Complex 5						
Filensin	74499	942.51	312-319	R.IIEIEGNR.L		
		1182.67	352-362	R.ALQDITAAKPR.Q		
		1279.65	147-157	K.EADEALLHNLR.L		
		1280.64	147-157	K.EADEALLHDLR.L	Deamidation	N155
		1310.68	78-90	R.LGELAGPEDALAR.Q		
		1634.87	144-157	R.LNKEADEALLHNLR.L		
		1635.86	144-157	R.LNKEADEALLHDLR.L	Deamidation	N155
		1635.86	144-157	R.LDKEADEALLHNLR.L	Deamidation	N145
		1671.9	240-254	R.VELQAQTTTLEQAIK.S		
		1725.94	294-308	R.QLAVAQQTLKNELDR.Y		
		1726.92	294-308	R.QLAVAQQTLKDELDR.Y	Deamidation	N304
		1788.93	158-173	R.LQLEAQFLQDDISAAK.D		
		1840.87	125-138	R.SKYENECECQLLLK.E	2 Propionamide	C131 C133
		1979.02	223-239	R.SQLEEGREVLSHLQAQR.V		
		2060.05	158-175	R.LQLEAQFLQDDISAAKDR.H		
		2639.18	255-275	K.SAHECYDDEIQLYNEQIETLR.K	Propionamide	C259
		2722.33	24-50	R.AAEPERPADEGWAGATSLAALQGLGER.V		
		2767.28	255-276	K.SAHECYDDEIQLYNEQIETLRK.E	Propionamide	C259
		2831.47	320-247	R.LTSAFIETPIPLFTQSHGVSLSTGSGGK.D		
		3316.73	320-351	R.LTSAFIETPIPLFTQSHGVSLSTGSGGKDLTR.A		
		3338.79	179-208	K.NLLEVQTYISILQQIIHTTPPASIVTSGMR.E	Oxidation	M207
		3466.89	178-208	K.KNLLEVQTYISILQQIIHTTPPASIVTSGMR.E	Oxidation	M207
		3724.97	179-211	K.NLLEVQTYISILQQIIHTTPPASIVTSGMREEK.L	Oxidation	M207
βB1-Crystallin	28006	1124.59	151-160	K.ISLFEGANFK.G		
		1449.76	61-72	R.LVVFELENFQGR.R		
		1456.7	203-214	R.GYQYLLEPGDFR.H		
		2007.02	93-110	R.SIIVSAGPWVAFEQSNFR.G		
αA-Crystallin	19897	979.57	71-78	K.FVIFLDVK.H		
		1036.53	13-21	R.TLGPFYPSR.L		
		1174.62	55-65	R.TVLDSGISEVR.S		
		1285.63	89-99	K.VQDDFVEIHGK.H		
αB-Crystallin	20146	920.5	75-82	R.FSVNLDVK.H		
		1164.65	93-103	K.VLGDVIEVHGK.H		
		1373.7	12-22	R.RPFFPFHSPSR.L		
		4003.02	23-56	R.LFDQFFGEHLLESDLFPTSTSLSPFYLRPPSFLR.A		
Serum Albumin	69321	1622.78	233-245	K.DVFLGMFLYEYAR.R		
		1638.77	233-245	K.DVFLGMFLYEYAR.R	Oxidation	M238
γS-Crystallin	20993	1516.73	8-19	K.ITFYEDKNFQGR.R		
		1896.98	132-146	K.VLEGVWIFYELPNYR.G		
Phakinin	45851	1359.79	77-89	R.ALGISSVFLQGLR.S		
βB2-Crystallin	23365	1407.74	109-120	K.IILYENPNFTGK.K		
Niban-like Protein 2	77364	2663.21	641-663	K.SSANWILAASLLSCSCFRSGFHR.D	Phosphorylation , Propionamide	S655 C656
Complex 6						
Filensin	74499	1182.67	353-362	R.LQDITAAKPR.Q		
		1279.65	147-157	K.EADEALLHNLR.L		
		1280.64	147-157	K.EADEALLHDLR.L	Deamidation	N155
		1310.68	78-90	R.LGELAGPEDALAR.Q		
		1634.87	144-157	R.LNKEADEALLHNLR.L		
		1635.86	144-157	R.LNKEADEALLHDLR.L	Deamidation	N155
		1635.86	144-157	R.LDKEADEALLHNLR.L	Deamidation	N145
		1671.9	240-254	R.VELQAQTTTLEQAIK.S		
		1725.94	294-308	R.QLAVAQQTLKNELDR.Y		
		1726.92	294-308	R.QLAVAQQTLKDELDR.Y	Deamidation	N304
		1788.93	158-173	R.LQLEAQFLQDDISAAK.D		
		1979.02	223-239	R.SQLEEGREVLSHLQAQR.V		
		2060.05	158-176	R.LQLEAQFLQDDISAAKDR.H		
		2722.33	24-50	R.AAEPERPADEGWAGATSLAALQGLGER.V		
		2831.47	320-347	R.LTSAFIETPIPLFTQSHGVSLSTGSGGK.D		
		3316.73	320-351	R.LTSAFIETPIPLFTQSHGVSLSTGSGGKDLTR.A		
		3338.79	179-208	K.NLLEVQTYISILQQIIHTTPPASIVTSGMR.E	Oxidation	M207

APPENDIX

		3466.89	178-208	K.KNLLEVQTYISILQQIIHTTPPASIVTSGMR.E	Oxidation	M207
		3756.96	312-347	R.IIEIEGNRLTSAFIETPIPLFTQSHGVSLSTGSGGK.D	Deamidation	N318
αB-Crystallin	20146	920.5	75-82	R.FSVNLDVK.H		
		1164.65	93-103	K.VLGDVIEVHGK.H		
		1191.62	73-82	K.DRFSVNLDVK.H		
		1373.7	12-22	R.RPFFPFHSPSR.L		
		2623.37	124-149	R.IPADVDPLTITSSLSSDGVLTVNGPR.K		
		2624.35	124-149	R.IPADVDPLTITSSLSSDGVLTVDGPR.K	Deamidation	N146
		2943.52	122-149	K.YRIPADVDPLTITSSLSSDGVLTVDGPR.K	Deamidation	N146
βB1-Crystallin	28006	1124.59	151-160	K.ISLFEGANFK.G		
		1449.76	61-72	R.LVVFELENFQGR.R		
		1456.7	203-214	R.GYQYLLEPGDFR.H		
		2007.02	93-110	R.SIIVSAGPWVAFEQSNFR.G		
Serum Albumin	69321	1622.78	233-245	K.DVFLGMFLYEYAR.R		
		1638.77	233-245	K.DVFLGMFLYEYAR.R	Oxidation	M238
αA-Crystallin	19897	979.57	71-78	K.FVIFLDVK.H		
		1036.53	13-21	R.TLGPFYPSR.L		
		1174.62	55-65	R.TVLDSGISEVR.S		
		1285.63	89-99	K.VQDDFVEIHGK.H		
γS-Crystallin	20993	1896.98	132-146	K.VLEGVWIFYELPNYR.G		
Phakinin	45851	1359.79	77-89	R.ALGISSVFLQGLR.S		
βB2-Crystallin	23365	1407.74	109-120	K.IILYENPNFTGK.K		
LIM Domain and Actin-binding Protein 1		1174.58	165-175	K.ISADEDSLAVR.S	2 Deamidation	N168 N170
Complex 7						
Filensin	74499	1182.67	352-362	R.ALQDITAAKPR.Q		
		1279.65	147-157	K.EADEALLHNLR.L		
		1280.64	147-157	K.EADEALLHDLR.L	Deamidation	N155
		1310.68	78-90	R.LGELAGPEDALAR.Q		
		1634.87	144-157	R.LNKEADEALLHNLR.L		
		1635.86	144-157	R.LNKEADEALLHDLR.L	Deamidation	N155
		1635.86	144-157	R.LDKEADEALLHNLR.L	Deamidation	N145
		1671.9	240-254	R.VELQAQTTTLEQAIK.S		
		1725.94	294-308	R.QLAVAQQTLKNELDR.Y		
		1726.92	294-308	R.QLAVAQQTLKDELDR.Y	Deamidation	N304
		1788.93	158-173	R.LQLEAQFLQDDISAAK.D		
		1840.87	125-138	R.SKYENECECQLLLK.E	2 Propionamide	C131 C133
		1979.02	223-239	R.SQLEEGREVLSHLQAQR.V		
		2060.05	158-175	R.LQLEAQFLQDDISAAKDR.H		
		2639.18	255-275	K.SAHECYDDEIQLYNEQIETLR.K	Propionamide	C259
		2722.33	24-50	R.AAEPERPADEGWAGATSLAALQGLGER.V		
		2767.28	255-276	K.SAHECYDDEIQLYNEQIETLRK.E	Propionamide	C259
		2831.47	320-347	R.LTSAFIETPIPLFTQSHGVSLSTGSGGK.D		
		3316.73	320-351	R.LTSAFIETPIPLFTQSHGVSLSTGSGGKDLTR.A		
		3338.79	179-208	K.NLLEVQTYISILQQIIHTTPPASIVTSGMR.E	Oxidation	M207
		3466.89	178-208	K.KNLLEVQTYISILQQIIHTTPPASIVTSGMR.E	Oxidation	M207
αB-Crystallin	20146	920.5	75-82	R.FSVNLDVK.H		
		1164.65	93-103	K.VLGDVIEVHGK.H		
		1373.7	12-22	R.RPFFPFHSPSR.L		
		2623.37	124-149	R.IPADVDPLTITSSLSSDGVLTVNGPR.K		
		2624.35	124-149	R.IPADVDPLTITSSLSSDGVLTVNGPR.K	Deamidation	N146
βB1-Crystallin	28006	1124.59	151-160	K.ISLFEGANFK.G		
		1449.76	61-72	R.LVVFELENFQGR.R		
		1456.7	203-214	R.GYQYLLEPGDFR.H		
Serum Albumin	69321	1622.78	233-245	K.DVFLGMFLYEYAR.R		
		1638.77	233-245	K.DVFLGMFLYEYAR.R	Oxidation	M238
αA-Crystallin	19897	1036.53	13-21	R.TLGPFYPSR.L		
		1171.59	79-88	K.HFSPEDLTVK.V		
		1174.62	55-65	R.TVLDSGISEVR.S		
Phakinin	45851	1359.79	77-89	R.ALGISSVFLQGLR.S		
		1878.98	122-137	K.VHALEQVSQELETQLR.M		
βB2-Crystallin	23365	1407.74	109-120	K.IILYENPNFTGK.K		
γS-Crystallin	20993	1516.73	8-19	K.ITFYEDKNFQGR.R		
Complex 8						

APPENDIX

Filensin	74499	1182.67	352-362	R.ALQDITAAKPR.Q		
		1279.65	147-157	K.EADEALLHNLR.L		
		1280.64	147-157	K.EADEALLHDLR.L	Deamidation	N155
		1310.68	78-90	R.LGELAGPEDALAR.Q		
		1634.87	144-157	R.LNKEADEALLHNLR.L		
		1635.86	144-157	R.LNKEADEALLHDLR.L	Deamidation	N155
		1635.86	144-157	R.LDKEADEALLHNLR.L	Deamidation	N145
		1671.9	240-254	R.VELQAQTTTLEQAIK.S		
		1725.94	294-308	R.QLAVAQQTLKNELDR.Y		
		1726.92	294-308	R.QLAVAQQTLKDELDR.Y	Deamidation	N304
		1788.93	158-173	R.LQLEAQFLQDDISAAK.D		
		1979.02	223-239	R.SQLEEGREVLSHLQAQR.V		
		2060.05	158-175	R.LQLEAQFLQDDISAAKDR.H		
		2722.33	24-50	R.AAEPERPADEGWAGATSLAALQGLGER.V		
		2767.28	255-276	K.SAHECYDDEIQLYNEQIETLRK.E	Propionamide	C259
		2831.47	320-347	R.LTSAFIETPIPLFTQSHGVSLSTGSGGK.D		
		3316.73	320-351	R.LTSAFIETPIPLFTQSHGVSLSTGSGGKDLTR.A		
		3338.79	179-208	K.NLLEVQTYISILQQIIHTTPPASIVTSGMR.E	Oxidation	M207
		3466.89	178-208	K.KNLLEVQTYISILQQIIHTTPPASIVTSGMR.E	Oxidation	M207
		3756.96	312-347	R.IIEIEGDRLTSAFIETPIPLFTQSHGVSLSTGSGGK.D	Deamidation	N318
αB-Crystallin	20146	920.5	75-82	R.FSVNLDVK.H		
		1164.65	93-103	K.VLGDVIEVHGK.H		
		1191.62	73-82	K.DRFSVNLDVK.H		
		1373.7	12-22	R.RPFFPFHSPSR.L		
		2623.37	124-149	R.IPADVDPLTITSSLSSDGVLTVNGPR.K		
		2624.35	124-149	R.IPADVDPLTITSSLSSDGVLTVDGPR.K	Deamidation	N146
		2943.52	122-149	K.YRIPADVDPLTITSSLSSDGVLTVNGPR.K		
βB1-Crystallin	28006	1124.59	151-160	K.ISLFEGANFK.G		
		1449.76	61-72	R.LVVFELENFQGR.R		
		1456.7	203-214	R.GYQYLLEPGDFR.H		
		2007.02	93-110	R.SIIVSAGPWVAFEQSNFR.G		
αA-Crystallin	19897	979.57	71-78	K.FVIFLDVK.H		
		1036.53	13-21	R.TLGPFYPSR.L		
		1174.62	55-65	R.TVLDSGISEVR.S		
		1285.63	89-99	K.VQDDFVEIHGK.H		
		3363.64	22-49	R.LFDQFFGEGLFEYDLLPFLSSTISPYYR.Q		
Phakinin	45851	1359.79	77-89	R.ALGISSVFLQGLR.S		
γS-Crystallin	20993	1896.98	132-146	K.VLEGVWIFYELPNYR.G		
βB2-Crystallin	23365	1407.74	109-120	K.IILYENPNFTGK.K		
Complex 9						
Filensin	74499	1182.67	352-362	R.ALQDITAAKPR.Q		
		1279.65	147-157	K.EADEALLHNLR.L		
		1280.64	147-157	K.EADEALLHDLR.L	Deamidation	N155
		1310.68	78-90	R.LGELAGPEDALAR.Q		
		1555.76	470-483	R.HVLVTGDADYVDPR.F	Deamidation	N478
		1634.87	144-157	R.LNKEADEALLHNLR.L		
		1635.86	144-157	R.LNKEADEALLHDLR.L	Deamidation	N155
		1635.86	144-157	R.LDKEADEALLHNLR.L	Deamidation	N145
		1671.9	240-254	R.VELQAQTTTLEQAIK.S		
		1725.94	294-308	R.QLAVAQQTLKNELDR.Y		
		1726.92	294-308	R.QLAVAQQTLKDELDR.Y	Deamidation	N304
		1788.93	158-173	R.LQLEAQFLQDDISAAK.D		
		1840.87	125-138	R.SKYENECECQLLLK.E	2 Propionamide	C131 C133
		1979.02	223-239	R.SQLEEGREVLSHLQAQR.V		
		2060.05	158-175	R.LQLEAQFLQDDISAAKDR.H		
		2639.18	255-275	K.SAHECYDDEIQLYNEQIETLR.K	Propionamide	C259
		2722.33	24-50	R.AAEPERPADEGWAGATSLAALQGLGER.V		
		2767.28	255-276	K.SAHECYDDEIQLYNEQIETLRK.E	Propionamide	C259
		2768.26	255-276	K.SAHECYDDEIQLYDEQIETLRK.E	Deamidation, Propionamide	N268 C259
		2831.47	320-347	R.LTSAFIETPIPLFTQSHGVSLSTGSGGK.D		
		3316.73	320-351	R.LTSAFIETPIPLFTQSHGVSLSTGSGGKDLTR.A		
βB1-Crystallin	28006	1124.59	151-160	K.ISLFEGANFK.G		
		1185.52	124-132	R.WNTWSSSYR.S		

APPENDIX

		1449.76	61-72	R.LVVFELENFQGR.R		
		1456.7	203-214	R.GYQYLLEPGDFR.H		
		1718.8	188-202	K.VSSGTWVGYQYPGYR.G		
		1934.99	236-252	K.QWHLEGSFPVLATEPPK.-		
		2007.02	93-110	R.SIIVSAGPWVAFEQSNFR.G		
		2439.13	161-182	K.GNTIEIQGDDAPSLWVYGFSDR.V		
αB-Crystallin	20146	920.5	75-82	R.FSVNLDVK.H		
		921.48	75-82	R.FSVDLDVK.H	Deamidation	N78
		1164.65	93-103	K.VLGDVIEVHGK.H		
		1191.62	73-82	K.DRFSVNLDVK.H		
		1373.7	12-22	R.RPFFPFHSPSR.L		
		1511.67	57-69	R.APSWFDTGLSEMR.L	Oxidation	M68
		1715.9	93-107	K.VLGDVIEVHGKHEER.Q		
		1881.9	57-72	R.APSWFDTGLSEMRLEK.D	Oxidation	M68
		2624.35	124-149	R.IPADVDPLTITSSLSSDGVLTVDGPR.K	Deamidation	N146
αA-Crystallin	19897	979.57	71-78	K.FVIFLDVK.H		
		1036.53	13-21	R.TLGPFYPSR.L		
		1171.59	79-88	K.HFSPEDLTVK.V		
		1174.62	55-65	R.TVLDSGISEVR.S		
		1192.63	12-21	K.RTLGPFYPSR.L		
		1285.63	89-99	K.VQDDFVEIHGK.H		
		3363.64	22-49	R.LFDQFFGEGLFEYDLLPFLSSTISPYYR.Q		
Phakinin	45851	1353.72	90-103	R.SSGLATVPAPGLER.D		
		1359.79	77-89	R.ALGISSVFLQGLR.S		
		1878.98	122-137	K.VHALEQVSQELETQLR.M		
		2081.01	174-191	R.LMLQTETIQAGADDFKER.Y	Oxidation	M175
γS-Crystallin	20993	1516.73	8-19	K.ITFYEDKNFQGR.R		
		1728.89	159-174	R.KPIDWGAASPAVQSFR.R		
		1896.98	132-146	K.VLEGVWIFYELPNYR.G		
βB2-Crystallin	23365	1407.74	109-120	K.IILYENPNFTGK.K		
		1725.81	173-188	K.DSSDFGAPHPQVQSVR.R		
		1759.83	146-160	R.VQSGTWVGYQYPGYR.G		
		2189.01	169-188	K.GDYKDSSDFGAPHPQVQSVR.R		
βA3-Crystallin	25134	1454.70	33-44	K.ITIYDQENFQGK.R		
		1499.74	126-137	K.MTIFEKENFIGURER.Q	Oxidation	M126
		1690.75	96-109	R.WDAWSGSNAYHIER.L		
γD-Crystallin	20715	1270.6	143-152	R.QYLLMPGDYR.R	Oxidation	M147
Phosphoglycerate Kinase 1	44586	2022.03	280-297	K.ITLPVDFVTADKFDENAK.T		
βA4-Crystallin	22360	1741.85		R.EWGSHAPTFQVQSIR.R		
Complex 10						
Filensin	74499	1014.54	484-492	R.FYVSSITAK.G		
		1094.5	484-492	R.FYVSSITAK.G	Phosphorylation	S488
		1131.6	621-630	K.TVEVVESIEK.I		
		1279.65	147-157	K.EADEALLHNLR.L		
		1280.64	147-157	K.EADEALLHDLR.L	Deamidation	N155
		1306.63	457-467	K.EPETPTELYTK.E		
		1310.68	78-90	R.LGELAGPEDALAR.Q		
		1386.6	457-467	K.EPETPTELYTK.E	Phosphorylation	T460
		1554.78	470-483	R.HVLVTGDANYVDPR.F		
		1555.76	470-483	R.HVLVTGDADYVDPR.F	Deamidation	N478
		1618.81	454-467	R.SPKEPETPTELYTK.E		
		1634.87	144-157	R.LNKEADEALLHNLR.L		
		1671.9	240-254	R.VELQAQTTTLEQAIK.S		
		1698.77	454-467	R.SPKEPETPTELYTK.E	Phosphorylation	T460
		1726.92	294-308	R.QLAVAQQTLKDELDR.Y	Deamidation	N304
		1725.9	294-308	R.QLAVAQQTLKNELDR.Y		
		1796.84	545-560	K.EIEPDGAELEGPEEKR.E		
		1840.91	468-483	K.ERHVLVTGDADYVDPR.F	Deamidation	N478
Phakinin	45851	1265.61	201-211	K.AAEEEINSLYK.V		
		1266.6	201-211	K.AAEEEIDSLYK.V	Deamidation	N207
		1268.72	286-297	K.NRVEAGALLQAK.Q		
		1269.7	286-297	K.DRVEAGALLQAK.Q	Deamidation	N286
		1307.63	221-231	K.MDLESQIESLK.E	Oxidation	M221
		1353.72	90-103	R.SSGLATVPAPGLER.D		
		1359.79	77-89	R.ALGISSVFLQGLR.S		
		1393.71	200-211	R.KAAEEEINSLYK.V		
		1394.69	200-211	R.KAAEEEIDSLYK.V	Deamidation	N207
		1660.77	401-415	K.DVASYHALLDREESG.-		
		1795.87	174-189	R.LMLQTETIQAGADDFK.E	Oxidation	M175
		1872.95	53-72	R.APGVYVGTAPSGCIGGLGAR.V	Propionamide	C65

APPENDIX

		2075.97	155-173	R.ASWASSCQQVGEAVLENAR.L	Propionamide	C161
		2081.01	174-191	R.LMLQTETIQAGADDFKER.Y	Oxidation	M175
Actin, cytoplasmic 1	41719	1176.61	316-326	K.EITALAPSTMK.I	Oxidation	M325
		1197.7	29-39	R.AVFPSIVGRPR.H		
		1515.69	360-372	K.QEYDESGPSIVHR.K		
		1789.88	239-254	K.SYELPDGQVITIGNER.F		
		1953.06	96-113	R.VAPEEHPVLLTEAPLNPK.A		
		2230.06	292-312	K.DLYANTVLSGGTTMYPGIADR.M	Oxidation	M305
αA-Crystallin	19897	1036.53	13-21	R.TLGPFYPSR.L		
		1174.62	55-65	R.TVLDSGISEVR.S		
		1192.63	12-21	K.RTLGPFYPSR.L		
		1285.63	89-99	K.VQDDFVEIHGK.H		
Vimentin	53619	1168.71	130-139	K.ILLAELEQLK.G		
		1322.61	197-207	R.EEAENTLQSFR.Q		
Glutathione Synthetase	52352	940.57	26-34	R.ALAEGVLLR.T		
		1027.57	222-230	R.AIENELLAR.N		
Paralemmin-1	42050	1085.64	42-51	R.VLSSTTLLPR.Q		
Spectrin α chain	284364	989.53	251-259	K.LFGAAEVQR.F		
		1084.62	286-295	R.DLASVQALLR.K		
Retinal Dehydrogenase 1	54827	1396.66	101-113	R.LLLATMESMDGGK.L	Deamidation, 2 Oxidation	N110 M106 M109
βB2-Crystallin	23365	1407.74	109-120	K.IILYENPNFTGK.K		
βB1-Crystallin	28006	1124.59	151-160	K.ISLFEGANFK.G		
αB-Crystallin	20146	920.5	75-82	R.FSVNLDVK.H		
		1164.65	93-103	K.VLGDVIEVHGK.H		
BASP 1	22680	2297.13	98-121	K.AEPPKAPEQEQAAPGPAAGGEAPK.A		
		2635.22	122-149	K.AAEAAAAPAESAAPAAGEEPSKEEGEPK.K		
Lactase-like Protein	65047	1097.64	93-101	K.VQEDIILLR.E		
NCAM	143800	1244.62	706-715	K.LSPYVNYSFR.V		
βA3-Crystallin	25134	1454.7	33-44	K.ITIYDQENFQGK.R		
Serum Albumin		926.49	12-18	K.YLYEIAR.R		

APPENDIX

Appendix 4

Tukey's test of percentage of deamidation for P7: Test performed using data presented in Table 5.5. Statistical significance at P≤0.01 shaded in light green, P≤0.05 shaded in dark green.

P7 (Q151)	ABC + heat	PBS	PBS + heat	Urea + heat
ABC + heat		0.19	0.002	0.12
PBS			0.03	0.98
PBS + heat				0.04
Urea + heat				

Tukey's test of percentage of deamidation for P8: Test performed using data presented in Table 5.5. Statistical significance at P≤0.01 shaded in light green, P≤0.05 shaded in dark green.

P8 (N146)	ABC + heat	PBS	PBS + heat	Urea + heat
ABC + heat		0	0.01	0.2
PBS			0.25	0.02
PBS + heat				0.65
Urea + heat				